Bond strength of reinforcing bars with different encasement qualities - Guidelines for the development length of reinforcing bars in shotcrete

Thèse

Pasquale Basso Trujillo

Doctorat en génie civil
Philosophiæ doctor (Ph. D.)

Québec, Canada

Bond strength of reinforcing bars with different encasement qualities

Guidelines for the *development length* of reinforcing bars in shotcrete

Thèse

Pasquale Basso Trujillo

Sous la direction de :

Marc Jolin, directeur de recherche
Bruno Massicotte, codirecteur de recherche
Benoît Bissonnette, codirecteur de recherche

Résumé

Depuis plusieurs années, le béton projeté a été utilisé pour la stabilisation des talus et le renforcement des structures dégradées. À ce jour, il est également utilisé pour construire des éléments complets tels que des murs de refend, colonnes, coquilles minces, revêtements de tunnels et poutres. Cependant, depuis quelques années, les ingénieurs en structures ont soulevé une préoccupation particulière concernant la qualité d'enrobage des barres d'armature. En effet, des imperfections peuvent être créées spécifiquement derrière les barres d'armature si le béton n'est pas projeté correctement ce qui pourrait provoquer la rupture prématurée des éléments structuraux. Essentiellement, peu de recherche a été faite à ce sujet et les recommandations courantes reposent sur des fondements entièrement empiriques servant uniquement à évaluer la qualité de l'enrobage de barres d'armature des carottes des panneaux de caractérisation.

Cette étude a pour but d'augmenter les connaissances scientifiques concernant la réduction de l'adhérence entre les barres d'armature et le béton causé par ces imperfections afin d'inclure ce phénomène dans les guides destinés à l'inspection et à la conception des structures en béton projeté. Pour contrebalancer la perte d'adhérence, le cas échéant, des facteurs de modification pour l'équation de la *longueur de développement* des barres d'armature en traction est proposée. À cette fin, l'étude présente une phase expérimentale, une phase de modélisation et finalement une phase analytique. La phase expérimentale inclut des éprouvettes de type « pull-out » faites en béton projeté et en béton coulé ayant des *vides artificiels* (pour recréer les imperfections parfois observées en béton projeté). Des éprouvettes de type « beam-end » coulées avec des *vides artificiels* ont également été testées. La phase de modélisation inclut seulement des éprouvettes de type « beam-end » et les principaux résultats étudiés comportent la charge maximale et le type de rupture des éprouvettes, lesquels se sont montrés influencés principalement par la longueur transversale des vides (périmètre *non-adhéré*) et le recouvrement du béton. Les résultats ont permis d'établir des périmètres *non-adhérés* limites pour lesquels une rupture par déchaussement pourrait survenir. Cependant, puisqu'une certaine perte d'adhérence a été observée même avant les limites établis, la phase analytique a permis de proposer des facteurs de modification pouvant être utilisés avec l'équation de la *longueur de développement*. Ainsi, des recommandations ont été développées pour permettre aux ingénieurs de prendre des décisions concernant l'intégrité des structures pendant les inspections ou d'inclure le béton projeté lors de la conception de ces structures si des vides sont relevées ou susceptibles d'être créés derrière les barres d'armature.

Abstract

For many years, shotcrete (sprayed concrete) has been used for slope stabilization and the reinforcement of degraded structures. Nowadays, it's also used to build full-depth structural reinforced concrete elements such as shear walls, columns, thin shells, tunnel linings and girders. However, concerns regarding the encapsulation quality of the reinforcing bars have been raised by structural engineers. Indeed, imperfections could be created specifically behind the reinforcing bars if concrete is inappropriately sprayed which could cause the premature failure of structural elements. Essentially, very little research has been completed on the subject and the current guidelines rely completely on empirical evidence which serves only to evaluate the encasement quality of reinforcing bars from cores taken from pre-construction panels.

This study aims to increase the scientific understanding regarding the bond stress reduction between reinforcing bars and concrete caused by the presence of such imperfections in order to include this phenomenon in the current inspection and design guidelines for shotcrete structures. To counteract the bond stress loss, if any, modification factors to be used in conjunction with the *development length* equation of reinforcing bars in tension is proposed. To do so, the study includes an experimental, a modeling and lastly an analytical phase. The experimental phase includes sprayed as well as cast in-place with *artificial voids* (to recreate the imperfections observed when shotcrete is incorrectly applied) "pull-out" specimens. Cast in-place "beam-end" specimens with *artificial voids* were also studied. The modeling phase only includes "beam-end" specimens and the main studied results were the ultimate load and the mode of failure of the specimens which were found to be mainly influenced by the transversal length of the voids (or *un-bonded* perimeters) and the concrete cover. The results allowed to establish *un-bonded* perimeters limits beyond which a possible reinforcing bar *pull-out* failure could occur. However, since a certain bar stress loss was still observed even below the limits established, the analytical phase served to propose modification factors to be used in conjunction with the *development length* equation. Thus, important guidelines have been created for structural engineers allowing them make decisions regarding the integrity of shotcrete structures during the inspection phase or to take into account shotcrete during the design phase of structures if imperfections are observed or are susceptible to be created behind the reinforcing bars.

Table of contents

List of tables

List of figures

List of symbols

A_b = Area of an individual reinforcing bar

$\widetilde{A}_j$ = Coefficient of a *fuzzy* regression

A_j = Mode of a *fuzzy* regression coefficient $\widetilde{A}_j$

A_{tr} = Total cross-sectional area of all transverse reinforcement within spacing s that crosses the potential plane of splitting through the reinforcement being developed

a_{ag} = Weighted coefficient of absorption for both sand and coarse aggregates in the shotcrete mixture

a_r = Base width of reinforcing bars' ribs

$b_{1,2,3}$ = Regression coefficients prior to the development of the current *development length* equation for reinforcing bars in tension

b_r = Top width of reinforcing bars' ribs

C_u = Unit conversion factor for the *development length* equation

C_1 = First curve-fitting factor for Cornelissen's uniaxial tensile relationship of concrete

C_2 = Second curve-fitting factor for Cornelissen's uniaxial tensile relationship of concrete

c_b = The concrete cover representing the lesser of:
a) The distance from the center of a bar to the nearest concrete surface; or
b) One half of the center-to-center spacing of the bars being developed

D = Either:
a) The core diameter of a reinforcing bar; or
b) The global desirability function

d_b = Nominal diameter of reinforcing bars

d_{cs} = The smaller of:
a) The distance from the closest concrete surface to the center of the bar being developed; or
b) Two thirds of the center-to-center spacing of the bars being developed

$d_{c,t}$ = Scalar damage variable for either the compressive and the tensile behavior

d_i = Desirability for the i^{th} surface response model

d_m = Desirability at the m^{th} surface response model

$E_{a.v.}$ = Elastic modulus of *artificial voids*

E_c = Elastic modulus of concrete

E_I = Internal energy of the Finite Element model

E_k = Kinetic energy of the Finite Element model

E_s = Elastic modulus of steel

e_i = Spread of a *fuzzy* output number i

$\bar{F}$ = Complement of a *fuzzy* number

$\tilde{F}$ = *Fuzzy* number $\tilde{F}$

f_{b0} = Equibiaxial stress of concrete

f_{b0}/f_c = Ratio between the equi-biaxial stress and the uniaxial compressive stress of concrete

f_c = Ultimate compressive strength of concrete

f_{cm} = Average compressive strength of concrete

f_{ct} = Average tensile strength of concrete

f'_c = Specified compressive strength of concrete

f_n = Lowest natural vibration frequency of the Finite Element model

f_s = Stress developed on a reinforcing bar

f_{smax} = Stress of the reinforcing bar at bond failure

f_{sp} = Splitting tensile strength of concrete

f_t = Tensile strength of concrete

f_u = Ultimate strength of reinforcement

f_y = Yield stress of reinforcement

f_{yt} = Yielding stress of the transverse reinforcement

G_F = Fracture energy of concrete

h = Fitting degree of the estimated value to the given data in a *fuzzy* model

h_r = Height of the reinforcing bars' ribs

$J(A,\alpha)$ = Vagueness or index of the spread of the interval in a *fuzzy* model

K_c = Constant defining the shape of the yield surface in the deviatoric plane of the Concrete Damage plasticity model in Abaqus 6.14

$K_{el,f}$ = Elastic friction stiffness for the Coulomb friction law of the Finite Element model

K_{tr} = Transverse reinforcement index

K_1 = Stiffness of the cohesive law in the normal direction of the Finite Element model

$K_{2,3}$ = Stiffness of the cohesive law in the two shear directions of the Finite Element model

k = Curve-fitting factor for uniaxial compressive relationship of concrete

k_1 = CSA A23.3-19 *development length* equation location factor of reinforcing bars

k_2 = CSA A23.3-19 *development length* equation coating factor of reinforcing bars

k_3 = CSA A23.3-19 *development length* equation concrete density factor of reinforcing bars

k_4 = CSA A23.3-19 *development length* equation bar size factor of reinforcing bars

$L^{-1}(h)$ = *Fuzzy* number function equal to (1 – h) for a symmetrical triangular *fuzzy* number

$|L_\alpha|$ = Length of an α-cut within a *fuzzy* number

ℓ_b = Bonded length of the "beam-end" specimens

ℓ_d = *Development length* of straight reinforcing bars in tension

ℓ_s = Splice length of reinforcing bars in tension

N = Necessity measure in *possibility theory*

n = Number of bars being developed or spliced in the plane of splitting

n = Curve-fitting factor for the uniaxial compressive relationship of concrete

P_{max} = Ultimate force of a reinforcing bar

P_{max}/A_b= Ultimate stress of a reinforcing bar

PS_{200} = Percentage of particles finer than the No. 200 sieve in the shotcrete mixture

p = Normal closing pressure between steel and concrete of the Finite Element model

R_r = *Relative rib* area of the reinforcing bar

S.D. = Standard deviation

s = Center-to-center spacing of transverse reinforcement

s_r = Spacing of reinforcing bars' ribs

T_n = Fundamental period of vibration of the Finite Element model

T_s = Tensional force of a reinforcing bar

u_c = Bond stress in the spliced reinforcement due to concrete contribution

u.p. = *Un-bonded* perimeter of a reinforcing bar

u_{tr} = Bond stress in the reinforcement due to the contribution of transverse reinforcement

V_L = Length of the voids placed in the Finite Element model of the "beam-end" specimen

$w_{c1,c2}$ = Weight of the fresh shotcrete sample 1 or 2

$w_{dry\ ag}$ = Weight of the shotcrete sample after 48 hours of drying in the oven

$w_{dry\ c1}$ = Weight of the shotcrete sample after several cycles of drying in the microwave

$\dot{w}_{machine}$ = Weight of the mix introduced in the *dry-mix* shotcrete machine per unit of time

$\dot{w}_{panel}$ = Weight of the shotcrete mixture sticking to the vertical panel per unit of time

$\dot{w}_{water}$ = Weight of water per unit of time

$\tilde{X}_j$ = *Fuzzy* input number of a *fuzzy* regression

x_{ij} = Mode of a *fuzzy* input number $\tilde{X}_j$

$\tilde{Y}$ = Estimated *fuzzy* number obtained from a *fuzzy* regression

$\tilde{Y}_{u.p.\,=\,0\%}$ = Estimated *fuzzy* number of a *fuzzy* regression at *u.p.* = 0%

$\tilde{Y}_{u.p.\,>\,0\%}$ = Estimated *fuzzy* number of a *fuzzy* regression at any *u.p.* greater than 0%

y_i = Mode of a *fuzzy* output number i

α-cut = Subset of values having a greater possibility ($\pi(x)$) than the threshold defined by the α-cut.

α_j = Bound of a *fuzzy* regression variable $\tilde{X}_j$

β = Either:

a) Width to length ratio of the bearing strips used in the concrete splitting tensile test

b) Inclination of reinforcing bars' ribs

γ_{ij} = Bound of a *fuzzy* input number $\widetilde{A}_j$

ϱ_c = Density of the concrete

ϱ_s = Density of the steel

δ = Cracking opening for the uniaxial concrete tensile behavior

δ_d = Post-peak separation of the cohesive law of the Finite Element model

δ_0 = Maximal crack opening for the uniaxial concrete tensile relationship

ε = Concrete uniaxial strain in compression

ε_c = Concrete uniaxial strain at failure in compression

ε_{max} = Elongation at rupture of reinforcement

ε_{cdp} = Eccentricity of the yield surface in the Concrete Damage Plasticity model in Abaqus 6.14

$\varepsilon_c^{\sim in}$ = Inelastic strain of the concrete in compression in Abaqus 6.14

λ = ACI 318-19 modification factor for lightweight concrete

μ = Static friction coefficient between steel and concrete

μ_c = Viscosity parameter in the Concrete Damage Plasticity model in Abaqus 6.14

ν_c = Poisson's coefficient of concrete

ν_s = Poisson's coefficient of steel

$\sigma_{c,t}$ = True (Cauchy) stress of concrete (or ultimate stress) in compression or in tension

$\bar{\sigma}_{c,t}$ = Effective stress of the concrete in compression or in tension

$\sigma_{i,j}$ = Variance of a population i and pair j

$\hat{\sigma}_{max}$ = Maximum principal effective stress

σ_1 = Cohesive strength in the normal direction

$\bar{\sigma}_1$ = Ultimate cohesive strength in the normal direction

σ_h = Tensile hoop stress around reinforcing bars

σ_r = Radial stress around reinforcing bars

Σ gaps = Sum of gaps transversal to the reinforcing bar other than the ribs (usually only the longitudinal ribs parallel to the longitudinal axis of the reinforcing bar)

θ = Face angle of reinforcing bars' ribs

Π = Possibility measure in possibility theory

$\pi(x)$ = Possibility distribution of a variable x

$\tau_{2,3}$ = Cohesive strength in the two shear directions

$\bar{\tau}_{2,3}$ = Ultimate cohesive strength in the two shear directions

τ_{crit} = Critical shear stress at the surface of the test bar

τ_{eq} = Equivalent shear stress at the surface of the test bar

ψ = Angle of concrete dilatancy in the Concrete Damage Plasticity model in Abaqus 6.14

Ψ_t = ACI 318-19 *development length* equation modification factor for reinforcement location

Ψ_e = ACI 318-19 *development length* equation modification factor for reinforcement coating

Ψ_s = ACI 318-19 *development length* equation modification factor for reinforcement size

Ψ_g = ACI 318-19 *development length* equation modification factor for reinforcement grade

Acknowledgements

During this project, I had the chance to work with extremely talented and interesting people. They might not know it but all of them have had a great impact on my professional career and my personal development and for that reason I would like to extend my most sincere gratitude to all of them. Of course, this investigation would have never happened without my research supervisor, Marc Jolin. His human approach for teaching and issue troubleshooting as well as his expertise on concrete technology made this period of my life extremely enjoyable. Marc always made sure the ambiance within the team was inclusive by making sure we participated in local and international events related to concrete technology and even by giving us responsibilities, like teaching assistance, to make sure once finished we would develop other academic and interpersonal skills that we could put into use professionally. For this and his useful advices, not only on research but life and personal related I thank him greatly. My research co-supervisors, Bruno Massicotte and Benoît Bissonnette also gave me lots of guidance on technical topics for this investigation, article writing and enhancement and other topics related to mechanical and durability properties of concrete structures. I even had the chance to take graduate classes from both Marc and Benoît, and even other extremely knowledgeable and passionate professors such as Benoît Fournier during my time as a Ph.D. student. An extremely valuable Finite Element coach and co-author during this time was Fabien Lagier. His large knowledge on concrete mechanics and his valuable advice greatly enhanced the scientific quality of the finite element phase within this investigation.

The support from other members of the CRIB (Centre de Recherche sur les Infrastructures en Béton) center at Université Laval was also fundamental for the completion of this research. I would especially like to thank Mathieu Thomassin and Jean-Daniel Lemay for their great help during the experimental phases of this investigation. They made sure that all of the equipment was functional and calibrated and that all of the material needed was in the laboratory. They also provided extremely valuable advice to enhance the experimental program of this research. I am also extremely grateful to René Malo, Richard Côté (R.I.P.) and Alain Melançon, concrete laboratory technicians, who helped me arduously set-up the testing apparatus and to cast and test all of the specimens in the laboratory. René Malo even helped me co-author a technical note on the modification of a testing equipment needed to complete the experimental program which appeared in a world renown peer-reviewed journal. The hard work that was needed in the lab

was also made possible with the help of concrete laboratory interns Benoît Chénard, David Bilodeau-Pelchat, Marc-Antoine April, Samuel Blackburn and Simon Paquet who helped with the casting operations of the specimens. Of course, the ambiance and functionality of the CRIB would not have been the same without Lyne Dupuis, administrative assistant, whose charisma and friendliness made my days in the university much easier.

The number of colleagues, and now friends, I had the chance to work with during this time was also remarkable. They are all extremely passionate about concrete research and extremely knowledgeable on this subject. It was really pleasant to exchange ideas and experiences in the students' lounge. I am speaking in particular of Isabelle Filly-Paré, Fabio Melo and Sebastien Girard whose research, like mine, focused on sprayed concrete technology. We all know how much laboratory work is needed with this particular method of concrete placement. During that period of time, I also had the chance to meet Sebastien Bilodeau, Jean-Sebastien Fortin, Anthony Allard, Felix-Antoine Villemure, Vincent Castonguay, Leandro Sanchez, Alexandre Rodrigue, Mathieu Fiset, Mathieu Champagne and Jessy-French Baronet with all of whom I had the chance to exchange research ideas and travel to conferences; I will never forget the good times we all had specially at International ACI conferences. Since I saw most of them finalize their research and leave, I had the chance to get to know another bunch of colleagues in the following years that were equally passionate and knowledgeable individuals. I am speaking in particular of Antoine Gagnon, Pierre Siccardi, Thomas-Jacob Vaillancourt, Christine Poulin, Alexandre Pépin Beaudet, Roxanne Ouellet, Xavier Berger, Fréderic Bédard, Simon Bérubé, Bruce Gandhi Menu, Mélodie Hilt, Émile Blouin-Dallaire, Achraf Laradh, Charles Lamothe and Fréderic Béland. Once again, I had a really good time with all of them exchanging research ideas and traveling to local and international ACI conferences.

One of the most important group of people I need to thank is my family. All of them, beginning with my parents, my brothers and sister, supported thoroughly my career (even from overseas) always with positive comments and great words of encouragement. My mother-in-law and father-in-law as well as my sister-in-law also encouraged me tremendously during this period of time and made it much easier for me. Perhaps the most important people in this part of my life has been my girlfriend Noémie Roy; I do not recall a time when she was not there to support me. She had to make a lot of hard decisions due to my wishes to pursue a Ph.D., so I would like to thank her enormously for her support and great patience.

Foreword

A total of four scientific articles and one technical note are included in this thesis; all of them have been (or are in the process of being) peer reviewed. The author of this thesis has been the main author in all of them. All of the co-authors, Dr. Jolin, Dr. Massicotte, Dr. Bissonnette and Dr. Lagier have contributed by reviewing them and proposing additional literature and analysis techniques so that their content could be improved and be of international scientific quality. The technical note was largely improved with the comments provided by Mr. Malo who acted as co-author and took care of developing the experimental set-up needed to test the laboratory specimens.

Regarding the status of the scientific articles, two of them have been published, one has been accepted for publication and the last one has been submitted; all of them in international scientific journals. The technical note has also been published in an internationally recognized journal. The layout of all of them has been modified to respect the formatting style of this thesis. Finally, the complete references, dates of submission and current status is enumerated below.

Article No. 1 (Chapter 3):

- Reference: Basso Trujillo, P., Jolin, M., Massicotte, B., and Bissonnette, B., "Bond strength of reinforcing bars encased with shotcrete," Construction and Building Materials, Vol. 169, 2018, pp. 678-688, doi.org/10.1016/j.conbuildmat.2018.02.218
- Submitted: August 23rd, 2017
- Status: Accepted on February 28th, 2018 and published on April 30th, 2018

Article No. 2 (Chapter 4):

- Reference: Basso Trujillo, P., Jolin, M., Massicotte, B., and Bissonnette, B., "Bond strength of reinforcing bars with varying encapsulation qualities," ACI Structural Journal, Vol. 115, No. 6, 2018, pp. 1707- 1717, doi.org/10.14359/51702415
- Submitted: November 1st, 2017
- Status: Accepted on February 19th, 2018 and published on November 1st, 2018

Article No. 3 (Chapter 5):

- Reference: Basso Trujillo, P., Lagier, F., Jolin, M., Massicotte, B., and Bissonnette, B., "Finite element model of "beam-end" specimen with different qualities of reinforcing bar encapsulation," Engineering Structures Journal (submitted).
- Submitted: September 28th, 2020
- Status: Under peer review

Article No. 4 (Chapter 6):

- Reference: Basso Trujillo, P., Jolin, M., Massicotte, B., and Bissonnette, B., "Shotcrete modification factors for the *development length* equation," ACI Structural Journal, Vol. 118, No. 3, 2021, pp. 305-314, doi.org/10.14359/51730539
- Submitted: July 13th, 2020
- Status: Accepted on October 22nd, 2020 and published on May 1st, 2021

Technical note (see Appendix A):

- Reference: Basso Trujillo, P., Jolin, M., Massicotte, B., and Bissonnette, B., "Alternative setup apparatus to test ASTM A944-10 "beam-end" specimens," Journal of Testing and Evaluation, Vol. 46, No. 4, 2018, pp. 1741-1748, https://doi.org/10.1520/JTE20170645
- Submitted: November 9th, 2017
- Status: Accepted on March 15th, 2018 and published on July 1st, 2018

Introduction

General introduction

Shotcrete is a method of concrete placement in which concrete is sprayed at high velocity onto a receiving surface. When the technique was first developed, at the beginning of the 1900s, it was mostly used for slope stabilization and restoration or reinforcement of degraded structures. However, with the development of better equipment, enhanced concrete mixtures (usually incorporating mineral and chemical admixtures and other by-products), and the improvement of guidelines regarding the placement techniques, shotcrete has become a viable and practical alternative with respect to cast in-place concrete to build full depth reinforced concrete elements such as domes [1], tunnel linings [2] (see Figure I.1a), columns [3] (see Figure I.1b), shear walls [4] and girders [2]. The advantage of using shotcrete includes the rapidity of construction, the use of one-sided formwork (if any) and the ability to place concrete on irregular surfaces; all reducing the expenses of a project if good practice guidelines are executed.

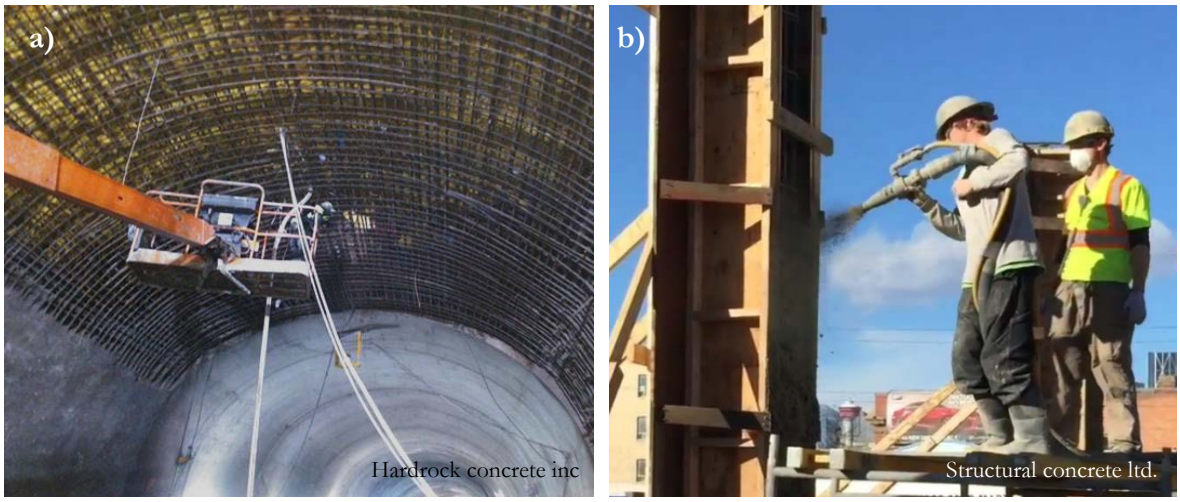

Figure I.1: a) Tunnel lining and b) columns being sprayed with concrete

Naturally, the design of reinforced sprayed concrete members must follow the requirements established in the ACI 318-19 [5] and the CSA A23.3-19 [6] design codes for concrete structures in the United States of America and Canada respectively. However, even if the sprayed material is still concrete, its properties and those of the interface around reinforcing bars are different than those of cast in-place concrete [7, 8]. Additionally, some issues like those related to the encapsulation of the reinforcement represent a typical concern among structural engineers, architects, contractors, and owners. Indeed, a certain area of the element is blocked by the

reinforcing bars themselves while the mixture is sprayed. To avoid the creation of imperfections (such as voids or entrapped aggregates) behind the bars as can be seen in Figure I.2, good practice guidelines recommend that an adequate shooting technique, in combination with an adequate mixture *consistency*, needs to be used [9-13]. Otherwise, imperfections might be created specifically behind reinforcing bars if, among others, the access to the element is difficult, the structural elements present heavily congested zones of reinforcement or if the nozzle operators (nozzlemen) do not have the proper skills or accreditation. If voids are created, the bond strength between reinforcing bars might be considerably reduced and consequently, the performance of the structural elements might be jeopardized as their mode of failure might become brittle with increasingly bigger imperfections.

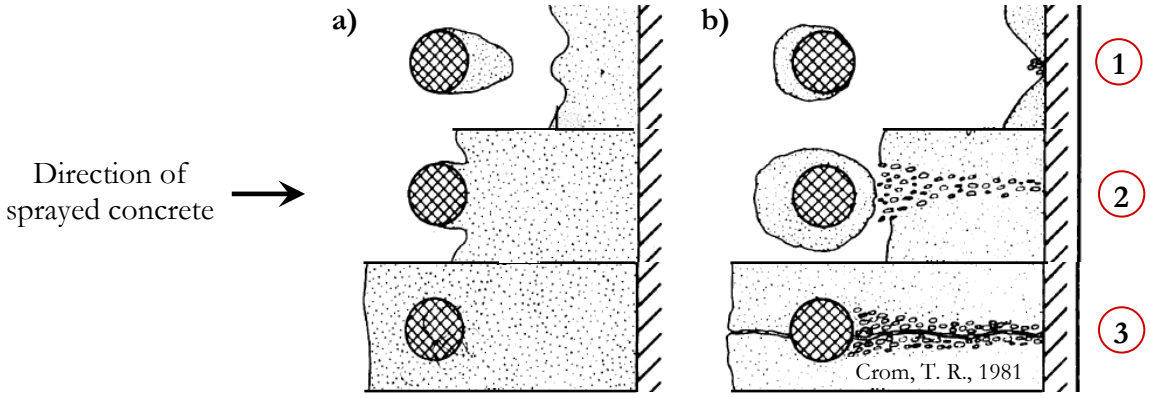

Figure I.2: a) Correct application of shotcrete and b) entrapped aggregates created behind a bar

A possible solution to take into account the assessed risk associated to the presence of defects on the bond strength between reinforcing bars and concrete is to adapt the *development length* (ℓ_d) equation for reinforcing bars in tension specified by North American design codes [5, 6] using modification factors when such defects are foreseen. The *development length* (ℓ_d) equation is used to calculate the extended length, or the lap splice length, of reinforcing bars within reinforced concrete members so that they can attain their yield stress at any section of the member and therefore comply with Ultimate Limit States (ULS) design criteria. In fact, the *development length* (ℓ_d) equation already incorporates modification factors accounting for the unfavorable effect of concrete bleeding and epoxy or zinc-coated bars as well as for the reinforcement grade and the more favorable bond performance of small size bars. However, in the case of shotcrete structures, the current practice is to assume a perfect reinforcing bar encapsulation during the

design phase and verify afterwards that it has actually been (or almost perfectly) achieved by visually inspecting cores extracted from pre-construction panels[1] [14, 15]. According to the most recent visual evaluation method of encapsulation quality established by the ACI [16], an encasement of 90%, 80%, and 70% of a reinforcing bar's perimeter is deemed to have a "very good", "good", and "satisfactory" quality of encapsulation respectively. However, despite all of the effort that has been put to fix these limits, they have been established based on empirical evidence (knowledge shared in ACI technical meetings mostly) and do not rely on actual laboratory tests in which the bar stress of reinforcing bars with varying encapsulation qualities was studied. Consequently, research is needed to determine the parameters that most impact the bat stress reduction of reinforcing bars when imperfections are present specifically behind them so that proper actions and decisions can be taken during the design of reinforced shotcrete structures and during the evaluation of cores taken from pre-construction panels.

Challenge

As a result of the current way to assess the encapsulation quality of reinforcing bars, structural engineers have no other option but to compute *development lengths* of reinforcing bars in tension for reinforced shotcrete elements in the same way as it is done for cast in-place concrete elements. Indeed, the different in-place concrete properties that are obtained with cast in-place concrete and shotcrete are overlooked in the current North American building code requirements for reinforced concrete. Therefore, rigorous encapsulation quality control procedures have been created for shotcrete i.e., spraying pre-construction panels whose cores are inspected and graded based on the encapsulation quality of reinforcing bars. Nonetheless, the current grading systems are based on empirical evidence and not on quantitative data taking into account the bar stress reduction as the encasement quality of reinforcing bars decreases. The fact is that reliable (scientific) data which can be used to determine the threshold between an acceptable or unacceptable size of imperfection is scarce; even the geometric parameters of the imperfections which contribute the most to the bar stress reduction are still not fully understood. The same uncertainty is encountered when cores are inspected as it is still almost impossible to evaluate the bond capacity of inadequately encased reinforcing bars with our current knowledge. Thus, a comprehensive investigation is needed to assess the stress of a reinforcing bar in the presence of different sizes of voids so that corrective measures can be

[1] Panels often sprayed in complex shotcrete projects to recreate the challenging parts of actual structures.

developed based on scientific data for the design and the inspection of shotcrete structures if imperfections are foreseen or are suspected to be present behind reinforcement.

Objectives and significance

The main objective of this investigation is to develop thorough knowledge and understanding regarding the main properties of imperfections that cause a bond strength reduction between reinforcing bars and shotcrete when they are specifically created behind the bars. On one hand, it intends to provide scientific data linking the bar stress of reinforcing bars to various qualities of reinforcing bar encapsulation and to validate and enhance the existing technical notes used to inspect shotcrete cores. On the other hand, it aims to develop a set of rigorous *modification factors* for the *development length* of deformed bars in tension equation (ℓ_d) specified by North American design codes [5, 6] so that voids up to a certain size can be considered (if any) during the design phase of shotcrete structures.

The specific objectives of the investigation are enumerated as follows:

1. Study the bond performance, including the load-slip (or stress-slip) relationship, the ultimate bar load (or bar stress), and the failure mode of two types of bond specimens having test bars with various qualities of reinforcing bar encapsulation. The bond specimens that will be studied are:

    a. Shotcrete and cast in-place "pull-out" specimens. The latter method of concrete placement is necessary to study the phenomenon with controlled void sizes using silicone inserts whose purpose is to recreate actual voids observed in shotcrete specimens (henceforth called *artificial voids*).

    b. Cast in-place ASTM A944-10 "beam-end" specimens [17] with *artificial voids*.

2. Validate laboratory results using a commercial Finite Element (FE) software and complement the experimental program by means of a parametric study using a larger set of variables.

3. Propose *modification factors* for the ACI 318-19 [5] and the CSA A23.3-19 [6] *development length* of deformed bars in tension equation (whenever needed) based on the experimental and the analytical campaign results.

The findings of this comprehensive investigation are intended to provide structural engineers with the required information to adequately specify *development lengths* if voids are suspected to be created with shotcrete. This will ultimately give the shotcrete crew a tolerable margin of error in terms of reinforcing bar encapsulation which will, in turn, guarantee the structural integrity of each structural element. Moreover, the investigation will provide reliable information regarding the impact of different void sizes on the bar stress loss of reinforcing bars that will help engineers to properly characterize the encasement quality of reinforcing bars from cores taken from pre-construction panels and determine if corrective measures in the design of the actual structural elements (if not already taken) is needed.

Scope

The global strategy of this investigation includes the three main phases enumerated below in order to achieve its objectives:

1. An experimental phase
2. A Finite Element (FE) phase
3. An analytical phase

Both "pull-out" and "beam-end" specimens were tested in the experimental phase. Initially, "pull-out" specimens made with *dry-mix* shotcrete were built to study the relationship between the *consistency*, the percentage of rebound[2] and the compressive strength of the concrete mixture in regard to the encapsulation quality of a reinforcing bar and its impact on the bar stress reduction. In that regard, imperfections were created specifically behind the test bar by the nozzlemen who deliberately varied the amount of water, and thus the *consistency* of the mixture, with the nozzle valve. Since it was difficult to control the size of the imperfections with shotcrete specimens, cast in-place "pull-out" specimens with *artificial voids* of known sizes were later used. In that way, the relationship between a precisely known void size and the bar stress reduction was determined. Such specimens served to establish the most significant geometrical properties of the *artificial voids* influencing the stress reduction of reinforcing bars. The studied parameters included the transversal length of the voids (0, 10, 20 and 30% of the reinforcing bars' perimeter) and the height of the voids (1x and 0.5x of the bars' diameter). A comparison between shotcrete

[2] The percentage mass of un-adhered material with respect to the total mass of sprayed material.

and cast in-place "pull-out" specimens allowed to determine the limitations associated to the use of *artificial voids*. This technique (cast in-place concrete with *artificial voids*), considering its limitations, was used thereafter with a more suitable bond specimen such as the "beam-end" specimen (their stress field is representative of most reinforced concrete members as the test bar and the concrete around it is placed in tension). The results obtained with this type of specimen were used to propose modification factors for the *development length* equation (ℓ_d). The parameters of the *artificial voids* that were investigated in such case included their transversal length (0, 10, 20 and 30% of the bars' perimeter), and their position (facing towards the top or the bottom of the "beam-end" specimen). Test bars 15M (No. 16) and 20M (No. 19) were investigated as the size of reinforcing bars represents a frequent concern regarding their encapsulation quality. For all the bond specimens tested in the laboratory ("pull-out" and "beam-end"), the *artificial voids* were placed over the entire bonded length of their test bars and the stability of the concrete mixture (especially for the "beam-end" specimens) was minimized to assure little bleeding and thus an insignificant bar stress reduction due to this phenomenon.

Because of the relative importance of the "beam-end" specimen over the "pull-out" specimen, only the former type was studied in the FE phase in which the commercial software Abaqus 6.14 was used. This phase served to explore variables that were not tested during the experimental phase and included the length of the voids over the bonded length of the test bars (100 and 50%), the concrete cover above the test bars (2.5 and 5.0 of the bar's diameter), the bonded length of the test bar (6.3 and 12.5 of the bar's diameter), and voids having a 40% transversal length even though past experience in shotcrete suggests that voids of such size would most likely cause excessive rebound. The FE results served to establish limits on the transversal size of voids in contact with the reinforcing bar beyond which an excessive bar stress loss and a possible element's failure mode change from concrete *splitting* to a bar *pull-out* could be observed. The transversal size of voids limits were dependant on the length of the voids over the bonded length of the reinforcing bar.

In the analytical phase, the ultimate bar stress obtained from the experimental cast in-place "beam-end" specimens was used to compute *bond performance ratios* (BPR) between specimens with a perfect encapsulation and those with various qualities of bar encasement. Such ratios were proposed to be used as a basis for the determination of modification factors for the *development length* equation (ℓ_d) of the North American reinforced concrete design codes [5, 6] whenever

voids in shotcrete elements (if any), and lying within the transversal size of voids limits established by the FE phase, are expected. The inherent size variability of actual shotcrete voids was incorporated to the proposed modification factors using principles of *possibility theory*. It has to be noted that the actual modification factors needed for a particular situation is out of the scope of the investigation as the judgment of structural engineers is still needed in all cases. The global procedure of this investigation, including the three main phases, that lead to the creation of *bond performance ratios* and guidelines for the encapsulation quality evaluation of reinforcing bars is shown in Figure I.3.

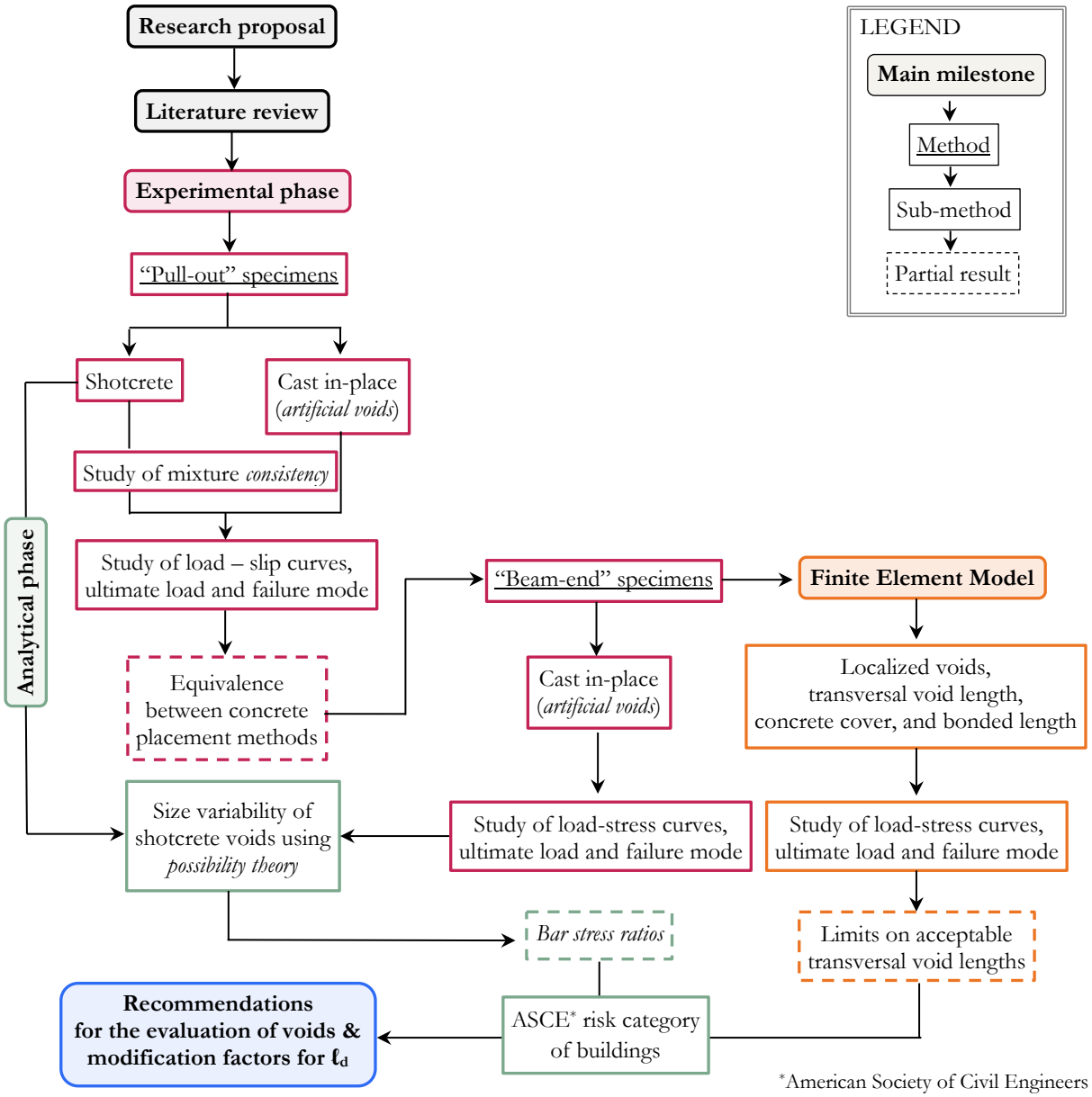

Figure I.3: Global strategy of this investigation

Structure of the thesis

This document is divided in eight chapters and includes four peer-reviewed articles as part of the body of the document and one peer reviewed technical note presented in Appendix A. Chapter 1 presents a literature review regarding the shotcrete process and the placement techniques that need to be followed to achieve an adequate reinforcing bar encapsulation. Thereafter, the current state of knowledge regarding the bar to concrete bond strength and the effect voids or imperfections behind reinforcing bars have on it is discussed. The way structural detailing for shotcrete structures is done by describing ACI 318-19 [5] and CSA A23.3-19 [6] equations to compute the *development length* of reinforcing bars in tension and the accepted correction factors that can be applied to them are also presented. Lastly, the most relevant FE modeling techniques to study the bar to concrete bond strength for this investigation are discussed. In Chapter 2, the experimental methods including the geometry and the testing apparatus of the selected bond specimens ("pull-out" and "beam-end") as well as all of the variables under study are presented. To shorten the text of this document, only a brief description of the set-up apparatus of the "beam-end" specimen following ASTM A944-10 [17] is presented as the Technical Note in Appendix A explains it in detail. More importantly, the way cast in-place bond specimens with *artificial voids* were built and compared to shotcrete specimens (only "pull-out" specimens) with imperfections is explained. In Chapters 3 and 4, presented in the form of peer-reviewed articles, the experimental results of the "pull-out" and "beam-end" specimens are presented respectively. In Chapter 5 the calibration and the results of the "beam-end" FE model are presented in the form of a peer-reviewed article. Chapter 6, also in the form of a peer-reviewed article, presents the analytical procedure (based on *possibility theory*) within which modification factors for shotcrete structures are proposed for the *development length* equation of the ACI 318-19 [5] and CSA A23.3-19 [6] design codes. The original contributions reported in each of the four journal articles and the technical note are described subsequently. A general discussion on the overall results from this investigation and on the future research still needed are presented in Chapter 7. Finally, the novel findings of this research are outlined in the conclusion.

Original contributions

Chapter 3 - Bond strength of reinforcing bars encased with shotcrete

This chapter describes an experimental study in which *dry-mix* shotcrete "pull-out" specimens were tested. Imperfections behind the single reinforcing bar of the specimens were deliberately created by the nozzlemen by varying the *consistency* of the mixture. Because imperfections of the desired sizes could not be created, cast in-place "pull-out" specimens with silicone inserts of different sizes were created and both methods of concrete placement were statistically compared.

Contrary to the well-known *wettest stable limit* that is usually sought to achieve a perfect reinforcing bar encapsulation, it was found that seeking the "driest" possible *consistency* (guaranteeing a proper reinforcing bar encapsulation and rebound not in excess of what is usually regarded as normal) is preferable to assure the best reinforcing bar to concrete bond performance. In terms of using *artificial voids*, it was found that only the bar stress at bond failure was comparable between shotcrete and cast in-place concrete specimens. In that regard, a considerable bar stress loss was found when voids of approximately 20% of the bar perimeter are present specifically behind a reinforcing bar. Beyond that void size, it is possible that the mode of failure of the specimens change from concrete *splitting* to the reinforcing bar *pull out*. In general, when comparing the bond performance of the reinforcing bars vis-à-vis the method of concrete placement, it was found that shotcrete enhances the *slip stiffness* of the bar relative to concrete in comparison to cast in-place concrete.

Chapter 4 - Bond strength of reinforcing bars with varying encapsulation qualities

This chapter describes an experimental study in which cast in-place "beam-end" specimens with silicone inserts of different sizes around the test bar, simulating possible shotcrete imperfections, were tested. Reinforcing bars of sizes 15M (No. 16) and 20M (No. 19) were used and the imperfections were placed over the bars either facing the top or the bottom of the specimens. In addition, the bond behavior of specimens having different concrete mixture's *w/b* ratios was compared to the one of specimens whose reinforcing bars had silicone inserts.

It was confirmed that a considerable bar stress is lost when approximately 20% of the bar perimeter is not in direct contact with the surrounding concrete. In fact, the impact of a void of

such magnitude on the bar stress loss was found to be comparable to the "top-bar" effect caused by bleeding around reinforcing bars. Additionally, it was observed that a change in the failure mode of specimens can occur if the transversal length of the voids become equal or greater than 30% for specimens with concrete covers of $2.5d_b$.

Chapter 5 - Finite Element model of "beam-end" specimen with different qualities of reinforcing bar encapsulation

A study in which the "beam-end" specimens presented in Chapter 4 were modeled using the commercially available Finite Element package Abaqus 6.14 and the generated data was compared to the experimental results obtained in the previous phase. Thereafter, a parametric study was undertaken to analyze the impact of the concrete cover and the size of imperfections on the bar stress loss and the failure mode of the specimens.

A void transversal length range of 0 - 20% was determined to be acceptable (minor bar stress reduction and bar slip relative to concrete) as long as measures are taken to overcome the bar stress loss of reinforcing bars. It was also determined that beyond this range, an excessive bar stress reduction and a possible failure mode change of specimens can occur. The range is valid for both concrete covers studied ($2.5d_b$ and $5.0d_b$) since allowing larger void lengths can considerably increase the slip of the bars for the smaller concrete covers and drastically reduce the bond stress at failure for the larger concrete covers fostering a mode of failure change of the specimens from concrete *splitting* to *pull out*. It was also found that a transversal void length of up to 30% could be allowed if imperfections cover half of the bonded length of a bar. This is because voids of 30% covering half of the bonded length of a bar present a similar bond performance as voids of 20% covering the entire bonded length of the bar. Similarly, voids of 20% covering half of the bonded length of a bar present a similar bond performance as voids of 10% covering the entire bonded length of the bar.

Chapter 6 - Shotcrete modification factors for the *development length* equation

An analytical investigation in which the experimental results from the "beam-end" specimens and the void size limits presented in chapters 4 and 5 respectively are used to propose modification factors for the *development length* of reinforcing bars in tension equation (ℓ_d) by means of *possibility theory* principles.

The modification factors can be chosen depending on the imperfections' transversal length around a reinforcing bar and, based upon *possibility theory*, on *bar stress ratios* associated to the risk category of a building as established by the American Society of Civil Engineers (ASCE).

Appendix A - Alternative set-up apparatus to test ASTM A944-10 "beam-end" specimens

A brief introduction of the "beam-end" specimen is presented and the set-up apparatus to test them in a vertical position is described in detail. The testing procedure and the way to interpret the results are also discussed.

A detailed way to adapt a high force vertical load frame which is normally available in structural laboratories is presented. This allows to use existing machines without having to build one as depicted in the ASTM A944-10 standard.

Chapter 1 Literature review

1.1 Shotcrete placement

1.1.1 Shotcrete placement processes

Shotcrete is a method of placement in which concrete is sprayed at high velocity onto a receiving surface. Shotcrete is classified in two processes depending on the way the materials are pumped and transported from the spraying machine up to the exit of the nozzle. In the first case, the *dry-mix* process, all of the mixture components (binder, coarse and fine aggregates, and powdered admixtures as well as fibers if needed) are transported through a hose from the spraying machine up to the nozzle using compressed air. The water is added to the dry mixture right before the end of the nozzle (Figure 1.1) by means of a water ring connected to an independent line. However, the water ring can be placed up to 3.0 m upstream from the nozzle (*long nozzle* configuration) to increase the mixing time from approximately 0.05 to 0.5 seconds [18].

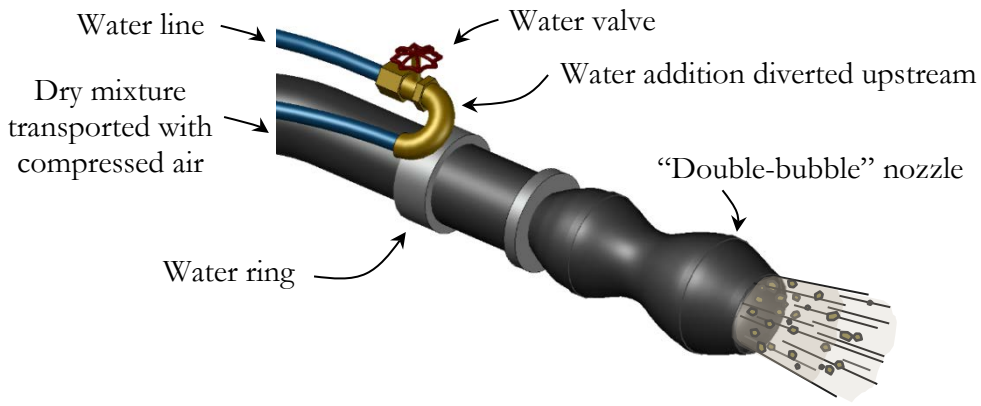

Figure 1.1: Typical *dry-mix* process nozzle

The machine operators (normally two or more) add the dry mixture into the hopper of the machine and regulate the flow of compressed air. The operator holding the nozzle, called often nozzleman, verifies the velocity of the air stream and communicates with the operators by hand signals to set the optimal air flow velocity. Thereafter, the nozzleman opens the water valve and then the operators release the flow of the dry mixture. Due to the nature of the process, the water to binder ratio (w/b) cannot be *a priori* known by the nozzlemen and thus, the optimal quantity of water is adjusted before the actual spraying operations by evaluating the *consistency* of

the fresh mixture on a panel. Usually, it is measured qualitatively by poking the fresh mixture and evaluating its surface glossiness. The paste is then characterized as adequate, " too wet" or " too stiff". However, it can be quantitatively measured using a penetrometer. In such case, the pressure required to penetrate the paste by a flat-headed tip (immediately after shotcrete has been placed) is regarded as the *consistency*.

In the second case, the *wet-mix* process, all of the materials are thoroughly mixed and pumped through the hose up to the nozzle using a pump. Then, the compressed air which is introduced at the nozzle using an independent line (refer to Figure 1.2) provides the mixture the acceleration needed to be placed at high speed. If needed, liquid set-accelerators can be added at the nozzle using an additional line [19]. Since the w/b ratio is known before the mixture is pumped, it is usually the slump of the mixture that is measured rather than its *consistency* to characterize the rheology of the mixture. Additional crew members are needed to activate the flow of the air and the mixture as well as to assure the correct functioning of the pump and the air compressor. More crew members may also be needed (in either process) depending on the circumstances. For instance, if *overspray*[3] is a substantial concern or if thick layers of shotcrete with double layers of reinforcement are being sprayed, an additional member should stand next to the nozzleman blowing away all of the un-adhered aggregates caused by rebound with an air lance (often called a blowpipe). More information regarding proper spraying of shotcrete can be found in the ACI "506R-16 Guide to shotcrete" [13].

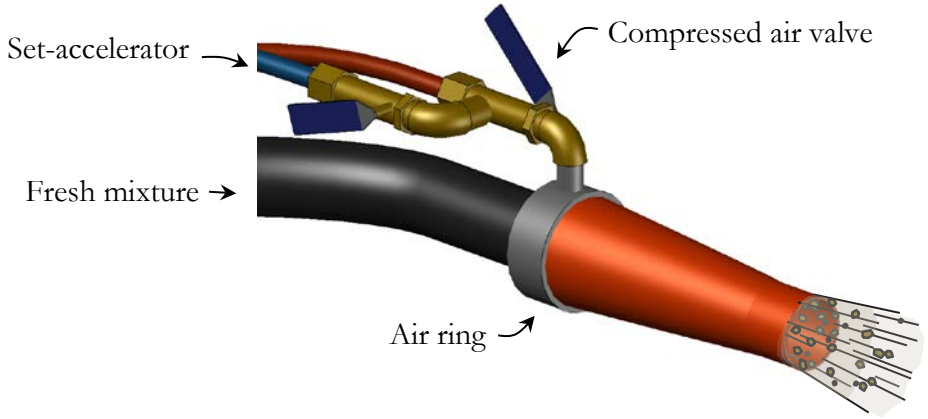

Figure 1.2: Typical *wet-mix* process nozzle

[3] Shotcrete material deposited away from the intended receiving surface.

1.1.2 Encasement of reinforcing bars

The main parameters that can influence the encasement quality of reinforcing bars with shotcrete can be grouped in four categories as follows:

a) The plasticity (or *consistency*) of the mixture

b) The experience of the nozzlemen and the applied spraying techniques

c) The airflow settings of the equipment

d) The amount of reinforcing bar congestion within an element

Regarding the *consistency,* the mixture should be plastic enough so the reinforcement can be properly encapsulated but not too much to cause the concrete to slough off the receiving surface. In *dry-mix* shotcrete this is usually assessed visually by the nozzleman who adjusts the amount of the added water accordingly. On one hand, shotcrete sprayed "too wet" can cause concrete sloughing and reduce the achievable build up thickness which is critical in vertical applications. On the other hand, shotcrete sprayed "too dry" can cause excessive rebound, dust, and difficulties for finishing causing, in turn, a reduction of the mechanical and durable properties of concrete. Historically, the *consistency* sought in *dry-mix* shotcrete has been called the *wettest stable consistency* and is achieved when the maximal amount of water before the concrete sloughs off the surface is used [10]. Obtaining the *wettest stable consistency* requires experienced nozzlemen and its actual value varies from one mixture to another. For a mixture[4] with 18% GU cement and 2% silica fume per total mass of dry materials for instance, the optimal *consistency* has been shown to range in between 0.5 and 1.4 MPa [11]. However, some admixtures used for, among others, rebound reduction and concrete sloughing enhancement may allow (unintentionally) the addition of more water by the nozzlemen and cause the mechanical and durable properties of the concrete to be reduced if the *wettest stable consistency* is sought [20, 21]. In the case of *wet-mix* shotcrete, obtaining the desired *plasticity* is often less problematic because the slump can be controlled before the concrete mixture is pumped. In that case, the slump that is usually specified ranges between 50 and 75 mm (based on ASTM C143-20 [22]) and in some cases even 100 mm when bars larger than 19.1 mm in diameter are used [23].

[4] T10+SF mixture as mentioned in the literature.

In terms of nozzlemen experience, past research has shown that reinforcing bars sprayed with a rather "wet" *consistency* mixture can be easily encased by nozzlemen of almost any level of experience. As the *consistency* of the mixture becomes "dryer", the experience of nozzlemen becomes a crucial factor as a better trained crew is needed to properly encase the bars. In fact, only highly experienced nozzlemen can properly encase the bars when the "driest" possible *consistency* (before creating excessive rebound) is used [10]. A proper spraying technique suggests that nozzlemen should make small circular movements with the nozzle while spraying the concrete in order to reduce rebound, overspray, and achieve a proper reinforcing bar encapsulation (Figure 1.3a) regardless of the mixture *consistency*. Also, the stream of shotcrete should impact the receiving surface at 90 degrees to achieve maximal compaction (refer to Figure 1.3b) and shotcrete should be placed from the bottom towards the top of the element. When spraying thick elements (even up to 0.9 m thick), the top surface of the in-place shotcrete should remain at approximately 45 degrees with respect to the ground [9] as shown in Figure 1.4. This technique, called "bench shooting", is done so that loose particles can fall down to the ground by gravity and trapped rebound is avoided [24].

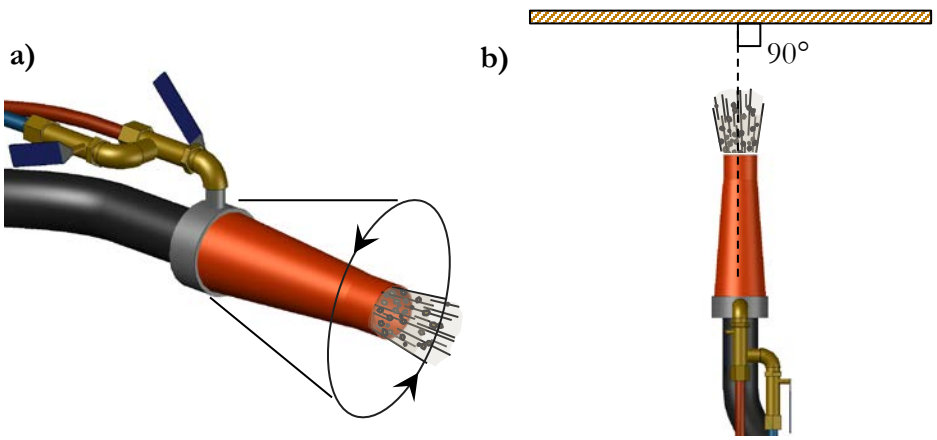

Figure 1.3: Adequate handling of the nozzle while spraying concrete

In terms of airflow settings, a proper air velocity assures the proper compaction of concrete around and behind the reinforcing bars. It also maintains their front surface clean (refer to Figure I.2a) and minimizes rebound. The ideal airflow should be selected based on the hose diameter and its length; as they become bigger and longer, the airflow should be increased. For a *dry-mix* equipment with a 15 m long and 50 mm diameter hose, the optimal airflow should range around 8.5 m^3/min (300 $ft.^3$/min). In projects where 300 m long and 75 mm diameter hoses are used,

the airflow can reach up to 19.8 m^3/min (700 $ft.^3$/min) [25, 26]. Compressors capable of ensuring as much as 28 m^3/min of airflow (1000 $ft.^3$/min) exist and are sometimes used. A lower airflow is normally required for the *wet-mix* process and, depending on the airflow selected, the nozzle should be located 0.6 to 3.0 m away from the receiving surface [9, 23]. In terms of reinforcing bar congestion, if the structural element is composed of more than one layer of reinforcement, the nozzlemen may need to get closer to the receiving surface and even introduce the nozzle beyond the first layer of reinforcement (the use of a blowpipe is required in this case). Usually, large diameter horizontal bars are more difficult to encase than vertical bars [27] so the use of non-contact lap splices is strongly recommended. It is worth mentioning that sufficiently rigid formwork is also needed to support the weight of the concrete and avoid undesired deformations of the elements.

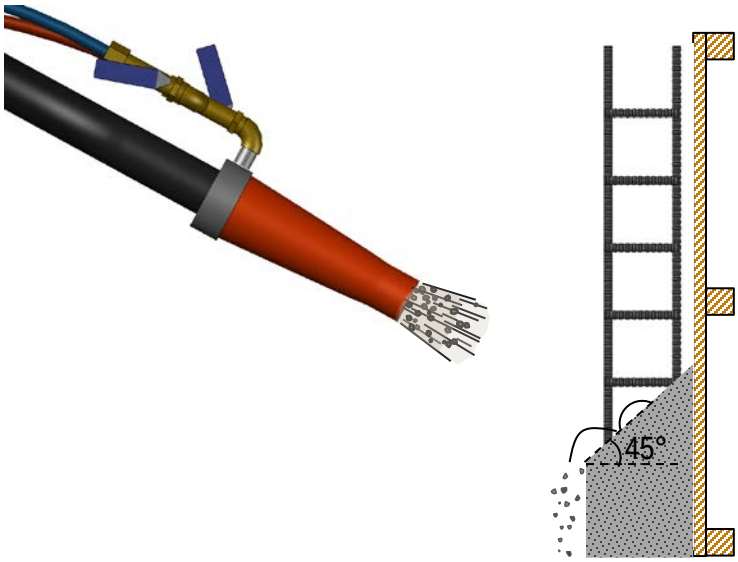

Figure 1.4: "Bench shooting" technique

If one or more of these guidelines are not followed, imperfections in the form of voids or entrapped aggregates (also called *sand lenses*) can be created behind the reinforcing bars as seen in Figure 1.5. In general, voids are mostly caused by an inadequate plasticity of the mixture whereas entrapped loose aggregates are mostly caused by an inappropriate spraying technique [12]. However, both types of imperfections may appear at the same time. Voids can also be created behind reinforcement if excessive sagging of concrete occurs while the reinforcement stays firmly in place.

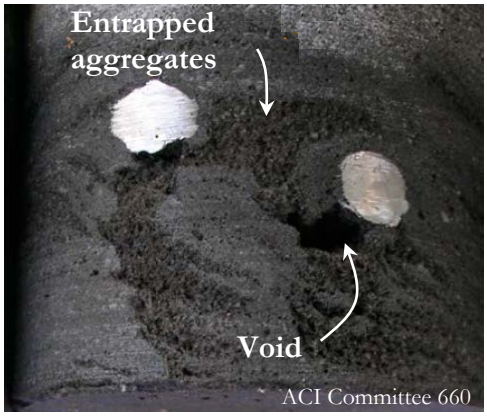

Figure 1.5: Imperfections created behind reinforcing bars (adapted from [30])

1.1.3 Inspection and evaluation of shotcrete

A common practice used in many projects in North America to determine the encasement quality of the reinforcing bars is to spray pre-construction panels (refer to Figure 1.6) and analyze cores extracted from them. Pre-construction panels normally represent one of the most challenging zones of the actual structure to spray on and the same equipment, crew members, and shotcrete mixture design are used to guarantee similar results on the actual structure. Up until 2013, the cores were evaluated using the *core-grading system* proposed in ACI "506.2-95 Specification for shotcrete" [28] in which the encasement quality was visually graded from 1 (perfect) to 5 (poorest). However, the *core-grading system* was strictly developed for the nozzlemen certification program established by ACI committee C660 [29, 30] and the grades had no correlation to the bond strength of the bars being encased. In fact, despite the effort made to create such grading system, its reliability has been widely questioned [31-33] and, even nowadays, it has led engineers make unsupported design decisions, i.e. using the ratio of cores of a given grade to establish a modification factor for the *development length* equation [34].

Figure 1.6: Pre-construction panel sprayed using the *wet-mix* process and an air lance

Consequently, the *core-grading system* was removed in the 2013 version of the document (ACI 506.2-13) [15] and was recently replaced (for evaluating the reinforcing bar encasement in actual structures) by ACI "506.6T-17 Visual shotcrete core quality evaluation technote" [16]. In this technical note, the size of the imperfections (if any) is reported as a percentage of the bars' perimeter and their size if they are in contact with the reinforcing bar. Still, the adopted percentage limits defining different qualities of encapsulation (from "very good" to "poor") were established based on experience and not on the actual bond strength performance of reinforcing bars with varying encapsulation qualities.

1.2 Fundamentals of bar-concrete bond strength

1.2.1 The bond mechanism

The mechanism that makes out the bond between reinforcing bars and concrete is activated progressively. Indeed, tensile stresses are transferred from the concrete towards the reinforcing bars gradually as a reinforced concrete element is loaded. Since both materials have different elastic moduli (E_s/E_c usually in between 6 and 8), slip relative to one another occurs but it is restrained by the bond between one another. In general, such bond can be grouped into three main mechanisms: *chemical adhesion*, *friction* and *mechanical anchorage* [35].

Chemical adhesion occurs when the cement paste, while nucleating into its different chemical phases, bonds to the surface of the reinforcing bars. However, this adhesion is rapidly lost when small loads are applied over the reinforced concrete elements and, from that moment on, *friction* between the concrete and the reinforcing bars is created while they slip relative to one another. The coefficient of friction depends on the surface roughness of both materials and the pressure over the bars provided by the confinement (concrete cover, transverse reinforcement, exterior reinforcement, etc.) or transverse loads on the element (as in a beam-column connection). The usual *static* coefficient of friction between reinforcing bars and concrete ranges between 0.57 and 0.70 [36]. *Mechanical anchorage* is caused by the bearing of the reinforcing bars' ribs against the surrounding concrete. For deformed bars, this represents the primary contributor to the bond mechanism [35]. Historically, the behavior of the bond mechanism has been studied with bond specimens tested in the laboratory and normally the information is represented using a stress (τ) - slip (δ) relationship like the one shown in Figure 1.7a.

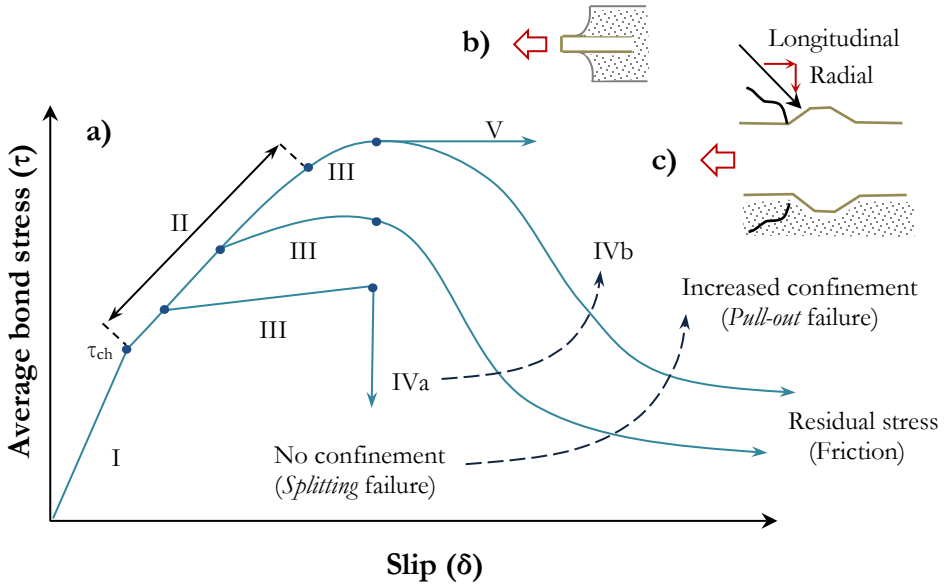

Figure 1.7: Bond stress - slip curve (adapted from [37])

Chemical adhesion, represented by Stage I, is the first mechanism to act. At this stage, even though some slip can be measured experimentally because of the elastic un-cracked concrete surrounding the bar (see Figure 1.7b), there is no actual relative slip between the bar and the concrete. When the stress reaches the maximal *chemical adhesion* resistance (τ_{ch}), the bars begin to slip relative to the concrete and the *friction* and the *mechanical anchorage* mechanisms are activated as depicted by Stage II. The reaction forces at the rib, divided into radial and longitudinal components as seen in Figure 1.7c, causes the formation of micro-cracks in front of the bar ribs as they bear on the surrounding concrete. As loading continues and the micro-cracks spread radially towards the outer surface of the element, the relative slip between the bar and the concrete increases (Stage III). The amount of slip depends on the quality of the bar-concrete interface (type of concrete, reinforcing bar geometry, etc.) and on the amount of confinement.

The type of bond failure, depicted by the descending branch of the curves in Figure 1.7a, also depends on the level of confinement and on the spacing between reinforcing bars. If the concrete cover is small, the micro-cracks will rapidly reach the outer faces of the member (before any other type of failure can occur) causing a concrete *splitting* failure (Stage IVa). If the spacing between the bars is smaller than the concrete cover, the *splitting* crack will form between the reinforcing bars. As the confinement and reinforcing bar spacing increases, the ribs of the bar will rather crush and shear the concrete in front of them before the micro-cracks can reach the

outer surface of the member causing a *pull-out* failure (Stage IVb); this will in turn cause an increase of the ultimate bond strength. Specimens having long development or spliced lengths, besides having an increased bond strength, will normally fail by a combination of *splitting* and *pull-out* mechanisms as the part of the reinforcing bar closest to the point of load application will be subject to a higher level of stress than the furthest part of the bar. When further loading is applied, residual stresses between the crushed and the surrounding concrete are developed. If sufficient confinement and bar spacing are provided, in combination with a long development or spliced length, the yielding of the bar is favored rather than a bond failure (Stage V). However, given the usual configuration of the reinforcement in most flexural members, the usual mode of bond failure is *splitting* [38-42].

1.2.2 Effect of the reinforcing bar and concrete properties on bond strength

Many properties of the reinforcing bars have an influence on bond strength. However, one of the most important factors is the geometry of the reinforcing bars [41]. The *relative rib* area (the ratio between the projected rib height normal to the bar axis and the center to center rib spacing) is particularly important as it influences, among others, the initial slope of the bond stress (τ) – slip (δ) curve; greater values of the *relative rib* area produce a stiffer initial slope [43]. In addition, it also increases the overall bond performance of the bars; tests indicate that doubling the *relative rib* area could reduce the *development length* by 20% [44]. In North America, its usual values range in between 0.057 and 0.087, however, bars having larger *relative rib* areas are also produced and those with values exceeding 0.100 are normally referred to as having high *relative rib* areas. Based on Fei et al. [45], the *relative rib* area (R_r) can be calculated using Equation 1.1:

$$R_r = \frac{h_r}{s_r}\left(1 - \frac{\sum gaps}{p}\right) \tag{1.1}$$

Where:

h_r = average height of the ribs

s_r = average center to center spacing between ribs

p = nominal perimeter of the bar

Σ gaps = sum of the transverse width of the longitudinal ribs or any other marking

The R_r value and the face angle of the ribs influence the mode of bond failure. Rehm [46] found that a *pull-out* failure is likely to occur if values of R_r exceed 0.143 and that the face angle of the ribs is greater than 40 degrees. With values of R_r smaller than 0.100 and rib face angles greater than 40 degrees, concrete crushing in front of the ribs is likely to occur initially producing an "effective rib" with a lesser angle because of the accumulated concrete after failure in front of the rib. In such case, a *splitting* failure is more likely to occur because the radial component of the bar stress at the rib would increase and the longitudinal one would decrease [35, 43, 46]. Whenever the rib face angle is less than 30 degrees, no crushing occurs and therefore a *splitting* failure is fostered. The confinement over the reinforcing bars (either by concrete cover or transverse reinforcement) also plays a significant role on the effect of the bars' geometry on bond strength. For a low confinement, bond is independent of deformation pattern and a *splitting* failure usually governs. On the contrary, with a high confinement, the bond strength is increased as the *relative rib* area also increases.

In terms of the concrete, both its fresh and hardened properties play a significant role on bond strength. As the compressive strength of the normal concrete increases, a *splitting* failure is favored instead of a *pull-out* one as crushing in front of the reinforcing bar ribs is prevented because the bearing capacity of the concrete increases. In descriptive and design equations, the contribution of the compressive strength of concrete to bond has been accounted by using $f'_c{}^p$. Values of p in the range of ¼ to 1 have been proposed depending on the absence or presence of transverse reinforcement. In general, a value for the exponent of ¼ has shown to provide the best correlation when no transverse reinforcement is present for both normal and high-strength concrete. For reinforcing bars confined by transverse reinforcement, a value ¾ has proven to be more adequate for a wide range of concrete compressive strengths. In general, as the compressive strength of concrete increases, the bond strength increases as a function of $f_c^{1/4}$ or $f_c^{3/4}$ depending on whether transverse reinforcement is absent or present. Interestingly, the 2010 fib model code for concrete structures links the *pull-out* failure of a reinforcing bar to $f'_c{}^{1/2}$ and a *splitting* failure to $f'_c{}^{1/4}$ [158].

The slump of concrete also impacts the bond strength of reinforcing bars. In general, the lower the slump (with proper consolidation), the higher the bond strength. This is because, higher slump (if produced by adding water or even with a water reducer and a somewhat high *w/b* ratio), increase the tendency of concrete segregation and bleeding which are likely to result in a

more porous zone and sometimes voids below reinforcing bars. This phenomenon, referred to as the "top-bar" effect, is only normally observed for reinforcing bars with considerable concrete placed below them. A "top-bar" effect can be avoided (up to a certain level) if the desired concrete rheology is obtained using a low *w/b* ratio and a water reducer. It must be noted that low temperatures, a high *w/b* ratio and an overdose of water reducers could increase the set time of concrete thereby increasing its bleeding time and additionally reducing the bond strength of reinforcing bars. Other properties of the reinforcing bars and the concrete affecting the bond behavior of reinforced concrete elements, usually to a lesser extent, are reviewed in detail in ACI "408R-03 *Bond and development of straight reinforcing bars in tension*" report [42].

1.3 Impact of imperfections on bond

1.3.1 Concrete placed by gravity

Imperfections or voids around reinforcing bars can be observed at a micro or a macroscopic level. Imperfections at the microscopic level refer to those present at the surface of reinforcing bars and to those in the thin layer of cement paste just around them. The surface defects of reinforcing bars exist because their crystalline surface referred to as "mill scale" presents cracks, voids and crevices due mainly to handling and bending. However, the presence of "mill scale", whose thickness typically ranges between 2-40 μm [47], causes no significant reduction in the bond strength of reinforcing bars [39]. Defects at the interface of reinforcing bars and cement paste exist because portlandite and ettringite crystals precipitate towards the reinforcing bar after the concrete is placed thus creating a porous area usually referred to as Interfacial Transition Zone (ITZ). The thickness of the ITZ is amplified, among others, by unstable mixes having an inadequate cement and fine size distribution [48], high slump mixtures with high *w/b* ratios or a high amount of water reducer admixture that might ease concrete segregation and therefore water accumulation under the reinforcing bars [42]. The thickness of the ITZ usually ranges between 50-100 μm (with *w/b* ratios in between 0.40 – 0.65) [49] but it may become larger in the event of concrete settlement and excessive bleeding, segregation, paste seepage from the formwork, re-vibration applied for extra consolidation, construction vibrations (in the case of high-slump concrete) and even if the "mill scale" of the bars is removed with a wire brush [50]. Indeed, the thickness of the ITZ has been reported to be around 186-320 μm when 70 mm of concrete is placed below reinforcing bars [49] whereas a thickness of 660 μm has been observed with 800 mm of concrete (w/b = 0.47) below the reinforcing bars [51]. The

position of the bar also influences the location of the concrete porosity around reinforcing bars. In the case of vertical reinforcing bars, the most porous zones are found at the underside of their ribs and in the case of longitudinal bars, this is found all along their bottom surfaces. The *defect factor* of this porous zone (defined as the ratio between the defect length and the perimeter of the bar) has been observed to vary widely depending on the mixture design [52-54]. These observations were made by examining the cross-sections of "pull-out" specimens with plain reinforcing bars extracted at different heights from 2.0 m columns as shown in Figure 1.8.

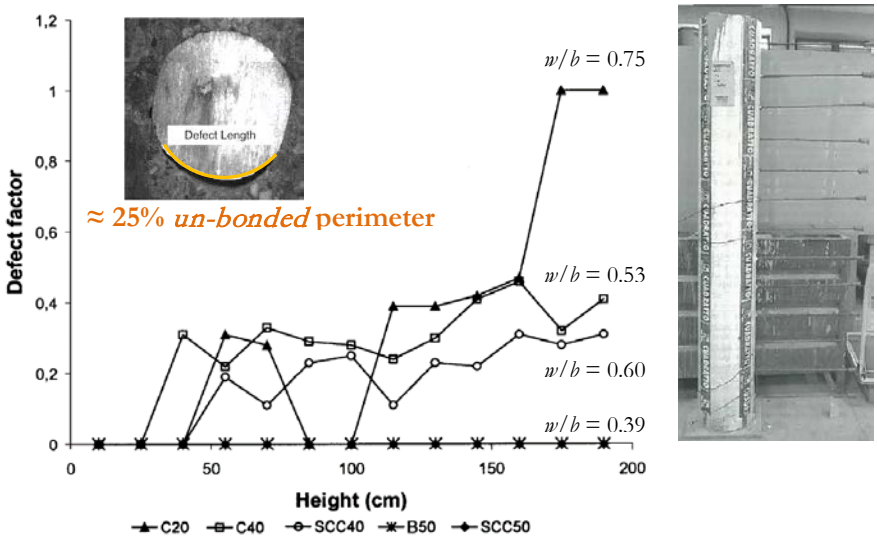

Figure 1.8: Impact of the height of concrete on the defect length (adapted from [52])

Defects on the bar to cement paste interface can be minimized with low *w/b* ratio mixes having enhanced plastic properties such as Self-Consolidating Concrete (SCC) made with supplementary cementitious materials (SCM), inert fillers and superplasticizers which will largely reduce bleeding. With 2.3 µm calcite fillers, the interface thickness has been reported to be approximately reduced by half from 100 µm to 50 µm [49]. With the use silica fume for instance, whose particles are about 100 times smaller (~0.1 µm) than cement grains [55] and react with the portlandite to create calcium silicate hydrate gel (C-S-H), a similar phenomenon occurs. In fact, no voids were created beneath the bars of SCC having silica fume even when they had 1.9 m of concrete below them as seen in Figure 1.8 for the 0.39 *w/b* mix (B50 mix).

Still, due to the different levels of porosity between top- and bottom-cast reinforcing bars caused by bleeding and settlement, the bond strength of reinforcing bars normally decreases. This effect

has been observed with as little as 150 mm of normal concrete below a reinforcing bar but not with SCC [42, 52]. Although the bond strength reduction has rarely been associated with the *un-bonded* perimeter[5] of imperfections and voids (refer to Figure 1.8), Soylev et al. [52-54] found a linear bond strength reduction tendency from about 40% to 80% (bond efficiency factor of 0.6 to 0.2) when the *un-bonded* perimeter increases from 10% to 40% respectively. This is observed in Figure 1.9 where a *defect factor* of approximately 0.25 (25% *u.p.*) causes a 0.4 bond efficiency factor[6] and thus a 40% reduction of the bond strength in comparison to a perfectly encapsulated bar.

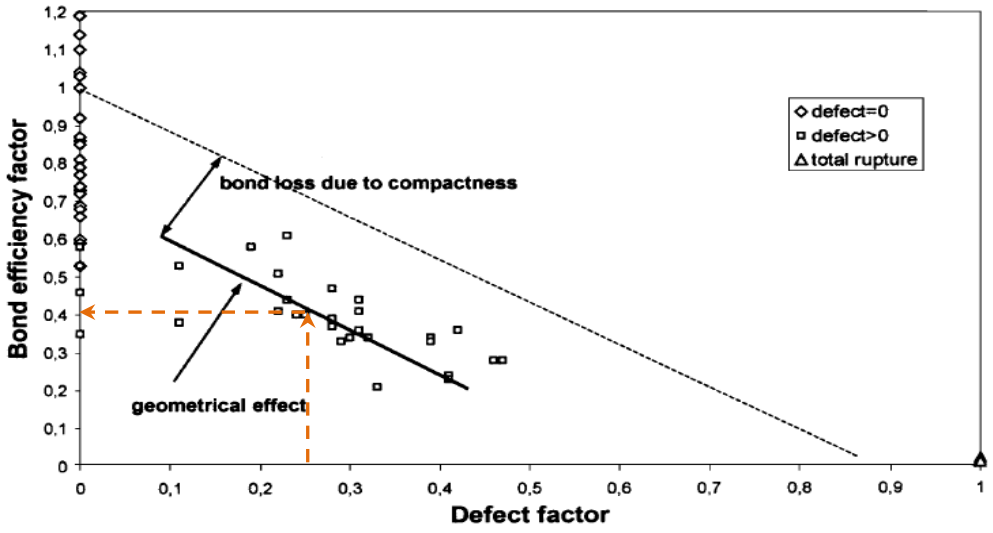

Figure 1.9: Impact of defect length and bond strength (adapted from [52])

It should be noted that because the bond strength of the specimens was not corrected to account for the different compressive strengths as the height of the concrete increases as it is usually done in this type of investigation [56-58], the actual bond strength reductions should be slightly smaller.

At the macro level, voids or entrapped air (usually larger than 1.0 mm) may be created and imprisoned at the surface of reinforcing bars if the concrete is not properly consolidated. As can be observed in Figure 1.10, the shape of these voids can be extremely irregular.

[5] Defined as the ratio, in percentage, between the *defect length* and the total perimeter of the reinforcing bar.
[6] Defined as the bond strength ratio between a bar cast at a given height and the bottom-cast bar.

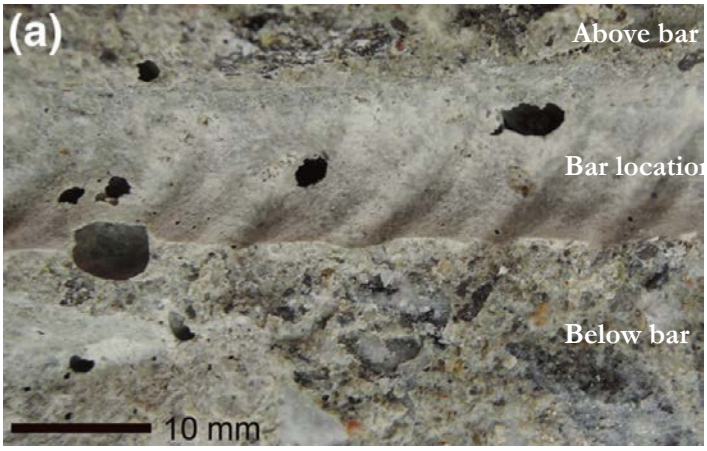

Figure 1.10: Entrapped air bubbles adjacent to a reinforcing bar [159].

Whiting et al. [59] reported that as little as 5% of under-consolidation[7] (referring to the amount of air of voids in the concrete matrix) can result in a bond strength reduction of approximately 63% of bottom-cast horizontal bars. Moreover, because of the somewhat poor bond between reinforcing bars and the surrounding cement paste, the failure mode of the specimens changed from concrete *splitting* to the reinforcing bar *pull-out*. The bond strength increased by about 10% for a 2% over-consolidation (5 min over a vibrating table). Similar tendencies have been observed by Darwin et al. [60, 61] who found bond strength reduction between vibrated and non-vibrated specimens of 6% and 23% for bottom- and top-cast reinforcing bars respectively. They attributed the difference between them to the fact that additional consolidation is provided to the bottom-cast reinforcing bars due to the self-weight of the concrete and thus, a smaller difference is observed in those cases. It must be noted that well distributed spherical voids as the ones found in air-entrained concrete do not cause a drastic decrease of the bond strength. However, above 4.5% of entrained air, a "true" bond reduction can be observed. Indeed, even though the compressive strength of concrete decreases as the amount of air entrained increases, the rate of the bond strength reduction is higher than the rate of the compressive strength reduction. This phenomenon did not occur when bars had a high *relative rib* area.

1.3.2 Imperfections in sprayed concrete

Only few investigations have studied the impact of voids and entrapped aggregates on the bond strength of sprayed concrete bond specimens. Gagnon et al. [12, 62] evaluated the

[7] Defined as the ratio between the bulk densities of mechanically vibrated and not-vibrated "pull-out" specimens.

bond strength of *wet-* and *dry-mix* "pull-out" specimens based on the ACI reinforcing bar encapsulation grades (see Section 1.1.3). They found that, for a given concrete compressive strength, the bar stress at failure decreased dramatically with an increase of the encapsulation deficiency as seen in Figure 1.11. Indeed, for reinforcing bars having an encapsulation grade 1 or 2 (which represents voids covering approximately 20% or less of the reinforcing bars used in the study), no significant bar stress reduction was observed. However, an important bar stress at failure decrease was observed beyond that point. Based on their findings, an average bar stress at failure reduction of 32% can be computed[8] for a grade 3 (voids' length in between 32 and 38 mm) reinforcing bars in comparison with perfectly encapsulated ones [29]. Still, the authors did not comment on the scatter observed for 39.0 MPa compressive strength specimens which might have been caused due to spraying or core grading attribution difficulties which is indeed a complex task to perform.

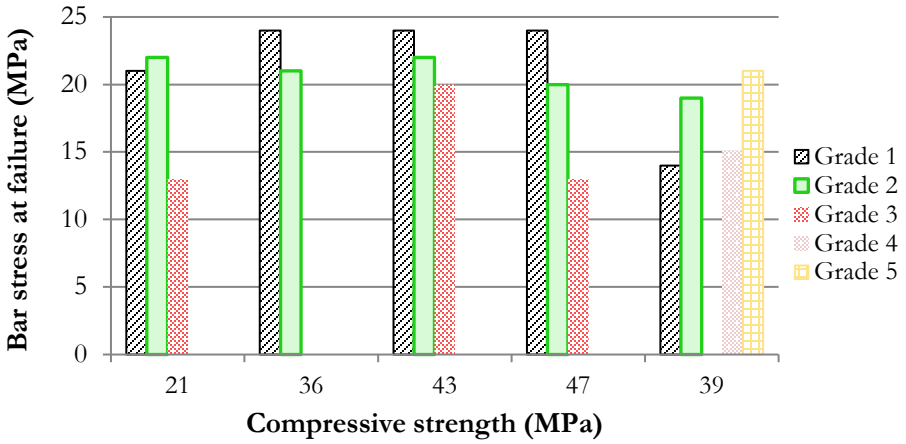

Figure 1.11: Bar stress results at failure of "pull-out" specimens (data from Gagnon et al. [62])

Ghio et al. [8] undertook an experimental research program in which they compared 8 *wet-mix* shotcrete and cast in-place concrete splice-beam specimens to study how the method of concrete placement affects the stress developed in reinforcing bars. They found that specimens with "top-cast" reinforcing bars performed better with shotcrete in comparison with cast in-place concrete and that "bottom-cast" reinforcing bars had a better performance with cast in-place concrete in comparison to shotcrete. They attributed the differences to the presence of imperfections and

[8] Including specimens whose bars yielded since the difference of bar stress at bond failure between bars that yield and those that don't, has been found to be only about 2% [ACI 408, 2003].

bleeding resulting from both placement techniques. Indeed, because of the small amount of segregation and bleeding (if any) occurring with shotcrete, "top-cast" reinforcing bars performed better *vis-à-vis* cast in-place concrete even though imperfections were possibly present behind the sprayed rebars. Imperfections, in turn, made "bottom-cast" reinforcing bars in sprayed specimens to underperform *vis-à-vis* cast in-place since bleeding did not occur in this case. If a perfect encapsulation is achieved with both concrete placement methods, the bond strength of "bottom-cast" reinforcing bars is comparable and can even be superior with shotcrete, especially for "top-cast" bars [12, 63]. However, regardless of recent advances on the subject and because the in-place sprayed material is still said to be concrete, it is still stated that the same structural design parameters used with cast in-place concrete should apply to shotcrete. This statement has unfortunately little (if any) scientific validity. In fact, it has already been proven that the behavior between cast in-place concrete and shotcrete is different [7] and thus, the design procedure for shotcrete structures may need to be adapted.

1.4 Finite Element method for bond modeling

1.4.1 Scales of modeling

The use of the Finite Element (FE) method to simulate the interaction between steel and concrete has played a significant role over the past few years. During the late 1960s, various models were created with the intention to interpret and understand the results obtained in the laboratory. Ultimately, the objective was to develop a reliable tool to evaluate existing or new structures (or its components) whose performance was predominantly defined by the interaction between reinforcing bars and concrete. In that regard, the bond mechanism has been studied at three different scales as shown in Figure 1.12 [64].

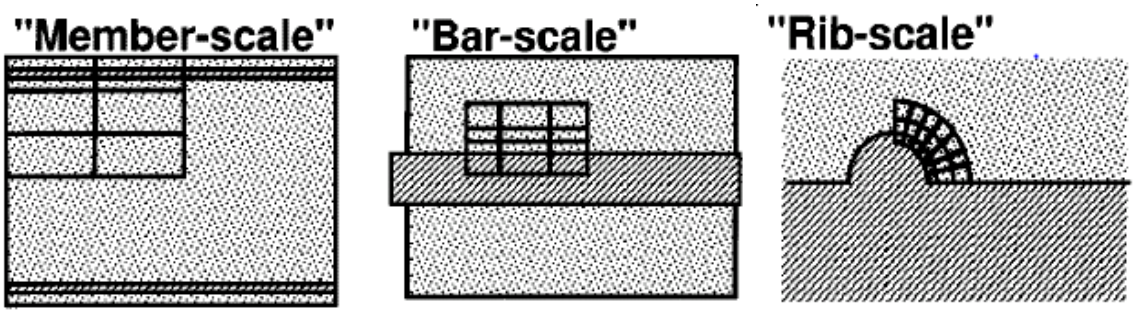

Figure 1.12: Scales used to study of bond between reinforcing bars and concrete [64]

The first models studied bond using a one-dimensional (1D) bond stress-slip law. This approach restrained the models from taking into account a possible *splitting* of concrete as a mode of failure by considering (indirectly) a high level of confinement, i.e. large concrete covers, large numbers of stirrups, etc. This has often been observed when a *member-scale* approach in combination with embedded 1D elements (truss [65] or surfaces [66]) representing the reinforcing bars is used. In these cases, elements are usually linked to the surrounding concrete using springs governed by a 1D linear or non-linear bond stress – slip relationships. If a perfect bond is assumed, the effect of a bar's slip can be indirectly accounted by introducing a softening post-peak branch in the tensional behavior of the concrete. Most of the elements modeled using a *member-scale* approach are too big to idealize the bar-concrete interaction in other ways due to computation constraints. However, when a two- (2D) or a three-dimensional (3D) interface representation between a reinforcing bar and concrete is used, the radial (σ_r) and the hoop (σ_h) stresses (refer to Figure 1.13) can be introduced to allow for a *splitting* failure in addition to a *pull-out* failure.

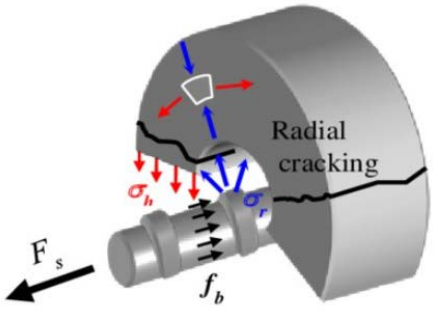

Figure 1.13: Radial or σ_r (blue) and hoop or σ_h (red) stresses as a bar is pulled [67]

The main difference between *bar-* and *rib-scale* models is the fact the latter explicitly models the geometry of the reinforcing bars in an attempt to consider parameters that cannot be taken into account, using other than correlation factors, with *bar-scale* models. In each of those cases, the approach to model the bar-concrete interface has varied widely. Indeed, bond has been idealized using layer, fracture mechanics, damage mechanics, discrete crack, micro-mechanics, inner softening bands, structural [37, 64] and even kinetic models [68]. The modeling techniques associated with each of the aforementioned strategies are extensive and a complete review of all of them is out of the scope of this document. Only research where bond has been studied using a *rib-scale* approach in conjunction with a structural model, where the inclusion of imperfections at the interface might be possible, will be discussed subsequently.

1.4.2 Mathematical and Finite Element models at *rib-scale*

One of the very first *rib-scale* models was developed by Reinhardt et al. [69] using a "slip-layer" between an axially symmetric reinforcing bar and bulk concrete as seen in Figure 1.14a. The "'slip-layer" itself was divided into two zones of different material properties as seen in Figure 1.14b. The zone adjacent to the bar (2.9 mm) possessed material properties characteristic of a mortar and the outer zone (17.1 mm) of either low-strength (f_c = 25.0 MPa) or high-strength (f_c = 50 MPa) concrete. The mortar only differed from the concrete due to a reduced Young's modulus by 60% and 80% in the case of low- and high-strength concrete. The "slip-layer" behaved as a linear-elastic material in both compression and tension before failure. A perfectly plastic and a tensile softening behavior were assigned in compression and tension respectively after failure. The onset of plasticity was defined using a Mohr-Coulomb *yield surface* defined with cohesion (c) values of 7.22 MPa and 14.44 MPa for the low- and the high-strength concrete respectively and an angle of friction (φ) of 15° in both cases. The model did not account for dilatancy (ψ = 0°) as it was argued that volume change would only be noticeable after reaching the ultimate stress. Slip between the reinforcing bar and the mortar was allowed (except in inclined front of the rib) using a friction coefficient of 0.40 and adhesion values of 1.0 and 2.0 MPa for low- and high-strength concrete respectively. The bulk concrete was treated as linear elastic and was represented by a spring. The model was implemented in the general-purpose finite element model DIANA and was compared with the results of "pull-out" tests. The bond behavior, the bar stress versus slip relationship and the onset of cracking were investigated.

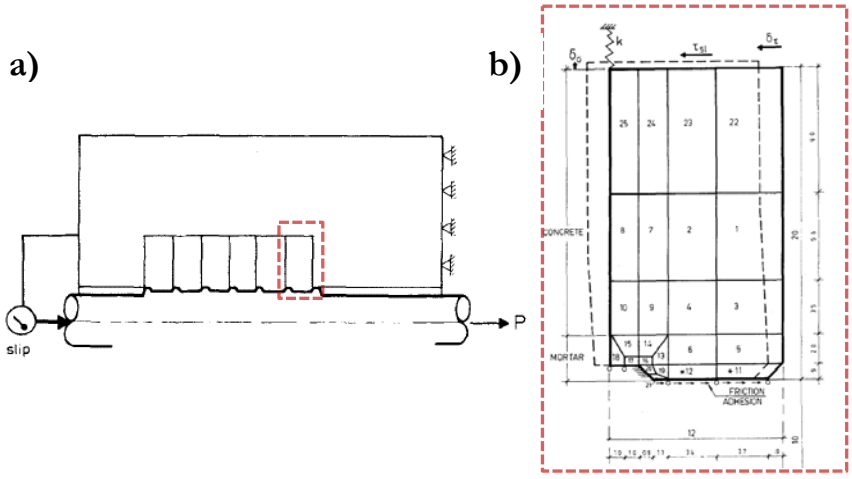

Figure 1.14: (a) Concept and (b) *rib-scale* model (adapted from Reinhardt et al. [69])

Ozbolt et al. [70] modeled a *rib-scale* axisymmetric "pull-out" specimen (Figure 1.15) using a generalized microplane model for concrete to study the behavior of the bar in monotonic and cyclic loading. The model considered concrete tensile cracking and a non-linear triaxial behavior in compression and shear. A 28.0 MPa compressive strength concrete along with other typical properties were used for the analysis. Displacement compatibility between the ribs and the concrete was assumed. Transverse reinforcement was modeled around the reinforcing bar to favor a *pull-out* failure. The results showed that the predicted bar stress at failure agreed well with experimental observations. However, the slip was largely underestimated. It was stated by the authors that this difference could have been corrected, as Reinhardt et al. [69] did, by decreasing the stiffness of the material adjacent to the reinforcing bar using a layer with different material properties.

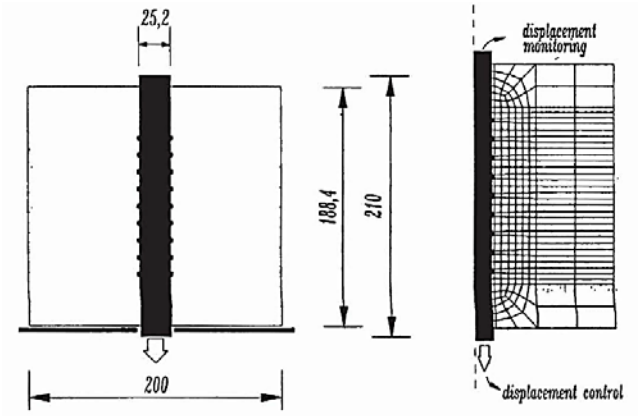

Figure 1.15: (a) Concept and (b) detail FE model of the *rib-scale* model proposed [70]

Brown et al. [41] used a *rib-scale* approach to model a portion of a "beam-end" specimen (refer to Figure 1.16a) and analyzed the effect of the height and angle of the reinforcing bar ribs', concrete cover, lead length[9], bonded length and confinement provided by transverse reinforcement on the bar stress – slip curve. Only one half of the specimen was modeled due to symmetry as seen in Figure 1.16b. Although their model was somewhat simplified as the reinforcing bar has a squared cross-section and ribs were only modeled on their sides, the results showed good agreement with experimental data. Both the concrete and the steel were modeled following a linear – elastic behavior and the plane of symmetry was considered to be the only

[9] The initial part of the test bar at the loaded-end that is prevented to have contact with the concrete to avoid a cone-type failure in the surface of the bond specimen.

possible fracture surface. For this reason, the concrete elements were connected to the nodes belonging to the plane of symmetry using rod elements which followed a Mode I non-linear fracture mechanics approach as the failure criterion. Contact between the bar and the concrete was modeled using special link elements whose behavior followed a Mohr-Coulomb surface failure criterion; the cohesion (c) value was set to 1.72 MPa and the friction coefficient (μ) to 0.3. Tholen et al. [71], also used this approach to study different concrete, steel and interface properties on the bond strength of reinforcing bars.

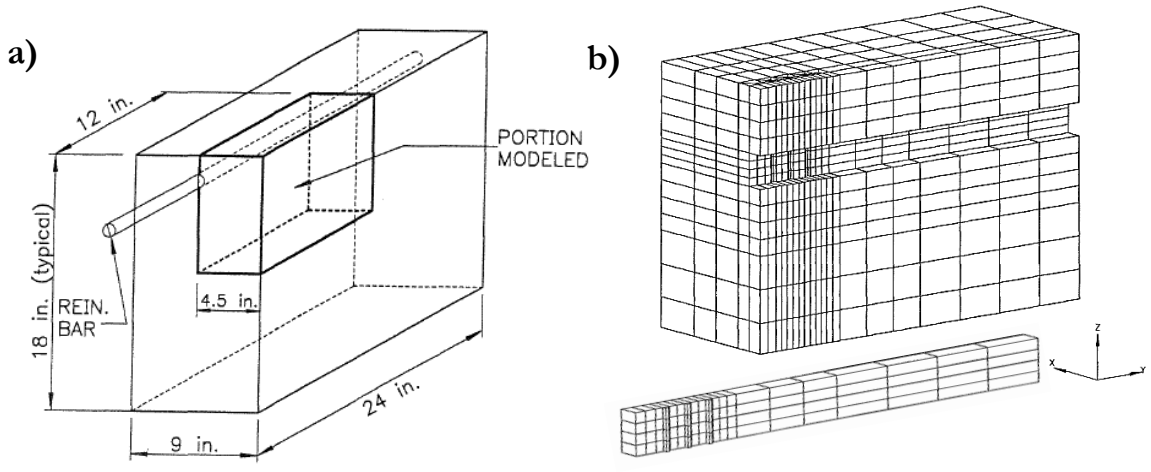

Figure 1.16: (a) "Beam-end" specimen and (b) discretization into FE of one part of it (adapted from Brown et al. [72])

Salem et al. [73] studied the pre- and post-yield bond behavior of a reinforcing bar in an axisymmetric "pull-out" specimen as seen in Figure 1.17a. The behaviour of steel and concrete was simulated using an elastoplastic Von Mises model with kinematic hardening and a fracture energy-based non-linear constitutive model respectively. Normal concrete and self-compacting concrete (SCC) were studied. The concrete around the reinforcing bar was divided in two zones: a "confined layer" which extended to $0.2d_b$ and a "soft layer" which extended to $1.0d_b$. For the normal concrete, the compressive strength of the "confined layer" was doubled and the stiffness of the "soft layer" was reduced by half in comparison to the bulk concrete. It is discussed that this assumption is made to take into account the porous zone close to the reinforcing bars due to higher *w/b* ratios in those areas caused by concrete settlement and bleeding. In the case of SCC, no "soft layer" was considered due to the usually low *w/b* ratios used in such type of concrete. To connect the steel and the concrete in the model, a joint element with an open-

closure (normal and shear) behavior was assumed. Its behavior was assumed as linear-elastic with a higher stiffness in the case of a closure in comparison with an opening as observed in Figure 1.17b. It was found that the opening-closure parameters have no significant effect of the results as long as the normal closure stiffness is very high. The results of the model agreed well with experimental results and emphasized the need to consider a "confined" and "soft layer" depending on the type of concrete under study.

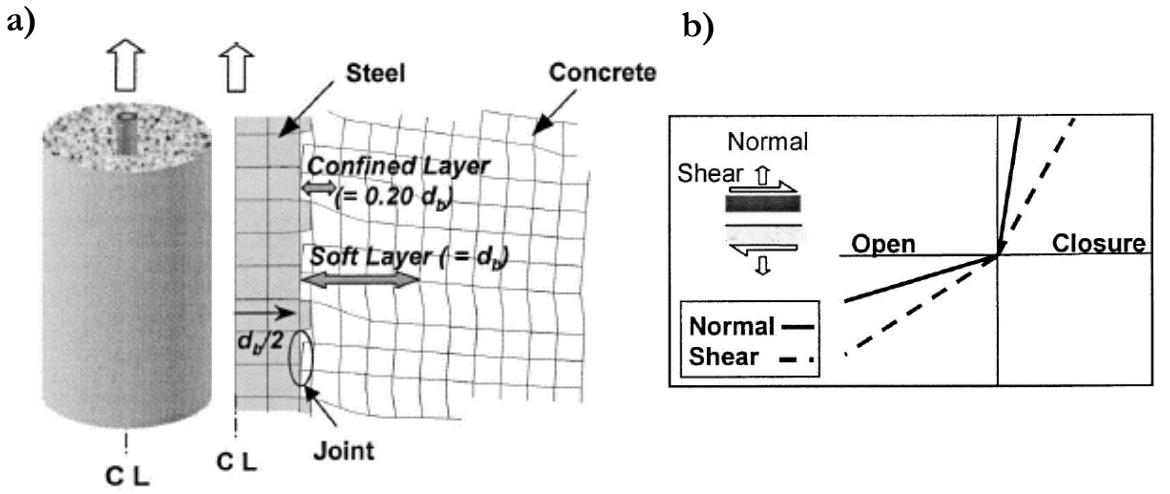

Figure 1.17: (a) FE model and (b) interface behavior (adapted from Salem et al. [73])

Lagier et al. [74] investigated the bond behavior of lap-splices in Ultra-High-Performance Fiber-Reinforced Concrete (UHPFRC) as shown in Figure 1.18a. The concrete was simulated using an orthotropic hypoelastic model based on a strain-rotating smeared crack approach. The model accounts for strain hardening before the peak load with three main phases (elastic behavior of the paste, microcracking associated with fiber activation and stable fine crack growth) and a stress softening behavior defined by the opening of macro cracks. The bond between the reinforcing bar and the concrete was set as a zero-thickness bond layer governed by a Mohr-Coulomb failure surface as seen in Figure 1.18b which allowed separation. During a contact/slip state, a friction model with a coefficient of 0.6 was used. At a contact/adhesion state, a normal and a shear behavior was defined with linear relationships. The ultimate normal resistance was set as 2.0 MPa whereas the ultimate shear resistance was set as 1.2 MPa in the two directions of the plane parallel to the reinforcing bar. In the same way as Salem et al. [73], the stiffness of the

normal behavior is considerably higher than the one at shear. Moreover, it was argued that a "slip-layer" was not needed as UHPFRC has a low *w/b* ratio and presents little (if any) bleeding.

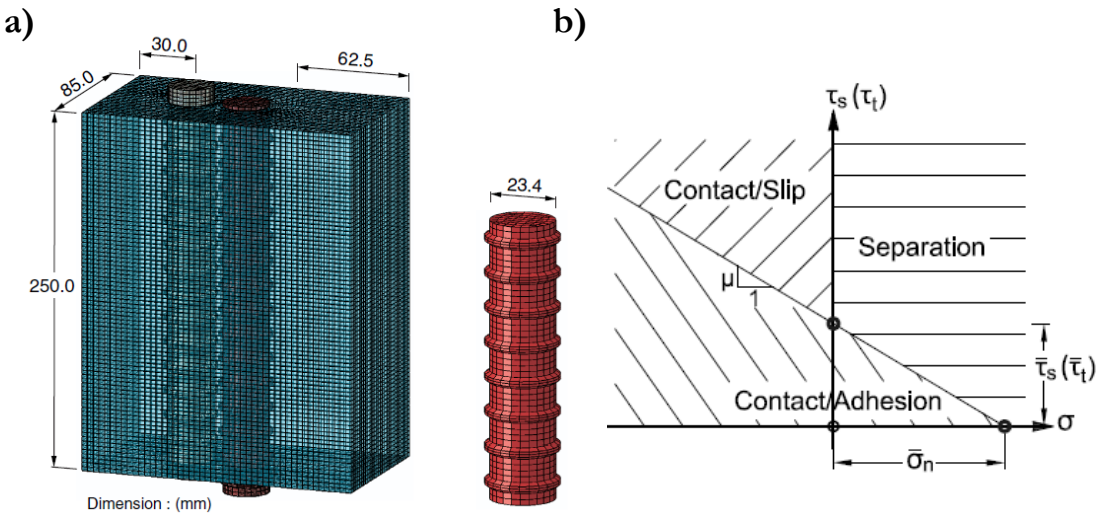

Figure 1.18: (a) Lap-splice FE model and (b) interface model (adapted from Lagier et al. [74]).

Bandelt et al. [75] used a *rib-scale* model to study the bond behavior of "beam-end" specimens under monotonic and cyclic loading using DIANA. The concrete was given a fracture energy-based plasticity constitutive model in compression and a total strain-based fixed crack model in tension. A uniaxial parabolic-softening behavior was used in compression whereas a linear tensile stress-strain hardening and softening behavior were assumed in tension. Three different concrete properties around the reinforcing bar were investigated due to the most-likely non-homogeneous properties in comparison with the bulk concrete. The first case was a zone with the same properties as the bulk concrete. In the second case, a mortar with voids was assumed and for this purpose, empirical relationships between compressive strength and the concrete's Young modulus were used to determine a certain level of porosity. Finally, a 50% reduction in the strength properties was assumed. The thickness of the interface varied in between 0 and 3 mm depending on the type of the interface or loading that was studied. Zero-thickness interface elements were used to allow a small amount of bond strength (attributed to friction) transfer between the reinforcing bar and the concrete. It was found that the model agreed well with the experimental results when a 2 mm mortar with void interface zone was used.

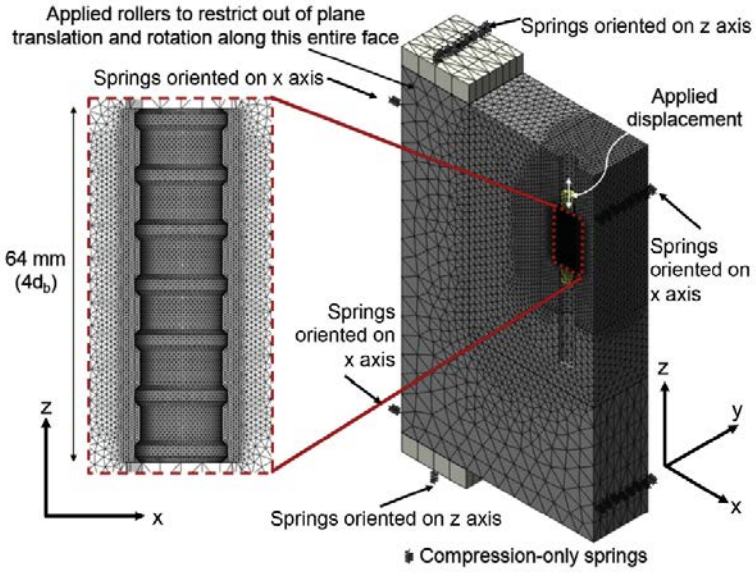

Figure 1.19: FE model of the "beam-end" specimen (Bandelt et al. [75]

1.5 The ACI *development length* equation

Up until 1971, the American Concrete Institute committee 318 – Structural Concrete Building Code treated the anchorage and splice requirements for reinforcing bars in tension in terms of bond stresses. The bond stress of a reinforcing bar to obtain a *splitting* failure was computed as $u = 9.5\sqrt{f'_c}/d_b$ in psi but less or equal to 800 psi because at that stress a *pull-out* failure would most likely occur. However, for practical reasons these requirements were set in terms of the *development length* (ℓ_d) of the reinforcing bars later that year by assuming a uniform bond stress distribution along the bar length as shown in Equation 1.2.

$$T_s = A_b f_s = u\pi \ell_d d_b \rightarrow \ell_d = d_b f_s / 4u \tag{1.2}$$

To do so, the computed bond stress (u) was introduced into Equation 1.2 and the bar stress (f_s) was replaced by $1.25f_y$ (to ensure a ductile failure) resulting in Equation 1.3 (expressed in U.S. customary units) which in turn requires a longer *development length* (ℓ_d).

$$\ell_d = 0.04A_b f_y / \sqrt{f'_c} \tag{1.3}$$

In the same way, the minimum *development length* was established by replacing the bond stress in Equation 1.2 with u = 800 psi and thus setting Equation 1.3 to a minimum of $\ell_d \geq 0.0004 d_b f_y$

(U.S. customary units). This is because bond stresses resulting from *pull-out* failures are greater than those resulting from *splitting* failures (due to the presence of a larger concrete cover or greater amounts of transverse reinforcement) and as a result they occur with smaller *development length*s. Consequently, by setting the minimal *development length* in regard to a *pull-out* failure, the yielding stress of the bar would be guaranteed.

However, Equation 1.3 was still based on ultimate bond stresses and for that reason an extensive revision was done in order to introduce a more realistic equation based on the analysis of experimental data [76, 77]. For this purpose, the rebar stress (f_s) developed in the spliced region of 62 "beam-splice" specimens without transverse reinforcement (refer to Figure 1.20a) and 27 of them with transverse reinforcement were used. The reinforcing bar stress in 27 "development length" specimens as shown in Figure 1.20b were also used.

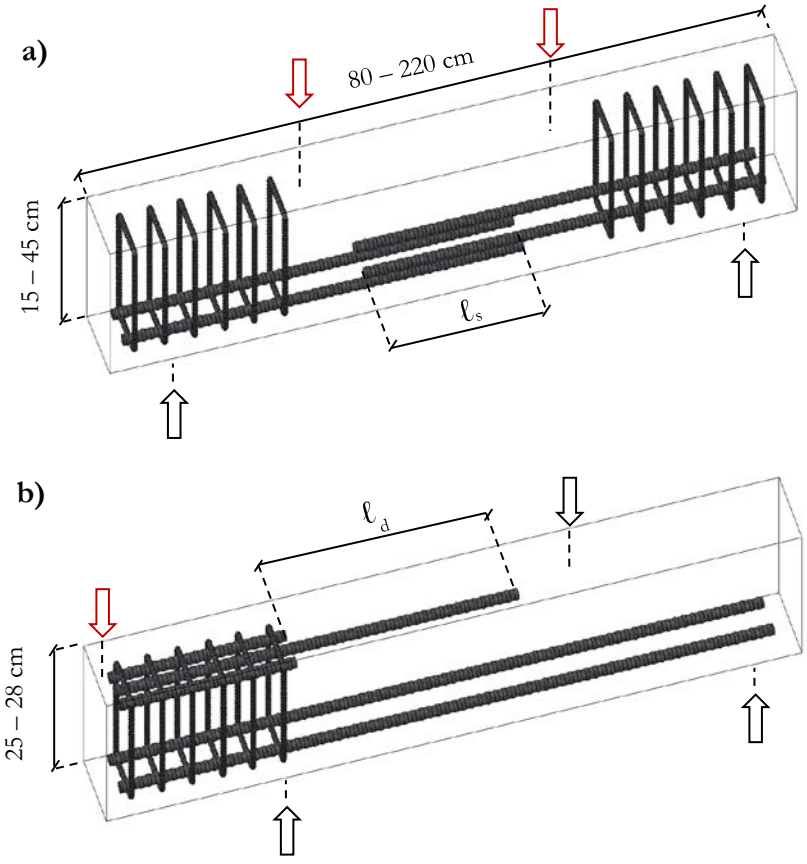

Figure 1.20: (a) "Beam-splice" and (b) a "development length" specimen (adapted from [42])

In order to develop a prediction equation of the bond stress in reinforcing bars with no transverse reinforcement, Equation 1.4 was fitted to the results of the first 62 "beam-splice" specimens. A non-linear regression analysis was used to find the coefficients b_1, b_2 and b_3 which resulted to be 1.2, 3 and 50 respectively. In Equation 1.4, u_c represents the bond stress developed in the spliced rebar due to the contribution of concrete, f_c represents the compressive strength of concrete, c_b represents the smaller of either the distance from the reinforcing bar to the outer face of the concrete member or half the distance between two reinforcing bars being spliced, d_b represents the diameter of the reinforcing bar being spliced, and ℓ_s represents the splice length.

$$\frac{u_c}{\sqrt{f_c}} = b_1 + b_2 \frac{c_b}{d_b} + b_3 \frac{d_b}{\ell_s} \tag{1.4}$$

Since the total bond stress (u_t) can be considered to be the sum of the bond contributed by concrete (u_c as per Equation 1.4) and that of the transverse reinforcement (u_{tr}), Equation 1.5 (expressed in U.S. customary units) was fitted using a linear regression analysis with the results of the "beam-splice" and "development length" specimens containing transverse reinforcement; the coefficient b_1 was found to be 1/500. In Equation 1.5, A_{tr} represents the area of the transverse reinforcement within the failure plane, f_{yt} represents the yielding stress of the transverse reinforcement and s represents the spacing between them.

$$u_t = u_c + u_{tr} = u_c + b_1 \left(\frac{A_{tr} f_{yt}}{s\, d_b} \right) \sqrt{f'_c} \tag{1.5}$$

Furthermore, the total bond stress (u_t) was substituted by the theoretical uniform stress developed along a rebar ($u = f_s d_b / 4\ell_d$). The splice length (ℓ_s) was replaced by the *development length* (ℓ_d) because it was observed that the mode of failure encountered in the "beam-splice" specimens was the same as the one observed with "development length" specimens. A comparison between the predicted values of bond stresses using Equation 1.4 and the calculated bond stresses of "development length" specimens presented by Ferguson and Thompson [78, 79] and Chamberlin [80] proved to be adequate. A visual representation of a "development length" specimen tested by the latter researcher is shown in Figure 1.21.

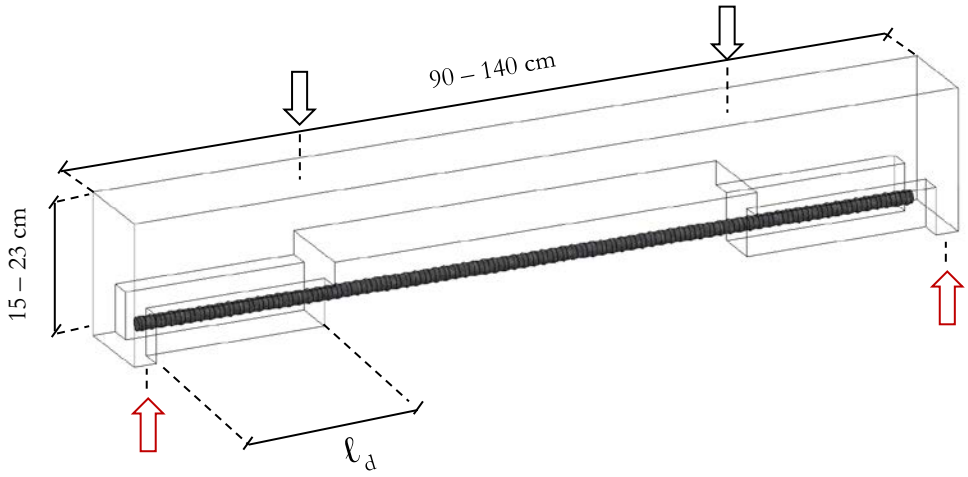

Figure 1.21: "Development length" specimen as tested by Chamberlin [80]

Finally, by adding Equation 1.4 to 1.5, replacing the total bond stress (u_t) by the theoretical uniform stress (u) and solving for ℓ_d, Equation 1.6 (expressed in U.S. customary units) was proposed as a way to calculate the *development length* (ℓ_d) of reinforcing bars in tension.

$$\ell_d = \frac{d_b\left(\frac{f_s}{4\sqrt{f'_c}} - 50\right)}{\left(1.2+3\frac{c_b}{d_b}+\frac{A_{tr}f_{yt}}{500\ s\ d_b}\right)} \tag{1.6}$$

The ACI 318 Structural Concrete Building Code committee then slightly modified Equation 1.6 [76] as expressed in Equation 1.7a and 1.7b (expressed in U.S. customary units) which appeared for the first time in the ACI 318-95 [81] design code.

$$\frac{\ell_d}{d_b} = \frac{3}{40}\frac{f_y}{\sqrt{f'_c}}\frac{\alpha\beta\gamma\lambda}{\left(\frac{c_b+K_{tr}}{d_b}\right)} \tag{1.7a}$$

$$K_{tr} = \frac{A_{tr}f_{yt}}{1500sn} \tag{1.7b}$$

As can be seen, the developed bar was limited to its yielding stress (f_y). Moreover, the transverse reinforcement contribution was grouped in the term K_{tr} where the number of bars being spliced or developed in the plane of splitting (n) were accounted for. Additionally, it was decided to limit

the term $(c_b+K_{tr})/d_b$ to a value of 2.5 or less in order to reduce the possibility of a *pull-out* failure. This is because Equation 1.6 was developed considering only specimens which had failed by *splitting*. The correction factors, α, β, γ and λ were included to account for the casting position, the coating material and the size of the developed reinforcing bars as well as for the use of lightweight concrete respectively. These factors will be discussed in detail in Section 1.6.

The current *development length* (ℓ_d) equation appearing in the ACI 318-19 [5] edition of the design code has been slightly modified since then as shown in Equation 1.8 (expressed in U.S. customary units). The lightweight concrete modification factor went from the numerator to the denominator and next to the square root of the compressive strength of the concrete term which is directly affected by it (as elsewhere in the code). The yielding stress for the transverse reinforcement (f_{yt}) was removed from the K_{tr} term because tests demonstrated that stirrups rarely yielded during bond tests. As a consequence, the constant multiplying this term changed from 1/1500 to 40 (considering the nominal yield strength of grade 60 reinforcing bars is 60,000 psi / 1500 = 40).

$$\ell_d = \frac{3}{40}\frac{f_y}{\lambda\sqrt{f'_c}}\frac{\Psi_t\Psi_e\Psi_s\Psi_g}{\left(\frac{C_b+K_{tr}}{d_b}\right)}d_b \; ; \; K_{tr}=\frac{40A_{tr}}{sn} \tag{1.8}$$

The parameters Ψ_t, Ψ_e, Ψ_s and Ψ_g represent the modification factors linked to the casting position, the coating material, the size and the grade of the developed bar. The latter has been added to the ACI 318-19 version of the code and did not appear in the ACI 318-14 [82] version. A summary of the current equation, as found in both the ACI 318-19 [5] design code and its Canadian equivalent (CSA A23.3-19 [6]) and including all of their constraints are shown in Table 1.1 in SI units. The equivalencies between both equations are demonstrated in Appendix B and the only difference resides now on the fact that the Canadian A23.3-19 version of the code does not account for the grade of the developed reinforcing bar.

Table 1.1: *Development length* equations of ACI and CSA design codes (SI units)

ACI 318M-19	CSA A23.3-19
$\ell_d = \dfrac{f_y}{1.1\lambda\sqrt{f'_c}} \dfrac{\Psi_t\Psi_e\Psi_s\Psi_g}{\left(\dfrac{c_b+K_{tr}}{d_b}\right)} d_b$	$\ell_d = 1.15 \dfrac{k_1k_2k_3k_4}{(d_{cs}+K_{tr})} \dfrac{f_y}{\sqrt{f'_c}} A_b$
Where: $K_{tr} = \dfrac{40A_{tr}}{sn}$	Where: $K_{tr} = \dfrac{A_{tr}f_{yt}}{10.5sn}$
Ψ_t = 1.3 when concrete below bar is 300 mm or more. 1.0 other cases	k_1 = 1.3 when concrete below bar is 300 mm or more. 1.0 other cases
Ψ_e = 1.5 when coated bars having a cover less than $3d_b$ or clear spacing less than $6d_b$ 1.2 other cases 1.0 uncoated and galvanized bars	k_2 = 1.5 when coated bars having a cover less than $3d_b$ or clear spacing less tan $6d_b$ 1.2 other cases 1.0 uncoated bars
λ = 0.75 for lightweight concrete $f_{ct}/0.56\sqrt{f_{cm}} \leq 1.0$, where f_{ct} is the average splitting tensile strength and f_{cm} the average compressive strength 1.0 for normal weight concrete	k_3 = 1.3 for structural low-density concrete 1.2 for structural semi-low-density concrete 1.0 for normal-density concrete
Ψ_s = 0.8 for No. 19 and smaller bars 1.0 for No. 22 and larger bars	k_4 = 0.8 for 20M and smaller bars 1.0 for 25M and larger bars
Ψ_g = 1.0 for Grade 40 or 60 1.15 for Grade 80 1.3 for Grade 100	
Constraints:	Constraints:
$\ell_d \geq 300$ mm	$\ell_d \geq 300$ mm
$\Psi_t\Psi_e \leq 1.7$	$K_1K_2 \leq 1.7$
$\left(\dfrac{C_b+K_{tr}}{d_b}\right) \leq 2.5$	$(d_{cs}+K_{tr}) \leq 2.5d_b$

1.6 Development of correction factors

1.6.1 The bar location factor

The bar location factor (Ψ_t) was first considered in the ACI 318-51 design code based on work done by Clark [83] where the bond stress of "bottom-cast" bars was compared to the one obtained with "top-cast" bars using "pull-out" specimens. The stress of "top-cast" bars, defined as bars having more than 300 mm of concrete below them, was found to be about 33% less than the one obtained with "bottom-cast" bars. Therefore, ACI committee 318 established the allowable stress of "top-cast" bars as 0.7 times the stress of bottom-cast bars. Thereafter, the ACI 318-71 issue of the code changed the bond stress calculation in terms of the *development length* (ℓ_d) and the modification factor for "top-cast" reinforcing bars became $1/0.7 \approx 1.4$.

In parallel, Jirsa and Breen [84] proposed a bar location factor varying from 1.0 to 2.2 based on the bond strength comparison of "bottom-cast" bars against "top-cast" bars having up to 1 775 mm of concrete below them and using two different concrete slumps. Moreover, Jeanty et al. [85] recommended a bar location factor of 1.22 based on the ratio of the reinforcing bar embedment length needed for "bottom-cast" bars to yield with respect to "top-cast" bars using 455 mm high "beam-splice" specimens.

Finally, ACI committee 318 decided to adopt the use of a 1.3 bar location factor for spliced or developed bars having more than 300 mm of concrete below them and a factor of 1.0 in all other cases. This specification first appeared in ACI 318-89 and since then, it has not been changed.

1.6.2 The bar coating factor

The bar coating factor (Ψ_e) first appeared in ACI 318-89 with values ranging from 1.0 to 1.5 depending on the coating material and the concrete cover (see Table 1.1) and it has not been changed since then. It was determined based on research done by Johnston and Zia [38] and Treece et al. [40].

In the first study, a factor of 1.15 was proposed by comparing "beam-end" specimens based on slip and bond strength criteria. Slip criteria was divided in two categories: the bond stresses corresponding to a slip of 0.254 mm (0.01 in.) when measured at the loaded end of the specimen and the ones corresponding to a slip of 0.051 mm (0.002 in.) when measured at their un-loaded end. In both cases, the ratio between stresses corresponding to mill scale and epoxy coated

reinforcing bars were computed. The bond strength criteria was defined in a similar way except that it was the bar strength at failure of specimens presenting a *pull-out* failure that was used. The only specimens considered were those having bonded lengths of 300 mm (12 in.) and longer, even though specimens with smaller bonded lengths were tested; the minimum *development length* of 12 in. (300 mm) specified in the ACI 318 design code was the basis for this decision.

The second study recommended a factor of 1.5 based on a similar analysis using "beam-splice" specimens. Their research indicated a bond strength at failure reduction of 33% between specimens with epoxy coated and uncoated reinforcing bars, i.e., a bond strength ratio of 0.67 was found. Based on this, a modification factor of 1 / 0.67 ≈ 1.5 was recommended. Because the specimens presented a relatively small concrete cover, they recommended the use of this value for members having less than $3d_b$ of concrete cover or $6d_b$ of clear spacing between two spliced reinforcing bars where a *splitting* failure is likely to occur. For larger concrete covers or bar spacings, they recommended the use of the 1.15 as suggested by Johnston and Zia [38].

Nonetheless, recent studies [39, 86] containing larger quantities of experimental data do not entirely agree with the specific factors selected by the ACI committee 318 and argue that they can be reduced.

1.6.3 The bar size factor

The bar size modification factor (Ψ_s) is the result of many "beam-splice" and "development length" bond test comparisons (around 635) performed over the past years documented by ACI committee 408 [87]. Based on this database, ACI committee 318 justified a reduction of the *development length* by 20% when using 20M (No. 19) and smaller reinforcing bars. Thus, they suggested the use of a 0.8 modification factor in such cases and a factor of 1.0 for larger reinforcing bars. However, it has been pointed out by ACI committee 408 that by the time the comparisons were made, the database only contained bond specimens with small size bars and *development length*s shorter than 12 in. (300 mm). Thus, ACI committee 408 does not recommend the use of a 0.8 factor [87].

1.6.4 The reinforcement grade factor

The reinforcement grade factor (Ψ_g) was reintroduced in the ACI 318-19 [5] design code and accounts for the effect of reinforcing yield strength on the required *development length* as

research has shown that the required *development length* increases disproportionately with an increase of the yield strength [77, 88]. Up until the ACI 318-89 version of the code, this effect was considered computing $\Psi_g = 2.0 - 60{,}000/f_y$ but it disappeared in the ACI 318-95 [81] version of the code. In the current version of the code [5], a similar approach has been adopted using slightly more forgiving values by substituting the 2.0 value by 1.9 in the previous equation.

1.7 Conclusion

As it was portrayed in this chapter, the bond between steel and concrete is a complex (progressive) phenomenon which involves many parameters. Some of these, like sprayed concrete as a method of concrete placement, are not accounted in the *development length* of reinforcing bars in tension equation (ℓ_d) of North American codes. This is because sprayed concrete presents various placement challenges and many of the parameters that need to be considered for its proper placement differ than those usually considered in regular cast in-place concrete. One of the biggest challenges concerns the possible creation of voids behind reinforcing bars while concrete is being sprayed and how these voids impact the bond performance of reinforcing bars.

However, this chapter has pointed out a current lack of knowledge and measures taken on both design codes and inspection guidelines when voids, specifically created behind reinforcing bars, cause a bar stress reduction. In fact, the use of existing guidelines for shotcrete structures resides in the fact that there is an incomplete comprehension of the subject and thus a comprehensive research on this matter is urgently needed. The effect of different void sizes and concrete covers on bond need to be further investigated to determine their impact on the failure mode of structural elements and the stress behavior of their reinforcing bars. The extensive shotcrete knowledge that has been developed internationally throughout the past years and numerical tools such as the Finite Element method in combination with different analytical tools represent the key to attain the objectives of this research and develop design guidelines in the form of modification factors to be used with the *development length* (ℓ_d) equation for reinforcing bars in tension.

Chapter 2 Methods

2.1 Introduction

To attain the objectives of this research, two types of bond specimens were tested. Initially, *dry-mix* "pull-out" specimens were built to investigate the relationship between the bond performance of a reinforcing bar *vis-à-vis*, among others, its encapsulation quality and the *consistency* of the mixture. However, a well-distributed range of voids was difficult to obtain in the laboratory so cast in-place "pull-out" specimens, in which voids were simulated with different sizes of *artificial voids* (silicone inserts), were tested. The advantages and drawbacks of this strategy as a way to recreate shotcrete specimens with varying encapsulation qualities were determined by statistically comparing the results obtained with both methods of concrete placement. Subsequently, only cast in-place ASTM A944-10 "beam-end" specimens were tested. Although it would have been ideal to spray this type of specimen, problems related to rebound, surface finishing, voids behind secondary reinforcement and testing difficulties were encountered during initial trials. The ASTM A944-10 "beam-end" specimen was also modeled using a commercial Finite Element (FE) package (Abaqus 6.14) to study parameters like the concrete cover and different sizes of voids in conjunction with a longer bonded length.

2.2 "Pull-out" specimens

2.2.1 Overview

"Pull-out" specimens are still the most common bond specimen used to study the bond strength between reinforcing bars and concrete. They are usually preferred over other types of specimens due to their construction, handling and testing easiness. Nonetheless, as the stress field developed during the test around the reinforcing bar differs from most situations encountered in practice where the concrete around the bars is placed in tension, these bond specimens are used mostly for comparative purposes. Indeed, while the bar is being pulled, radially distributed compressive struts as depicted in Figure 2.1 are developed and the concrete prevents the bar from slipping more strenuously than it would occur in typical flexural reinforced concrete members or other anchorages where the reaction plate (if any) is located at some distance away from the reinforcing bar.

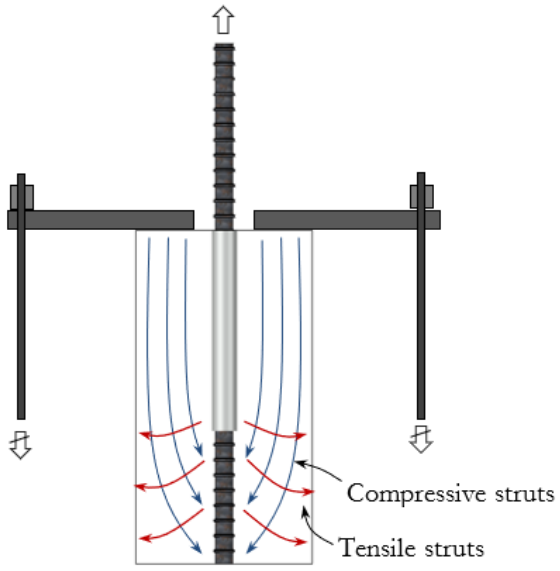

Figure 2.1: Stress distribution in a "pull-out" specimen

Consequently, the bar stress at bond failure obtained will be greater than most types of bond specimens with the same bonded length, concrete cover and the mechanical properties of the concrete and the reinforcing bar [42, 89]; the reinforcing bar could even attain its yield limit. In this research, this type of specimen has been used to compare the bond performance of reinforcing bars with different qualities of encapsulation with the intention to determine which variables are the most important to consider and use them posteriorly with the "beam-end" specimens.

2.2.2 Construction and geometry of specimens

Shotcrete specimens were built by spraying a pre-bagged mixture onto 450 x 680 x 150 mm square wooden molds using the *dry-mix* process as shown in Figure 2.2. The spraying operations took place in the spraying chamber of the Université Laval. The *dry-mix* process was used to allow the nozzlemen change the water flow at the nozzle, and consequently the *consistency* of the mixture, to intentionally produce a wide range of void sizes behind the reinforcing bars. An ALIVA 246.5 spraying machine with the water ring installed 2.2 meters upstream from a "double-bubble" nozzle was used with a 38 mm internal diameter hose. Each mold contained three 150 x 285 x 150 mm prism-shaped specimens with a single reinforcing bar concentric with their longitudinal axis. As the ASTM standard [90] regulating their construction was withdrawn, the size of the specimens was chosen based on similar studies [12, 62]. All reinforcing bars were

positioned so their longitudinal ribs were oriented facing the sides of the molds. The initial length of the bar at the loaded end of the specimen (referred to as lead length) was protected with a PVC sleeve to control the portion of the bar in contact with the concrete (referred to as bonded length). The top end of the sleeve was glued to the mold using hot glue and its bottom end was sealed with duct tape to prevent mortar or rebound seepage. The bonded length was set to $2.5d_b$ to avoid the bar from yielding. Before spraying the concrete, the molds were oiled with special care to avoid contaminating the surface of the bars.

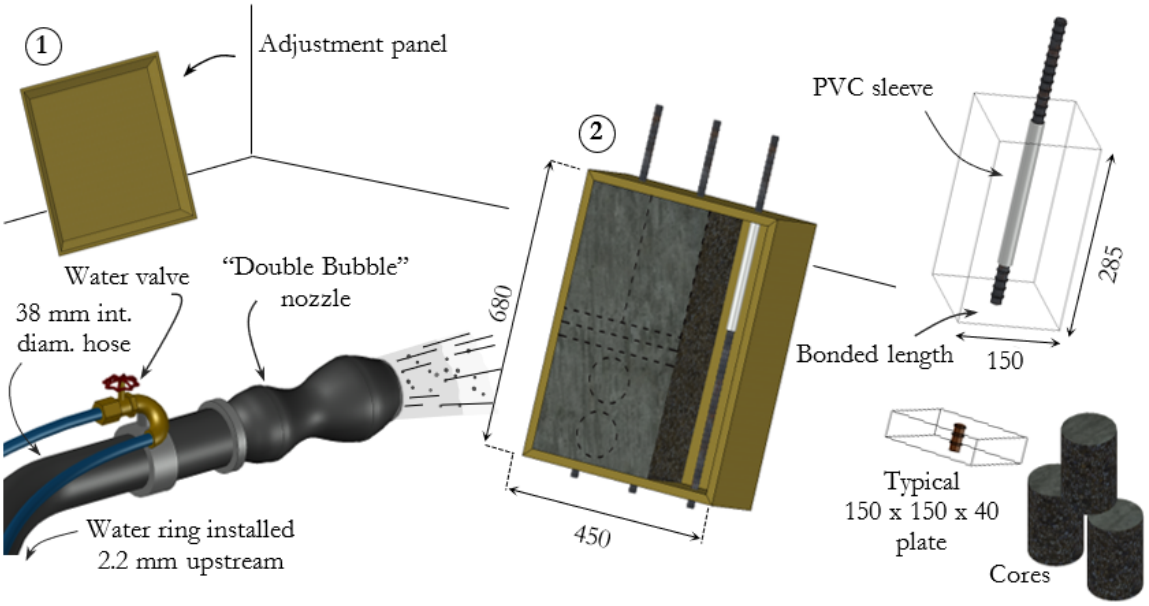

Figure 2.2: Representation of the spraying operations

The beginning of the spraying operations started when the machine operator released the flow of compressed air. The nozzleman then indicated to the machine operator to increase or decrease the airflow. Once the adequate air velocity was established, the nozzleman opened the water valve and indicated to the machine operator to release the flow of the dry mixture. Subsequently, the nozzlemen adjusted the water content while spraying into the wooden panels (number 1 in Figure 2.2) and once the desired *consistency* was visually obtained, the concrete was sprayed into the "pull-out" molds (number 2 in Figure 2.2). The bottom corners were first sprayed (refer to Figure 2.3) and then, by constantly making small circular movements with the nozzle, the mold was filled towards the top. The overall shotcrete placement procedure followed the recommendations stated in the CCS-4(08) "Shotcrete for the craftsman" document [91].

Figure 2.3: Molds containing the "pull-out" specimens

Once the molds were filled, the excess concrete was cut off with a metal trowel and the molds were covered with a plywood board (to avoid overspray) and a plastic membrane (without touching the fresh concrete) to limit water evaporation until the initial set of the concrete. Thereafter, wet burlap was placed over the plywood board and under the plastic membrane until the next day, when the blocks were demolded. Curing with the wet burlap continued subsequently for one week. The blocks were then wet cut to obtain the "pull-out" specimens (refer to the dotted lines of the mold in Figure 2.2). In addition, two 40 mm plates were cut beneath the "pull-out" specimens (refer to Figure 2.2) so the size of the voids (if any) could be measured at five locations (two for each plate and 1 beneath the specimen). The aforementioned sequence was repeated by two nozzlemen who sprayed three molds each using different mixture *consistencies*; from "wettest" to "driest". The air flow speed chosen by each nozzlemen was not modified in between *consistencies* and a proper shooting technique was always sought. The first nozzleman (referred to as nozzleman N1 in Chapter 3) had a considerable amount of experience in the laboratory whilst the other one (referred to as nozzleman N2 in Chapter 3) had no previous experience. Three "pull-out" specimens were created for each of the *consistencies* chosen by each nozzleman.

The cast in-place specimens had the same dimensions as the sprayed specimens but a constant w/b ratio of 0.45 was chosen to avoid as much as possible bleeding as there is no evidence of

this phenomenon with shotcrete. In order to make the mixture workable, a slight amount of a polycarboxylate-based multi-range water reducer was added. The fresh concrete was consolidated in accordance to ASTM C192/C192M-16a [92]. The *artificial* voids, whenever used, were placed directly over the reinforcing bars as described in detail in Section 2.2.3. The concrete was screeded with a metal trowel and was then protected from evaporation, demolded, cured and cut in the same way as shotcrete specimens. In this case, only two specimens were built for each parameter studied.

2.2.3 *Artificial voids*

The *artificial voids* were made of silicone and were only used in combination with cast in-place specimens. To build them, a silicone gasket maker was inserted into hollow plastic tubes and once it had cured, the hardened silicone was extracted from the plastic tubes (as they only acted as molds) and was cut longitudinally in two halves. The resulting pieces were then glued over the bonded length of reinforcing bars using the same material. To ensure no silicone was deposited elsewhere over the surface of the reinforcing bars, the position of the voids was delimited with masking tape which was removed once the *artificial voids* were securely glued in place. A detailed description of this process is presented in Appendix C. Voids of nominal transversal lengths of 10, 20 and 30% were created and are referred to as *unbonded* perimeters in subsequent chapters (see Figure 2.4). These values were chosen based on the ACI committee 506 visual shotcrete core quality evaluation technote [16] and are expressed as a percentage of the nominal perimeter of the bars.

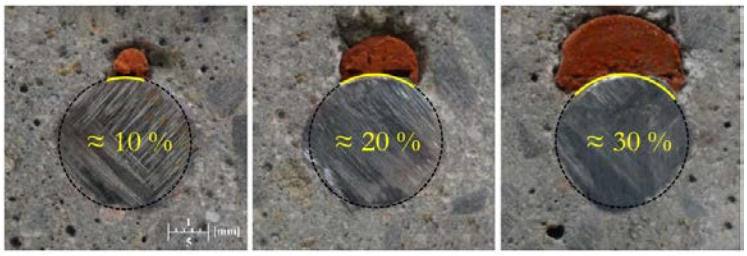

Figure 2.4: Tested *un-bonded* perimeters

The *un-bonded* perimeters were precisely measured at the bottom of the specimens (and on the 40 mm plates for shotcrete specimens) using high-quality photographs in combination with a Computer Aided Design (CAD) software. The measurements were performed by placing a circle over the image (dotted line in Figure 2.4) of equal nominal perimeter as the one of the bar and

then by measuring the length of the arc in contact with the void (solid line in Figure 2.4). Additional *artificial voids* with constant *un-bonded* perimeter and twice the initial height were also built by placing two cut silicone halves on top of each other as seen in Figure 2.5.

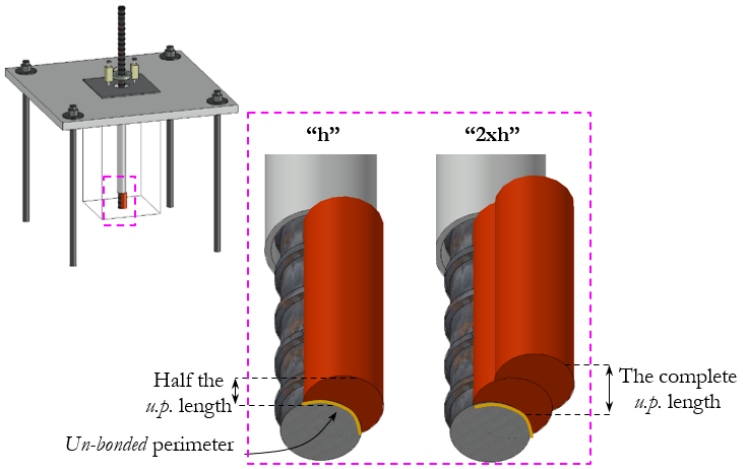

Figure 2.5: Different heights of the *artificial voids*

2.2.4 Concrete properties

After the molds were filled with shotcrete, concrete was sprayed onto a vertical steel panel pin-connected to the wall of the spraying chamber (number 3 in Figure 2.6) and instrumented with a load cell to calculate the amount of rebound as expressed in Equation 2.1.

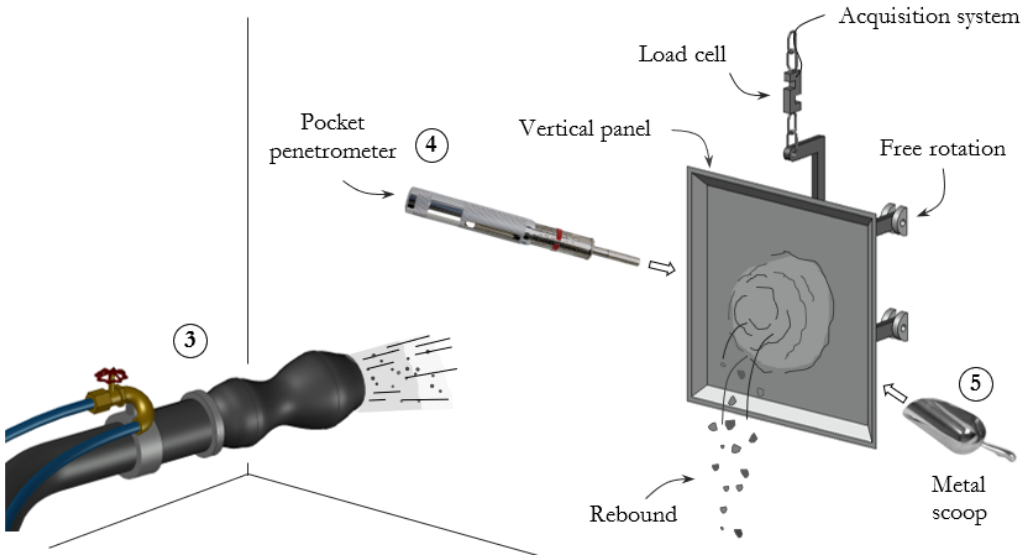

Figure 2.6: Spraying operations on the vertical panel

On one hand, the mass of the mixture sticking to the panel per unit of time ($\dot{w}_{panel}$) was measured by a load cell supporting the vertical panel. On the other hand, the total weight of the mixture and water used per unit of time ($\dot{w}_{machine}$ and $\dot{w}_{water}$) were recorded as the spraying machine laid permanently on a scale and a flowmeter was used in the water line. A detailed explanation on how rebound is measured is presented by Jolin [18].

$$\text{Rebound} = 1 - \left(\frac{\dot{w}_{panel}}{\dot{w}_{machine} + \dot{w}_{water}} \right) \tag{2.1}$$

Also, the *consistency* of the mixture was measured with a pocket penetrometer right after the concrete was sprayed on the vertical panel (number 4 in Figure 2.6). Ten effective measurements were taken; the ones in which the tip of the penetrometer intercepted a coarse aggregate were discarded and were taken again. Thereafter, two samples of approximately 1.5 kg were taken from the vertical panel to calculate the water and the binder content of the in-place mixture (number 5 in Figure 2.6). The available water for the hydration of the cement was calculated by determining the weight evaporated from one of the samples after several cycles of drying using a microwave oven [93, 94]. The binder content was calculated assuming it was composed of particles finer than 75 μm and by determining their weight when the sample was washed over a No. 200 sieve [95]. The fraction between both values was considered as the in-place *w/b* ratio of the mixture. The complete procedure is detailed in Appendix D.

For the cast in-place specimens, the slump and the air content were measured following the ASTM C143/C143M-20 [22] and C231/C231M-17 [96] standards. As it was done for the shotcrete specimens, the remaining concrete in the molds was used to extract cores [97] for the boiled absorption and permeable voids volume and the compressive strength of the concrete in accordance to the ASTM C642-13 [98] and C39/C39M-20 [99] standards respectively.

2.2.5 Specimen identification

The labeling system of the "pull-out" specimens depended on the method of concrete placement (shotcrete or cast in-place) which was used to build them. Subsequently, attributes proper to each method were used to identify individual specimens. For shotcrete specimens, they referred to the nozzleman (N1 or N2) followed by the water content used by each one of them (Highest, Medium, or Lowest). For cast in-place specimens, they referred to the height of

the *artificial voids* (h or 2xh respectively). Regardless of the method of concrete placement, the value of the *un-bonded* perimeter was indicated and lastly, each replica was identified alphabetically (A to B or A to C). The complete labeling system is shown Figure 2.7

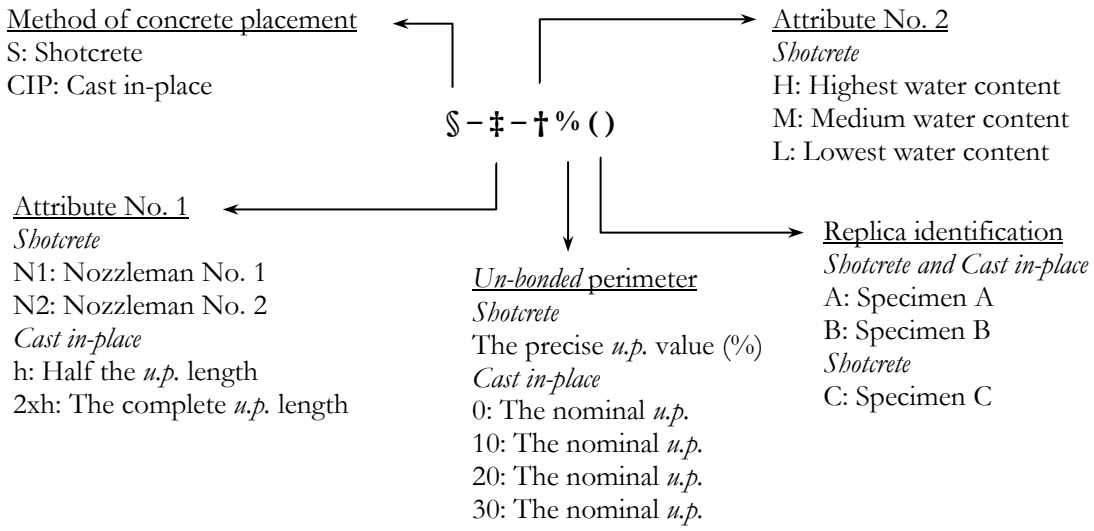

Figure 2.7: Labeling system of the "pull-out" specimens

2.2.6 Testing

The specimens and their respective material properties were tested 21 days after spraying or casting using a 322 MTS test frame equipped with a 647 MTS hydraulic wedge grip. The tests were performed at 1.0 mm/min displacement control and the slip of the reinforcing bars was recorded at the loaded end with two linear position sensors with return spring attached to a steel shaft collar as shown in Figure 2.8 (refer to Appendix E for their detailed specifications). The collar was placed around the reinforcing bar and was tightened as the tip of a thumb screw, passing through the collar, bore against the barrel of the bar. A 25 mm thick steel plate attached to the base of the press by four plain round steel rods retained each specimen. A system of two layers consisting of a 2 mm thick rubber sheet and a 9 mm thick steel plate were placed above each specimen to assure the load was applied uniformly and to reduce the frictional resistance between concrete and steel. Shotcrete "pull-out" specimens were capped with self-leveling epoxy because their surface presented entrapped rebound in some areas. An additional 9 mm steel plate was placed on top of the 25 mm thick plate over which the probe tips of the position sensors were laid on to provide an un-deformed surface while the specimens were tested.

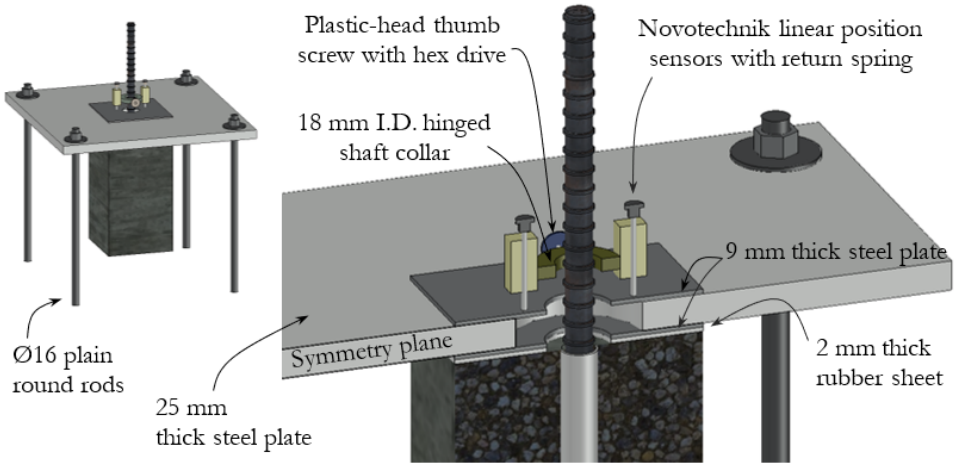

Figure 2.8: Test set-up of "pull-out" specimens

2.3 "Beam-end" specimens

2.3.1 Overview

The ASTM A944-10 "beam-end" specimen [17] has gained more acceptance for the study of the bond strength between reinforcing bars and concrete because the stress distribution, as shown in Figure 2.9, represents in a more realistic way the stress field found in actual reinforced concrete flexural members. Indeed, because only a portion of the concrete block is retained away from the applied load, the bonded length and the concrete around it are placed in tension while at the opposite side of the specimen the concrete is placed in compression. This, in combination with a relatively small concrete cover, usually allows the concrete along the bonded length to split as it would normally occur in flexural members who fail by bond.

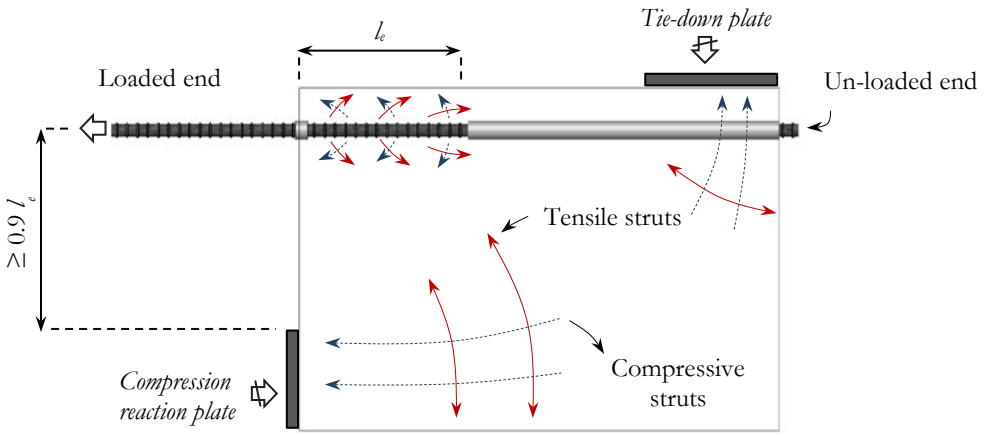

Figure 2.9: Stress distribution in a "beam-end" specimen

Because of the specimen's configuration, the results closely match those obtained with other specimens designed to represent full-scale reinforced concrete members in flexure [42] and therefore, their results are well suited for developing rational criteria for the design and inspection of reinforced concrete structures at a reduced cost and effort than larger bond specimens.

2.3.2 Construction and geometry of specimens

The "beam-end" specimens were built in accordance with the ASTM A944-10 standard [17] and consisted of 210 x 600 x 450 mm prisms with the test bar placed eccentrically near the top of the specimen. The reinforcing bar had a concrete cover of $2.5d_b$ which represents the maximal theoretical confinement value when the *development length* of straight bars in tension is calculated (refer to Section 1.5) and the concrete cover required for elements exposed to weather or in contact with the ground according to the ACI 318-19 design code [5]. The test bar passed through a PVC bond breaker at the loaded end (or lead length) to prevent a conical failure at the front of the specimen and another one at the un-loaded end intended to control the bonded length of the test bar (see Figure 2.10).

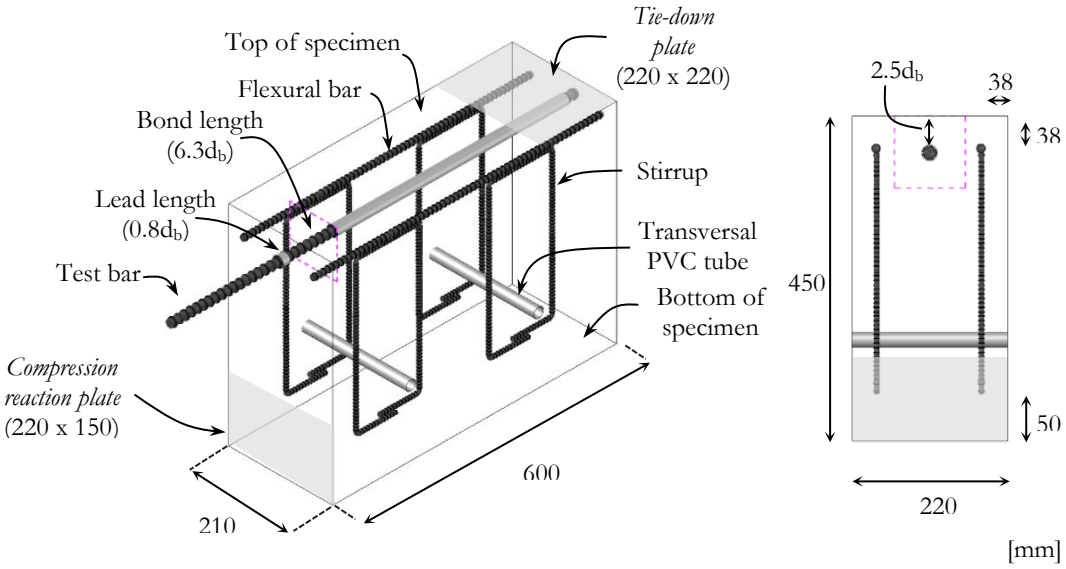

Figure 2.10: Geometry of the "beam-end" specimen

The lead length and the bonded length were set to $0.8d_b$ and $6.3d_b$ respectively for all specimens. The interior ends of the PVC bond breakers were sealed with duct tape to prevent mortar seepage and all test bars were placed with their longitudinal ribs facing the sides of the molds.

Flexural bars and stirrups are required to favor a bond failure rather than a flexure or a shear failure of the "beam-end" specimen. The stirrups are oriented parallel to the sides of the specimen to avoid the presence of transversal reinforcement along the plane of cracking. Additional 25.4 mm diameter PVC tubes were placed transversally with respect to the test bar in between the stirrups so that they could be transported after being demolded. The top and side concrete cover of the flexural bars and stirrups were 38 mm and the concrete below the stirrups was 50 mm.

The specimens were cast in reusable molds consisting of detachable 19.1 mm thick plywood panels reinforced with 50.8 x 50.8 mm studs as seen in Figure 2.11a. The panels were retained together using three 9.5 and two 2.5 mm steel threaded rods at their bottom and top sections respectively. Before pouring the concrete, the bolts of the threaded rods were tightened and all joints were caulked with silicone to prevent water from the concrete mixture to seep. Thereafter, the test bar along with its front and back bond breakers were secured in place and the molds were covered with release agent. The flexural bars and the stirrups (attached together using tie wraps) were then placed inside the molds and lastly the transversal PVC tubes were installed. All of the holes in the formwork holding the pieces in place were also caulked. This sequence guaranteed a wider space between the mold and the test bar to avoid contaminating the bars with release agent.

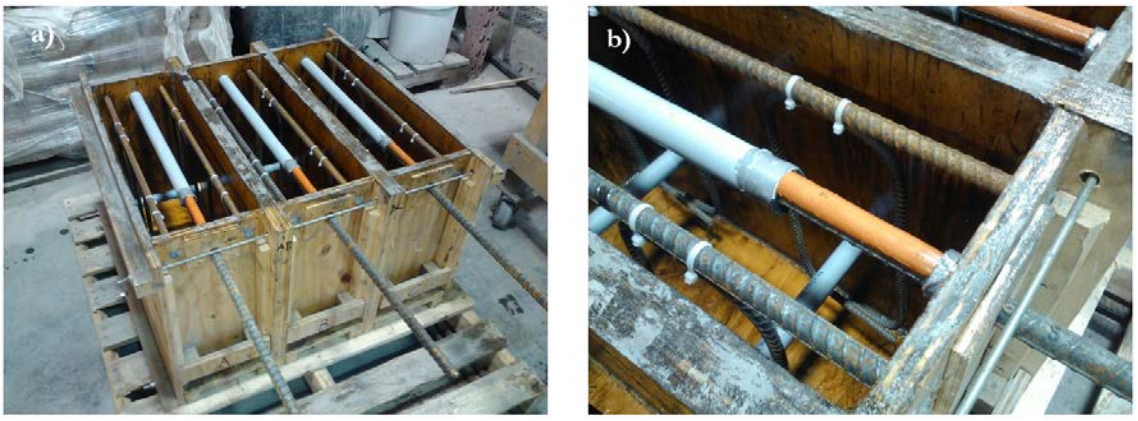

Figure 2.11: Molds of the "beam-end" specimens

The *artificial voids* were built in the same way as it was described in Section 2.2.3 and they were glued all along the bonded length of the test bars as seen in Figure 2.11b. As voids in shotcrete

structures can be created facing the exterior or the interior of an element depending on the location of the bar and the direction of the shotcrete stream, the impact of the position of the void on the bond strength of the bars was also investigated. For this purpose, a top and bottom void configuration were studied as seen in Figure 2.12. Since these types of specimens were not cut to verify the actual size of the voids, the *un-bonded* perimeter was taken as the nominal one.

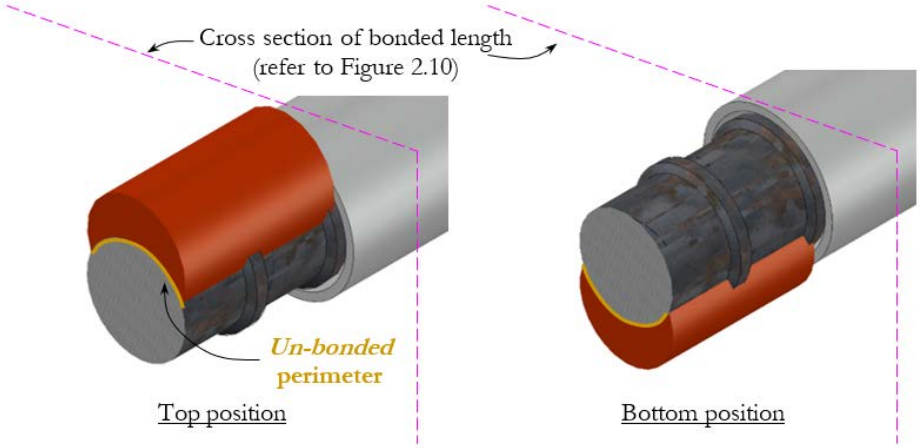

Figure 2.12: Position of *artificial voids* on the bonded length of "beam-end" specimens

Because the molds of the "beam-end" specimens were higher than those of the "pull-out" specimens, a semi-self consolidating concrete mixture with a 0.45 w/b ratio was used. This was done to reduce the required consolidation and thus, the possible bleeding of the mixture. The effectiveness of this action was verified by comparing the bond strength of "beam-end" specimens and their concrete bleeding properties against specimens made with a w/b ratio of 0.55. The fresh concrete was transferred into the molds in two lifts (the first layer was placed in all specimens before placing the second one) and minimal consolidation was provided; only a few strokes were given on the corners of the molds. The top surface of the specimens was screeded with a metal trowel and a plastic membrane was placed over them (making sure it did not touch the fresh concrete) to limit water evaporation until the initial set of the mixture where a wet burlap was laid over the molds and under the plastic membrane. The specimens were demolded 1 day after the concrete was poured and curing continued for one week with the same protective system. For this type of specimen, three replicas of each configuration were built.

2.3.3 Concrete tests

The slump and the slump flow along with the Visual Stability Index (VSI) were measured in accordance to ASTM C143/C143M-20 [22] and ASTM C1611/C1611M-18 [100] standards for the 0.45 and the 0.55 *w/b* ratio mixtures respectively. In both cases, the air content was also measured following the ASTM C231/C231M-17 [96] standard. Additionally, 100 x 200 mm cylinders were cast to test the compressive strength, the splitting tensile strength, the modulus of elasticity and the poisson's ratio of the concrete in accordance to ASTM C39/C39M-20 [99], ASTM C496/C496M-17 [101] and ASTM C469/C469M-14 [102] standards respectively. All of the aforementioned tests were performed with concrete from the second lift with which the test bar of the "beam-end" specimens was encased.

As the concrete below the test bar was considerable, the average bleeding rate (R) and the bleeding capacity (ΔH) of the mixture were quantified as proposed by Josserand et al. [103] to make sure the bond strength reduction caused by the presence of *artificial voids* would not be amplified by excessive water accumulating under the test bars. The procedure requires filling with concrete 3 circular molds of different heights[10] as those shown in Figure 2.13a. Then, the bleed water is drawn off the intersection of two orthogonal, and inclined towards the center, grooves at a regular time interval using a pipet as shown in Figure 2.13b.

Figure 2.13: (a) Equipment for the bleeding test and (b) bleeding water being drawn

During the entire test, the tallest mold laid on a 0.1g accurate scale so the average evaporation of bleed water (and then considered for all other molds) could be measured. To avoid this as

[10] All molds must possess a diameter-to-height ratio greater than 0.24.

much as possible, the cylinders were covered during the entire test and the covers were only removed to draw off the bleed water. The bleed water, measured using a ±0.001g precision balance, was used to calculate the bleeding capacity (ΔH) for each mold (refer to Figure 2.14).

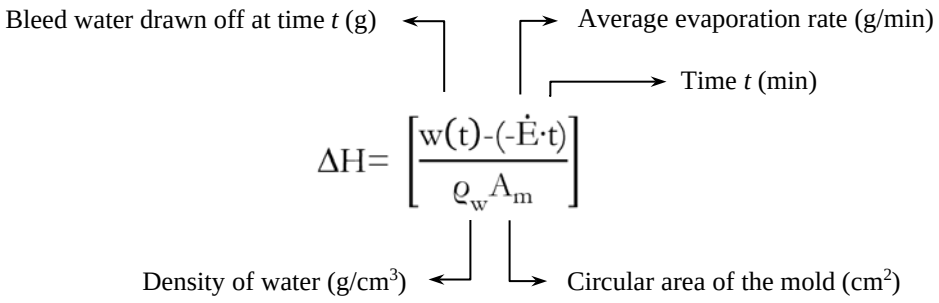

Figure 2.14: Expression to calculate the bleeding capacity of the concrete

The rate at which bleeding occurs (R), which is independent of the mold's height, was calculated based on the increase of ΔH over time. In this investigation, the three chosen cylinders were 150, 210 and 430 mm high and had an inner diameter of 150 mm. The tallest mold was intended to approximately represent the amount of concrete under the test bar of the "beam-end" specimens. Moreover, the concrete was consolidated in the same manner as it was done with the specimens. This method is advantageous over similar ones such as ASTM C232/C232M-20 [104] because the molds do not need to be tilted to draw off the bleed water. Yet, it gives the opportunity to calculate the amount of bleeding in the same way the ASTM standard does.

2.3.4 Specimen identification

The labeling system of the "beam-end" specimens, as shown in Figure 2.15, referred to the size of the test bar, the water to binder ratio (*w/b*) and the position of the *artificial voids*. Subsequently, the encapsulation quality of the test bars was indicated by means of the nominal *un-bonded* perimeter and lastly, each one of the three replicas was identified alphabetically with letters A to C.

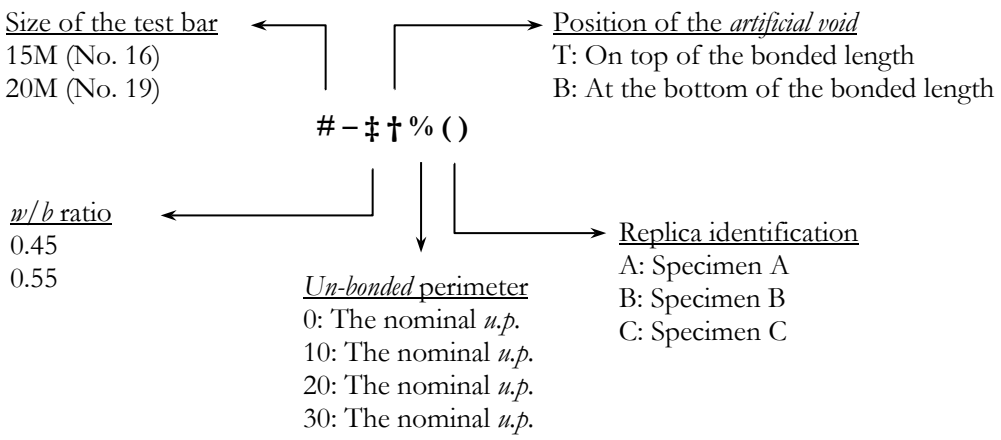

Figure 2.15: Labeling system of the "beam-end" specimens

2.3.5 Testing

The "beam-end" specimens and their respective concrete properties were tested 24 ± 2 days after casting using a 311 MTS test frame and the set-up show in Figure 2.16. The tests were performed at 0.5 mm/min displacement control and the slip of the reinforcing bars was recorded at the loaded and at the un-loaded end of the test bar using two linear position sensors with return spring on each side. The sensors were attached to the test bar as explained in Section 2.2.6.

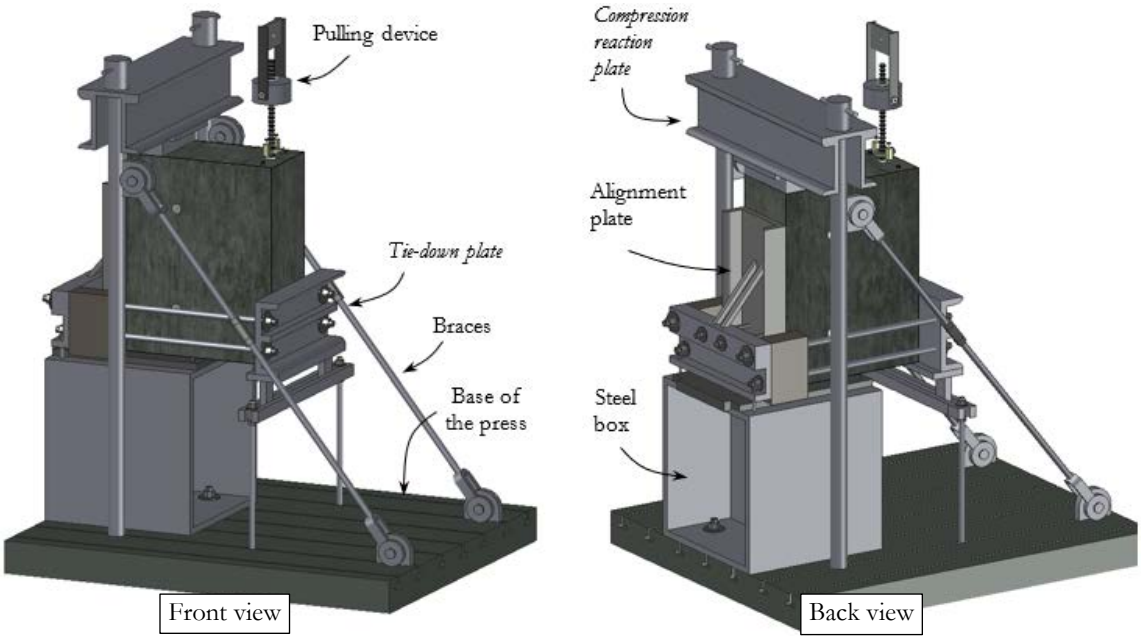

Figure 2.16: Test set-up of "beam-end" specimens

The specimens were lifted with a crane using the holes provided by the transversal PVC tubes (refer to Figure 2.10) and its un-loaded side was laid on a steel plate resting over a steel box anchored to the base of the press as shown in Figure 2.16.

The steel plate was equipped with bolts intended to tilt the specimen slightly to position the test bar vertically in case the "beam-end" specimen was not perfectly rectangular. Subsequently, the test bar was aligned with the press actuator's longitudinal axis by pushing the specimen with the alignment plate. Then, the specimen was gradually tightened with the *compression reaction plate* and the *tie-down plate*.

Two inclined braces retained the columns which in turn retained the *compression reaction plate* in place. The *tie-down plate* was attached to a steel plate which was in turn attached to the steel box. Finally, the pulling device, which consisted of two square shafts pin-holding a 65 mm thick cylinder with a hole in its middle, was installed. The test bar passed through the cylinder's hole and a conical wedge was placed around the bar so that the cylinder would bear against the wedge while the bar was pulled. A detailed description of the testing apparatus is presented in Appendix A.

2.4 Materials

2.4.1 Reinforcing bars

The mechanical and geometrical properties of the reinforcing bars used for each type of bond specimen are listed in Table 2.1. The mechanical properties were obtained in accordance with ASTM A370-20 standard [105] and the geometrical properties were obtained with samples cut longitudinally at 45 and 90 degrees with respect to the longitudinal plan of the ribs. The mechanical properties represent the mean of 3 samples whereas the geometrical ones represent the average from 20 ribs (10 for each longitudinal cut at a different angle) using high-resolution photographs and a CAD software.

Table 2.1: Properties of the reinforcing bars

	Properties	"Pull-out" 15M (No. 16‡)	"Beam-end" 15M (No. 16§)	"Beam-end" 20M (No. 19§)
Mechanical	Young's modulus, E_s (GPa)	197	197	208
	Yield strength at 0.2%, f_y (MPa)	378	733	475
	Ultimate strength, f_u (MPa)	562	962	742
	Elongation at rupture, $\varepsilon_{max.}$ (%)	17.7	10.5	12.7
Geometrical	Nominal diameter, d_b (mm)	16.0	15.9	19.1
	Core diameter, D (mm)	15.1	14.8	17.7
	Ribs' height, h_r (mm)	1.0	0.9	1.3
	Ribs' top width, b_r (mm)	2.1	1.0	1.2
	Ribs' base width, a_r (mm)	5.5	4.9	5.6
	Ribs' spacing, s_r (mm)	10.8	10.8	12.6
	Ribs' face angle, θ (degrees)	31	25	30
	Ribs' inclination, β (degrees)	53	67	68
	Σ gaps (mm)	7.6	4.0	4.0
	Relative rib area, R_r (mm/mm)†	0.088	0.080	0.100

‡Obtained in a local hardware store, Québec, Canada
§Supplied by HarMac Rebar & Steel, Maine, U.S.A.
† Calculated as per Equation 2.1

The geometrical nomenclature appearing in Table 2.1 is represented in Figure 2.17 where a 90 degree longitudinal cut with respect to the longitudinal plan of the ribs is depicted.

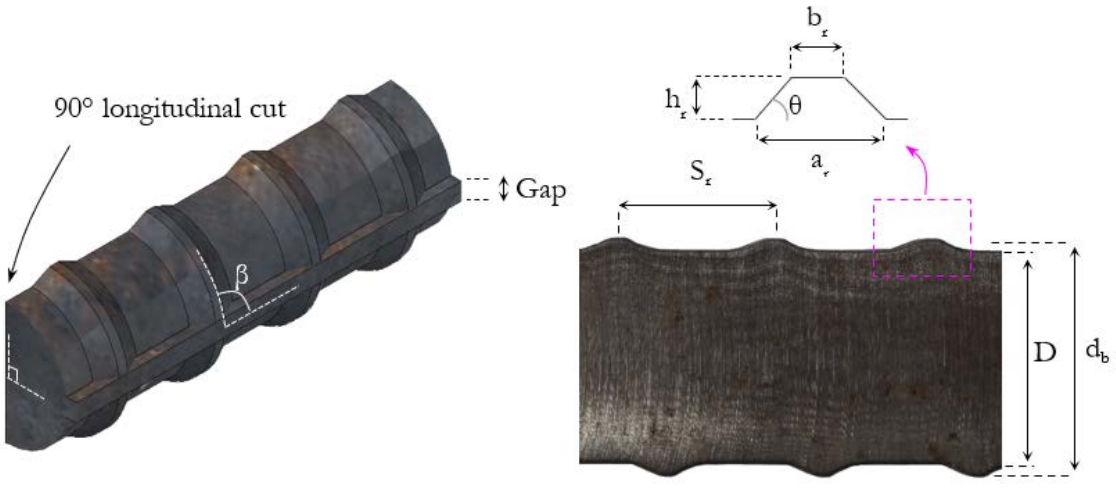

Figure 2.17: Longitudinal cut of a bar showing the geometry parameters

2.4.2 Concrete mixing and composition

Contrary to the *dry-mix* shotcrete process in which mixing occurs inside the hose, the nozzle and seconds after the material is projected, the concrete intended for the cast in-place specimens was mixed using an 80 L planetary mixer. Initially, all of the pre-bagged *dry-mix* shotcrete materials were mixed a few seconds before the water was slowly added at a constant rate. Once all the water was added, mixing continued for 3 minutes followed by a 3-minute rest period and a final 2-minute mixing period. The quantity of each component of the mixture as a function of the method of concrete placement and the type of bond specimen is presented in Table 2.2.

Table 2.2: Properties of the concrete mixture

Component	**"Pull-out"** Shotcrete	**"Pull-out"** Cast in-place	**"Beam-end"** Cast in-place	**"Beam-end"** Cast in-place
Ordinary Portland cement (kg/m³)	388.3	388.8	393.1	376.7
Silica fume[++] (kg/m³)	33.9	34.0	34.3	32.9
Coarse aggregate 2.5 – 10 mm[†] (kg/m³)	556.8	702.6	708.6	680.7
Fine aggregate 0.08 – 5 mm[•] (kg/m³)	1152.6	1008.0	1016.6	976.5
Water (kg/m³)	190.1	189.6	191.2	224.8
Polypropylene fibers (kg/m³)	1.0	-	-	-
Air (%)	4.5[‡]	4.5[§]	3.4[§]	2.1[§]
Water reducer (ml/100 kg of binder)	-	500	750	-
w/*b* ratio	0.45[*]	0.45	0.45	0.55

[++] Surface area = 22~24 m²/g, relative density = 2.24~2.27

[†] Crushed limestone (Mirabel, QC): Maximum nominal diameter = 10 mm, bulk specific gravity = 2.77, absorption: 0.39~0.71

[•] Sand (St-Gabriel, QC): fineness modulus: 2.68~2.92, bulk specific gravity = 2.68, absorption: 0.60

[‡] Air content based on the pre-bagged shotcrete's manufacturer range of values

[§] Air content measured based on ASTM C231/C231M-17

[*] Established for comparison purposes

As can be observed, polypropylene fibers were not used with the cast in-place specimens. This should not significantly impact the mechanical properties of the resulting concrete since they are only added to resist relatively low stresses caused by plastic shrinkage. Moreover, the multi-range water reducer used for cast in-place specimens was an ASTM Type A and F polycarboxylate based plasticizing admixture complying with the ASTM C494/C494M-19 [106] standard. The liquid admixture was incorporated in the water prior to the beginning of the mixing procedure described above. Its use was intended to enhance the workability of the pre-bagged shotcrete

mixture prepared with a0.45 *w/b* ratio. Based on the aspect of the cast in-place mixture, the use of a viscosity modifier to further reduce segregation was not deemed necessary.

2.5 Summary of the experimental program

The principal variable studied was the transversal length of the void (or *un-bonded* perimeter) to investigate its impact the bond strength of a reinforcing bar. The maximum *un-bonded* perimeter investigated in the laboratory was 30% as higher values would normally entail rejecting the shotcrete due to excessive rebound. Additionally, the height of the voids and their position were also studied in the "pull-out" and the "beam-end" specimens respectively. Only in the case of the "beam-end" specimens, the size of the bar and the bleeding capacity of the mixture were also investigated. A summary of the studied parameters are presented in Table 2.3 with the intention to consolidate the information presented in the previous sections of this chapter.

Table 2.3: Summary of variables and parameters of bond specimens

	Parameters	"Pull-out" (Chapter 3)	"Pull-out" (Chapter 3)	"Beam-end" (Chapter 4)	"Beam-end" (Chapter 4)
Specimen	Concrete placement	Shotcrete	Cast in-place	Cast in-place	Cast in-place
	w/b ratio	0.25 to 0.44	0.45	0.45 and 0.55	0.45
	Test bar	15M (No. 16)	15M (No. 16)	15M (No. 16)	20M (No. 19)
	Flexural bars	-	-	No. 13	15M (No. 16)
	Stirrup	-	-	No. 10	No. 10
	Concrete cover (mm)	67 ($4.2d_b$)	67 ($4.2d_b$)	40 ($2.5d_b$)	50 ($2.5d_b$)
	Lead length (mm)	245 ($15.3d_b$)	245 ($15.3d_b$)	12.5 ($0.8d_b$)	15.5 ($0.8d_b$)
	Bonded length (mm)	40 ($2.5d_b$)	40 ($2.5d_b$)	100 ($6.3d_b$)	120 ($6.3d_b$)
	Number of specimens	15	14	21	18
	Number of replicas	3†	2	3	3
Voids	Type	Stream created	*Artificial*	*Artificial*	*Artificial*
	Transversal length (%)	0 to 36	0, 10, 20, 30	0, 10, 20, 30	0, 10*, 20, 30
	Height§	Variable	0.5, 1.0	0.5	0.5
	Position	Bottom	Bottom	Top and Bottom	Top and Bottom
Hardened concrete	Compressive strength	Cores	Cores	Cylinders	Cylinders
	Splitting tensile	-	-	Cylinders	Cylinders
	Modulus of Young	-	-	Cylinders	Cylinders
	Poisson ratio	-	-	Cylinders‡	-
Fresh concrete tests	In-place *w/b* ratio	yes	-	-	-
	Boiled absorption	yes	-	-	-
	Rebound	yes	-	-	-
	Consistency	yes	-	-	-
	Slump	-	yes	-	-
	Slump flow	-	-	yes	yes
	Visual Stability Index	-	-	yes	yes
	Air percentage	-	yes	yes	yes
	Bleeding test	-	-	yes	-

† Only two replicas sprayed by Nozzleman N1 could be tested
§ The height of the voids is relative to the *un-bonded* perimeter of a given specimen
‡ Only for the 0.45 *w/b* ratio mixture
* Specimens' results were discarded due to a malfunction in the equipment

2.6 Finite Element modeling with Abaqus 6.14

2.6.1 Overview

The commercially available Finite Element (FE) package Abaqus 6.14 was selected to complete this part of the research. In Abaqus 6.14, there are three different pre-defined materials in the library to choose from in order to define the properties of concrete. These represent the *smeared crack* model, the *cracking* model and the *concrete damage plasticity* model [107]. The latter was selected for this study as it assumes isotropic damage to represent the inelastic behavior of concrete by considering the degradation of the elastic stiffness of the concrete by using plastic straining both in tension and in compression. This makes the material useful for many situations such as monotonic, cyclic, and dynamic loading but specifically for low confining pressures as in this study. Regarding the reinforcing bars, their properties can be defined based on their uniaxial behavior and they can either be modeled as three-dimensional elements or as truss elements embedded in the concrete (no slip between them and the surrounding concrete occurs). In the former case, the interaction between materials can be specified based on contact by applying an interface constitutive laws.

2.6.2 Specimen geometry

The complete "beam-end" specimen, as shown in Figure 2.18, was modeled with the test bar and the concrete using 8-node linear brick elements with a one-point integration scheme (type C3D8R) and a *relaxed hourglass stiffness* control method (to avoid a zero-energy mode deformation caused by a zero stiffness matrix). Only "beam-end" specimens with 15M (No. 16) bars were considered (refer to Table 2.1 for the bar's geometry) and the ribs were modeled normal to the longitudinal axis of the test bar and the longitudinal ribs were omitted.

The flexural bars and stirrups were modeled using 2-node linear truss elements (type T3D2) and were embedded in the concrete elements assuming perfect bond. The T3D2 elements were assigned a cross-sectional area corresponding to the bars used in the experimental campaign; the overlapped portions of the flexural bars and the stirrups were also considered.

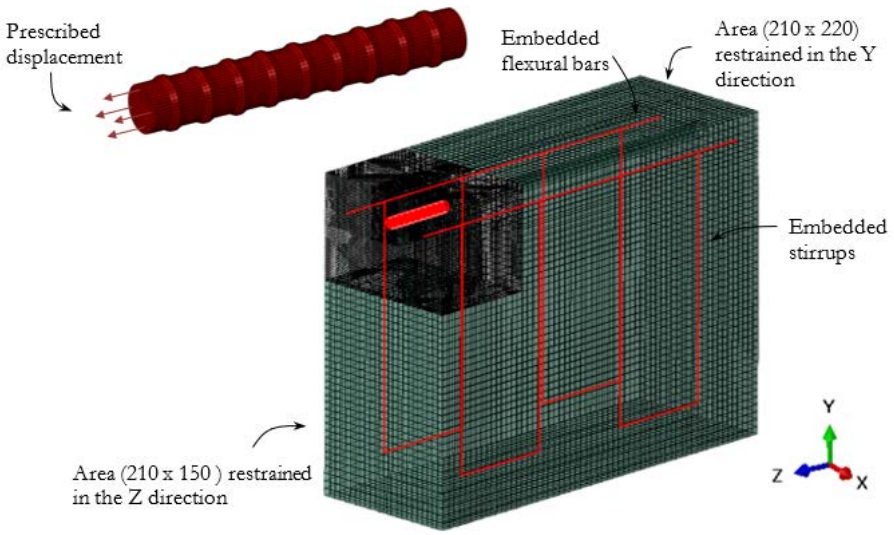

Figure 2.18: Geometry of the "beam-end" specimen

The imperfections were introduced explicitly by removing the necessary concrete elements around the test bar to uncover its ribs (facing the top surface of the specimen). The *un-bonded* perimeters that were studied represent up to 40% of the nominal perimeter of the bar as shown in Figure 2.19.

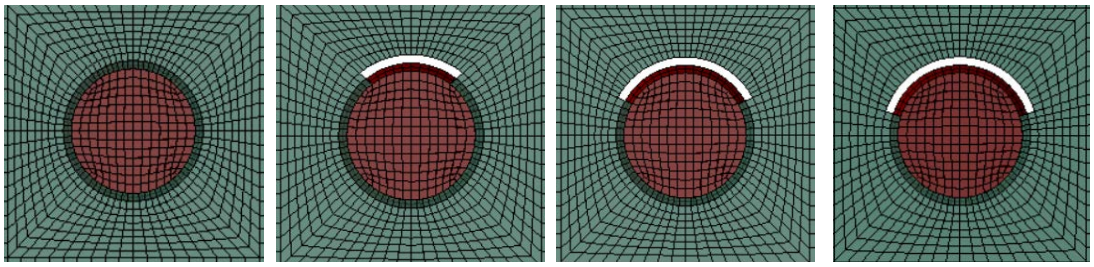

Figure 2.19: Size of voids investigated

The translational displacement of the nodes covering the same area of the *compression reaction plate* and the *tie-down plate* (refer to Figure 2.10) were restrained in the Z and in the Y direction respectively. Moreover, the load was uniformly applied on the exterior end of the test bar by imposing a prescribed "smooth" displacement fifth-degree polynomial function.

The concrete was divided in three parts (connected to one another using a tie constraint) with different mesh sizes. A *very fine* mesh (#1 in Figure 2.20) was used approximately $1.0d_b$ around

the test bar but was extended to the top surface of the specimen assuming the cracking (running along the bonded length of the test bar) should normally develop first in that area. The *fine* mesh (#2 in Figure 2.20) was used on the region of the specimen showing further cracking and the *coarse* mesh (#3 in Figure 2.20) was used elsewhere where cracking was not expected to occur. Both the *very fine* and the *fine* mesh were extended approximately $1.0c_b$ towards the back of the specimen beyond the bonded length of the test bar. The characteristics of the three different concrete mesh sizes and the one of the test bar are presented in Figure 2.20**.** The longitudinal cut is only used to represent in a clearer way the topology of the model; symmetry was in fact not used to alleviate the calculations because it could have induced a preferential *splitting* pattern of the concrete along the symmetry region.

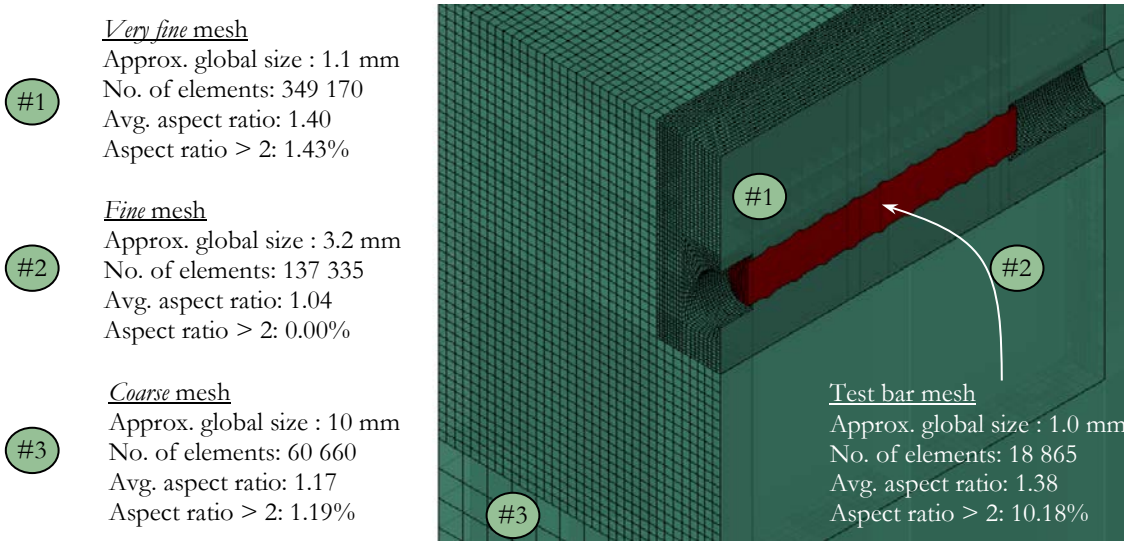

Figure 2.20: Mesh of the "beam-end" specimen

2.6.3 Materials constitutive laws

The *Concrete Damage Plasticity* (CDP) constitutive model is a scalar plastic damage model that is defined with the three fundamental assumptions of the incremental theory of plasticity: the shape of an initial *yield surface* in the three-dimensional principal-stress space, the evolution of subsequent loading surfaces based on a *hardening rule* and the formulation of an appropriate *flow rule*.

The *yield surface*, which defines the stress level at which plastic deformation begins, is defined by the function $F_{(\bar{\sigma},\varkappa)}$ [108, 109] as shown in Equation 2.2. Elasticity is present as long as $F_{(\bar{\sigma},\varkappa)}$ is less than 0 and yielding occurs when $F_{(\bar{\sigma},\varkappa)}$ equals 0.

$$F_{(\bar{\sigma},\varkappa)} = \frac{1}{1-\alpha}\left[\alpha I_1 + \sqrt{3J_2} + \beta_{(\varkappa,\alpha)}\langle\hat{\sigma}_{max}\rangle - \gamma\langle-\hat{\sigma}_{max}\rangle\right] - C_{c_{(\varkappa)}} \quad (2.2)$$

This *yield surface* is a function of the *effective stress* ($\bar{\sigma}$) and a *hardening variable* ($\varkappa$). However, for practical reasons $\varkappa$ is represented by means of a scalar *degradation damage* variable $D_{(\varkappa)}$. In order to introduce the damage in $F_{(\bar{\sigma},\varkappa)}$, the Cauchy stress ($\sigma$) is defined using the relationship expressed in Equation 2.3.

$$\sigma = [1 - D_{\varkappa}]\bar{\sigma} \quad (2.3)$$

The variable D is defined independently for the tensile (d_t) and the compressive (d_c) degradation damage. Each of these variables can take values in the range of 0 (no damage) and 1 (complete degradation). Since $\bar{\sigma}$ should reduce to the stress in the uniaxial test, the tensile and compressive uniaxial stress – strain relationships are defined in Abaqus 6.14 independently. In compression, the initial behavior is elastic, followed by some stress-hardening and finally, strain softening after the ultimate stress (σ_c) is attained. In tension, the behavior is elastic until the ultimate stress (σ_t) is reached and post-failure behavior is characterized by strain softening. If the concrete specimen is unloaded after the elastic limit has been attained, the elastic modulus (E) is reduced as expressed in Equation 2.4 to simulate some level of *degradation damage* of the initial elastic modulus (E_0).

$$E = [1 - D]E_0 \quad (2.4)$$

Moreover, α and γ represent dimensionless material constants which can be determined from experimental data [110]; α takes into account the equibiaxial (f_{b0}) and uniaxial (f_c) compressive stresses and γ depends on the constant K_c, which in turn, defines the shape of the *yield surface* in the deviatoric plane[11]. Both material constants are defined as expressed in Equation 2.5 and 2.6.

[11] The plane perpendicular to the hydrostatic axis in which $\sigma_1 = \sigma_2 = \sigma_3$.

$$\alpha = \frac{(f_{b0}/f_c) - 1}{2(f_{b0}/f_c) - 1} \tag{2.5}$$

$$\gamma = \frac{3(1 - K_c)}{2K_c - 1} \tag{2.6}$$

The *hardening rule*, which assures the evolution of the hardening variables and thus the shape of subsequent loading surfaces beyond the *yield surface*, is expressed with Equation 2.7 where $\dot{\varepsilon}^p$ represents the plastic strain rate vector.

$$\dot{\varkappa} = h(\bar{\sigma}, \varkappa) \cdot \dot{\varepsilon}^p \tag{2.7}$$

The *flow rule* then establishes the connection between the plastic stress – strain relationships and the subsequent loading surfaces based on the relationship expressed in Equation 2.8.

$$\dot{\varepsilon}^p = \dot{\lambda} \frac{\partial G_{(\bar{\sigma})}}{\partial \bar{\sigma}} \tag{2.8}$$

The variable $\dot{\lambda}$ represents a positive (only when plastic deformations occur) scalar hardening parameter which can vary throughout the straining process and $G_{(\bar{\sigma})}$ a plastic potential function with a Drucker-Prager hyperbolic shape as expressed in Equation 2.9**.** The eccentricity ε determines the rate at which the function approaches the asymptote (as ε tends to 0, the plastic potential tends to a straight line). Moreover, σ_t represents the uniaxial tensile stress at failure and ψ the angle of dilatancy. Smaller values of ψ result in less dilatancy and therefore a more brittle behavior.

$$G_{(\bar{\sigma})} = \sqrt{(\varepsilon \sigma_{t0} \tan\psi)^2 + 3J_2} + \frac{I_1}{3} \tan\psi \tag{2.9}$$

Since the gradient of the potential surface ($\partial G_{(\bar{\sigma})}/\partial \bar{\sigma}$) defines the direction of the plastic strain rate vector (and thus the volume change of an element at the onset of plastic deformation) and because $G_{(\bar{\sigma})} \neq F_{(\bar{\sigma},\varkappa)}$ (a *non-associated flow rule* is used), the change of volume of an element will be greater near the apex of the surface at the tension zone. The steel was considered as a perfectly elastic material.

2.6.4 Interface constitutive laws

The interaction between the test bar and the concrete was defined through a general contact algorithm. In order to recreate the three components of the bond mechanism, a cohesive law (zero-thickness), a Coulomb friction law and a "hard" pressure-overclosure relationship (with allowed separation) were specified over different sections of the test bar's surface according to Figure 2.21 (refer to Lagier et al. [74]). Thus, as the load was applied to the test bar, the different sections of the interface were progressively placed on *contact/stick*, *contact/slip* or *separation* states.

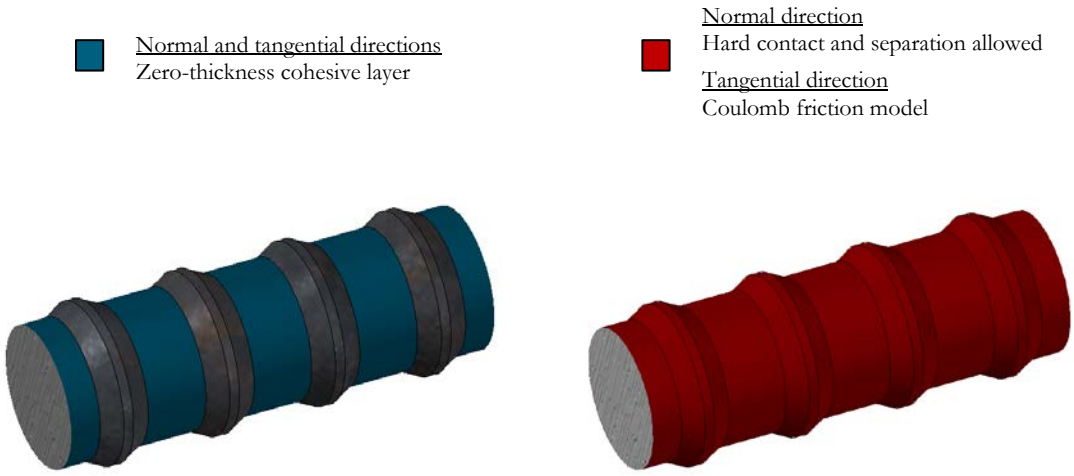

Figure 2.21: Distribution of interface laws over the test bar's surface

The pressure-overclosure relationship guarantees the load transfer from the bar's ribs to the concrete; a penalty contact constraint was used. Although the penalty constraint induces additional stiffness to the model because the nodes of the test bar are allowed to slightly penetrate the concrete elements, its impact on the model's response is usually insignificant and avoids over-constraint issues. The cohesive layer was defined using uncoupled *traction-separation* laws in the normal (σ_1) and in the two shear ($\tau_{2,3}$) directions. The cohesive law was only assigned to the surface in between the ribs where its impact is more important. The cohesive laws were assumed as linear elastic with stiffness K_1 and $K_{2,3}$ for the normal and the two shear directions as shown in Figure 2.22a. At the onset of the ultimate cohesive strength ($\overline{\sigma}_1$ or $\overline{\tau}_{2,3}$), the damage of the cohesive laws is linear and is specified by means of a displacement δ_d. When the cohesive layer is completely damaged, a *separation* state occurs in the normal direction whilst in the shear

direction the Coulomb friction law is activated (refer to Figure 2.22b). Relative slip between the test bar and the concrete occurs if the equivalent shear stress at the surface ($\tau_{eq} = \sqrt{\tau_2{}^2+\tau_3{}^2}$) exceeds the critical shear stress (τ_{crit}) equal to the static friction coefficient between the steel and the concrete (μ) multiplied by the normal closing pressure between both materials (p). Because a penalty contact constraint was used, an *elastic friction stiffness* ($K_{el,f}$) specified by the user causes some relative slip between the test bar and the concrete before τ_{crit} is attained. On the surface of the ribs, the friction law is actively functioning in the tangential direction (if there is contact between the concrete and the test bar) because the cohesive law was not assigned in that area.

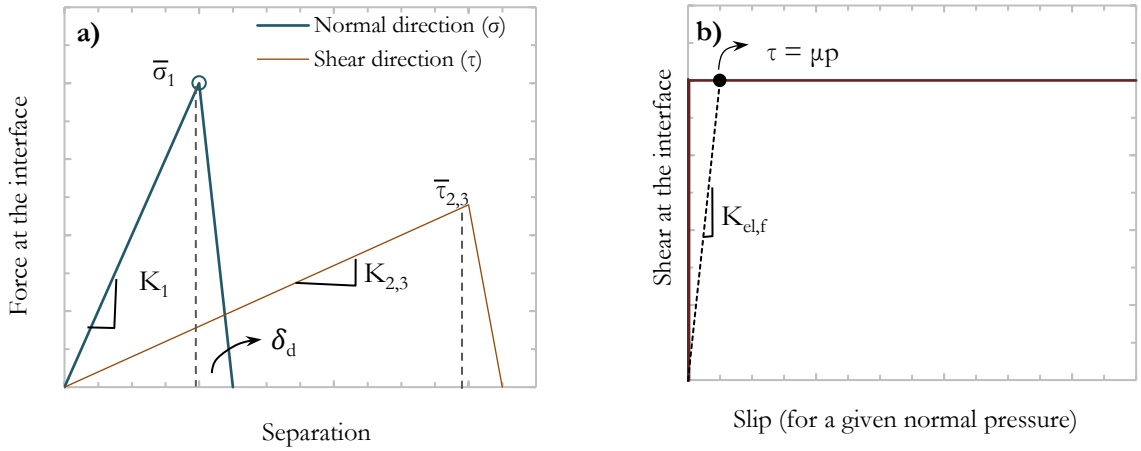

Figure 2.22: (a) Cohesive and (b) friction laws

2.6.5 Solution Strategy

A quasi-static explicit dynamic analysis was used. The explicit formulation is very effective in highly non-linear problems under quasi-static loading such as bond between a reinforcing bar and concrete around it. A direct integration of the equations of motion are solved using the explicit central-difference method with very small time increments; a static solution can be obtained with this strategy when the loading rate is very slow. For such purpose, the time to reach the maximum load is suggested to be less than 10 times the fundamental period of vibration to assure that the ratio between the kinetic (E_k) and the internal energy (E_I) of the model lies below 5% at the onset of concrete cracking [74, 111]; these recommendations minimize inertial effects.

Chapter 3 Bond strength of reinforcing bars encased with shotcrete

Pasquale Basso Trujillo[a], Marc Jolin[a], Bruno Massicotte[b], Benoît Bissonnette[a]
[a] *Dept. of Civil and Water Engineering, Université Laval*
[b] *Department of Civil, Geological and Mining Engineering, École Polytechnique de Montréal*

This paper is part of the Construction and Building Materials Journal, ISSN 0950-0618, doi.org/10.1016/j.conbuildmat.2018.02.218. Paper submitted on January 11th, 2018; approved on February 28th, 2018 and published on April 30th, 2018.

3.1 Résumé

Alors que l'utilisation du béton projeté pour construire des éléments structuraux en entièreté en Amérique du Nord augmente, la qualité de l'enrobage des barres d'armature devient un sujet de grande préoccupation. Dans cette recherche, l'influence de la consistance du mélange et la taille des imperfections (crée délibérément) derrière les barres d'armature sur la force d'adhérence des barres ont été étudiées en utilisant des éprouvettes « pull-out » en béton projeté par *voie sèche*. Cependant, puisque les tailles des imperfections recherchées n'ont pas pu être créées, des éprouvettes « pull-out » ont été coulées en place en utilisant des *vides artificiels*. Cette stratégie a permis d'étudier la réduction de la force d'adhérence en contrôlant précisément la taille des vides. Les résultats suggèrent que la meilleure performance des barres, en ce qui concerne l'adhérence, est obtenue lorsqu'une technique de projection adéquate est utilisée et quand une combinaison optimale entre la *consistance* du mélange et la vitesse de projection est utilisée. De plus, des barres d'armature encapsulées avec béton projeté glissent moins, relativement au béton, que celles encapsulées avec béton coulé en place à cause de la grande compaction avec laquelle le béton est mis en place. Aussi, une longueur transversale du vide (en contact avec la barre d'armature) d'approximativement 20% a été définie comme la limite après laquelle la performance des barres concernant l'adhérence change grandement.

3.2 Abstract

As the use of shotcrete (sprayed concrete) to build full-depth structural elements increases in North America, the encapsulation quality of reinforcing bars has become a subject of growing concern. In this investigation, the influence of the mixture *consistency* and the size of imperfections (created deliberately) behind reinforcing bars on the bond strength of the bars

was studied using shotcrete "pull-out" specimens sprayed with the *dry-mix* process. However, as the desired range of the imperfection sizes could not be obtained, cast in-place "pull-out" specimens were built with artificially created voids. This strategy allowed to study the reduction of the bond strength by knowing the precise size of the voids. The results suggest that the best bond performance of a bar is obtained, given an appropriate spraying technique, when the optimal combination between the mixture *consistency* and the airflow rate is used. Moreover, reinforcing bars encased with shotcrete slip less, relative to concrete, than those encased with cast in-place concrete because of the high compaction with which the mixture is placed. Additionally, a void's transversal length (in contact with the bar) of about 20% of the bar's nominal perimeter was found to be the threshold beyond which an important change of the bond performance occurs.

Keywords: Shotcrete; Sprayed concrete; Consistency; Voids; Artificial voids; Encapsulation; Bond strength; Hypothesis testing.

Highlights:

- Concrete sprayed properly offers better *slip stiffness* than cast in-place concrete
- Shotcrete voids were recreated using *artificial voids* made of silicone
- A void's transversal length of approximately 20% sets a bond performance threshold
- The height of the voids does not greatly influence the bond strength of a bar
- The optimal combination between the *consistency* and the airflow rate must be sought

3.3 Introduction

Shotcrete is a method of concrete placement in which the mixture is sprayed at high velocity onto a surface using compressed air. Nowadays, its use in North America has increased substantially and structural elements such as shear walls [4], columns [3], girders [2] and shells [1, 2] are being built entirely with it, mostly, because little formwork (if any) is needed. However, concerns regarding the encapsulation quality of the reinforcing bars have been raised due to the "shadow" zone existing behind the bars. To avoid the creation of imperfections[12] in that area, good practice guidelines state that an appropriate spraying technique, in combination with an

[12] Imperfections may take the form of entrapped aggregates (*sand lenses*) or voids.

adequate mixture *consistency*, needs to be used [9-13]. Nozzle operators (often called nozzlemen) are required to, among others, continuously move the nozzle in small circles, stand at the right distance from the receiving surface and hold the nozzle at the right angle relative to the receiving surface while spraying the concrete [9]. Albeit this is true for both processes of shotcrete available (*dry-* and *wet-mix*), the peculiarity of the *dry-mix* process is that the nozzlemen control the flow of water and thus, their experience plays a more important role than in the case of the *wet-mix* process regarding the encapsulation of reinforcing bars [10]. With the *dry-mix* process, mixtures sprayed "too wet" (with high water content) will probably slough off the surface before the desired buildup thickness is attained whereas mixtures sprayed "too dry" (with low water content) will lack sufficient plasticity to flow around the bars and voids behind them may be created. Nonetheless, for a given *consistency* above the optimal, voids created by experienced nozzlemen will be smaller than those created by unskilled nozzlemen [10]. In general, it has been suggested to spray *dry-mix* shotcrete at its *wettest stable consistency* which refers to a mixture having the maximum amount of water before it sloughs off the receiving surface [10, 112]. For *dry-mix* process mixtures with an 8-10% cement replacement with silica fume, a *consistency* ranging between 0.5 and 1.4 MPa should be sought [11] to avoid excessive rebound (the mass of un-adhered particles expressed as a percentage of the total mass of the sprayed mixture) and to maximize the buildup thickness. Unfortunately, recommendations regarding the optimal mixture *consistency* to achieve the proper encapsulation of reinforcing bars in combination with their best bond performance have not been suggested.

Despite the use of the proper *consistency* and spraying technique, imperfections may also be created, among others, due to heavily congested zones of reinforcing bars within members, difficult conditions at the job site or the use of set-accelerators (mostly when using the *wet-mix* process). In these cases, the bond strength of the bars is expected to decrease since the bond stress will not be transferred uniformly to the bar from the surrounding concrete. Indeed, it has been shown that the ultimate bond strength of a bar will drastically decrease as the size of the imperfections behind it (which were qualitatively characterized) increases for a given concrete compressive strength [12]. In contrast with cast in-place concrete, the height of the concrete below the bars should not cause an additional reduction of the bond strength (unless the mixture is sprayed "too wet" and plastic settlement occurs) because less bleeding is observed in shotcrete [8]. Nonetheless, detailed information about the dimensions, type, and distribution of the

imperfections and their effect on the bond strength and the slip performance of the bars is almost inexistent in the literature. To the knowledge of the authors, only the transversal length of a void has been investigated in the past [52]. The results showed how the bond strength of plain round bars decrease linearly and proportionally, regardless of the concrete compressive strength, as the transversal length of a void increases. The purpose of this paper is to assess the impact of the mixture *consistency* and of the transversal dimensions of imperfections on the bond strength of deformed reinforcing bars encased with shotcrete. The results will ultimately be useful to set acceptance criteria for the evaluation of cores taken from shotcrete pre-construction panels[13] and even for the future development of guidelines regarding the detailing of the reinforcement during the design phase of a structure.

3.4 Experimental program

3.4.1. Test specimens

Shotcrete "pull-out" specimens were built in the laboratory using the *dry-mix* process so the nozzlemen could intentionally change the water added to the mixture and create a wide range of reinforcing bar encapsulation qualities. The mixture was sprayed into wooden rectangular panels as the one shown in Figure 3.1 in which all of the reinforcing bars were positioned with their longitudinal ribs facing the sides of the panels.

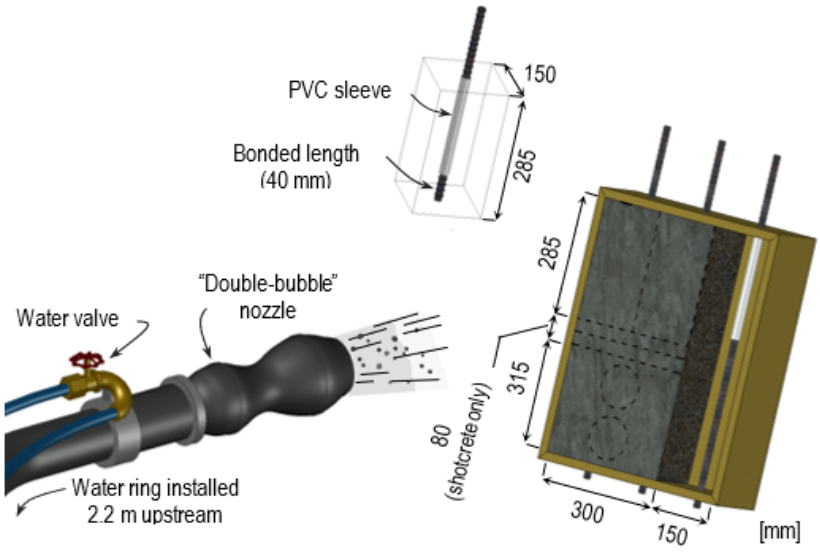

Figure 3.1: Representation of the spraying operation

[13] Panels often used in complex shotcrete projects to recreate the challenging parts of the actual structure.

Two nozzlemen (referred henceforth as N1 and N2) sprayed the concrete using an ALIVA® 246.5 spraying machine with the water ring installed 2.2 meters upstream from a "double-bubble" nozzle. Both nozzlemen were asked to spray the concrete using three different flows of water ranging from high (the "wettest" *consistency*) to low (the "driest" *consistency*) without changing the chosen rate of airflow and using a proper spraying technique. In that manner, only the ability of each nozzleman to specify the appropriate rate of airflow before shooting and to choose the mixture *consistency* would influence the creation of imperfections. However, as the desired range of imperfection sizes could not be obtained, cast in-place specimens (using the same pre-bagged shotcrete mixture) in which the voids were recreated using silicone were built. Such strategy allowed to better correlate the measured bond strength to the known void sizes by overcoming the difficulties related to spraying. Moreover, similar mixture properties from one specimen to another were obtained. In such cases, the concrete was placed and consolidated in accordance with the ASTM C192/C192M-16a standard [92].

The blocks were stripped 1 day after the spraying or the casting operations and were subsequently cured for one week using wet burlap. The blocks were then cut following the dotted lines shown in Figure 3.1 over the mold to obtain three specimens per panel. Each specimen consisted of a 150 x 150 x 285 mm prism with a single 16 mm nominal diameter (d_b) reinforcing bar concentric with the longitudinal axis of the prism as shown in Figure 3.1. The initial length of the reinforcing bar was protected with a 245 mm long PVC sleeve to leave a 40 mm ($2.5d_b$) bonded length (the portion of the bar in contact with concrete) at the opposite end of the specimen from which the bar was pulled. The relatively short bonded length was chosen to avoid the yielding of the reinforcing bars during the tests and did not contain any grade or manufacturer markings.

3.4.2. *Artificial* and shotcrete voids

Artificial voids were made of silicone and were used in combination with cast in-place specimens only. First, the fresh silicone was inserted into hollow plastic tubes to create voids' nominal transversal lengths, referred to as *un-bonded* perimeters (or *u.p.*) henceforth, of 10, 20 and 30% (refer to Figure 3.2a); the *un-bonded* perimeters are expressed as a percentage of the nominal perimeter of the bar. The hardened silicone was then extracted from the plastic tubes, whose only objective was to act as molds, and were subsequently cut longitudinally in two halves.

The resulting pieces were then glued over the entire bonded length of the reinforcing bars using the same material.

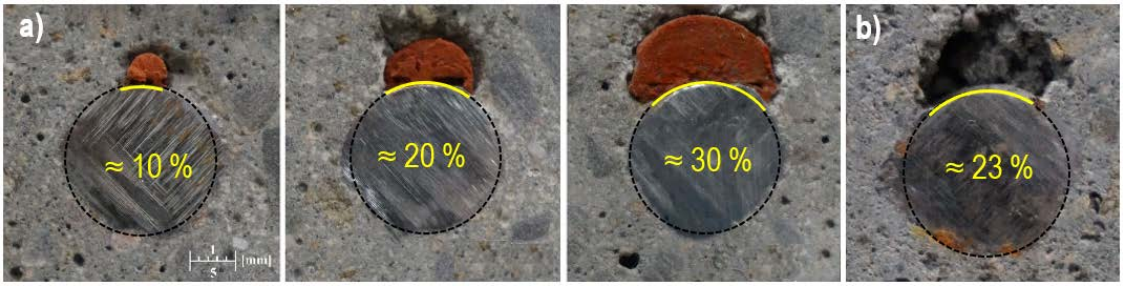

Figure 3.2: (a) Typical *un-bonded* perimeters (*u.p.*) of cast in-place and (b) of *dry-mix* shotcrete specimens

The *un-bonded* perimeter was precisely measured at the bottom of each "pull-out" specimen (for both cast in-place and shotcrete), once they had been cut-out, using high-quality photographs in combination with a CAD software. The values of the *u.p.* were obtained by measuring the length of a circular arc placed over the photograph at the interface between the bar and the void. Only for shotcrete specimens, two (2) 40 mm thick concrete slices were cut from the blocks adjacent to the location of the "pull-out" specimens (see Figure 3.1) resulting in four (4) additional measures of the *u.p.*; a typical shotcrete void is shown in Figure 3.2b.

3.4.3 Properties of concrete

The remaining concrete from the blocks was cored to obtain cylinders [97, 113] for compressive strength [99] and boiled water absorption (B.W.A.) and permeable voids (P.V.) [98] tests for both methods of concrete placement. For shotcrete specimens, the percentage of rebound was measured by spraying each mixture onto a vertical steel panel pin-connected to the wall and supported by a load cell. The *consistency* of the mixture on the panel was then measured using a pocket penetrometer. The measurements in which the tip intercepted a coarse aggregate were discarded and taken again. Moreover, to calculate the in-place *w/b* ratio of each mixture, the mass of the water evaporated from a sample of fresh paste using a microwave oven [93] and the mass of the particles finer than 75 µm lost when a sample of fresh paste was washed over a No. 200 sieve [95] were obtained. The rate of the airflow could not be recorded due to a malfunction issue with the equipment. In the case of cast in-place specimens, the slump [22] and the air content [96] were also measured.

3.4.4 Mixture design

Due to the different nature of the mixing process between sprayed and cast in-place concrete, a slight change in the latter's mixture design was done to obtain comparable concrete properties. Firstly, a constant *w/b* ratio of 0.45, which lies between the common range of shotcrete values [114], was chosen for all cast in-place specimens. Secondly, a polycarboxylate based ASTM C494/C494M-19 [106] type A and F water reducer was used to make the cast in-place mixture workable, yet stable enough, to avoid excessive bleeding. In this manner, the *artificial voids* were properly encased without creating undesired additional imperfections around them. Lastly, the polypropylene fibers were removed to facilitate mixing. Since fibers are only incorporated to withstand relatively low stresses caused by plastic shrinkage, the mechanical properties of the concrete were not considerably altered. The mixture composition of both methods of concrete placement is shown in Table 3.1.

Table 3.1: Mixture composition of the concrete placement methods

Component	*Dry-mix* shotcrete	Cast in-place mixture
Ordinary Portland cement (kg/m^3)	388.3	388.8
Silica fume (kg/m^3)	33.9	34.0
Coarse aggregate 2.5 – 10 mm (kg/m^3)	556.8	702.6
Sand 0.08 – 5 mm (kg/m^3)	1152.6	1008.0
Water (kg/m^3)	190.1	189.6
Polypropylene fibers (kg/m^3)	1.0	-
Air (%)	4.5‡	4.5§
Water reducer (ml/100 kg of binder)	-	500
w/b ratio	0.45*	0.45

‡ Based on the range of values obtained by the manufacturer; § Based on the ASTM C231/C231M-14 standard; * Set for comparison purposes

3.4.5 Reinforcing bars

The reinforcing bars came from the same heat of steel and their mechanical properties were obtained from three (3) samples. Additional samples were cut longitudinally at 45 and 90 degrees with respect to the plan of the longitudinal ribs to measure the geometrical properties as shown in Figure 3.3.

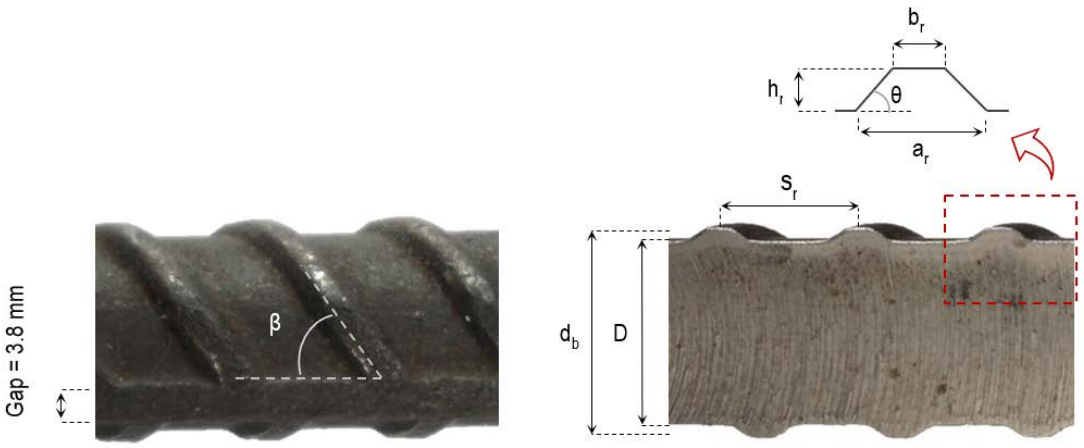

Figure 3.3: Longitudinal cut of a bar with its geometry nomenclature

The measurements were performed over 10 ribs using high-resolution photographs and a CAD software for each longitudinal cut. Table 3.2 summarizes the mean mechanical and geometrical properties from the three (3) and 20 measurements respectively.

Table 3.2: Mechanical and geometrical properties of the reinforcing bars

Type	Parameter	Test bar #16
Mechanical	Young's modulus, Es (GPa)	197
	Yield strength at 0.2%, *fy* (MPa)	378
	Ultimate strength, *fu* (MPa)	562
	Elongation at rupture, εmax (%)	17.7
Geometrical	Nominal diameter, db (mm)	16.0
	Core diameter, D (mm)	15.1
	Ribs' height, hr (mm)	1.0
	Ribs' top width, br (mm)	2.1
	Ribs' base width, ar (mm)	5.5
	Ribs' spacing, sr (mm)	10.8
	Ribs' face angle, θ (degrees)	31
	Ribs' inclination, β (degrees)	53
	Σ gaps (mm)	7.6
	Relative rib area*, Rr (adim)	0.088

*Based on Fei et al. [45]

3.4.6 Testing procedure

The specimens were tested using a 322 MTS test frame and the slip of the reinforcing bars was recorded by two linear position sensors with return spring attached to the loaded end of the bar as shown in Figure 3.4. A 25 mm thick steel plate attached to the base of the test frame by 4 plain steel rods retained each specimen. Additionally, a 2 mm thick rubber sheet and a 9 mm thick steel plate were placed over the top surface of each specimen to assure the load was applied uniformly and to reduce the frictional resistance between the concrete and the steel. An additional 9 mm steel plate was placed on top of the 25 mm thick plate over which the probe tips of the position sensors were laid on to provide an un-deformed surface during the test.

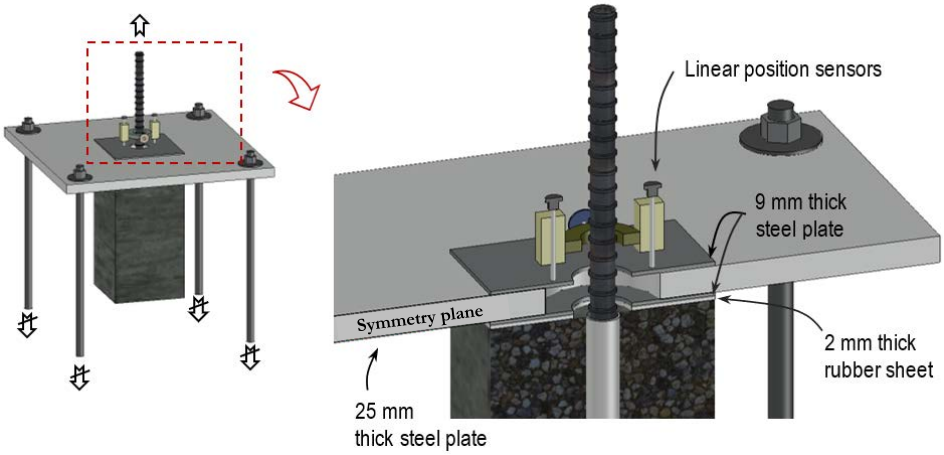

Figure 3.4: Test set-up for the "pull-out" specimen

Shotcrete specimens had to be capped with self-leveling epoxy because of their sometimes less perfect top surface due to the presence of entrapped aggregates at the corners. Tests were conducted at 1.0 mm/min displacement control and were performed 21 days after the specimens were cast or sprayed; this represented the minimal time required to prepare the specimens for testing (curing, cutting, drilling cores, capping, etc.).

3.4.7 Test parameters

The parameters studied for each method of concrete placement and their respective material properties, measured at 21 days, are summarized in Table 3.3 (refer to Section F.1 in Appendix F for additional data). The specimens have been divided into families whose label indicates the method of concrete placement (S: shotcrete or CIP: cast in-place) followed by specific attributes proper to each one of them. The attributes of the shotcrete families indicate

the number assigned to each nozzleman (N1: number 1 or N2: number 2) followed by the water content used by each one of them (H: highest, M: medium or L: lowest). For cast in-place specimens, the first number indicates the height of the *artificial void*; "h" and "2xh" being half and the complete transversal length of the *un-bonded* perimeter respectively as shown in Figure 3.5.

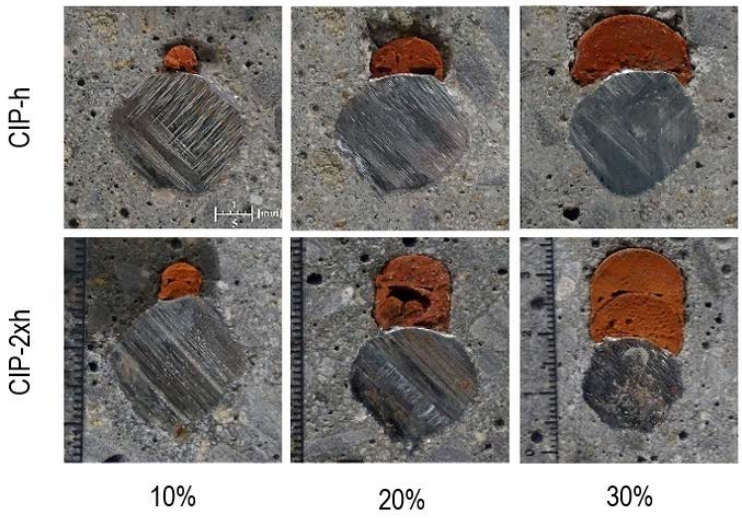

Figure 3.5: The heights of the *artificial voids* tested

Only *un-bonded* perimeters ranging from 0 (perfect encapsulation) to 30% were tested because larger values would probably produce unacceptable rebound producing a poor quality shotcrete which in turn, would induce durability issues. The label used to designate specimens having perfect encapsulation is not followed by any specific attribute since no voids were present.

Three (3) and two (2) specimens were built for each configuration of the shotcrete and the cast in-place families respectively, however, only two (2) out of three (3) specimens sprayed by nozzleman N1 could be tested due to excessive rebound in some areas of the panel. Individual specimens within each family of both methods of concrete placement were labeled alphabetically (A, B or C). The standard deviation is presented in parentheses in Table 3.3 wherever it was deemed pertinent. The *consistency* values represent the mean of 10 readings and in the case of mixture S-N2-L, all readings reached the maximum scale of the pocket penetrometer (4.8 MPa). Specific comments relative to the plastic state of the mixture, the type of voids and the

encapsulation quality of the bars have been added to Table 3.3 for each mixture. A total of 29 "pull-out" specimens were tested; 15 were sprayed and 14 were cast in-place.

Table 3.3: Results of concrete properties for the cast in-place and *dry-mix* mixtures

Placement method	Family	Nominal *un-bonded* perimeter, *u.p.* (%)	*w/b*	$f'_{c\ 21d}$ (MPa)	B.W.A. (%)	P.V. (%)	Rebound (%)	*Consistency* (MPa) / Slump (mm)	Air (%)	Comments§
Dry-mix shotcrete	S-N1-H (A-B)	Measured after spraying	0.40	41.9	7.8	16.8	19	1.4 (0.2)	-	P.E.
	S-N1-M (A-B)		0.35	44.7	7.5	16.5	28	2.2 (0.5)		V.
	S-N1-L (A-B)		0.32	47.3	6.4	14.1	16	2.9 (0.3)		V.
	S-N2-H (A-C)		0.44	40.0	7.9	16.9	22	0.8 (0.1)		C.S., ν.
	S-N2-M (A-C)		0.36	49.7	6.7	14.6	20	1.4 (0.2)		P.E.
	S-N2-L (A-C)		0.25	44.7	7.8	16.9	40	≥ 4.8 (-)		V.
Cast in-place	CIP (A-B)	0 - - -	0.45	49.3 (0.5)	6.8 (0.4)	15.1 (0.9)	-	180 (20.6)	4.7 (0.3)	P.E.
	CIP-h (A-B)	- 10 20 30								*Artificial voids*
	CIP-2xh (A-B)	- 10 20 30								

§ P.E.: Perfect encasement, ν.: Voids of negligible size (≤ 1% *u.p.*), V.: Voids (≥ 20% *u.p.*), C.S.: Concrete sloughing

3.5 Results and discussion

The following section presents the results of the "pull-out" specimens divided into 3 main sections. Firstly, the bond strength of the bars is correlated to the mixture *consistency*, secondly, to the *un-bonded* perimeter and finally, to the failure mode of the specimens. Different values obtained from the load – slip curves have been used for comparison purposes. The load – slip performance of shotcrete specimens has also been compared to the one of cast in-place specimens to validate and assess the limitations of using *artificial voids* to the study bond strength of a bar. The elastic elongation of the bars was subtracted from the measured slip and therefore, the values represent the net slip of the bars. All assertions are supported by well-established statistical tests.

3.5.1 Shotcrete application in terms of bar-concrete bond strength

The loads measured at 0.25 mm of the bars' slip ($P_{0.25}$) and the ultimate load (P_{max}) have been correlated to the mixture *consistency* of each shotcrete family and are shown in Figure 3.6a and b. The 0.25 mm slip has been chosen since it is considered a "critical" slip value which onsets excessive damage in reinforced concrete structures [59, 115].

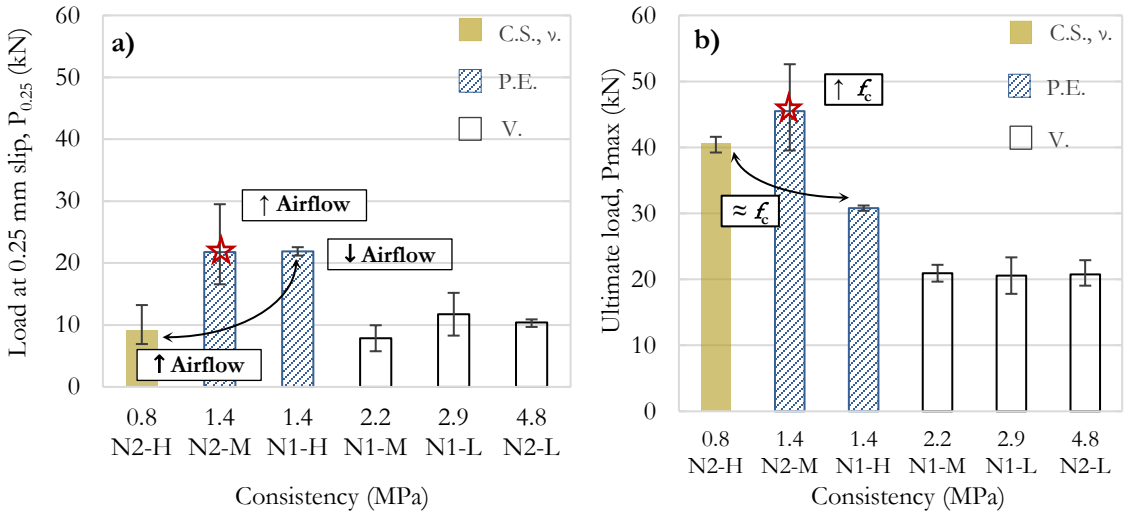

Figure 3.6: (a) Loads at 0.25 mm slip and (b) the ultimate load vs. *consistency*

The whiskers indicate the minimal and the maximal values measured away from the means. Moreover, the results have been categorized into three groups based on the comments made in the last column of Table 3 which emphasize the encapsulation quality of the bars and the plastic state of the mixture. Even though the compressive strength of concrete (f_c) varies from one family to the other, the loads were not normalized relative to one particular f_c because the bond strength is preferentially influenced by the size of the voids (if present) rather than by the mechanical properties of the concrete [52].

From Figure 3.6a and b, it can be seen that the specimens sprayed with a mixture *consistency* of 1.4 MPa (perfect encapsulation) were able to achieve higher loads than the rest of the specimens at 0.25 mm of the bars' slip. Although the ultimate loads of the specimens sprayed by nozzleman N1 using this *consistency* were not as high as those sprayed by nozzlemen N2, their bond strength exceeded the ones achieved by specimens in which voids were created behind the bars. The slower airflow rate used by nozzlemen N1, as it was perceived during the spraying operations,

may have caused this bond strength reduction relative to specimens sprayed by nozzleman N2 even though in both cases the bars were perfectly encased and the same mixture *consistency* was used with an adequate spraying technique. Since the bond strength obtained with specimens from family S-N2-M had the greatest values (mean values enclosed with a star in Figure 3.6a and b) they will be subsequently used as the reference family for comparison purposes.

The considerably lower $P_{0.25}$ values that were obtained using a *consistency* of 0.8 MPa (family S-N2-H) were probably caused by the presence of a lower strength concrete surrounding the bars. Since the rate of the airflow used was the same as with the reference family and the bars were also perfectly encapsulated, their ultimate loads were similar but higher slip values were obtained with a 0.8 MPa *consistency* as seen from the load - slip curves in Figure 3.7a. Conversely, the opposite effect was observed with bars belonging to family S-N1-H in which nozzlemen N1 used a *consistency* of 1.4 MPa (which proved to be the most adequate for this mixture) but perhaps not the optimal airflow rate. In such case, the *slip stiffness* (the ascending slope of the slip – load curve) was similar to the reference family but because the optimal compaction was not achieved due to the observed lower airflow rate used, the ultimate load was considerably reduced. Therefore, it seems that the approximately equal f_c of families S-N1-H and S-N2-H (refer to Figure 3.6b) is the result of two different events which compensate one another; either a high content of water was used with a higher airflow rate (S-N2-H) or a low water content was used with a lower airflow rate (S-N1-H). The differences of bond performance cannot be attributed to different in-place mixture proportions since the rebound of families in Figure 3.7a were all similar (between 19 and 22%) as shown in Table 3. Specimens sprayed with *consistencies* of 2.2 MPa and higher resulted in considerably lower loads at any slip in comparison with the reference family, regardless of the nozzle operator (refer to Figure 3.6a and b), because imperfections behind the bars were present. Moreover, the loads at any slip and the *slip stiffness* among them were almost the same as shown in Figure 3.7b; this occurred even though imperfections varied in size (*un-bonded* perimeters from 21 to 36% as shown in Section F.2 in Appendix F), the specimens were shot using different airflow rates and the mixtures possessed different properties (*w/b* ratio, rebound, and *consistency*).

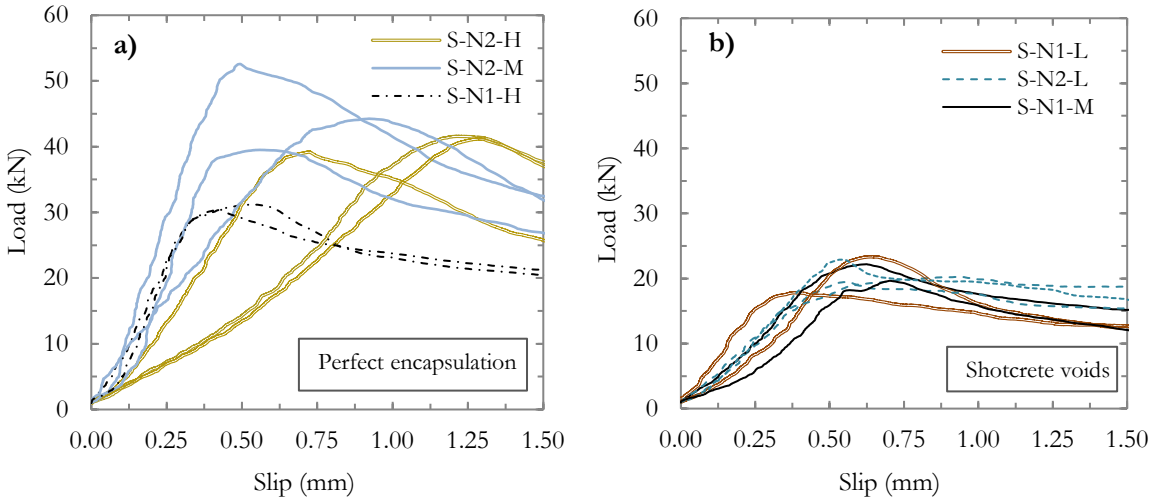

Figure 3.7: (a) Load-slip curve of perfectly encased bars and (b) those having voids

However, it was not certain if such similarities occurred because the aforementioned range of *un-bonded* perimeters was similar enough to cause the same bond strength reduction or because the large variability of the shotcrete *un-bonded* perimeters makes the use of a mean value a somewhat imprecise representation of the encapsulation quality of the reinforcing bars. What is certain is that there is an optimal combination of the mixture *consistency* and the airflow rate with which the best bond performance of the reinforcing bars is achieved. Despite lower consistencies (high water content) are usually preferred to ease the proper encapsulation of the bars [12], excessively low ones need to be avoided to obtain an optimal slip stiffness and prevent the plastic settlement of the mixture. Additionally, spraying with excessively high consistencies (low water content) may create voids behind the bars, even if the adequate airflow rate and the appropriate spraying technique are used. Targeting the highest possible limit of the mixture *consistency* (without producing excessive rebound) and controlling the airflow rate will guarantee the proper compaction of the mixture around the bars and their proper encapsulation (given the use of an adequate spraying technique) and therefore the best bond performance of the reinforcing bars will be obtained. In fact, for the mixture under study, a *consistency* of around 1.4 MPa, which represents the upper limit recommended for this type of mixture [11], seems to be the most adequate. Actual values regarding the adequate airflow rates for *dry-mix* shotcrete can be obtained from Armelin [25] for different hose diameters and distances away from the receiving surface.

3.5.2 One-way ANOVA

To formally support our previous assertions and to determine if differences between the population means (μ) of $P_{0.25}$, P_{max} and the ultimate *slip stiffness* (K_{su}) of each family truly exist, an ANOVA (*analysis of variance*) test was performed. This is formally done by defining a *null* (H_0) and an *alternative hypothesis* (H_a) which test if the means of each family are equal or if at least one pair between them is different as expressed in Equation 3.1. For the purpose of this study, K_{su} was defined as the ascending slope of the load – slip curve between 40 and 70% of P_{max}.

$$H_0: \mu_1 = \mu_2 = \ldots = \mu_n \text{ for n families}$$

$$\text{vs.} \tag{3.1}$$

$$H_a: \mu_i \neq \mu_j \text{ for at least one pair (i, j)}$$

The outcome of the test, most frequently expressed with a *p-value*, determines if there is enough evidence to accept H_0 or if it should be rejected. The *p-value* represents the level of risk a *decision-maker* is willing to take at the moment H_0 is accepted or rejected; a decision based on a *p-value* equal to 0.05 implies taking a risk of 5% to falsely reject H_0. The *p-value* is obtained based on the calculated $F_{0(u,v)}$ test-statistic (distributed as *F*) using each sample mean ($\bar{y}$) in which *u* and *v* represent the degrees of freedom corresponding to the mean square between the treatments and of the error respectively. When a precise level of risk is established as the threshold to accept or reject H_0, its value is called the *level of significance* (α) of the test. In this case, a *p-value* smaller than α would imply that H_0 should be rejected in favor of H_a.

Here, the ANOVA test resulted in a *p-value* = 0.011 ($F_{0(5, 9)}$ = 5.90) for comparisons between $P_{0.25}$, a *p-value* < 0.000 ($F_{0(5, 9)}$ = 25.28) for comparisons between P_{max} and a *p-value* = 0.027 ($F_{0(5, 9)}$ = 4.34) for comparisons between K_{su} (refer to Section F.3 in Appendix F for additional data). As suspected, there exists sufficient evidence to reject H_0 in favor of H_a based on α = 0.05. Therefore, we can conclude that there is at least one mean which differs from the rest for all three (3) parameters under study. The results, however, do not explicitly indicate which means are different from one another. For that purpose, a pairwise comparison between all of the 15 possible combinations between the means was done for each of the three (3) groups. The preferred comparison method was the Fisher's Least Significant Difference (LSD) method

because the ANOVA results were significant at $\alpha = 0.05$ [116]. The results of the test are shown in Table 3.4 for a *level of significance* equal to 0.05. The mean values of each parameter associated to the same letter (A, B or C) indicate a statistical equivalency.

All of the assumptions needed to use the ANOVA test were verified; perhaps the most important one, stating that the families should possess equal variances, was checked using the Modified Levene Test. Additional information about the ANOVA test and the LSD method is provided by Montgomery [117] and Quinn et al. [118].

Table 3.4: Results of the Fisher's LSD method ($\alpha = 0.05$)

Family	*Consistency* (MPa)	$\bar{y}$ of K_{su} (kN/mm)	LSD	$\bar{y}$ of $P_{0.25}$ (kN)	LSD	$\bar{y}$ of P_{max} (kN)	LSD
S-N2-H	0.8	52.2	C	9.1	B	40.7	A
S-N2-M	1.4	108.9	A	21.8	A	45.5	A
S-N1-H	1.4	108.4	A B	21.9	A	30.8	B
S-N1-M	2.2	46.0	C	7.9	B	20.9	C
S-N1-L	2.9	57.2	B C	11.7	B	20.6	C
S-N2-L	> 4.8	46.4	C	10.4	B	20.8	C

In general, the results confirm the presence of significant differences between specimens sprayed with *consistencies* of 1.4 MPa and those in which concrete sloughing and voids were observed for all three (3) parameters under study. As stated in the previous section, the best bond performance was achieved with specimens belonging to the reference family (S-N2-M) in which a higher airflow rate and the optimal amount of water were used. The consequences of increasing the water content and producing a *consistency* of 0.8 MPa, as for specimens belonging to family S-N2-H, can be clearly observed as their mean K_{su} and $P_{0.25}$ are statistically equal to the values obtained with specimens having voids behind the bars (letter C and B respectively). A significantly lower P_{max} was also detected for specimens belonging to family S-N1-H (letter B) which were sprayed with a slower airflow rate in comparison with those sprayed by nozzleman N2 (letter A). Moreover, all the mean $P_{0.25}$, P_{max}, and K_{su} obtained with specimens having voids, independently of the nozzlemen, resulted in statistically similar results and provided the lowest values.

3.5.3 The *un-bonded* perimeter

Although the spraying technique used by both nozzlemen followed good practice guidelines [9], the evaluation of shotcrete imperfections (as discussed in Section 3.4.2) revealed that they consisted of both voids and entrapped aggregates all along the bonded length of the specimens' test bar as shown in Figure 3.8. The imperfections were only observed behind the bars and despite their presence, the quality of the mixture elsewhere was determined as "good" for all of the specimens based on Morgan's scale [119] in which the B.W.A. and the P.V. measurements presented in Table 3.3 are taken into account.

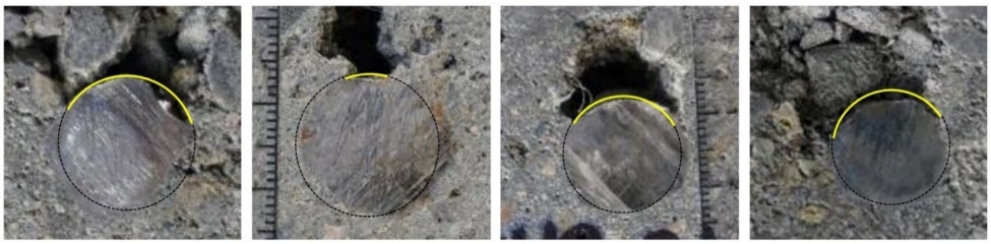

Figure 3.8: Typical shotcrete imperfections behind reinforcing bars

To study their impact on the reduction of the bond strength, the *un-bonded* perimeters of the shotcrete specimens was plotted against P_{max} as shown in Figure 3.9a. Only the minimal and the maximal values of the voids' *un-bonded* perimeter, depicted by the whiskers, are shown. However, their complete sampling distribution (including the 25, 50 and 75 percentiles) based on the 5 cuts discussed in Section 3.4.2 are shown in Figure 3.9b. Additionally, their order of vertical appearance is the same as it is in Figure 3.9a.

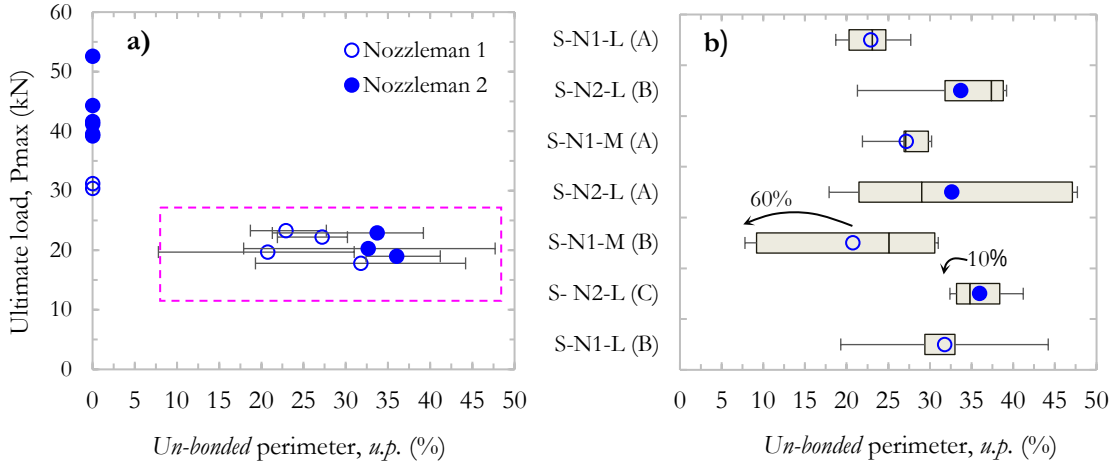

Figure 3.9: (a) Loss of bond strength caused by imperfections and (b) their distribution

As can be observed, the scatter away from the mean *un-bonded* perimeter varies highly from one specimen to another and ranges from as much as 60% to as little as 10%. Moreover, their distribution does not seem to be normal. Based on this and because *un-bonded* perimeters around 10% were not obtained, it became clear that assessing the reduction of the bond strength as a function of the *un-bonded* perimeter would be a difficult task to accomplish with shotcrete specimens; even if an increased number of them were built.

The use of *artificial voids* was intended to tackle these limitations because their mixture had the same fresh and hardened properties and because the geometry of the voids was precisely known. Figure 3.10 shows the average load evolution, from $P_{0.25}$ towards P_{max}, as a function of the mean *un-bonded* perimeter obtained with cast in-place specimens having *artificial voids*.

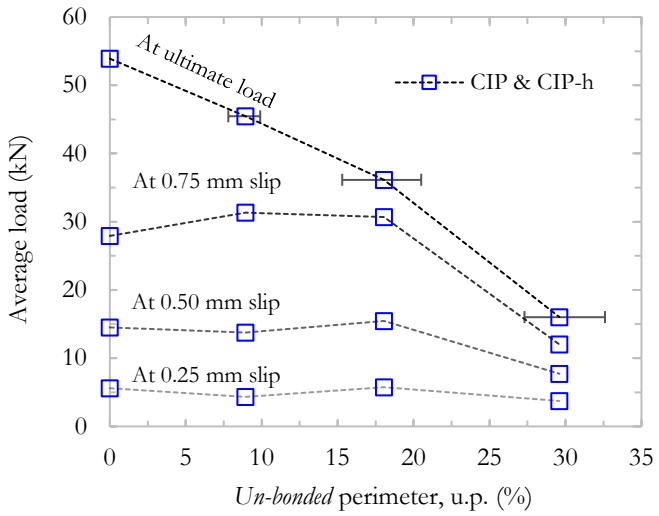

Figure 3.10: Evolution of the average load as a function of the *u.p.*

The minimal and maximal values of each mean *un-bonded* perimeter are indicated using horizontal whiskers which are only shown in the ultimate load curve for clarity reasons. As it can be observed, the ultimate bond strength reduction is linear (but it is not proportional to the *un-bonded* perimeter). However, before the ultimate load is reached, the loads obtained with specimens having nominal *un-bonded* perimeters of 20% and less are approximately equal to the loads obtained with specimens having a perfect encapsulation; nominal *un-bonded* perimeters greater than 20% cause a drastic bond strength reduction.

Thus, the results obtained with *artificial voids* successfully complement those obtained with shotcrete specimens. Indeed, cast in-place specimens with *artificial voids* made it possible to limit the scatter associated to the *un-bonded* perimeter measurements of shotcrete specimens and made it possible to visualize the different bond performance prior to and once the ultimate load was attained. This apparent change in bond performance may be attributed to the redistribution of the stress that can only occur with *un-bonded* perimeters below 20%. This vale, albeit unconservative because "pull-out" specimens slightly overestimate the bar-concrete bond strength, defines the threshold beyond which the bond performance results inadequate. Beyond this threshold, the ultimate load was reduced approximately by almost 50% to 70% once the *un-bonded* perimeter reached 30%.

3.5.4 The effect of a void's height

To assess if the use of the *un-bonded* perimeter alone was sufficient to adequately explain the reduction of the bond strength, the ultimate load of specimens belonging to family CIP-2xh, in which the height of the voids was doubled, was compared to the ultimate load of specimens belonging to family CIP-h. As can be seen from Figure 3.11, even though the linear function belonging to family CIP-2xh lies below the one belonging to family CIP-h, the reduction does not seem to be significant.

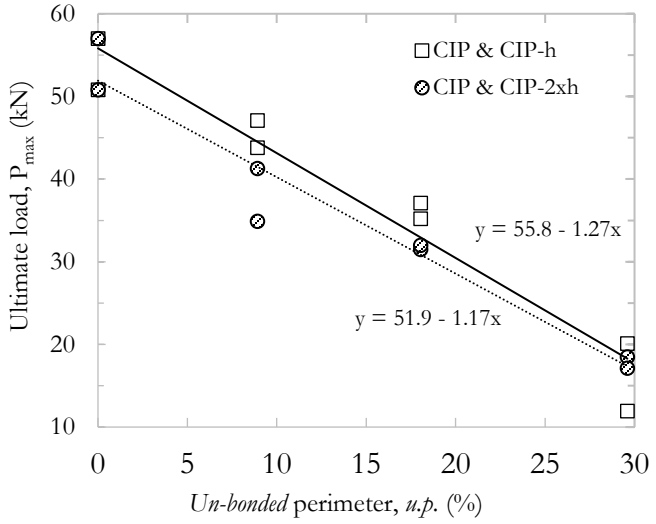

Figure 3.11: Influence of the voids' height on the ultimate bond strength of a bar

To confirm this, both linear functions were compared based on a hypothesis testing procedure [120] designed to test whether the intercept (β_{0i}) and the slope (β_i) of both functions are equal or not. Once it was verified that each function was significant and adequately linear with an ANOVA test, the *null* (H_0) and the *alternative hypothesis* (H_a) were defined as expressed in Equation 3.2.

$$H_0: \begin{bmatrix} \beta_{01} \\ \beta_1 \end{bmatrix} = \begin{bmatrix} \beta_{02} \\ \beta_2 \end{bmatrix}$$

$$\text{vs.} \tag{3.2}$$

$$H_a: \begin{bmatrix} \beta_{01} \\ \beta_1 \end{bmatrix} \neq \begin{bmatrix} \beta_{02} \\ \beta_2 \end{bmatrix}$$

The test resulted in a *p-value* = 0.391 ($F_{0(2,12)}$ = 1.02) from which we can conclude that, at any relevant *level of significance* ($\alpha \leq 0.05$), there is not enough evidence to reject H_0 and that the bond strength reduction is not significantly influenced by the height of the voids (refer to Section F.4 in Appendix F for additional data). The meaning of the outcome is extremely relevant because the height of actual shotcrete voids would have been extremely difficult to characterize. Thus, whenever the encapsulation quality of a bar may need to be evaluated *vis-à-vis* its bond performance, the use of the *un-bonded* perimeter as the sole parameter to do so would be sufficient.

3.5.5 Shotcrete vs. *artificial voids*

At this point, the suitability of using *artificial voids* to capture the response of actual voids created with shotcrete needs to be studied. For this purpose, comparisons between parameters obtained from the load – slip curve of shotcrete and cast in-place specimens were performed. Both perfectly encapsulated bars and those having voids behind them were used. In the former case, specimens from the family S-N2-M were compared to specimens from the family CIP since they had approximately the same hardened concrete properties (refer to Table 3.3). In the latter case, families S-N2-L and CIP-h 30 were compared because the *un-bonded* perimeters (which ranged between 30 and 36%) were fairly similar. Since the height of the specimens showed to have no significant impact on the ultimate bond strength of a bar, specimens belonging to family CIP-2xh 30 were also included in the comparison. Only specimens sprayed by nozzleman N2

were considered since the results suggest that a more appropriate airflow rate was used. Both groups under comparison and the labels corresponding to each specimen are shown in Figure 3.12.

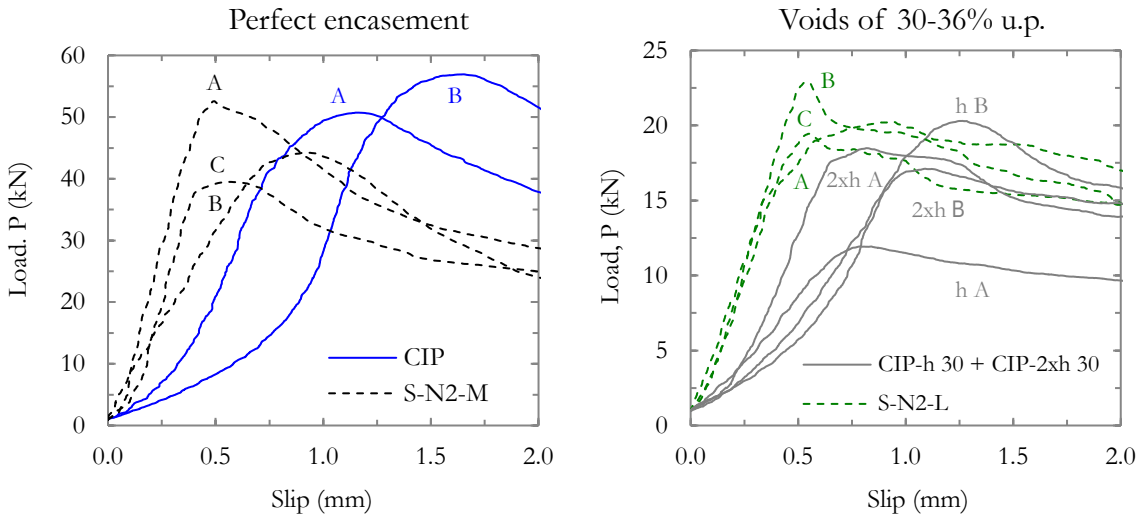

Figure 3.12: Load – slip curves for shotcrete and CIP groups under comparison

As can be observed, the *slip stiffness* of the cast in-place specimens was initially small but it increased as the ultimate load was reached. In contrast, the *slip stiffness* of shotcrete specimens remained constant until the ultimate load was reached. Nonetheless, the *slip stiffness* of the last segment of the ascending curve appears to be approximately the same for both methods of concrete placement. The initial difference between their *slip stiffness* may be due to the inexistence of a "wall effect" around the bars encased with shotcrete because of the high compaction with which shotcrete is placed. Regardless of these bond performance differences, it seems that cast in-place specimens, with and without *artificial voids*, can effectively reproduce the ultimate load obtained with shotcrete specimens.

To formally support these statements, a pairwise comparison between the ultimate load (P_{max}) and the *slip stiffness* was performed. Since the *slip stiffness* of cast in-place specimens changed as the load increased, a distinction between the initial (K_{so}) and the ultimate *slip stiffness* (K_{su}) was made. For the purpose of this investigation, K_{so} was defined as the slope from the beginning of the measurements until 20% of P_{max} and K_{su} as it was done in Section 3.5.2 As before, the comparison relies on a hypothesis testing procedure in which the sample mean ($\bar{y}$) of P_{max}, K_{so},

and K_{su} between the groups are compared to determine if their population means (μ) are equal or not. In this case, the *null* (H_0) and the *alternative hypothesis* (H_a) are expressed in Equation 3.3.

$$H_0: \mu_1 = \mu_2$$

$$\text{vs.} \tag{3.3}$$

$$H_a: \mu_1 \neq \mu_2$$

The *p-value* is obtained based on the calculated $t_{0,v}$ test-statistic (distributed as t) using each sample mean ($\bar{y}$) where v represents the degrees of freedom relative to the sample size. In this case, the population variance of the shotcrete and the cast in-place specimens were not considered to be equal due to the different nature of both concrete placement techniques which normally produces a different spread of the results' distributions. The results of the comparison are shown in Table 3.5 where the resulting decision, based on $\alpha = 0.05$, has been added for each parameter under comparison. Additional information about this test is given by Montgomery [117].

Table 3.5: Unequal variance *t-test* results

Group	Parameter	n*	$\bar{y}$	S†	t_0	v	*p-value*	Result (α = 0.05)
Perfect encasement	P_{max} (kN)	3	45.4	6.6	1.70	2.9	0.189	*E.*
		2	53.8	4.4				
S-N2-M vs. CIP 0	K_{so} (kN/mm)	3	65.3	20.3	3.29	2.8	0.051	*E.*
		2	22.1	8.4				
	K_{su} (kN/mm)	3	108.6	44.1	0.67	2.1	0.572	*E.*
		2	91.5	4.5				
30 - 36% mean *u.p.*	P_{max} (kN)	3	20.7	2.0	1.76	4.8	0.142	*E.*
		4	17.0	3.6				
S-N2-L vs. CIP-h 30 + CIP-2xh 30	K_{so} (kN/mm)	3	30.0	4.7	6.73	2.6	0.010	*N. E.*
		4	10.6	2.1				
	K_{su} (kN/mm)	3	46.4	6.5	4.11	4.8	0.010	*N. E.*
		4	24.9	7.3				

* Number of observations per group; † Standard deviation
E.: Equal; *N.E.*: Not equal given the *level of significance*

The results support the assertion that the ultimate load obtained with shotcrete specimens can be adequately reproduced using cast in-place specimens. Indeed, *p-values* greater than any relevant *level of significance* ($\alpha \leq 0.05$) were obtained for specimens having perfectly encapsulated bars and voids behind the bars. The results also indicate that the same K_{su} is obtained between both methods of concrete placement for perfectly encapsulated bars. This does not happen when voids are present as the *slip stiffness* of the cast in-place specimens changes little as the load increases; it is believed that specimens fail before K_{su} can be developed in that case. Regarding the initial *slip stiffness* (K_{so}), there is strong evidence that the values differ from one method of concrete placement to another. For perfectly encapsulated bars, even though the test result indicates that the values are equivalent, the *p-value* is substantially equal to the *significance level* of 0.05; it would not be unreasonable to say that they are not equal with a risk of falsely rejecting H_0 of 5.1%. In the case where voids are present behind the bars, the results do indicate a difference from one method to the other.

Thus, *artificial voids* represent an interesting approach to study the impact of the *un-bonded* perimeter on the ultimate bond strength of a bar. Moreover, even though the absolute slip values overestimate those obtained with actual shotcrete specimens, it is believed that comparing the relative performance among them can still provide useful information that would be applicable to shotcrete. Indeed, even if the 20% *un-bonded* perimeter threshold was determined with *artificial voids*, it would also have been found with shotcrete specimens if a large number of shotcrete specimens were tested.

3.5.6 Failure mode of the specimens

After specimens failed, their bottom surface was inspected to determine if a *splitting* or a *pull-out* failure had occurred. In the former case, apparent cracks running from the reinforcing bar to the side of the specimens were observed (the concrete cover was forced outward due to the wedging action of the ribs) whereas no cracks were observed in the latter case (the ribs crushed and sheared the concrete in front of them). The results are presented in Table 3.6 for each individual specimen where the range of mean *un-bonded* perimeters and the nominal *un-bonded* perimeter for each family of shotcrete and cast in-place specimens respectively are shown.

Table 3.6: Failure mode of specimens

Placement method	Family	Avg. / Nom. *u.p.* (%)	Comment (see Table 3.3)	Type of failure§		
				Specimen A	Specimen B	Specimen C
Dry-mix shotcrete	S-N1-H	0	P.E.	*SP*	*SP*	-
	S-N1-M	21 - 27	V.	P	P	-
	S-N1-L	23 - 32	V.	P	P	-
	S-N2-H	0	C.S., v.	*SP*	*SP*	*SP*
	S-N2-M	0	P.E.	*SP*	*SP*	*SP*
	S-N2-L	33 - 36	V.	P	*SP*	P
Cast in-place	CIP	0	P.E.	P	SP	-
	CIP-h	10	*Artificial voids*	P	P	-
		20		SP	P	-
		30		P	P	-
	CIP-2xh	10		P	P	-
		20		P	P	-
		30		P	P	-

§*SP*: *Splitting* failure, P: *Pull-out* failure

The general trend, albeit more obvious for the shotcrete specimens, is that the presence of voids induces a *pull-out* failure whereas specimens whose bars are perfectly encased tend to fail by *splitting*. Indeed, for cast in-place specimens, *pull-out* failures prevailed and *splitting* failures occurred sporadically when bars had *un-bonded* perimeters equal to and below 20%, however, a clear tendency could not be truly observed. On the other hand, for shotcrete specimens this tendency was clear since all specimens with perfectly encased bars failed by *splitting* whereas most of those having *un-bonded* perimeters over 20% failed by *pull-out*. Again, this strongly supports the existence of a 20% *un-bonded* perimeter threshold beyond which the bond performance of a bar is considerably altered. Additionally, it highlights the capability of shotcrete to more efficiently compact concrete around reinforcing bars relative to cast in-place concrete.

3.6 Conclusions

The influence of the mixture *consistency* on the bond strength of a reinforcing bar was studied in the first part of this investigation. For this purpose, *dry-mix* shotcrete "pull-out" specimens were built in the laboratory by two nozzlemen who intentionally produced different

qualities of reinforcing bar encapsulation by varying the water added to the mixture. The results indicate that only when the adequate *consistency* is used, in combination with the proper airflow rate and the proper spraying technique, the optimal bond performance of a bar can be achieved. The "driest" *consistency* (slightly above the well-known *wettest stable* limit) within the acceptable limits of a given mixture should be sought to maximize the bond performance of the reinforcing bars whilst their proper encasement and the maximum buildup thickness is achieved and excessive rebound is avoided. Using *consistencies* below the optimal value ("too wet") will cause the bars to attain similar ultimate bond strengths (if they are well encapsulated) as those in which the optimal *consistency* was used but will cause the reinforcing bars to slip faster relative to concrete. Using *consistencies* above the optimal value ("too dry") will increase the chances of creating imperfections behind the reinforcing bars. Thus, *consistency* measurements taken at different stages of a project could provide valuable information regarding the quality of the shotcrete and the bond performance of the bars. In contrast with cast in-place concrete, it was found that the *slip stiffness* of reinforcing bars encased with shotcrete is enhanced due to the high compaction of the mixture around the bars resulting from the spraying process.

Since voids may be created even if the adequate *consistency* is used, the influence of the voids' dimensions on the bond strength of a reinforcing bar was studied in the second part of this investigation. As the desirable range of the voids' sizes could not be created with the shotcrete specimens, cast in-place "pull-out" specimens with *artificial voids* were built. The results showed that whenever the encapsulation quality of a bar may need to be evaluated *vis-à-vis* its bond performance, the use of the *un-bonded* perimeter as the sole parameter to do so is sufficient. Reinforcing bars having voids with *un-bonded* perimeters of about 20% and less develop a similar bond performance as perfectly encapsulated bars before the ultimate load is attained and show a drastic bond strength decrease once the *un-bonded* perimeter exceeds this threshold. Nonetheless, at the ultimate load, the reduction is linear (but not proportional) as the *un-bonded* perimeter increases. The existence of this threshold was also supported by the change of the failure mode of shotcrete specimens (from *splitting* to *pull-out*) once the *un-bonded* perimeter exceeded about 20%. However, because "pull-out" specimens overestimate the bar-concrete bond of most structural elements, its actual value might be slightly smaller.

The findings could help set *un-bonded* perimeter thresholds to avoid the excessive slip of the bars and thus, to prevent the excessive deflection, cracking and the premature failure of structural

elements. Such threshold could be verified during the evaluation of cores taken from pre-construction panels. If *un-bonded* perimeters of a certain size are considered during the design phase nonetheless, modification factors should be developed and specified for the *development length* equation appearing in design codes [5, 6] to assure the ductility of the structural elements. Further studies should be carried out using bond specimens which simulate the stress distribution of flexural elements like the ASTM A944 [17] "beam-end" specimen. Such type of specimen allows to test longer bonded lengths because, opposite to "pull-out" specimens, the concrete around the bar is placed in tension and small concrete covers are used. This would allow to study the bond performance of reinforcing bars with *artificial voids* placed only over a small portion of their bonded length to simulate other possible cases that may be encountered in practice. The use of self-compacting concrete (SCC) to better reproduce the *slip stiffness* of shotcrete specimens when using *artificial voids* should be considered as less bleeding and a better bar-concrete interface, like in shotcrete, are expected. Nonetheless, the results obtained with cast in-place specimens having *artificial voids* should be interpreted with care as only the absolute values of the ultimate load are representative of what is obtained with shotcrete specimens.

3.7 Acknowledgements

The authors are grateful to the Concrete Infrastructure Research Center (CRIB) of Québec, the Natural Sciences and Engineering Research Council of Canada (NSERC), King Packaged Materials and Co., the Canadian Council of Independent Laboratories (CCIL), The American Shotcrete Association (ASA) and the Québec and East Ontario Chapter of the American Concrete Institute (ACI) for their financial support. Furthermore, special thanks are extended to Jean-Daniel Lemay and Mathieu Thomassin-Mailhot (research engineers), to René Malo (expert laboratory technician) and to Pierre-André Tremblay and Alain Melançon (laboratory technicians) of the Department of Civil and Water Engineering at Université Laval for their outstanding work and support during the casting and the testing operations.

3.8 References

[1] Davis, B., "Holcim New Zealand cement terminal," Shotcrete Magazine, Vol. 19, No. 1, 2017 pp. 26-30.

[2] Townsend III, F. E., "Northern boulevard crossing tunnel CQ039," Shotcrete Magazine, Vol. 18, No. 1, 2016, pp. 34-36.

[3] Townsend III, F. E., "The plaza substation and queen structures," Shotcrete Magazine, Vol. 18, No. 1, 2016, pp. 22-23.

[4] Panian, L., Steyer, M., Tipping, S., "Post-tensioned shotcrete shearwalls," Concrete International, Vol. 29, No. 10, 2007, pp. 39-45.

[5] ACI Committee 318, "318-19 Building code requirements for structural concrete and commentary," American Concrete Institute, Michigan, 2019, 559 p.

[6] CSA, "A23.3-19 Design of concrete structures," Canadian Standards Association, Ontario, 2019, 297 p.

[8] Ghio, V. A., Monteiro, P. J. M., "Bond strength of reinforcing bars in reinforced shotcrete," ACI Materials Journal, Vol. 94, No. 2, 1997, pp. 111-118.

[9] Crom, T. R., "Dry mix shotcrete nozzling," Concrete International, Vol. 3, No. 1, 1981, pp. 80-93.

[10] Beaupré, D., Jolin, M., "Effect of shotcrete consistency and nozzleman experience on reinforcement encasement quality," Shotcrete Magazine, Vol. 3, No. 4, 2001, pp. 20-23.

[11] Jolin, M., Beaupré, D., Mindess, S., "Quality control of dry-mix shotcrete during construction," Concrete International, Vol. 24, No. 10, 2002, pp. 69-74.

[12] Jolin, M., Gagnon, F., Beaupré, D., "Determination of criteria for the acceptance of shotcrete for certification," Shotcrete: More engineering developments, 2004, pp. 175-181.

[13] ACI Committee 506, "506R-16: Guide to shotcrete," American Concrete Institute, Michigan, 2016, 52 p.

[17] ASTM, "A944-10(2015) standard test method for comparing bond strength of steel reinforcing bars to concrete using beam-end specimens," American Society of Testing and Materials, 2015, 4 p. https://doi.org/10.1520/A0944-10R15

[22] ASTM, "C143/C143M-20 standard test method for slump of hydraulic-cement concrete," American Society of Testing and Materials, 2020, 4 p. https://doi.org/10.1520/C0143_C0143M-20

[25] Armelin, H. S., "Rebound and toughening mechanisms in steel fiber reinforced dry-mix shotcrete," The University of British Columbia, British Columbia, 1997, 262 p.

[45] Fei, J., Darwin, D., "Fatigue of high relative rib area of reinforcing bars," University of Kansas Center for Research, Kansas, 1999, 76 p.

[52] Soylev, T. A., François, R., "Quality of steel-concrete interface and corrosion of reinforcing steel," Cement and Concrete Research, Vol. 33, No. 9, 2003, pp. 1407-1415. https://doi.org/10.1016/S0008-8846(03)00087-5

[59] Whiting, D., Seegebrecht, G. W., Tayabji, S., "Effect of degree of consolidation on some important properties of concrete," Special Publication 96, 1987, pp. 125-160.

[92] ASTM, "C192/C192M-16a standard practice for making and curing concrete test specimens in the laboratory," American Society of Testing and Materials, 2016, 8 p. https://doi.org/10.1520/C0192_C0192M-16A

[93] Nagi, M., Whiting, D., "Determination of water content of fresh concrete using a microwave oven," Cement, Concrete and Aggregates, Vol. 16, No. 2, 1994, pp. 125-131. https://doi.org/10.1520/CCA10290J

[95] ASTM, "C117-13 standard test method for materials finer than 75-μm (No. 200) sieve in mineral aggregates by washing," American Society of Testing and Materials, 2013, 3 p. https://doi.org/10.1520/C0117-17

[96] ASTM, "C231/C231M-17 standard test method for air content of freshly mixed concrete by the pressure method," American Society of Testing and Materials, 2017, 9 p. https://doi.org/10.1520/C0231_C0231M-17A

[97] ASTM, "C1604/C1604M-05(2019) standard test method for obtaining and testing drilled cores of shotcrete," American Society of Testing and Materials, 2012, 5 p. https://doi.org/10.1520/C1604_C1604M-05R19

[98] ASTM, "C642-13 standard test method for density, absorption, and voids in hardened concrete," American Society of Testing and Materials, 2013, 3 p. https://doi.org/10.1520/C0642-13

[99] ASTM, "C39/C39M-17a standard test method for compressive strength of cylindrical concrete specimens," American Society of Testing and Materials, 2017, 8 p. https://doi.org/10.1520/C0039_C0039M-17B

[106] ASTM, "C494/C494M-19 Standard specification for chemical admixtures for concrete," American Society of Testing and Materials, 2019, 15 p. https://doi.org/10.1520/C0494_C0494M-19

[112] Studebaker, C. H., "Report on gunite at Arrow dam," U.S. Bureau of Reclamation Memorandum, 1939, 66 p.

[113] ASTM, "C42/C42M-20 standard test method for obtaining and testing drilled cores and sawed beams of concrete," American Society of Testing and Materials, 2020, 7 p. https://doi.org/10.1520/C0042_C0042M-20

[114] Austin, S. A., Robins, P. J., "Sprayed concrete: properties, design and application," McGraw-Hill, New York, 1995, 382 p.

[115] Mor, A., "Steel-concrete bond in high-strength lightweight concrete," ACI Materials Journal, Vol. 89, No. 1, 1992, pp. 76-82.

[116] Carmer, S. G., Swanson, M. R., "An evaluation of ten pairwise multiple comparison procedures by Monte Carlo methods," Journal of the American Statistical Association, Vol. 68, No. 341, 1973, pp. 66-74. https://doi.org/10.2307/2284140

[117] Montgomery, D. C., "Design and analysis of experiments," 7th ed, 2009, 725 p.

[118] Quinn, G. P., Keough, M. J., "Experimental design and data analysis for biologists," Cambridge University Press, New York, 2002, 537 p.

[119] Morgan, D. R., McAskill, N., Neill, J., Duke, N. F., "Evaluation of silica fume shotcrete," International workshop on condensed silica fume in concrete, Montréal, 1987, 34 p.

[120] Milliken, G. A., Johnson, D. E., "Analysis of messy data - Volume III: Analysis of covariance," Champman & Hall / CRC, New York, 2002, 605 p.

Chapter 4 Bond strength of reinforcing bars with varying encapsulation qualities

Pasquale Basso Trujillo[a], Marc Jolin[a], Bruno Massicotte[b], Benoît Bissonnette[a]
[a] *Dept. of Civil and Water Engineering, Université Laval*
[b] *Department of Civil, Geological and Mining Engineering, École Polytechnique de Montréal*

This paper is part of the ACI Structural Journal, ISSN 0889-3241, doi.org/10.14359/51702415. Paper submitted on November 1st, 2017; approved on February 19th, 2018 and published on November 1st, 2018.

4.1 Résumé

La qualité de l'enrobage des barres d'armature représente une préoccupation commune parmi les ingénieurs lors de la conception de structures en béton projeté. Puisque très peu d'information scientifique est disponible concernant la perte potentielle de la force d'adhérence des barres d'armature présentant des vides d'enrobage sur leur longueur, des éprouvettes ASTM A944-10 « beam-end » dont la barre d'armature possédait différentes qualités d'enrobage ont été testées. Afin de limiter la variabilité de la taille des vides pendent les opérations de projection, les vides ont été créés en utilisant des morceaux de silicone ce qui a également permis de connaître leur taille et position précise. Des *vides artificiels* représentant jusqu'à 30% de la circonférence des barres d'armature ont été encapsulés en coulant sur place un mélange conçu pour béton projeté. Un faible rapport *e/l* a été utilisé pour garantir une capacité de ressuage du mélange minime tel qu'observé en béton projeté. Les résultats concordent avec les résultats des recherches antérieures en démontrant qu'une longueur transversale de vide plus grande que 20% cause un changement important dans la pente de la courbe contrainte-glissement et une réduction importante de la contrainte ultime d'adhérence.

4.2 Abstract

The encapsulation quality of reinforcing bars represents a common concern among structural engineers when shotcrete structures are designed. Since little scientific information is available regarding the potential bond strength reduction of bars with adjacent defects along their length, ASTM A944-10 "beam-end" specimens with different encasement qualities were tested. To limit the size variability of voids when spraying, voids were created using silicone inserts which also made it possible to control their exact size and position. *Artificial voids* were

encased with a poured shotcrete mixture and transversal lengths of up to 30% of the bars' perimeter were investigated. A low *w/b* ratio was employed to guarantee an insignificant bleeding capacity of the mixture as is commonly observed in shotcrete. The results support previous investigations by showing that transversal void lengths beyond 20% induce a considerable change in the slope of the stress – slip curve and an important reduction of the ultimate bond stress.

Keywords: Shotcrete; Sprayed concrete; Beam-end; Voids; Artificial voids; Encapsulation; Bond strength; Hypothesis testing.

4.3 Introduction

Ever since the 1933 Long Beach earthquake in California, the use of shotcrete as a way to retrofit structural elements has rapidly increased in North America[31]. Its use has grown so quickly that nowadays it is not unusual to see tunnel linings[2], domes[1], shear walls[4] or even columns[3] and girders[2] being entirely built with shotcrete. The main reasons for this include the small amount (if any) of formwork needed and the ability to build structural elements of almost any shape, which often results in considerable time and cost savings. However, using the current design criteria may not be completely adequate for reinforced shotcrete elements because of the different placement process between shotcrete and cast in-place concrete. In particular, a recurring concern among structural engineers has been the possibility to encounter voids or entrapped aggregates (usually referred to as *sand pockets*) behind reinforcing bars. In *wet-mix* shotcrete, such defects are in general caused by the use of excessive set-accelerating admixtures and in *dry-mix* shotcrete by the inadequate selection of the water content by the nozzlemen. However, imperfections can be caused with the use of both processes if inadequate placement techniques are used. In reality, the concern regarding the encapsulation quality of reinforcement is widespread and covers many aspects from the design of structures to the evaluation of cores taken from pre-construction panels[*]. Up until now, this issue has been addressed only for evaluation of shotcrete quality and not design. The approach has been to quantitatively characterize the size of the voids observed in cores[16] and then determine if the individual/crew is sufficiently experienced to place good quality shotcrete. Unfortunately, the limits determining what is "acceptable" and "unacceptable" have been chosen empirically. An alternative and perhaps a more advantageous way to deal with both the evaluation and the design might be to establish a void size threshold (based on the bond strength performance of bars) beyond which

design criteria applicable specifically for shotcrete should be adopted. Accordingly, the evaluation of cores could be relaxed knowing that preventive measures were taken during the "design phase" to overcome the structural effect of such imperfections. The *development length* of reinforcing bars required to be computed by North American design codes [5, 6] may represent a suitable parameter to be adapted in such situations. However, a considerable amount of scientific information regarding the effect of different void sizes on the bond strength of a bar is lacking and would be needed for this purpose.

Early results within this research project using "pull-out" specimens [121] have shown that the height of the voids behind reinforcing bars contributes little to the reduction of the bond strength and that a void's transversal length in contact with the bar (referred to as the *un-bonded* perimeter) exceeding approximately 20% of the bar's perimeter represent the onset of a significant bond reduction and a change of failure mode from *splitting* to *pull-out*. In that investigation, *artificial voids* created with silicone inserts and encased with a poured shotcrete mixture were used to overcome the difficulty to obtain specific void sizes and limit their size variability when spraying. A statistical comparison between the results obtained with such type of specimens and equivalent ones made with *dry-mix* shotcrete showed that the ultimate loads were statistically equivalent between them and that, although the shape of their load – slip curve differed, *artificial voids* represented a valuable method to ultimately set rational evaluation and design criteria[121].

In this research, the ASTM A944-10 [17] "beam-end" specimens were used to study the impact of defects on the bond behavior of reinforcing bars. This type of specimen is advantageous since it accurately recreates the stress distribution around tensioned bars of most structural elements[42]. However, since spraying specimens in the laboratory to obtain imperfect encapsulation qualities has proven to be a difficult task, the specimens were cast in-place using a self-compacting concrete (SCC) mixture poured by gravity into the molds. As in the past investigation[121], the voids were recreated using *artificial voids*. This was done to obtain the most representative mechanical properties possible of typical shotcrete whilst minimizing the bleeding capacity of the mixture and to obtain a "reliably imperfect" bar – concrete interface with known void sizes.

4.4 Research significance

This experimental investigation intends to broaden our knowledge regarding the bond strength reduction caused by the possible presence of voids specifically behind reinforcing bars created with improperly placed shotcrete. Ultimately, the information will serve to develop reliable guidelines for the design of shotcrete structures (in particular for the computation of the *development length* of bars in tension specified by North American design codes [5, 6]) and for the evaluation of concrete cores as the values in existing tools were chosen subjectively and not based on the actual bond behavior of specimens tested in the laboratory.

4.5 Experimental investigation

4.5.1 Test specimens

"Beam-end" specimens were built in accordance with the ASTM A944-10 standard [17] and consisted of 210 x 600 x 450 mm [8.3 x 23.6 x 17.7 in.] prisms with a single test bar passing through a PVC sleeve at the loaded end (called the lead length) and a second sleeve at the un-loaded end as seen in Figure 4.1.

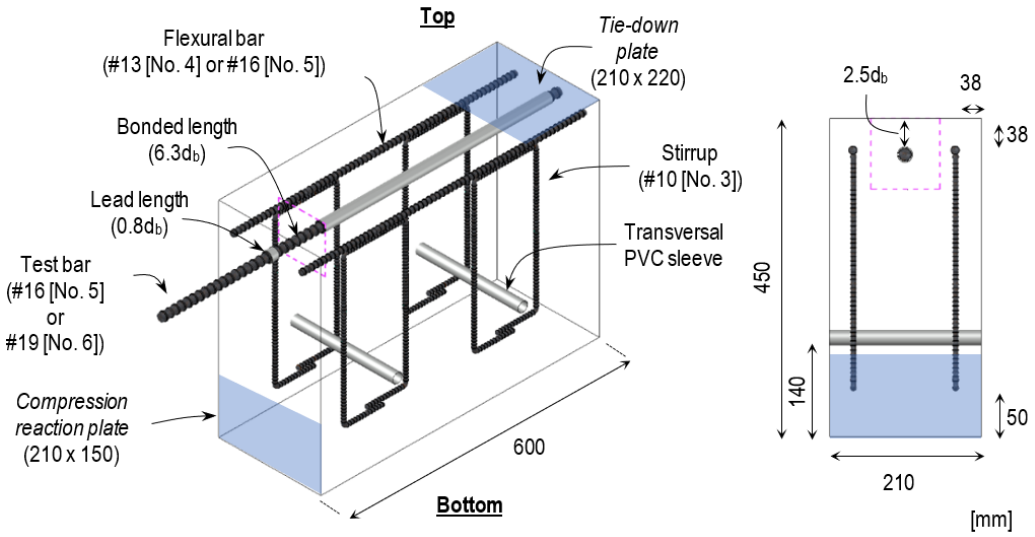

Figure 4.1: ASTM A944-10 "beam-end" specimen (Note: 25.4 mm = 1 in.)

The bonded length of the test bar was therefore controlled by these bond breaking sleeves. Test bars of 15.9 mm [$^5/_8$ in.] and 19.1 mm [$^6/_8$ in.] nominal diameter (d_b) were tested and placed with their longitudinal ribs facing the sides of the forms. The lead length and the bonded length were

set as $0.8d_b$ and $6.3d_b$ respectively for all specimens. The flexural bars were 12.7 mm [$^4/_8$ in.] and 15.9 mm [$^5/_8$ in.] in nominal diameter for each of the test bars respectively. The flexural bars (9.5 mm [$^3/_8$ in.] or 12.7 mm [$^4/_8$ in.] depending on the test bar size) and the stirrups (9.5 mm [$^3/_8$ in.] for all specimens) are required by the standard to assure proper behavior in flexure and in shear. Additional PVC sleeves were placed transversally (with respect to the test bar) in between the stirrups so they could be used to move the specimens after being stripped. The concrete cover of the test bars was set to $2.5d_b$ for all specimens which represents the cover beyond which the bond strength does not increase if a *pull-out* failure occurs (as this type of failure become more predominant over a *splitting* failure as the concrete cover increases) [76, 122]. Specimens were cast in detachable wooden panels held together by steel threaded rods. After the test bar and its front and back sleeves were secured in place, the forms were carefully oiled. Subsequently, the flexural bars and the stirrups (attached together using cable ties) were placed inside the forms and lastly, the transversal PVC sleeves were installed. This sequence guaranteed a wider space between the form and the test bar to avoid staining the bars with the form release agent. Prior to casting, all of the joints and holes in the formwork holding the bars and PVC sleeves in place were caulked with silicone. Twenty-four hours after, the specimens were stripped and were cured for 1 week using wet burlap.

4.5.2 Reinforcing bars

The reinforcing bars came from the same heat of steel and complied with the ASTM A615/A615M-16 standard [123]. Their mechanical properties were averaged from 3 specimens and tested in accordance with ASTM A370-17 [105]. Additional specimens were cut longitudinally at 45° and 90° with respect to the longitudinal ribs' plan to measure their geometrical properties as shown in Figure 4.2.

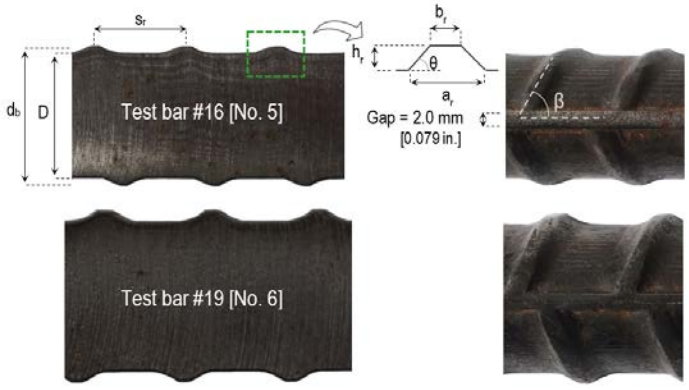

Figure 4.2: Longitudinal cut with the nomenclature of #16 [No. 5] and #19 [No. 6] bars

The measurements were performed over 10 ribs using high-resolution photographs and a CAD software for each longitudinal cut. Table 4.1 summarizes the mean mechanical and geometrical values from the three and twenty measurements of each bar size respectively.

Table 4.1: Geometrical and mechanical properties of the reinforcing bars

Type	Parameter	Test bar # 16 [No. 5]	Test bar # 19 [No. 6]
Mechanical	Young's modulus, GPa (ksi)	197 (28570)	208 (30170)
	Yield strength at 0.2%, MPa (ksi)	733 (106.3)	475 (68.9)
	Ultimate strength, MPa (ksi)	962 (139.5)	742 (107.6)
	Elongation at rupture, %	10.5	12.7
Geometrical	Nominal diameter d_b, mm (in.)	15.9 (0.63)	19.1 (0.75)
	Core diameter D, mm (in.)	14.8 (0.58)	17.7 (0.70)
	Ribs' height h_r, mm (in.)	0.9 (0.035)	1.3 (0.051)
	Ribs' top width b_r, mm (in.)	1.0 (0.039)	1.2 (0.047)
	Ribs' base width a_r, mm (in.)	4.9 (0.193)	5.6 (0.220)
	Ribs' spacing s_r, mm (in.)	10.8 (0.425)	12.6 (0.496)
	Ribs' face angle θ, degrees	25	30
	Ribs' inclination β, degrees	67	68
	Σ gaps*, mm (in)	4.0 (0.16)	4.0 (0.16)
	Relative rib area* R_r, adim	0.080	0.100

*Based on Fei et al.[60]

4.5.3 *Artificial voids*

To create the *artificial voids*, fresh silicone was inserted into hollow plastic tubes and extracted once the silicone had hardened. The resulting tubes were subsequently cut longitudinally into two halves and one piece was then glued over the entire bonded length of the test bars using the same material. To ensure no silicone was deposited elsewhere over the surface of the bars, the position of the voids was defined with masking tape which was removed once the *artificial voids* were securely glued in place. Voids of nominal transverse lengths of 10, 20 and 30% of the test bars' perimeter were created and are referred to as *un-bonded* perimeters (*u.p.*) henceforth. A "top" and "bottom" void configuration, as seen in Figure 4.3a and 4.3b respectively were also studied since, depending on the location of a bar and the direction of the shotcrete flow, voids could be created facing either the exterior or the interior of a reinforced shotcrete element.

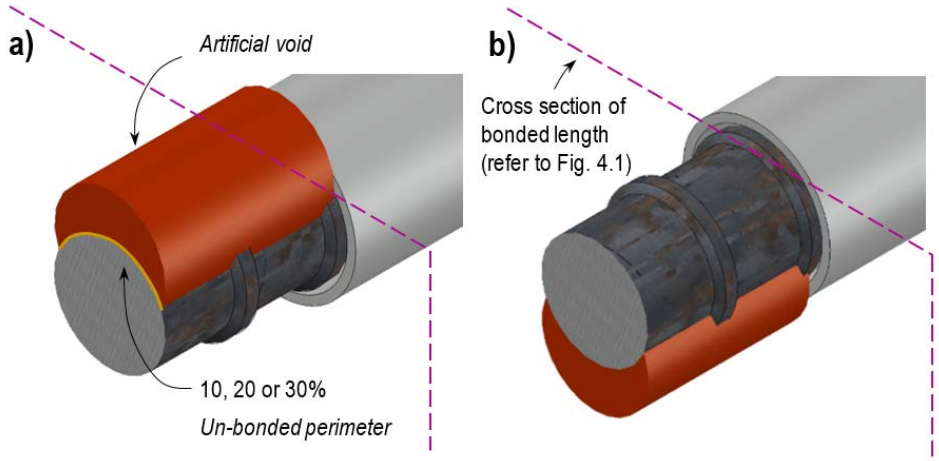

Figure 4.3: (a) Top and (b) bottom position of the artificial voids

4.5.4 Mixture design

Specimens were cast using a pre-bagged mixture intended for *wet-mix* shotcrete (max. aggregate size of 10 mm) which was poured into the forms. A constant *w/b* ratio of 0.45 was used in combination with a polycarboxylate based water reducer complying with types A and F categories of the ASTM C-494/C494M-19 [106] standard. This produced a SCC mixture with which it was possible to properly encase the *artificial voids* by providing only a minimal amount of external consolidation; only the corners of the forms were carefully tapped a few times. All of the forms were filled in two lifts and the first layer was placed in all specimens before the second layer. Since a considerable amount of concrete was placed below the test bars and a possible bond performance deterioration (additional to the presence of the voids) caused by excessive water accumulation under the test bars was a concern, a family of specimens having a 0.55 *w/b* ratio mixture was also tested. In that case, no water reducer was added and the consolidation was done in accordance with ASTM C192/C192M-16a [92]. The proportions of both mixtures are shown in Table 4.2.

Table 4.2: Mixture composition of both types of concrete

Component	w/b = 0.45	w/b = 0.55
Ordinary Portland cement, kg/m³ (lb/yd³)	393.1 (663)	376.7 (635)
Silica fume, kg/m³ (lb/yd³)	34.3 (58)	32.9 (55)
Coarse aggregate 2.5 – 10 mm, kg/m³ (lb/yd³)	708.6 (1194)	680.7 (1147)
Sand 0.08 – 5 mm, kg/m³ (lb/yd³)	1016.6 (1714)	976.5 (1646)
Water, kg/m³ (lb/yd³)	191.2 (322)	224.8 (379)
Air, %	3.4§	2.1§
Water reducer, ml/100 kg of binder (fl. oz./100 lb)	750 (11)	-

§ Based on ASTM C231/C231M-14

4.5.5 Properties of concrete

Cylinders (100 x 200 mm [4 x 8 in.]) were prepared to test the compressive strength (f_c)[99], the splitting tensile strength (f_s)[101] and the modulus of Young (E_c) [102] of all the concrete mixtures. The cylinders were cured in the same way (for 1 week using wet burlap) and were tested at the same age as the "beam-end" specimens. Moreover, the slump [22] and the *slump flow* along with the *visual stability index* (VSI) [100] were documented for the 0.55 and the 0.45 w/b ratio mixtures respectively; the air content was also measured for both of them [96]. All tests were performed using the concrete from the second lift with which the test bar was encased. The bleeding properties of both types of concrete mixtures i.e. their average bleeding rate (R) and their bleeding capacity (ΔH), were quantified following the method proposed by Josserand et al. [103]. The procedure requires 3 cylindrical containers of different heights (as those shown in Figure 4.4a) to be filled and to collect the bleed water from the intersection of two orthogonal tracks made on the surface of the concrete (and inclined towards the center) at a regular time interval using a pipet as shown in Figure 4.4b.

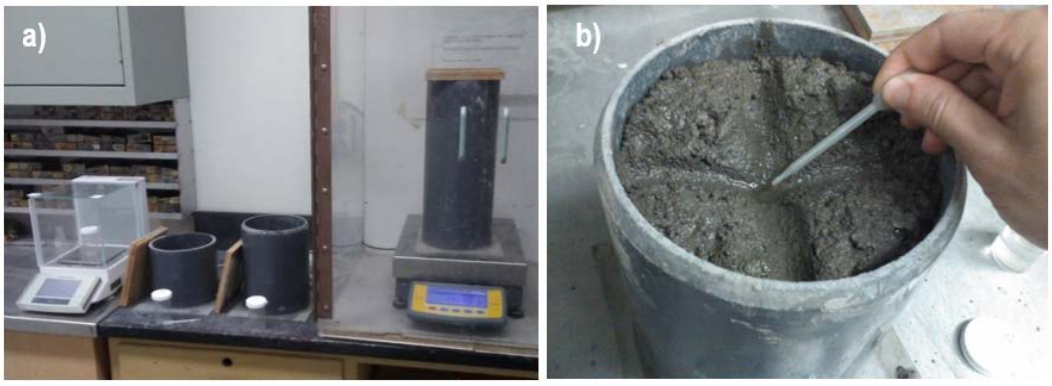

Figure 4.4: (a) Equipment for the bleed test and (b) bleed water collected

The bleed water is used to calculate "ΔH" which in turn serves to calculate "R" (whose values are independent of the container's height) and determine its maximal value (R_{max}). During the entire test, the tallest container rests on a 0.1g [0.04 oz.] accurate scale so its weight loss rate can be measured and later considered as the average bleed water evaporation of all the containers. In this investigation, the containers were 150 mm [5.9 in.], 210 mm [8.3 in.] and 430 mm [16.9 in.] tall and had an inner diameter of 150 mm [5.9 in.]. Moreover, the concrete was consolidated in the same manner as was done to cast the "beam-end" specimens. This method is advantageous over similar methods such as the ASTM C232/C232M-14 [104] standard because the containers do not need to be tilted to collect the bleed water. However, it stills provides the opportunity to calculate the bleeding in the same way as the standard does. All of the concrete test results are summarized in Table 4.3.

Table 4.3: Test results of the concrete mixtures

Family	*u.p.*, %				*w/b*	f'_c, MPa (psi)	f_s, MPa (psi)	E_c, GPa (ksi)	Air, %	*Slump flow*, mm (in.) / Slump, mm (in.)	VSI	R_{max}, µm/min (mils/min)	Test§, days
#16-0.45	0	-	-	-	0.45	57.7 (8370)	3.9 (570)	33.3‡ (4830)	3.4	550 (21.7)	0 ~ 1	2.2† (0.1)	24 ± 2
#16-0.45 T	-	10	20	30									
#16-0.45 B	-	-	20	30									
#19-0.45	0	-	-	-									
#19-0.45 T	-	10*	20	30									
#19-0.45 B	-	-	20	30									
#16-0.55	0	-	-	-	0.55	34.7 (5030)	2.5 (360)	25.4 (3680)	2.1	140 (5.5)	-	6.5† (0.3)	8

§In reference to both the "beam-end" specimens and the mechanical properties of the concrete
* Specimens' results were discarded due to a malfunction in the equipment
‡A Poisson's ratio of 0.14 was measured at the same time
† Mean from the 3 molds of different heights and only 1 mixture

4.5.6 Testing procedure

The "beam-end" specimens were tested using a 311 MTS frame and the set-up shown in Figure 4.5. The tests were performed at 0.5 mm/min displacement control and the slip of the reinforcing bars was recorded at the loaded end and at the un-loaded end of the test bar using two linear position sensors with return spring on each side. The "beam-end" specimen was lifted using the holes provided by the transversal PVC sleeves and then laid on a steel box anchored to the base of the test frame. After the specimen was pushed with the alignment plate so as to align the test bar with the actuator's longitudinal axis, the specimen was gradually tightened with the *compression reaction plate* and the *tie-down plate*. Finally, the pulling device, which consisted of two square shafts pin-holding a thick cylinder with a hole in its middle, was inserted around the test bar. A conical wedge was then placed around the test bar so that the cylinder from the pulling device would bear against it while the bar was tensioned. A detailed description of the testing apparatus and procedure to test ASTM A944-10 "beam-end" specimens is given by Basso et al. [124]. The properties of the hardened concrete were measured right after the "beam-end" specimens were tested and are presented in Table 4.3.

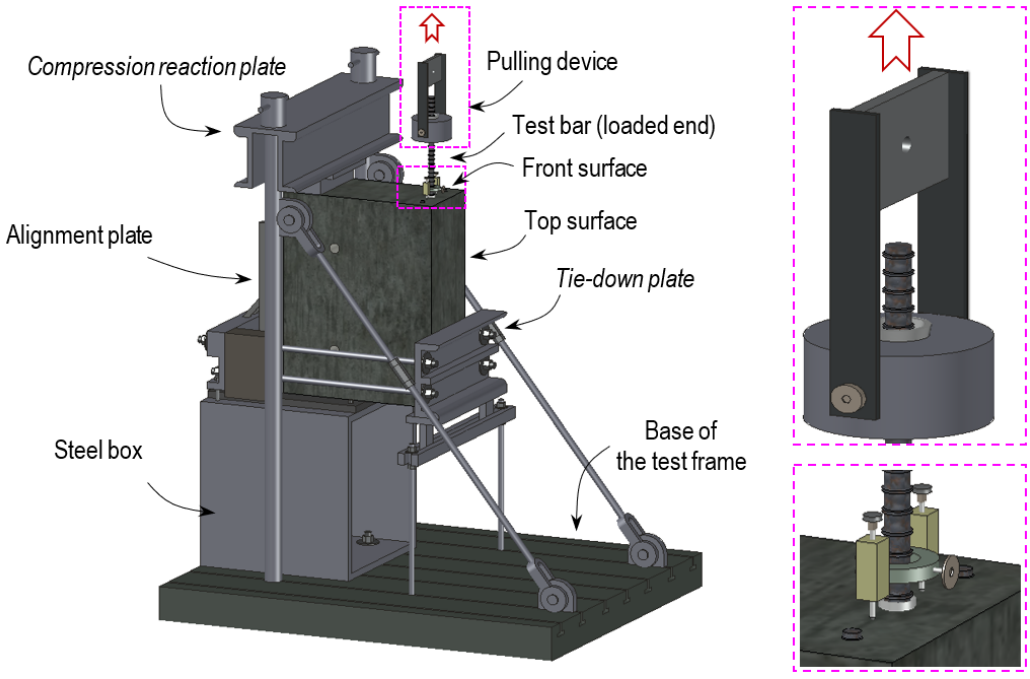

Figure 4.5: Test set-up of the ASTM A944-10 "beam-end" specimen

4.5.7 Test parameters

Specimens were grouped in families using labels which indicate the size of the test bar (#16 [No. 5] or #19 [No. 6]), the *w/b* ratio of the mixture (0.45 or 0.55) and the orientation of the *artificial voids* (T or B for top and bottom respectively and based on Figure 4.1 and 4.3) if they were used. Three replicas were built for each configuration. The 10% *u.p.* was not tested for the "Bottom" configuration as early results showed that the bond strength was not significantly reduced in comparison with perfectly encapsulated bars (*u.p.* = 0%). Considering all of the *u.p.*'s for each family (13) and the replicas for each one of them (3), a total of 13 x 3 = 39 "beam-end" specimens were built. However, only the results of 36 of them are presented in the following section as explained in Table 4.3.

4.6 Results and discussion

4.6.1 Stress – slip curves

The measured load (P) has been normalized with respect to the nominal transversal area of the test bars (A_b) and is plotted against the slip of the bars for the different *u.p.*'s under study. At the loaded end only, the elastic elongation of the portion of the test bars between the attachment of the linear position sensors and the end of the lead length was subtracted from the measured slip. Moreover, only the test bars with a "top" void configuration and a *w/b* ratio of 0.45 are presented in this section. The curves of the loaded and the un-loaded ends are shown in Figure 4.6a and 4.6b for the #16 [No. 5] test bars and in Figure 4.7a and 4.7b for the #19 [No. 6] test bars.

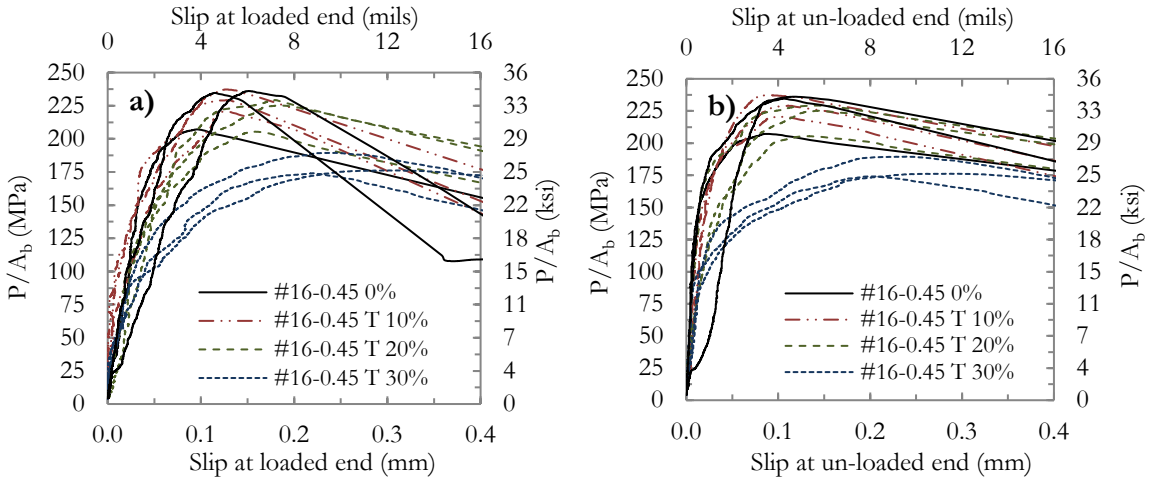

Figure 4.6: (a) Stress – slip curves of the #16 [No. 5] test bars at the <u>loaded end</u> and (b) at the <u>un-loaded end</u>

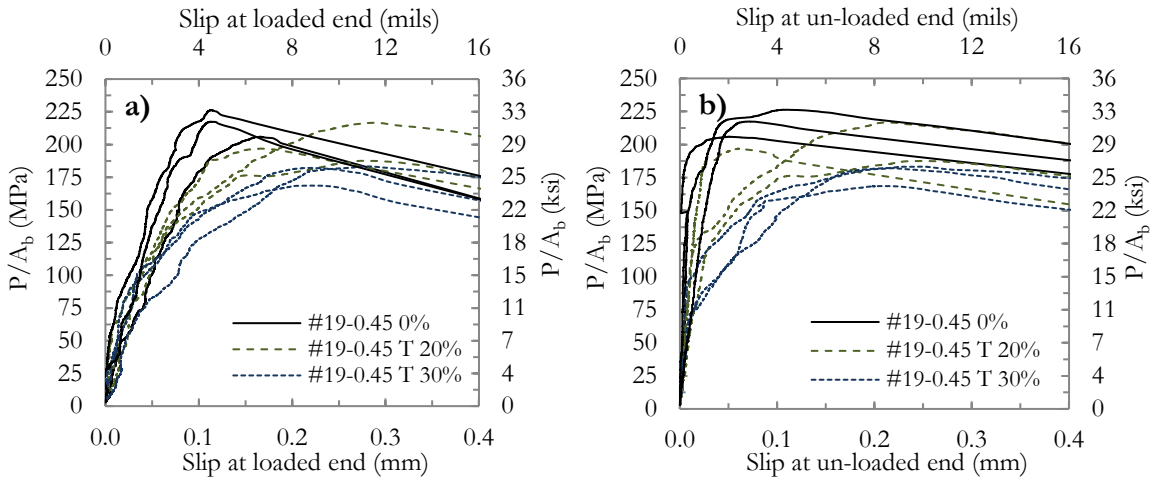

Figure 4.7: (a) Stress – slip curves of the #19 [No. 6] test bars at the <u>loaded</u> and (b) at the <u>un-loaded end</u>

As expected, the slip associated to the loaded end is larger than the one measured at the un-loaded end as the latter captures the "stiffness" of the entire bonded length. The difference between both measures represents the lengthening of the reinforcing bar and its absolute value increases as the bonded length is increased. As can be seen in Figure 4.6a and 4.6b, an *u.p.* of 10% causes no apparent change in the overall bond behavior of a bar in comparison to a perfectly encapsulated bar (0% *u.p.*). Indeed, in both cases, the slope of the ascending curve (referred to as the *slip stiffness* henceforth), remains constant until the ultimate bond stress (P_{max}/A_b) is attained. Beyond that point, the ribs of the bar crush the concrete in front of them creating residual stresses as the bar continues to slip relative to the concrete. In all cases, the transition from a 10% to a 30% *u.p.* causes the *slip stiffness* to decrease progressively as the ultimate bond stress is attained as can be observed in Figure 4.6a and 4.6b as well as in Figure 4.7a and 4.7b. At a 20 % *u.p.*, the ultimate bond stress had been reduced in the range of 3-8% and at a 30% *u.p* in the range of 20-25% relative to perfectly encapsulated test bars.

Despite the fact that the concrete was not actually sprayed, the bond behavior of the specimens provides useful evidence to define threshold values defining bond behavior changes between specimens with different encapsulation qualities. In reality, according to the investigation of Basso et al.[121] in which the bond performance of shotcrete and cast in-place "pull-out" specimens were compared, the *slip stiffness* of shotcrete specimens would be slightly greater than those shown in Figure 4.6a and 4.6b as well as those shown in Figure 4.7a and 4.7b due to the

high compaction of the concrete obtained upon its impact on the forms. Nonetheless, the ultimate bond stress between both methods of concrete placement should be the same despite the different slip performance. It is for this reason that the ultimate bond stress is used subsequently for the analysis and thus, the values obtained with both test bar sizes are plotted in Figure 4.8 as a function of the *u.p.* In general, the ultimate bond stress for different qualities of encapsulation seems to be independent of the tested bar sizes (#16 [No. 5] and #19 [No. 6]) and the reduction is best characterized by a second-order polynomial regression. This model is both significant (F_0 = 28.89 and *p-value* < 0.000) and adequate (F_0 = 0.00 and *p-value* = 1.000) based on an *analysis of variance* [117] and possesses an adjusted Pearson coefficient (R^2_{adj}) of 0.736 (refer to Section G.1 in Appendix G for additional data).

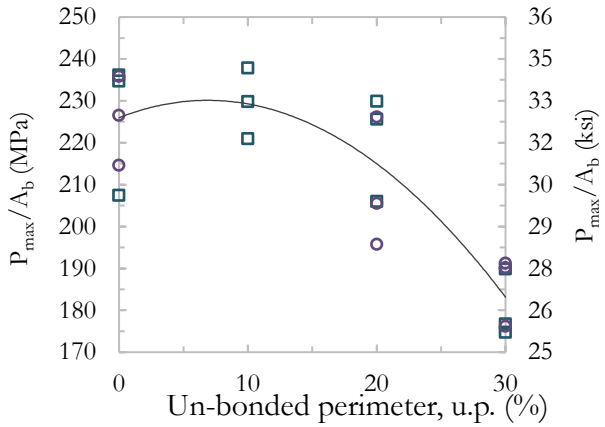

Figure 4.8: Effect of the *u.p.* on the ultimate stress of bars #16 [No. 5] and #19 [No. 6]

4.6.2 The size of the bars

To support the assertion that the reduction of the ultimate bond stress is independent of the bar size, an equal variance pairwise comparison *t-test* was performed. This is formally done by defining a *null* (H_0) and an *alternative hypothesis* (H_a), as expressed in Equation 4.1, to determine if the ultimate bond stresses of the entire population (μ_i) of specimens with one bar size are equal or not to another one having a different bar size but the same *u.p.*

$$H_0: \mu_1 = \mu_2$$

$$\text{v.s.} \qquad (4.1)$$

$$H_a: \mu_1 \neq \mu_2$$

The outcome of the test, most frequently expressed with a *p-value*, determines if there is enough evidence to accept H_0 or if it should be rejected. The *p-value* represents the level of risk a *decision-maker* is willing to take at the moment H_0 is accepted or rejected; a decision based on a *p-value* equal to 0.05 implies taking a risk of 5% to falsely reject H_0. The *p-value* is obtained based on the degrees of freedom (*v*) associated with the size of the combined sample and the calculated t_0 test-statistic (distributed as *t*), which in turn, is calculated using the mean of each families' ultimate bond stress (Avg. P_{max}/A_b). In this case, *v* equals $n_1 + n_2 - 2 = 4$ where n_i is the size of each family. When a precise level of risk is established as the threshold to accept or to reject H_0, its value is called the *level of significance* (α) of the test. The results of the comparison based on $\alpha = 0.05$ are shown in Table 4.4. Because the resulting *p-values* are greater than any relevant *level of significance* ($\alpha \leq 0.05$) in all cases, there is not sufficient evidence to reject H_0 and thus we can conclude that the ultimate bond stress in the presence of voids is independent of the sizes of the bars tested herein. It is worth noticing that as the *u.p.* increases, the standard deviation (S.D.) seems to decrease. Indeed, it is mostly due to the variability of the concrete properties that dispersion within specimens occurs and thus, the lesser the concrete around the bar, the lesser the standard deviation.

Table 4.4: Equal variance *t-test* results for the size of the bars

***u.p.*, %**	**Bar No.**	**n**	**Avg. P_{max}/A_b, MPa (ksi)**	**S.D. , MPa (ksi)**	**t_0**	**v**	**p-value**	**Result***
0	16	3	226.1 (32.8)	16.2 (2.3)	0.04	4	0.972	Equal
	19	3	225.7 (32.7)	10.7 (1.6)				
20	16	3	220.5 (32.0)	12.8 (1.9)	0.98	4	0.384	Equal
	19	3	209.2 (30.3)	15.5 (2.2)				
30	16	3	180.5 (26.2)	8.2 (1.2)	0.80	4	0.467	Equal
	19	3	185.9 (27.0)	8.4 (1.2)				

*Based on a level of significance $\alpha = 0.05$

4.6.3 The position of the voids

An equal variance *t-test* was also performed to assess the impact of a void's position on the bond strength of a bar. The comparisons were made between specimens having "top" and "bottom" void configurations but having the same bar size and *u.p.*'s. The results are shown in Figure 4.9 in which the error bars represent one standard deviation away from P_{max}/A_b.

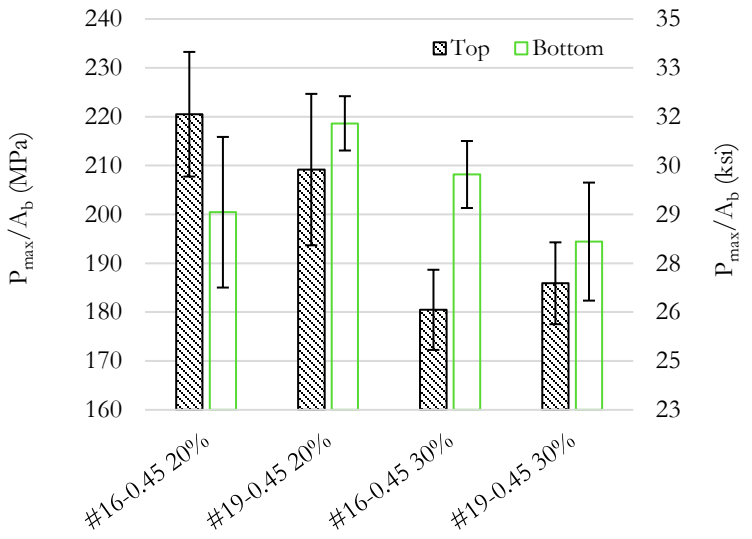

Figure 4.9: Ultimate bond stress of the bars with different void position

The results of the test are presented in Table 4.5 and, based on the same analysis procedure described previously, the position of the void did not have a significant impact on the ultimate bond stress in most situations.

Table 4.5: Equal variance *t-test* results for the position of the voids

Family	Position	*u.p.*, %	n	Avg. P_{max}/A_b, MPa (ksi)	*S*, MPa (ksi)	t_0	*v*	*p-value*	Result*
#16-0.45	T	20	3	220.5 (32.0)	12.8 (1.9)	1.74	4	0.157	*Equal*
	B		3	200.4 (29.1)	15.4 (2.2)				
#19-0.45	T	20	3	209.2 (30.3)	15.5 (2.2)	1.00	4	0.376	*Equal*
	B		3	218.6 (31.7)	5.6 (0.8)				
#16-0.45	T	30	3	180.5 (26.2)	8.2 (1.2)	4.49	4	0.011	*Not Equal*
	B		3	208.2 (30.2)	6.9 (1.0)				
#19-0.45	T	30	3	185.9 (27.0)	8.4 (1.2)	1.00	4	0.372	*Equal*
	B		3	194.4 (28.2)	12.1 (1.8)				

*Based on a *level of significance* $\alpha = 0.05$

In the case of family #16-0.45 30%, the test detected a difference between the population's means. Surprisingly, the mean bond stress of this family with a "bottom" void configuration presented higher values than the one obtained with an *u.p.* of 20% for the same bar size (208.2 MPa [30.2 ksi] vs. 200.4 MPa [29.1 ksi]); it is for this unexpected and unrealistic difference that

the bond stresses of bar sizes #16 [No. 5] and #19 [No. 6] were not combined for a given *u.p.* despite the fact that results are independent of the sizes of the bars as described in the previous chapter. Since in all other three cases the results lead to the conclusion that mean bond stresses are equal between "top" and "bottom" void configurations, there is strong evidence that a void facing the surface of a structural element and another of the same size facing its interior would have approximately the same impact on the bond strength of the bar.

4.6.4 The *w/b* ratio

The *visual stability index* (VSI) of the 0.45 *w/b* ratio mixture resulted mainly in grade 0 values (refer to Figure 4.10) and sporadic grade 1 values; these observations provided preliminary evidence that the SCC mixture had a very low propensity to bleed.

Figure 4.10: Typical *consistency* of the 0.45 *w/b* ratio mixture showing a VSI of 0

Quantitatively, this was confirmed by the average bleeding rate (R) and the bleeding capacity (ΔH) measurements (shown respectively in Figure 4.11 and 4.12) in comparison with those obtained with the 0.55 *w/b* ratio mixture; in Figure 4.11 the error bars represent one standard deviation away from the mean. Only the ΔH of the 430 mm tall container is presented since it represents the approximate height of the concrete below the test bars in the "beam-end" specimens (refer to Section G.2 in Appendix G for additional data).

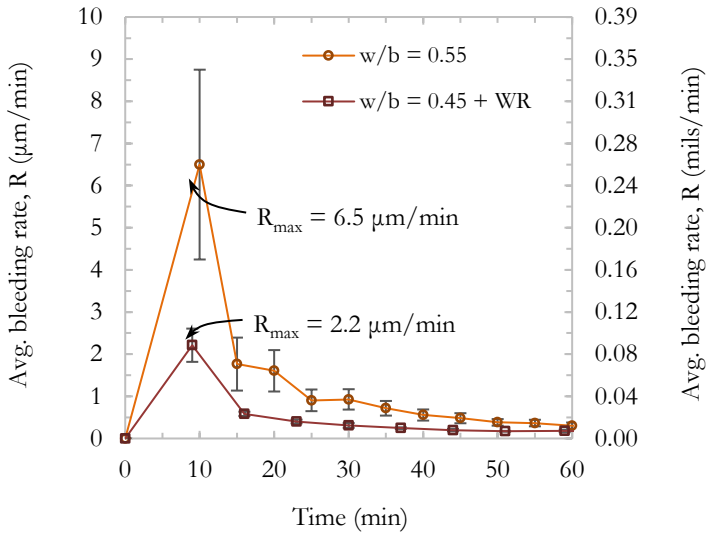

Figure 4.11: Average bleeding rate of the mixtures (Note: 1 µm/min = 0.039 mils/min)

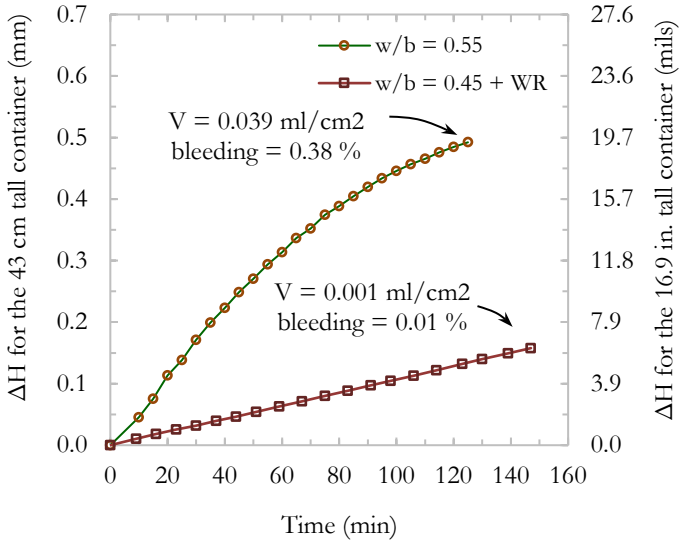

Figure 4.12: Bleeding capacity of the mixtures (Note: 1 ml/cm^2 = 0.218 fl. oz./in.^{2})

In addition, the volume of bleed water per unit area (V) and the accumulated bleed water (*bleeding*) expressed as a percentage of the mixture's net mixing water of each container are presented in Figure 4.12 for both mixtures. Both V and *bleeding* were calculated based on the ASTM C232/C232M-14[104] standard using the total amount of bleed water collected from the containers before the concrete hardened. As can be observed, the maximum average bleeding rate (R_{max}) and ΔH were reduced by about 66% as the *w/b* ratio was lowered by approximately

20% with the addition of the water reducer. In fact, based on the ASTM C232/C232M-14[104] standard's results (see Figure 4.12), it can be said that the reduction of the *w/b* ratio produced a mixture with "essentially no bleeding"*[125]* as the amount of *bleeding* was 0.01%. In terms of bond strength, the almost complete lack of bleeding produced a superior ultimate bond stress as can be observed in Figure 4.13a and 4.13b where the stress – slip response of the "beam-end" specimens belonging to families #16-0.45 0%, 20%, 30% and #16-0.55 0% are plotted. To properly compare the response of all specimens, the bond stresses of the higher *w/b* ratio family were normalized relative to the f_c of the lower *w/b* ratio family. Therefore, the bond stresses of the #16-0.55 0% family of specimens were multiplied by $(57.7/f_c)^{¼}$ assuming that the bond strength is proportional to the ¼ power of the compressive strength. In past research, either a value of ½ or ¼ has been used as a normalization coefficient but it has been shown that the latter is more accurate when f_c is greater than 55 MPa [56-58]). This assured the specimens' response was equivalent in terms of bulk compressive strength with the only difference being the increased porosity around the bar of the specimens cast with a higher *w/b* ratio mixture.

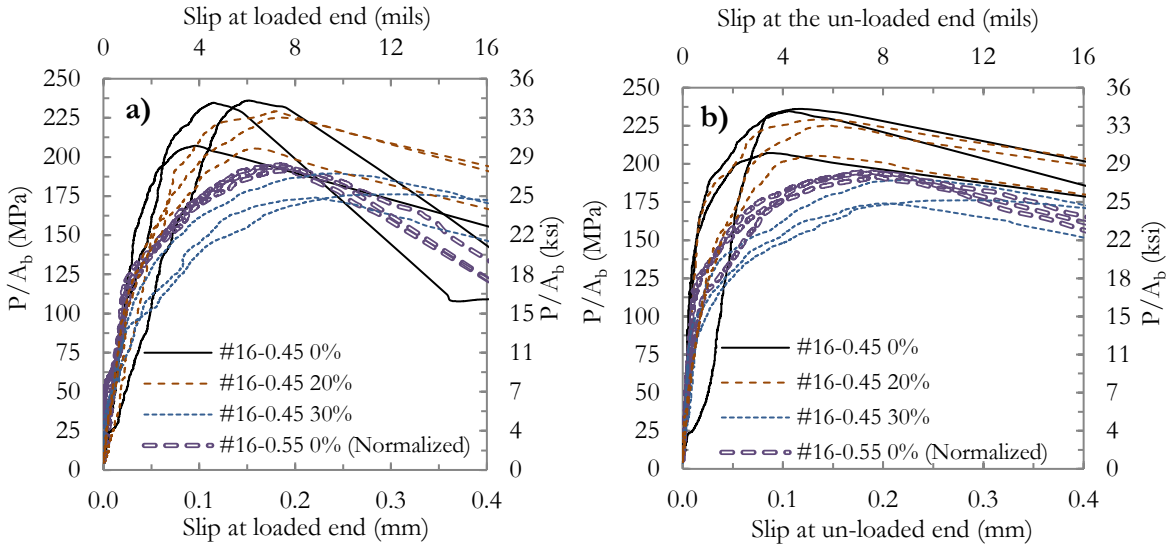

Figure 4.13: (a)Stress – slip curves of the 0.45 and 0.55 *w/b* ratio mixtures at the <u>loaded</u> and (b) at the <u>un-loaded end</u>

As can be observed, using a 0.45 *w/b* ratio mixture with a water reducer caused the initial branch of the stress – slip curve to have a more or less constant slope which best approximates the behavior of shotcrete specimens[121]. This effect may be explained due to the possibly lower porosity in the vicinity of the bars obtained with the SCC mixture in comparison to regular

concrete[73] as no internal vibration is necessary with the former type of concrete. Surprisingly, besides the evident difference of the ultimate bond stress between perfectly encapsulated bars (which is strongly linked to the normalization coefficient used), the bond behavior of the bars encased with the 0.55 *w/b* ratio was considerably degraded and produced a similar bond to bars having *artificial voids* in between 20 and 30% *u.p.*'s. This is extremely relevant because it emphasizes how crucial the properties of the bar-concrete interface are on both shotcrete and cast in-place concrete and how each effect needs to be addressed with appropriate measures.

4.6.5 The failure mode

All the specimens (except one) failed by *splitting* (refer to Section G.3 in Appendix G for additional data). At the top surface (refer to Figure 4.1 and 4.5), a crack ran parallel and above the test bar and fanned out to the sides after the length of the bonded section of the bar had been passed. At the front surface, two different types of *splitting* patterns occurred. In the first case (Y-shape pattern), two diagonal cracks grew towards the bottom of the specimen at approximately 120 degrees between one another and with respect to the top surface crack as shown in Figure 4.14a. In the second case (T-shape pattern), one single crack grew towards the bottom of the specimen parallel to the top surface crack and then fanned out towards the sides of the specimen before the *compression reaction plate* was reached as shown in Figure 4.14b. The two types of *splitting* patterns were observed on all specimens and no correlation was found between the size of the voids or the family of the specimens. In fact, these two *splitting* patterns are usual and can even be observed between specimens having a concrete compressive strength difference as low as 2.5 MPa (0.36 ksi)[60]. The only specimen with an unusual mode of failure belonged to family #16-0.45 T 30%. Initially, it failed by splitting and an initial crack appeared on the top surface of the specimen. However, as loading continued, the crack stopped to grow and the mode of failure transformed into a *pull-out* mode. The crack did not extend all the way towards the end of the bonded length and did not appear on the front surface.

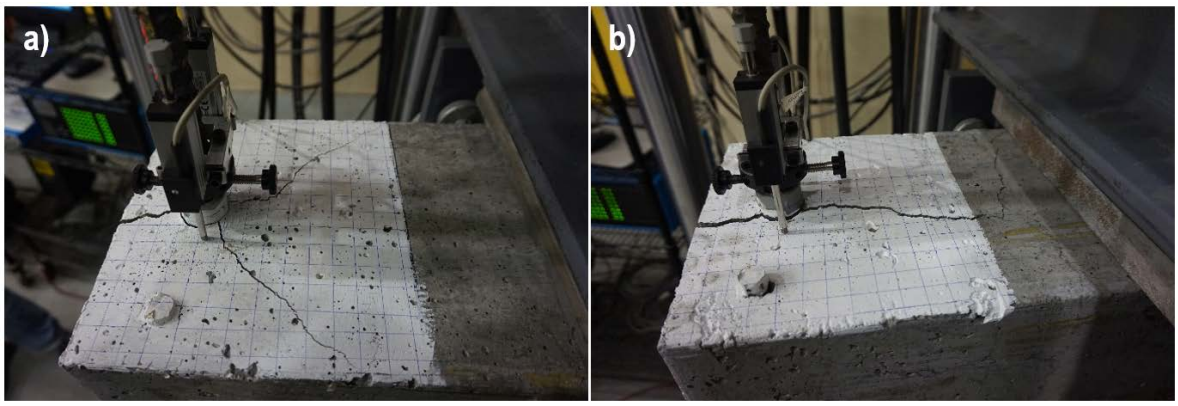

Figure 4.14: (a) Y- and (b) T-shape splitting patterns at the front surface (grids are 15 x 15 mm [0.6 x 0.6 in.])

4.7 Further research

Although the results presented herein are essential to understand the impact of defects on the bond strength of reinforcing bars, the experimental campaign recreated only the "worst-case" scenario in which the defects covered the entire bonded length of the test bars. Thus, it is of vital importance to further explore the impact of "localized voids" (voids covering only a portion of the bonded length of the bar) as this may occur in congested areas of reinforcement or lap splice regions. The impact of the confinement (concrete cover and transverse reinforcement) should also be investigated as this may influence the failure mode of the specimens. This is of prime importance as it will allow the establishment of design and evaluation criteria considering not only the *u.p.* if voids might be created or are observed but also in regard of how frequently they appear in a given structural element or pre-construction panel.

4.8 Conclusions

In this research, *artificial voids* encased with a low *w/b* ratio mixture were used to simulate the types of encasement deficiencies that are sometimes found in reinforced shotcrete elements when congested elements are sprayed in combination with deficient shooting techniques, inadequate mixtures or when difficult job site conditions exist. The methodology not only made it possible to obtain stress – slip curves with similar characteristics to those that have been observed in shotcrete (due to the insignificant amount of the mixture's bleeding capacity) but also to obtain clear tendencies and a reduced dispersion of the results. Moreover, the results show how the *slip stiffness* of the stress – slip curves starts to decrease when *artificial voids* pass

from *un-bonded* perimeters of 10 to 20%. In terms of the ultimate bond stress, the values start decreasing at an *un-bonded* perimeter of 20% and are considerably reduced with *un-bonded* perimeters of 30% reaching reduction values of up to 25% in comparison with perfectly encapsulated bars. In addition, the position of the voids (either facing the exterior or the interior of the element) does not seem to have a great impact on the bond strength of the bars for equal void sizes. In terms of the mode of failure, the majority of the specimens failed by *splitting* in the same manner as has been reported in the literature[60]. Nonetheless, it is believed that voids with an *un-bonded* perimeter larger than 30% might cause the mode of failure to change from *splitting* to *pull-out* when voids cover the entire bonded length. The results also showed how the impact of voids is as important as the one caused by excessive bleeding in cast in-place concrete since a bleeding increase of about 3 times (from a condition of almost no bleeding) caused a bond behavior similar to the one observed with specimens with *artificial voids* of *un-bonded* perimeters larger than 20%.

Therefore, based on the results of this investigation and those available in the literature, it seems that actions to counteract the change in the stress – slip behavior and the ultimate bond stress reduction should be considered in the design of reinforced shotcrete structures once voids having *un-bonded* perimeters equal to or larger than 20% are expected. Indeed, *un-bonded* perimeters of around 10% *u.p.* have little impact on the bond performance of a bar in comparison with perfectly encapsulated bars; this holds even in the *worst-case* scenario in which the length of the voids covered the entire bonded length of the test bar. *Un-bonded* perimeters equal to or larger than 20% should be carefully treated as bigger confinement provided by concrete cover or transverse reinforcement may induce a change in the mode of failure and consequently a brittle behavior of the reinforced concrete elements. It is the hope of the authors that the results can already serve as a solid background to enhance or validate the current evaluation methods intended for shotcrete structures and pre-construction panels. As future work will be completed (the effect of "localized voids", concrete cover and transverse reinforcement), proper guidelines for the design are intended to be developed.

4.9 Acknowledgements

The authors are grateful to the Concrete Infrastructure Research Center (CRIB) of Québec, the Natural Sciences and Engineering Research Council of Canada (NSERC), King Packaged Materials and Co., the Canadian Council of Independent Laboratories (CCIL), The

American Shotcrete Association (ASA) and the Québec and East Ontario Chapter of the American Concrete Institute (ACI) for their financial support. Furthermore, special thanks are extended to Jean-Daniel Lemay and Mathieu Thomassin-Mailhot (research engineers), to René Malo (expert laboratory technician) and to Pierre-André Tremblay and Alain Melançon (laboratory technicians) of the Department of Civil and Water Engineering at Université Laval for their outstanding work and support during the casting and the testing operations.

4.10 References

[1] Davis, B., "Holcim New Zealand cement terminal," Shotcrete Magazine, Vol. 19, No. 1, 2017 pp. 26-30.

[2] Townsend III, F. E., "Northern boulevard crossing tunnel CQ039," Shotcrete Magazine, Vol. 18, No. 1, 2016, pp. 34-36.

[3] Townsend III, F. E., "The plaza substation and queen structures," Shotcrete Magazine, Vol. 18, No. 1, 2016, pp. 22-23.

[4] Panian, L., Steyer, M., Tipping, S., "Post-tensioned shotcrete shearwalls," Concrete International, Vol. 29, No. 10, 2007, pp. 39-45.

[5] ACI Committee 318, "318-19 Building code requirements for structural concrete and commentary," American Concrete Institute, Michigan, 2019, 559 p.

[6] CSA, "A23.3-19 Design of concrete structures," Canadian Standards Association, Ontario, 2019, 297 p.

[16] ACI Committee 506, "Visual shotcrete core quality evaluation technote (ACI 506.6T-17)," American Concrete Institute, Michigan, 2017, 4 p.

[17] ASTM, "A944-10(2015) standard test method for comparing bond strength of steel reinforcing bars to concrete using beam-end specimens," American Society of Testing and Materials, 2015, 4 p. https://doi.org/10.1520/A0944-10R15

[22] ASTM, "C143/C143M-20 standard test method for slump of hydraulic-cement concrete," American Society of Testing and Materials, 2020, 4 p. https://doi.org/10.1520/C0143_C0143M-20

[31] Warner, J., "Understanding shotcrete - Structural applications," Concrete International, Vol. 17, No. 10, 1995, pp. 55-61.

[42] ACI Committee 408, "408R-03 Bond and development of straight reinforcing bars in tension," American Concrete Institute, Michigan, 2003, 49 p.

[56] Darwin, D., Zuo J., Tholen M. L., Idun, E. K., "Development length criteria for conventional and high relative rib area reinforcing bars," ACI Structural Journal, V. 93, No. 3, 1996, pp. 347-359, https://doi.org/10.14359/9694

[57] Zuo, J., Darwin, D., "Splice strength of conventional and high relative rib area bars in normal and high-strength concrete," ACI Structural Journal, Vol. 97, No. 4, 2000, pp. 630-641, https://doi.org/10.14359/7428

[58] Miller, G. G., Kepler J. L., Darwin, D., "Effect of epoxy coating thickness on bond strength of reinforcing bars," ACI Structural Journal, Vol. 100, No. 3, 2003, pp. 314-320, https://doi.org/10.14359/12606

[60] Brettmann, B. B., Darwin, D., Donahey, R. C., "Bond of reinforcement to superplasticized concrete," Journal of The American Concrete Institute, Vol. 83, No. 1, 1986, pp. 98-107. https://doi.org/10.14359/1743

[73] Salem, H. M., Maekawa, K., "Pre- and postyield finite element method simulation of bond of ribbed reinforcing bars," Journal of Structural Engineering, Vol. 130, No. 4, 2004, pp. 671-680, https://doi.org/10.1061/(ASCE)0733-9445(2004)130:4(671)

[76] Orangun, C. O., Jirsa J.O., Breen J.E., "The strength of anchor bars: A revaluation of the test data on development length and splices," The University of Texas, Texas, 1975, 78 p.

[92] ASTM, "C192/C192M-16a standard practice for making and curing concrete test specimens in the laboratory," American Society of Testing and Materials, 2016, 8 p. https://doi.org/10.1520/C0192_C0192M-16A

[96] ASTM, "C231/C231M-17 standard test method for air content of freshly mixed concrete by the pressure method," American Society of Testing and Materials, 2017, 9 p. https://doi.org/10.1520/C0231_C0231M-17A

[99] ASTM, "C39/C39M-17a standard test method for compressive strength of cylindrical concrete specimens," American Society of Testing and Materials, 2017, 8 p. https://doi.org/10.1520/C0039_C0039M-17B

[100] ASTM, "C1611-14 Standard test method for slump flow of self-consolidating concrete," American Society of Testing and Materials, 2014, 6 p. https://doi.org/10.1520/C1611_C1611M-14

[101] ASTM, "C496-17 Standard test method for splitting tensile strength of cylindrical concrete specimens," American Society of Testing and Materials, 2017, 5 p. https://doi.org/10.1520/C0496_C0496M-17

[102] ASTM, "C469-14 Standard test method for static modulus of elasticity and poisson's ratio of concrete in compression," American Society of Testing and Materials, 2014, 5 p. https://doi.org/10.1520/C0469_C0469M

[103] Josserand, L., de Larrard F., "A method for concrete bleeding measurement," Materials and Structures, Vol. 37, 2004, pp. 666-670. https://doi.org/10.1007/BF02480511

[104] ASTM, "C232-20 Standard test method for bleeding of concrete," American Society of Testing and Materials, 2020, 3 p. https://doi.org/10.1520/C0232_C0232M-20

[105] ASTM, "A370-20 Standard test methods and definitions for mechanical testing of steel products," American Society of Testing and Materials, 2020, 50 p. https://doi.org/10.1520/A0370-20

[106] ASTM, "C494/C494M-19 Standard specification for chemical admixtures for concrete," American Society of Testing and Materials, 2019, 15 p. https://doi.org/10.1520/C0494_C0494M-19

[117] Montgomery, D. C., "Design and analysis of experiments," 7th ed, 2009, 725 p.

[121] Basso Trujillo, P., Jolin, M., Massicotte, B., Bissonnette, B., "Bond strength of reinforcing bars encased with shotcrete," Construction and Building Materials, Vol. 169, 2018, pp. 678-688. https://doi.org/10.1016/j.conbuildmat.2018.02.218

[122] Jirsa, J.O., Lutz L.A., Gergely P., "Rationale for suggested development, splice, and standard hook provisions for deformed bars in tension," Concrete International, Vol. 1, No. 7, 1979, pp. 47-61.

[123] ASTM, "A615-20 Standard specification for deformed ad plain carbon-steel bars for concrete reinforcement," American Society of Testing and Materials, 2020, 8 p. https://doi.org/10.1520/A0615_A0615M-20

[124] Basso Trujillo, P., Malo, R., Jolin, M., "Alternative set-up apparatus to test ASTM A944-10 beam-end specimens," Journal of Testing and Evaluation, Vol. 46, No. 4, 2018, pp. 1741-1748. https://doi.org/10.1520/JTE20170645

[125] ASTM, "Significance of tests and properties of concrete and concrete-making materials," American Society of Testing and Materials, 2006, 664 p., https://doi.org/10.1520/STP169D-EB

Chapter 5 Finite Element model of "beam-end" specimen with different qualities of reinforcing bar encapsulation

Pasquale Basso Trujillo[a], Fabien Lagier[b], Marc Jolin[a], Bruno Massicotte[b], Benoît Bissonnette[a]
[a] *Dept. of Civil and Water Engineering, Université Laval*
[b] *Department of Civil, Geological and Mining Engineering, École Polytechnique de Montréal*

This paper is part of the Engineering Structures Journal, ISSN 0141-0296. Paper submitted on September 28th, 2020 and is currently under peer review.

5.1 Résumé

L'enrobage adéquat des barres d'armature en béton projeté représente toujours une inquiétude parmi des ingénieurs en structure. Ainsi, des études récentes ont été entamées pour étudier l'impact des imperfections spécifiquement créées derrière les barres d'armatures en utilisant des éprouvettes ASTM A944-10 « beam-end » dans le laboratoire. Dans cette étude, un modèle non linéaire 3D en éléments finis à l'échelle de la crènelure ayant différentes qualités d'enrobage autour de la barre d'armature a été développé pour valider les résultats des expériences obtenues dans le passé ainsi que pour créer des données additionnelles; différents recouvrements du béton et tailles et longueurs des vides autour de la barre d'armature ont été étudiés. Les résultats de cette étude concordent avec les résultats des études passées en démontrant que des vides au-delà de 20% du périmètre *non-adhéré* causent une importante réduction de la contrainte d'adhérence et une augmentation du glissement de la barre d'armature. De plus, au-delà de cette limite, le mode de rupture des éprouvettes est soupçonné de changer de *fendage* à *déchaussement* de la barre d'armature. La limite augmente à 30% lorsque les vides recouvrent seulement la moitié de la longueur de la barre d'armature. Ces limites pourront ultérieurement aider les ingénieurs à déterminer si des actions ou des corrections sont nécessaires à effectuer afin de garantir un comportement adéquat des éléments structuraux.

5.2 Abstract

The proper encapsulation of reinforcing bars in shotcrete has represented for many years a concern among engineers. Thus, recent research has investigated the impact of imperfections specifically behind reinforcing bars using ASTM A944-10 "beam-end" specimens in the laboratory. Here, a 3D non-linear Finite Element model at *rib-scale* with different reinforcing bar encapsulation qualities was developed to validate such experimental results and obtain additional

data; different concrete covers and void sizes and lengths around the bar were investigated. The results support recent findings by suggesting a 20% un-bonded bar perimeter limit beyond which an excessive bar stress reduction and slip are observed. Beyond this limit, the failure mode of the specimens is thought to change from *splitting* to *pull-out*. The limit becomes 30% when voids cover half of the bar's length. These limits could allow engineers to determine if design actions or corrections guarantee the proper bond behavior of structural elements.

Keywords: Encapsulation quality; Shotcrete; Bond strength; Non-linear Finite Element analysis; Rib-scale; Concrete Damage Plasticity

Highlights:

- A *rib-scale* Finite Element model was used to study the impact of voids around bars
- Concrete cover and voids greatly affect the failure mode, slip and stress of bars
- Voids of 20% length set a bond threshold when covering the entire bonded length
- Voids of 30% length set a bond threshold when covering half of the bonded length
- The void size limits can be used for the design and inspection of shotcrete members

5.3 Introduction

5.3.1 General introduction

The possibility to create imperfections behind reinforcing bars has long been recognized when using shotcrete. This may arise because, among others, an excessive dose of set-accelerator is used, placement is done by inexperienced nozzle operators or because elements are heavily congested with reinforcement. Historically, the solution has been to emphasize on using robust shotcrete mixtures (proper thixotropy to achieve pumpable yet stable mixes) and a proper spraying technique to reduce as much as possible the appearance of imperfections behind reinforcement [9, 10, 126]. However, whenever a perfect encapsulation cannot be completely guaranteed, appropriate structural solutions to compensate for the bar stress loss have not yet been determined due to a lack of knowledge and data on the subject. To this day, structural engineers have limited tools when designing reinforced shotcrete structures or when evaluating the encasement quality of reinforcement in the field. In an effort to overcome these limitations, the American Concrete Institute (ACI) introduced the core-grading system to evaluate the

encasement quality of reinforcing bars with its 506.2-95 "Specification for shotcrete" document [28]. The system required evaluators to determine the size of imperfections on the surface of the cores (if any) taken from pre-construction panels[14] and then to associate their size to grades ranging from 1 (perfect encapsulation) to 5 (poorest encapsulation). Even though this system represented a great improvement for quality control purposes, the grades were being wrongly averaged to obscure the presence of large voids in some areas. Therefore, the grading system was removed in the 2013 edition of the guide [15] and the ACI created the 506.6T-17 "Visual shotcrete core quality evaluation technote" [16] where imperfections are given qualitative grades ranging from "very good" to "poor" depending on the percentage of the bar's transversal perimeter covered by imperfections (here called *un-bonded* perimeter or *u.p.*) and on their overall size. Nonetheless, the grades are still not associated to the bar stress loss. To do so, bond specimens can be tested in the laboratory. Among the most used small-scale standardized ones are the "pull-out" (formerly ASTM C234-91a [90]) and the ASTM A944-10 "beam-end" specimens [17]. The latter is usually preferred over the former since the stress state of flexural reinforced concrete members is accurately duplicated (both the test bar and the concrete around it are placed in tension). Experimental results in which ASTM A944-10 "beam-end" specimens were used to recreate various encapsulation qualities have shown that *un-bonded* perimeters of approximately 20% represent the onset of considerable bar slip and stress reduction [121, 127]. The results also suggest that voids equal to or greater than 30% *u.p.* may change the specimens' mode of failure from concrete *splitting* to a reinforcing bar *pull-out* increasing the chances of elements to fail in a brittle manner. Still, the mechanism by which reinforcing bar stresses are reduced as the size of *un-bonded* perimeters increase is not fully understood.

In the past, many experimental bond specimens have been successfully recreated using Finite Element (FE) models and in some cases the results have aid to establish rational criteria for the design of concrete structures [71-75, 128]. Indeed, FE models help to avoid expensive and time-consuming tests in the laboratory and provide valuable data which is difficult to obtain experimentally such as the stress state of the concrete around reinforcing bars. To the authors' knowledge, a 3D non-linear FE model in which the geometry of the reinforcing bar is explicitly modeled (*rib-scale*) to study the impact of imperfections located around the bars has not yet been reported. In this research, ASTM A944-10 "beam-end" specimens were modeled using the FE

[14] Panels often sprayed in complex shotcrete projects to recreate the challenging parts of actual structures.

package Abaqus 6.14 [107] to validate the results obtained in the laboratory [127] and to study the impact of the concrete cover and different sizes of voids over the test bar in conjunction the longest possible bonded length of the test bar given the geometry of the bond specimen. Ultimately, the main goal of this research paper is to determine *un-bonded* perimeter limits that can be deemed acceptable during the inspection of shotcrete structures (by evaluating cores taken from pre-construction panels) or even considered during the design of reinforced shotcrete structures to apply corrective measures (if voids are expected) possibly in the form of modification factors for the *development length* equation required by North American structural codes [5, 6]. However, proposing their actual value of modification factors is out of the scope of this paper.

5.3.2 Typical configuration of a "beam-end" specimen

The typical configuration of an ASTM A944-10 "beam-end" specimen, including all its parts, is shown in Figure 5.1.

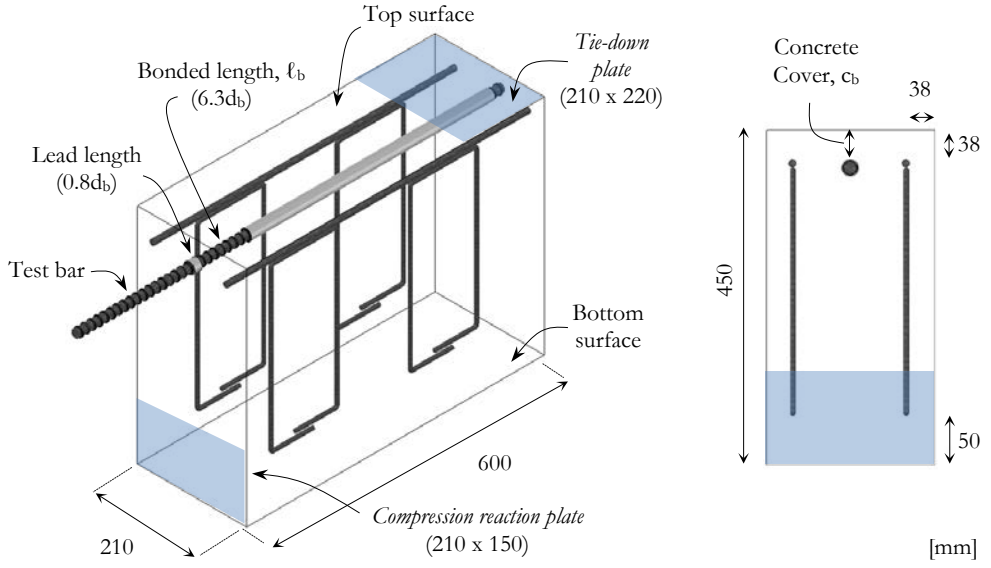

Figure 5.1: Configuration of the ASTM A944-10 "beam-end" specimen

As can be seen, the bonded length of the test bar and its location are controlled by front and back PVC sleeves. The length of the front sleeve is referred to as the *lead length* and is required to prevent a cone-type failure of the concrete on the front surface of the specimen. Additional longitudinal and transverse reinforcement guarantee that the specimen will not fail in flexure nor

in shear. The transverse reinforcement is placed parallel to the test bar so the bars do not cross the failure plane of the concrete. To test the specimen, tension needs to be applied to the test bar while the specimen is retained by plates referred to as *compression reaction* and *tie-down plates*. The displacement of the test bar is measured relative to the front and back concrete surfaces using position sensors attached to the test bar. The dimensions of the "beam-end" specimen analyzed herein are shown in Figure 5.1 and represent those tested by Basso et al. [127] using a test bar of 15.9 mm nominal diameter. A detailed description of the testing apparatus and the procedure is given by Basso el al. [124].

5.4 Finite Element model

5.4.1 Model assumptions

The concrete was assumed to be a homogeneous material and the steel as a perfect elastic material since the intention of the experiments was not to achieve steel yielding. Moreover, the ribs of the test bar were explicitly incorporated into the model; this has formerly been identified as a *rib-scale* model [64]. The ribs were modeled normal to the longitudinal axis of the test bar and the longitudinal ribs were omitted for mesh simplicity. While a *rib-scale* model presents some limitations, mainly because it increases computational time, its main advantage is that the stress – slip relationship between the test bar and the concrete results from the analysis rather than it being defined as a model input. As a consequence, the three components of the bond mechanism, i.e., adhesion, friction and mechanical anchorage [37, 40, 77], have to be defined *a priori*. Chemical adhesion occurs when the cement paste, while nucleating into its different chemical phases, bonds to the surface of the reinforcing bars. However, this adhesion is rapidly lost when small loads are applied over the reinforced concrete elements and, from that moment on, friction between the concrete and the reinforcing bars is created while they slip relative to one another. Mechanical anchorage is caused by the bearing of the reinforcing bars' ribs against the surrounding concrete. For deformed bars, this represents the primary contributor to the bond mechanism [35] providing the advantage of explicitly simulating bond with a *rib-scale* model.

5.4.2 Geometry and boundary conditions

The "beam-end" specimen was modeled using 8-node linear brick elements with a one-point integration scheme (C3D8R) and a *relaxed hourglass stiffness* control method for the test bar

and the concrete. The geometrical properties of the test bar used in the model are shown in Table 5.1.

Table 5.1: Geometrical properties of the test bar

Geometrical properties	Value
Nominal diameter, mm (d_b)	15.9
Core diameter, mm (D)	14.8
Ribs' height, mm (h_r)	0.9
Ribs' top width, mm (b_r)	1.0
Ribs' base width, mm (a_r)	5.0
Ribs' spacing, mm (s_r)	11.0
Ribs' face angle, degrees (θ)	24.2
Relative rib area*, mm/mm (R_r)	0.082

*In the absence of longitudinal ribs, $R_r = h_r / s_r$ as per Fei et al. [45]

The flexural bars and the stirrups were modeled using 2-node linear truss elements (T3D2) and were embedded in the concrete assuming perfect bond. The truss elements were assigned a cross-sectional area corresponding to those of the bars used in the experimental program [121, 127]; the overlapped section between the flexural bars and the stirrups was also considered. Regarding the boundary conditions of the model, the translational displacement of the nodes covering the same area as the *compression reaction* and the *tie-down plates* (refer to Figure 5.1) were restrained in the Z and the Y direction respectively. Moreover, the load was uniformly applied on the exterior end of the test bar using a "smooth" displacement function. The *un-bonded* perimeters simulating a poorly encapsulated reinforcing bar were explicitly introduced by removing the concrete elements on top of the test bar (facing the top surface of the specimen). The aforementioned parts of the model and examples of different encapsulation qualities around the test bar are shown in Figure 5.2.

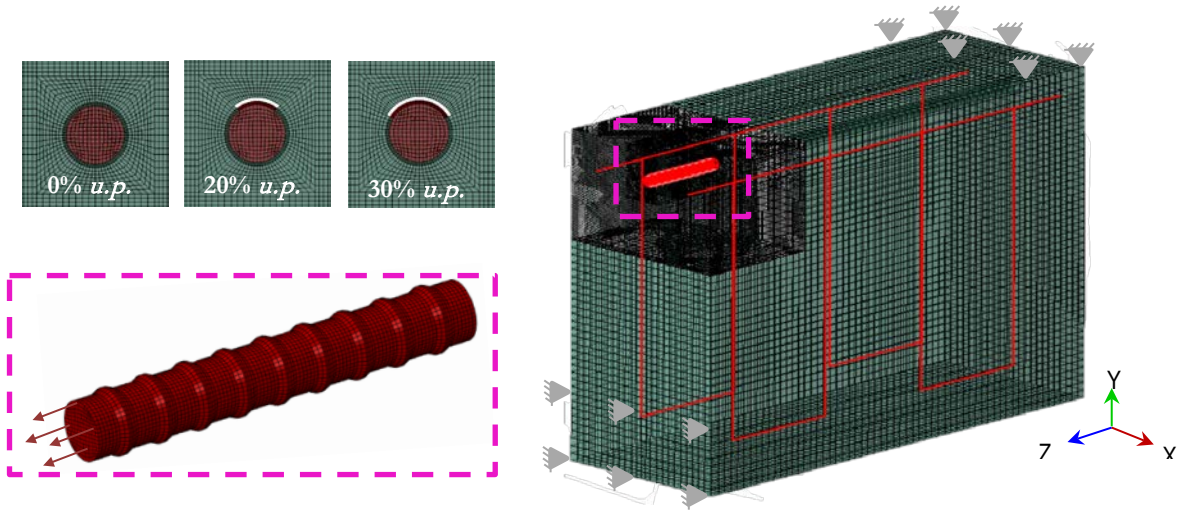

Figure 5.2: Finite Element model of the ASTM A944-10 "beam-end" specimen

5.4.3 Meshing

The concrete was divided in three sections with different mesh sizes and were connected to one another using a tie constraint. A "very fine" mesh of about 1.1 mm was created around the test bar approximately one bar diameter (d_b) away from it but was also extended to the top surface of the specimen since the initial concrete *splitting* cracks typically propagate through that location. A "fine" mesh of about 3.2 mm was used on the region of the specimen typically showing additional cracking after the ultimate load is reached and a "coarse" mesh of about 10.0 mm was used elsewhere. Both the "very fine" and the "fine" meshes were extended beyond the bonded length of the test bar (towards the back of the specimen) the equivalent length of one concrete cover (c_b). The mesh size of the test bar was set to 1.0 mm and, along with the three different concrete mesh sizes, its properties are presented in Figure 5.3.

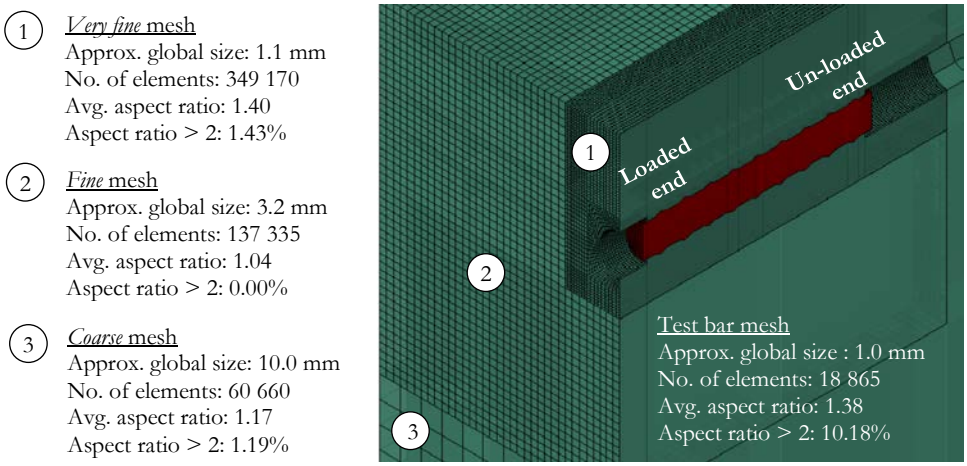

Figure 5.3: Mesh properties of the concrete and the test bar

Despite a cut section of the "beam-end" specimen is shown in Figure 5.3, symmetry was not used because the state of the concrete stresses around the bar could have been wrongly affected.

5.4.4 Material properties

The concrete was defined using the *Concrete Damage Plasticity* (CDP) constitutive model available in Abaqus 6.14 [107]. The CDP model is best suited to simulate low confining pressure conditions where concrete crushing and cracking govern in compression and in tension respectively. As a scalar plastic damage model, the CDP model is defined by the three fundamental assumptions of the incremental theory of plasticity: a *yield surface*, a *hardening rule* and a *flow rule* [129].

In the CDP constitutive model, the shape of the *yield surface*, described in detail by Lubliner et al. [108] and Lee et al. [109], is defined by two dimensionless constants; the ratio between the equi-biaxial stress and the ultimate uniaxial compressive stress (f_{b0}/f_c) and the constant K_c defining its shape in the deviatoric plane. The *yield surface* is also a function of the *effective stress* ($\bar{\sigma}_{c,t}$) and *hardening variables* which in turn, are defined using scalar *damage* variables for the compressive (d_c) and the tensile (d_t) behavior. The *true stress* ($\sigma_{c,t}$), expressed in Equation 5.1, is then computed with the user specified uniaxial stress relationships.

$$\sigma_{c,t} = \left[1 - d_{c,t}\right]\bar{\sigma} \tag{5.1}$$

The *hardening rule* of a plasticity model is used to define the evolution of subsequent loading surfaces (beyond the *yield surface*) and the *flow rule* links the plastic stress – strain relationships to such surfaces. In the CDP model, the *flow rule* is defined by a Drucker-Prager hyperbolic surface whose shape is determined by two constants. The eccentricity (ε_{cdp}) determines the rate at which the function approaches the asymptote (in the meridian plane) and the angle of concrete dilatancy (ψ) represents the volume of concrete expansion at high confining pressures. A *viscosity* parameter (μ_c) can also be specified to help improve the convergence of the model at each iteration.

In this research, the compressive stress ($\bar{\sigma}_c$) – strain (ε) curve was defined according to Popovics [130] and Thorenfeldt et al. [131] using Equation 5.2. Such relationship has been demonstrated to be applicable to f_c ranging from 15 to 125 MPa [132]. The value of f_c and the modulus of elasticity (E_c) of the concrete were set to 58.0 MPa and 33.3 GPa respectively according to

experimental results [127] and the strain at compressive strength (ε_c) was set to 0.0025 according to De Nicolo et al. [133]. The parameter n represents a curve-fitting factor whose value results in 3.3 according to Equation 5.3 established by Popovics [130]. The factor k was calculated using Equation 5.4 as proposed by Collins et al. [134, 135].

$$\bar{\sigma}_c / f_c = \frac{n\,(\varepsilon/\varepsilon_c)}{n - 1 + (\varepsilon/\varepsilon_c)^{nk}} \tag{5.2}$$

Where:

$$n = E_c / (E_c - f_c / \varepsilon_c) \tag{5.3}$$

$$k = \begin{cases} 1.0 & \text{for } \varepsilon/\varepsilon_c \leq 1 \\ 0.67 + \left(f_c / 62\right) & \text{for } \varepsilon/\varepsilon_c > 1 \end{cases} \tag{5.4}$$

As required by Abaqus 6.14, Equation 5.2 was defined in terms of compressive inelastic strains ($\tilde{\varepsilon}_c^{in}$) using Equation 5.5. The onset of concrete plasticity was assumed to occur at $0.4f_c$ and a Poisson's ratio (ν_c) of 0.14 was used based on the experimental results [127].

$$\tilde{\varepsilon}_c^{in} = \varepsilon - (\bar{\sigma}_c / E_c) \tag{5.5}$$

The behavior in tension was defined in terms of a tensile stress ($\bar{\sigma}_t$) – crack opening (δ) relationship to avoid as much as possible mesh sensitivity arising from the lack of reinforcement in some areas of the model [107]. The relationship established by Cornelissen et al. [136] as expressed in Equation 5.6 was used for this purpose. The recommended coefficients for normal weight concrete C_1 and C_2 of 3.0 and 6.93 respectively were used.

$$\bar{\sigma}_t / f_t = \left(1 + (C_1\delta / \delta_0)^3\right)^{(-C_2\delta / \delta_0)} - (\delta / \delta_0)\left(1 + C_1^3\right)^{-C_2} \tag{5.6}$$

The relationship begins at the tensile strength (f_t) for a null crack opening and ends at the maximal crack opening (δ_0) at which stress cannot be longer transferred. The tensile strength of concrete (f_t) was calculated as 3.8 MPa based on Equation 5.7 [137] where f_{sp} represents the splitting tensile strength of 3.9 MPa obtained experimentally [127] and β the width to length ratio of the bearing strips equal to 0.1 used in the laboratory as per ASTM C496 [101]. The value of δ_0 was approximated as $5.14\,G_F / f_t = 0.129$ mm where the fracture energy of concrete (G_F) was

estimated as 0.095 N/mm [138]. The *damage* variables d_c and d_t were calculated as $d_{c,t} = 1 - \bar{\sigma}_{c,t} / f_{c,t}$ for $\bar{\sigma}_{c,t} \geq f_{c,t}$ and 0 for $\bar{\sigma}_{c,t} < f_{c,t}$ [139]. The selection of the plasticity parameters f_{b0}/f_c, ε_{cdp}, K_c, and ψ is discussed in Section 5.5.

$$f_t = f_{sp}\left(1 - \beta^2\right)^{3/2} \tag{5.7}$$

For the steel, a Young modulus (E_s) of 200 GPa according to the experimental results [127] was used and a Poisson ratio (ν_s) of 0.3 was assumed.

5.4.5 The bar – concrete interface

The interaction between the test bar and the concrete was defined through a general contact algorithm. In order to recreate the three components of the bond mechanism, a cohesive law (zero-thickness), a Coulomb friction law and a "hard" pressure-overclosure relationship (with allowed separation) were specified over different sections of the test bar's surface (refer to Lagier et al. [74]). Thus, as the load was applied to the test bar, the different sections of the interface were progressively placed on contact/stick, contact/slip or separation states.

The pressure-overclosure relationship guarantees the load transfer from the bar's ribs to the concrete; a penalty contact constraint was used. Although the penalty constraint induces additional stiffness to the model because the nodes of the test bar are allowed to slightly penetrate the concrete elements, its impact on the model's response is usually insignificant and avoids over-constraint issues. The cohesive layer was defined using uncoupled traction-separation laws in the normal (σ_1) and in the two shear ($\tau_{2,3}$) directions. The cohesive law was only assigned to the surface in between the ribs where its impact is more important. The cohesive laws were assumed as linear elastic with stiffness K_1 and $K_{2,3}$ for the normal and the two shear directions. At the onset of the ultimate cohesive strength ($\bar{\sigma}_1$ or $\bar{\tau}_{2,3}$), the damage of the cohesive laws is linear and is specified by means of a displacement δd. When the cohesive layer is completely damaged, a separation state occurs in the normal direction whilst in the shear direction the Coulomb friction law is activated. Relative slip between the test bar and the concrete occurs if the equivalent shear stress at the surface ($\tau_{eq} = \sqrt{\tau_2{}^2 + \tau_3{}^2}$) exceeds the critical shear stress (τ_{crit}) equal to the static friction coefficient between the steel and the concrete (μ) multiplied by the normal closing pressure between both materials (p). Because a penalty contact constraint was used, an elastic friction stiffness ($K_{el,f}$) specified by the user causes some relative

slip between the test bar and the concrete before τ_{crit} is attained. On the surface of the ribs, the friction law is actively functioning in the tangential direction (if there is contact between the concrete and the test bar) because the cohesive law was not assigned in that region. The properties of the bar – concrete interface that were used are shown in Table 5.2 and were chosen based on research performed by Lagier et al. [74] and Rabbat et al. [36].

Table 5.2: Bar-concrete interface parameter values used in the FE model

Property	Parameter	Value
Friction	μ (-)	0.6
	$K_{el,f}$ (N/mm^3)	80
Cohesive	$\bar{\sigma}_1$ (MPa)	2.0
	$\bar{\tau}_{2,3}$ (MPa)	1.2
	K_1 (kN/mm^3)	0.10
	$K_{2,3}$ (kN/mm^3)	0.02
	δ_d (mm)	0.005

5.4.6 Solution strategy

A quasi-static explicit dynamic analysis was used. The explicit formulation is very effective in highly non-linear problems under quasi-static loading such as bond between a reinforcing bar and concrete around it. A direct integration of the equations of motion are solved using the explicit central-difference method with very small time increments; a static solution can be obtained with this strategy when the loading rate is very slow. For such purpose, the time to reach the maximum load is suggested to be less than 10 times the fundamental period of vibration to assure that the ratio between the kinetic (E_k) and the internal energy (E_I) of the model lies below 5% at the onset of concrete cracking [74, 111]; these recommendations minimize inertial effects. In this study, the lowest natural vibration frequency (f_n) of the "beam-end" specimen was 380 Hz. Thus, the analysis time was set to $t = 10(1/f_n) \approx 0.02$ s. The density of the concrete and the steel were considered as $\varrho_c = 2350$ and $\varrho_s = 7850$ kg/m^3 respectively.

5.5 Validation of the model

5.5.1 Calibration of the plasticity parameters

The selection of the model's plasticity parameters f_{b0}/f_c, ε_{cdp}, K_c, and ψ needed thoughtful consideration since biaxial and triaxial tests are needed to determine their values but were not

available. However, preliminary analysis with the FE model showed that the parameters that most influence the bond performance of the test bar were K_c and ψ for this particular case. Accordingly, such parameters were chosen based on a statistical calibration procedure [140] in which the ratios of the bar stress at failure obtained with the FE model (f_{smax}) and those obtained in the experiments (f_{exp}) [127] were optimized to achieve the highest "desirability" value. First, two first-order surface models of the $f_{smax}/f_{exp.}$ ratio were built with various combinations of K_c and ψ; one surface for a 0% *u.p.* and another one for a 30% *u.p* FE model. Each surface was created using two values of K_c (0.610 and 0.667) and ψ (30° and 38°) for a total of 4 combination. An additional f_{smax}/f_{exp} ratio was computed to analyze a center point (K_c = 0.640 and ψ = 34°) and validate that the surface models were in fact planes and did not present curvature. Then, each f_{smax}/f_{exp} ratio was linked to a "desirability" value in between 0 and 1 using the triangular *desirability function* given by Equation 5.8. As can be seen, the target "desirability" was set to 1 whereas the lower and upper limits for a 0 "desirability" were set to 0.9 and 1.1 respectively.

$$d_i = \begin{cases} 0 & f_{smax}/f_{exp} < 0.9 \\ (f_{smax}/f_{exp} - 0.9) \,/\, 0.1 & 0.9 \leq f_{smax}/f_{exp} \leq 1.0 \\ (1.1 - f_{smax}/f_{exp}) \,/\, 0.1 & 1.0 \leq f_{smax}/f_{exp} \leq 1.1 \\ 0 & f_{smax}/f_{exp} > 1.1 \end{cases} \tag{5.8}$$

All "desirability" values obtained with each FE model were transformed into a *global desirability* using Equation 5.9 and ultimately, the K_c and ψ values having the maximal *global desirability* were selected. In this case, such values were K_c = 0.667 and ψ = 33° so they were selected for the rest of the study.

$$D = (d_i \cdot \ldots \cdot d_m)^{1/m} \tag{5.9}$$

The f_{b0}/f_c ratio was set to 1.16 based on the biaxial tests performed by Kupfer et al. [121] where concretes with compressive strengths ranging between 20 and 60 MPa were studied. A 1.16 value also agrees with biaxial tests reported by Hussein et al. [141] for concretes with compressive strengths ranging between 40 and 70 MPa and 6.0 mm maximum size aggregates as the ones used in the experimental investigation [127]. The value of ε_{cdp} was set to 0.1 according to the Abaqus 6.14 user manual [107] and the value for the viscoplastic regularization (μ_c) was set to 0.

5.5.2 The influence of the interface laws

The importance of considering both the cohesive and the frictional laws in a *rib scale* model has been discussed in detail by Lagier et al. [74]. It has been shown that, contrary to the frictional law, the cohesive law does not considerably influence the computed reinforcing bar stress at bond failure. Nonetheless, because it can contribute to the concrete crack opening, it was included in this study. With this modeling technique, the parameter that most influenced the behavior of the stress-slip curve was found to be the *elastic friction stiffness* ($K_{el,f}$). Ideally, the largest possible value of $K_{el,f}$ should be used to best recreate the theoretical shear-slip behavior (no slip before τ_{crit} is attained). However, the chosen value of $K_{el,f}$ = 80 MPa/mm was selected as higher ones created a "too stiff" interface which caused the stress state of the concrete to behave in a similar manner as if the test bar was "tied" to the surrounding concrete.

5.5.3 Adequacy of the model and discussion

The bar *stress-slip* curves at the un-loaded end of the bar are presented in Figure 5.4a, 4b and 4c for *un-bonded* perimeters of 0, 20 and 30% respectively. The slip from the FE model was calculated as the displacement difference between the test bar and the concrete at the approximate location where the linear position sensors were placed in the experimental program. In addition, the bar stress at bond failure (f_{smax}) obtained with the FE model and those obtained in the laboratory (including 19.0 mm nominal diameter bars) are shown in Figure 5.4d.

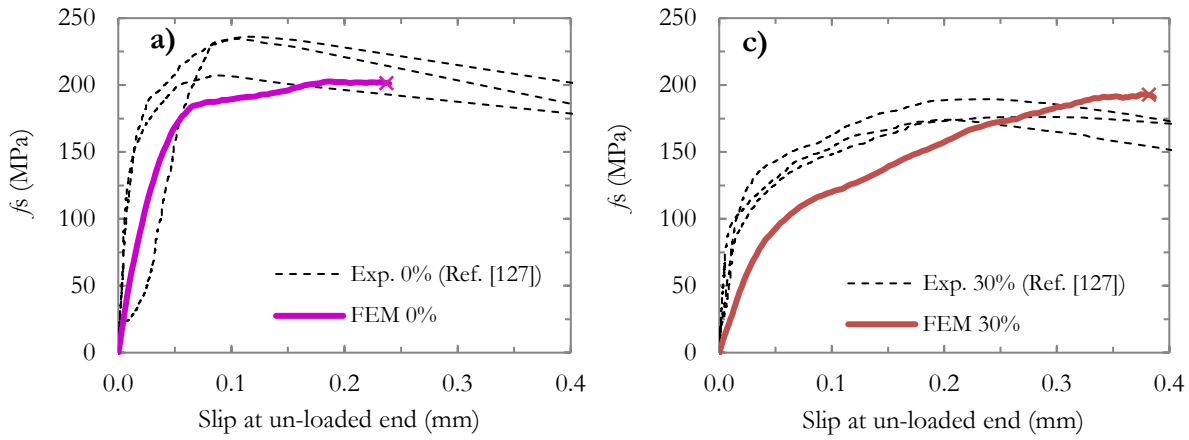

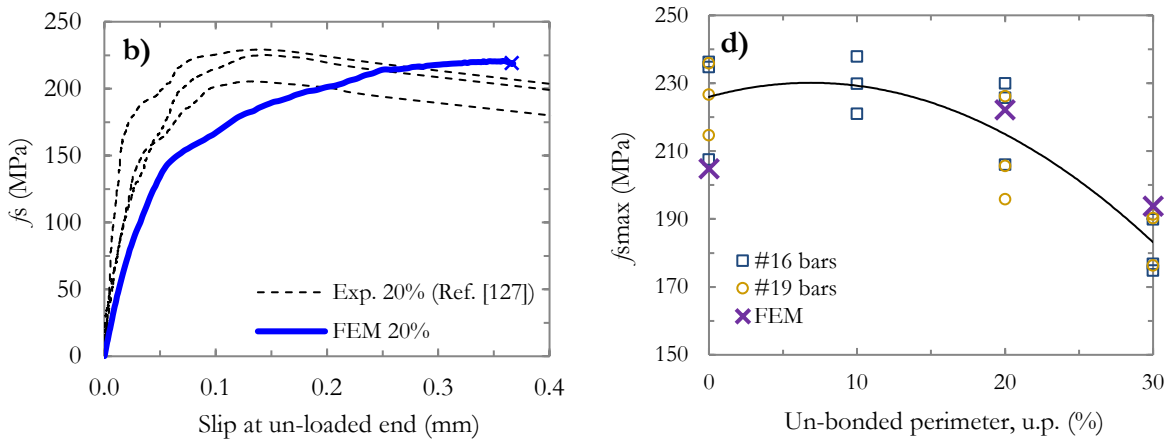

Figure 5.4: Stress-slip curves of the FE model at (a) 0% (b) 20% (c) 30% *u.p* and (d) stresses at bond failure

As observed, the model has some limitations. Firstly, the slip stiffness is slightly underestimated in comparison with the results from the experimental campaign. The joint effect of average values assigned to materials, the geometry of the bar as well as the inherent assumptions behind the CDP model may be the reason for these differences. As a scalar plastic damage model, CDP cannot compute actual cracking and the width of cracks. Instead, damage can be considered by reducing the mechanical properties of concrete once failure, and therefore plasticity, is attained. This makes it impossible for the model to truly account for residual stresses after the ultimate load is attained in the same way it is observed in the laboratory. Consequently, the post-peak part of the stress-slip curves can differ from the FE model and those obtained with the laboratory specimens. It is for this reason that only the pre-peak part of the curve will be studied henceforth. In terms of the bar to concrete interface properties, it should be noted that larger values for the cohesive and friction laws, besides being unrealistic, did not considerably change the slip stiffness of the model's bond behavior. Moreover, the error of the bar stresses at bond failure away from the average represent -9% and +6% for the 0% and the 30% *u.p.* respectively and are deemed acceptable. For this reason, the selected values of the model were kept for further analysis.

5.6 Parametric study

5.6.1 Design

A parametric study was performed to determine the influence of the concrete cover (c_b), the *un-bonded* perimeter (*u.p.*) and the length of the voids (V_L) over the test bars with a constant bonded length of $\ell_b/d_b = 12.5$. The variables under study are represented in Figure 5.5.

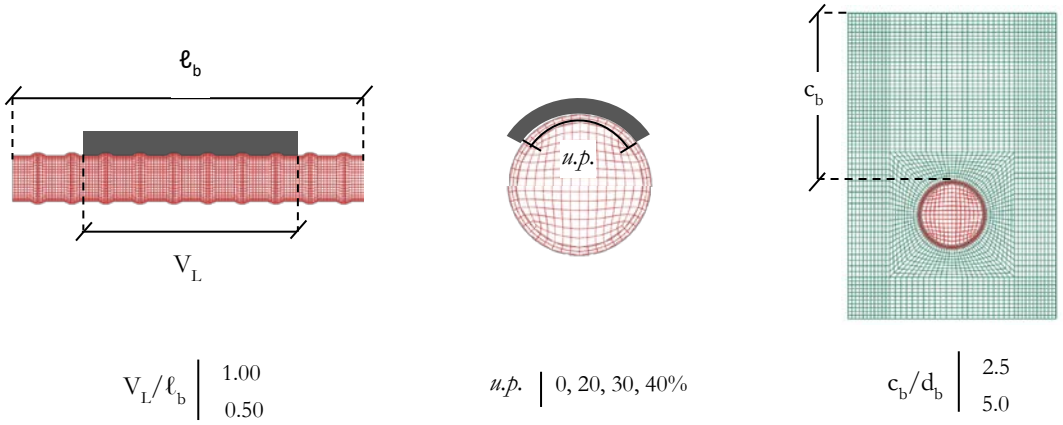

Figure 5.5: Variables of the parametric study

Concrete covers of 40 and 80 mm ($c_b/d_b = 2.5$ and 5.0 respectively), as it would normally be used in shotcrete structures given their exposure to the ground or weather [5], were chosen. In regard of void sizes, *un-bonded* perimeters (*u.p.*) up to 40% were investigated and were considered all along the test bar's length ($V_L/\ell_b = 1.0$) for both concrete covers. Voids covering 50% of the bonded length were also investigated for specimens with 30% and 40% *u.p.* For such purpose, voids were placed in the middle of the bar; placing them in other position over the bar's length did not influence considerably the computed bar stress at bond failure. It should be noted that preliminary results showed that the height of the voids did not have a significant impact on the bar stress at bond failure (as it had already been observed experimentally [121]) and for that reason this parameter was not investigated. Specimens are subsequently named by their concrete cover, the *un-bonded* perimeter and the void's length over the bar, i.e. 2.5cb-20up-1.0VL or 5.0cb-30up-0.5VL. In total, 6 cases per concrete cover were studied. The bar stress-slip curves as well as the state of stress in the surrounding concrete (maximum principal, radial and hoop stresses) are presented subsequently.

5.7 Results and discussion

5.7.1 Stress-slip curves

The bar stress (f_s) is plotted against the slip of the reinforcing bars for the different *un-bonded* perimeters (*u.p.*) and the concrete covers (c_b) under study in Figure 5.6a and 5.6b. Each bar stress – slip is plotted up to f_{smax} to focus specifically on the bond behavior of the reinforcing bars before and at failure. The slip in the figures represents the relative displacement between the concrete and the reinforcing bars. The curves belonging to the c_b/d_b = 2.5 concrete cover specimens are shown in Figure 5.6a whereas those belonging to specimens with a c_b/d_b = 5.0 concrete cover are shown in Figure 5.6b for the un-loaded end of the bar.

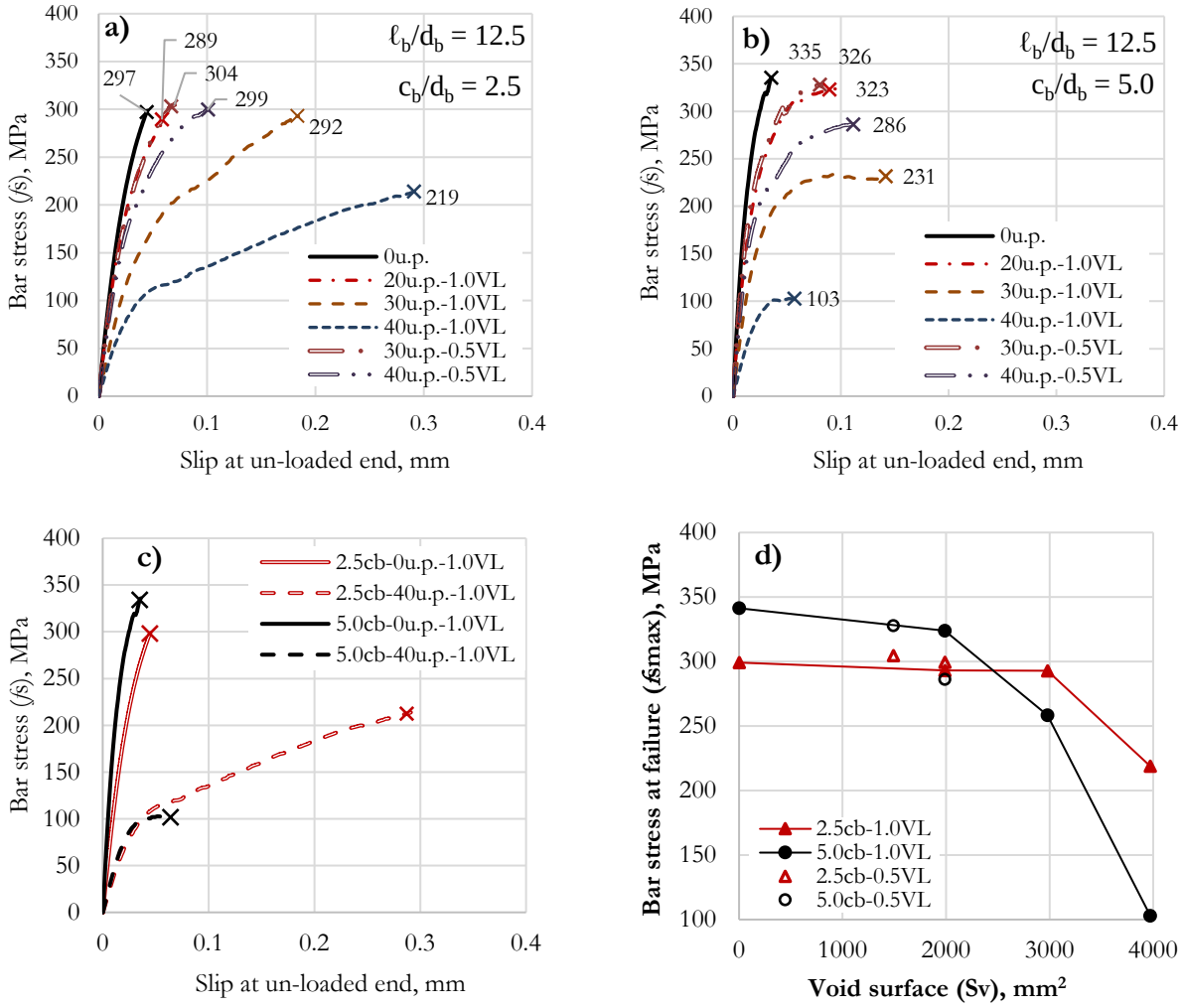

Figure 5.6: Stress-slip curves at the un-loaded end for (a) c_b/d_b = 2.5 (b) c_b/d_b = 5.0 (c) both concrete covers with and without voids and (d) the bar stress at failure of all specimens

As can be observed, the numerical model adequately captures the increase of f_{smax} and the stress-slip slope, or *slip stiffness*, as the bonded length and the concrete cover of the specimens are increased for perfectly encapsulated bars. Indeed, a (297-199)/199 = 49% increase of f_{smax} is computed with a ℓ_b/d_b = 12.5 in comparison to a ℓ_b/d_b = 6.3 specimen with a c_b/d_b = 2.5 concrete cover (refer to Section 5.5.3). In addition, a (335-297)/297 = 13% increase of f_{smax} is obtained when the concrete cover is increased from c_b/d_b = 2.5 to 5.0 for a ℓ_b/d_b = 12.5 bonded length specimen. The increase of f_{smax} matches well those found in past research with similar parameters [39] and in both cases the *slip stiffness* increases as it would be expected with a longer bond length and a larger concrete cover (refer to Figure 5.6c).

However, it should be noted that the 13% increase of f_{smax} is relatively small (considering that the concrete cover was doubled) indicating that the c_b/d_b = 2.5 concrete cover specimen is close to a mode of failure transition from *splitting* to *pull-out* where usually not a significant gain of f_{smax} is observed [142].

When the presence of voids is analyzed, it can be seen that f_{smax} decreases as the *u.p.* increases from 0% to 40% for both concrete covers; the same tendency is observed for the *slope stiffness*. However, the overall behavior between specimens is different depending on their amount of concrete cover. Indeed, f_{smax} decreases gradually with a large slip increase for c_b/d_b = 2.5 concrete cover specimens whereas its decrease for specimens with a c_b/d_b = 5.0 concrete cover is somewhat abrupt without any significant slip increase.

The more pronounced reduction of f_{smax} for c_b/d_b = 5.0 concrete cover specimens as the *u.p.* increases could be due to a premature mode of failure change from concrete *splitting* to a reinforcing bar *pull-out* as the *u.p.* increases in comparison to a c_b/d_b = 2.5 concrete cover specimen. It is possible that a larger concrete cover (or other type of bar confinement such as stirrups and concrete fibers) could favor a higher and more localized stress concentration in front of the first reinforcing bar ribs (at the loaded end) and thus cause concrete crushing in front of them while bearing on a smaller surface with the increase of the *u.p.* This is supported by the considerably smaller slip attained at f_{smax} with 5.0cb-40u.p.-1.0VL specimens in comparison to 2.5cb-40u.p.-1.0VL specimens as shown in Figure 5.6c. The effect of the concrete cover and the increase of the *u.p.* shows that beyond a 20% *u.p.*, f_{smax} decreases even more for c_b/d_b = 5.0 specimens than those with a c_b/d_b = 2.5 concrete cover as shown in Figure 5.6d. In

that figure, the size of the voids is expressed as the surface they cover over the bar's bonded length in order to plot all specimens. Indeed, it can be seen that f_{smax} obtained with 5.0cb-40u.p.-1.0VL is smaller by (219-103)/219 = 53% in comparison with 2.5cb-40u.p.-1.0VL. Regarding voids covering half of the reinforcing bar's bonded length, it is noted that its size has a considerable influence on the stress-slip behavior. Indeed, the 30up-0.5VL specimen shows approximately the same behavior as the 20up-1.0VL specimen and the 40up-0.5VL shows a better stress-slip performance than the 40up-1.0VL specimens for both concrete covers.

Based on the above discussion, it seems adequate to set a 20% *u.p.* as an imperfection size limit if voids cover the entire bonded length of a reinforcing bar being developed. Indeed, the un-loaded end slip at bond failure for a 2.5cb-30up-1.0VL specimen is considerable and represents (0.185-0.045) / 0.045 = 311% in comparison to a perfectly encapsulated bar whereas it is only (0.064-0.045) / 0.045 = 42% for a 2.5cb-20up-1.0VL specimen. Moreover, for c_b/d_b = 5.0 concrete cover specimens, it is not the slip of the bar but the reduction of f_{smax} that may compromise the performance of a structural element. The reduction of f_{smax} in the case of a 5.0cb-30up-1.0VL specimen with respect to a perfectly encapsulated bar represents (335-231) / 335 = 31% whereas it only represents (335-323) / 335 = 4% for a 5.0cb-20up-1.0VL. In a similar way, a 30% *u.p.* could be accepted if the voids cover 50% or less of the bar's bonded length.

5.7.2 Stress state of concrete around reinforcing bars

The 20% *u.p.* limit suggested before can be supported when analyzing the concrete's Maximum Principal tensile stresses (S_{max}) as well as the radial (σ_r) and the hoop (σ_h) stresses around the specimens' reinforcing bars. To compare the bond behavior of reinforcing bars, the stress states at 80% of f_{smax} is used. A value slightly before f_{smax} was selected to avoid comparing values for a completely "plasticized" concrete based on the CDP model's hypothesis. The Maximum Principal tensile stresses are shown in Figure 5.7 and 5.8 for 0u.p, 20u.p.-1.0VL and 40u.p.-1.0VL specimens having c_b/d_b = 2.5 and 5.0 concrete cover respectively. A 30% *u.p.* is not presented as the stress state of the concrete around the bar was found to be similar to the one around a 40% *u.p.* A cut along the reinforcing bar's longitudinal axis and three sections transversal to the reinforcing bar are presented in each figure. The sections are labeled depending on the rib they lie ahead from considering the first rib as the one closest to the loaded end of the reinforcing bar, i.e. where the highest values of the principal stress in tension can be

observed. The tensile stresses range from 3.8 MPa (red) to 0.0 MPa (dark blue) in 0.3 MPa increments.

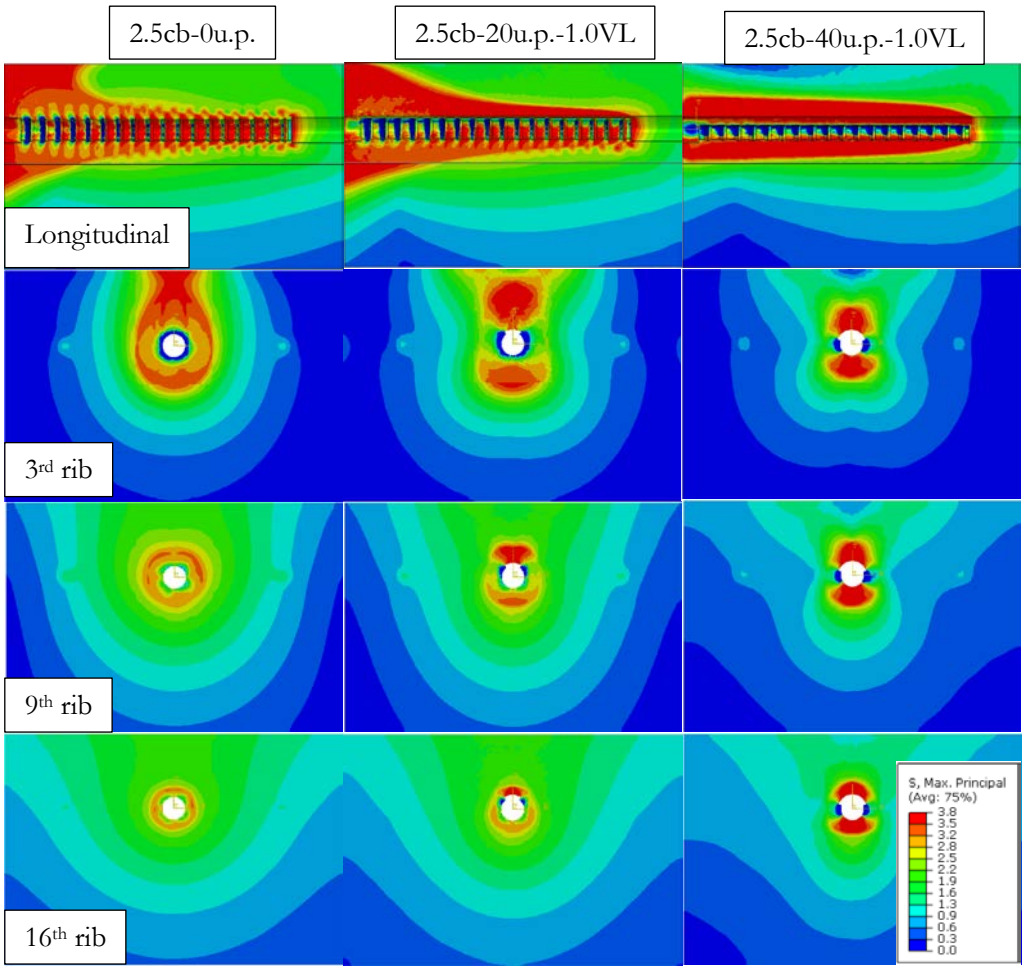

Figure 5.7: Principal stresses in tension of specimens with 2.5d_b c_b at 80% of f_{smax}

From Fig. 5.7 and 5.8, a distinction can be made from specimens that might potentially fail by *pull-out* rather than by concrete *splitting*. Indeed, for both concrete covers under study, an *u.p.* of 40% will cause an undesirable *pull-out* failure since stresses close to the tensile strength of the concrete are mainly concentrated nearby the ribs along the entire bonded length of the reinforcing bar. In contrast, for specimens with 0% and 20% *u.p.*, the principal stress distribution shows a clear variation along the *development length*. The 20% *u.p.* can be regarded as the transition point where clearly the stress distribution around the bar is disrupted in comparison to a perfectly encapsulated bar but not enough to cause a drastic f_{smax} or slip stiffness loss. This seems to be true for 2.5cb-20up-1.0VL and 5.0cb-20up-1.0VL specimens where a *splitting* failure is most likely

to occur based on the stress distribution around the bar. Again, the 20% *u.p.* is believed to be the limit beyond which a failure mode change can occur.

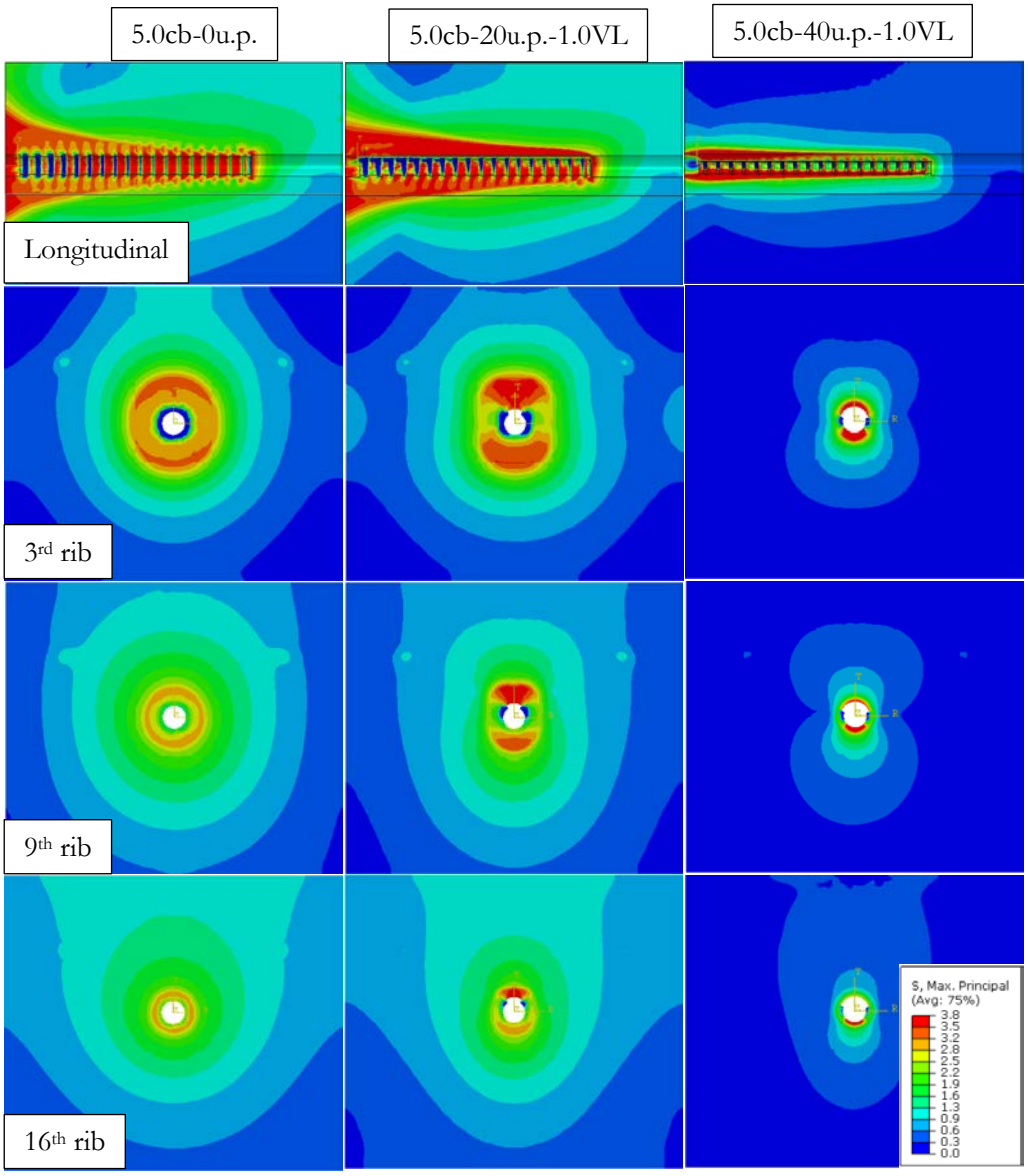

Figure 5.8: Principal stresses in tension of the specimens with 5.0d_b c_b at 80% of f_{smax}

From Fig. 5.9 and 5.10, where the radial stresses (σ_r) and the tensile hoop stress (σ_h) are shown (ranging from from +3.8 MPa to -10MPa) for 5.0cb-20up-1.0VL specimens at 80% f_{smax}, the 20% *u.p.* limit can also be noted. The radial stresses (σ_r) give an indication of the stress transfer between the concrete and the steel and, as can be observed, σ_r is uniformly acting in compression (blue) around the bar for a perfectly encapsulated bar. As mentioned before, the distribution of σ_r is inevitably distorted with the presence of a void. Indeed, the distribution of the radial stresses

change to act in tension (red); first only above the bar and then below it as the size of the void increases. However, σ_r still acts in compression all around the bar except at the location of the void with a 20% *u.p.*; tensile stresses appear below the bar beyond this value of *u.p.*

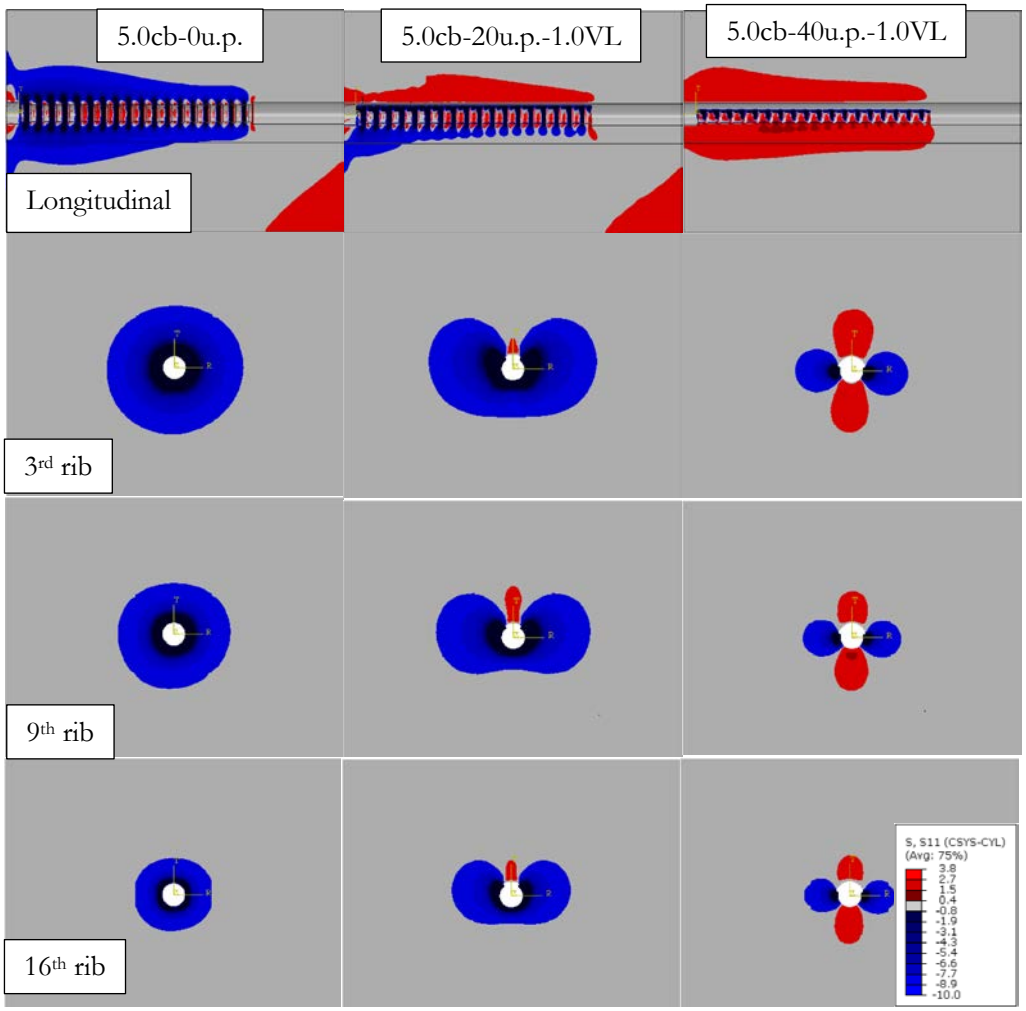

Figure 5.9: Radial stresses (σ_r) around the bar of 5.0d_b c_b specimens at 80% of f_{smax}

A uniform tensile hoop stress (σ_h) is also computed around reinforcing bars with perfect encapsulation as can be seen in Figure 5.10. As expected, the extent of σ_h decreases as the size of voids increases and a considerable change is observed when *un-bonded* perimeters change from 20% to 40%. This is especially true at the loaded end of the reinforcing bar and as seen with the maximal principal stresses, the extent of the hoop stresses becomes uniform all along the bonded length of the reinforcing bar for 5.0cb-40u.p.-1.0VL in comparison to 5.0cb-20u.p.-1.0VL or 5.0cb-0u.p.

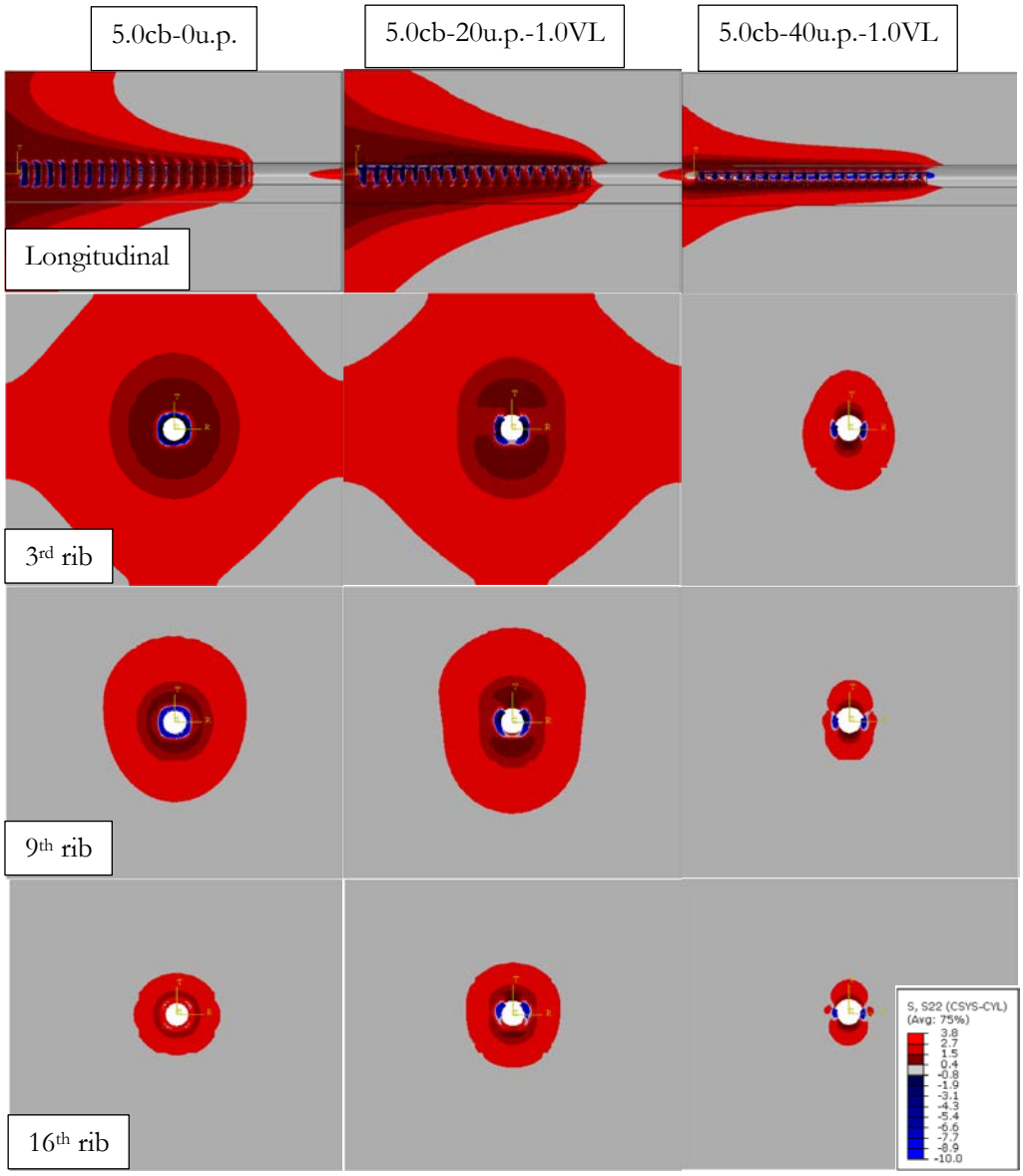

Figure 5.10: Hoop stresses (σ_h) around the bar of 5.0d_b c_b specimens at 80% of f_{smax}

5.8 Recommendations for the design and assessment of shotcrete structures

5.8.1 Towards recommendations

Albeit it is difficult to extrapolate findings with small-scale bond specimens to full-size structural members, first recommendations can be made from this numerical study in combination with recent experimental findings [121, 127]. Here, guidelines are focused on determining an acceptable *u.p.* limit at which measures to compensate for the bar stress loss could still be used to avoid compromising the structural behavior of reinforced shotcrete

elements. As discussed in previous research [121, 127], such measures could take the form of modification factors for the *development length* equation required to be computed by reinforced concrete design codes in North America [5, 6]. The aim of this research is that such limits are used if imperfections behind reinforcing bars are foreseen when shotcrete is considered (depending on nozzlemen expertise, level of reinforcement congestion, etc.) or if voids are found after cores taken from pre-construction panels are inspected.

5.8.2 First recommendations

Based on the analysis made above, imperfections may be limited to the following constraints:

- Imperfections around reinforcing bars should be limited to a 20% *un-bonded* perimeter if there is evidence that they will cover all (or most) of the bonded length of a reinforcing bar being developed. Nonetheless, proper actions to counteract the bar stress reduction should still be taken into account. This might be achieved with the use of modification factors applied to the *development length* of reinforcing bars in tension equation as prescribed by North American design codes [5, 6].

- Imperfections around reinforcing bars could be limited to a 30% *un-bonded* perimeter if there is evidence that they will cover less than half of the developed reinforcing bar's bonded length. The extent of the voids over the bonded length could be determined based on the percentage of cores taken from pre-construction panels and therefore, the judgment of a qualified structural engineer or inspector is needed.

- Larger *un-bonded* perimeters should not be accepted unless enough data exists to prove that their presence will not jeopardize the structural performance of a reinforced concrete element. Imperfections of greater size than those previously discussed can greatly increase either the risk of a *pull-out* failure (and thus the brittle failure of an element) or an excessive reinforcing bar slip.

5.9 Conclusion

ASTM A944-10 "beam-end" specimens were modeled using a three-dimensional Finite Element (FE) model at *rib-scale* using Abaqus 6.14. As a consequence of the modeling technique,

the bar stress-slip response resulted from the numerical analysis itself instead of it being defined as an input for the model. The *Concrete Damage Plasticity* (CDP) was used as the constitutive law for the concrete elements and a statistical procedure was used to calibrate two of its parameters based on results available from experimental tests. Thereafter, a parametric analysis using the longest possible bonded length in accordance with the ASTM A944-10 standard for the specimen under study ($\ell_b/d_b = 12.5$) was undertaken to study the influence of the concrete cover and different sizes and lengths of voids on the bond behavior of the specimen. The bar stress-slip curves as well as the stress state of the concrete around the bar, i.e., the Maximum Principal stresses (S_{max}), the radial (σ_r) and the hoop (σ_h) stresses, were studied for this purpose. The stresses were evaluated at 80% of the bar stress at failure.

The numerical results showed that the *rib-scale* model adequately reproduced the stress-slip response of reinforcing bars with different qualities of encapsulation. Both the stress-slip response and the stresses around the concrete bar helped to establish a 20% *un-bonded* perimeter as a limit beyond which the anchorage capacity of a bar could be compromised. It was found that concrete cover, in the presence of voids, played a significant role in establishing such limit. On one hand, a relatively small cover could cause an excessive slip of a reinforcing bar. On the other hand, larger concrete covers could reduce the bar stress at failure due to a likely failure mode change from concrete *splitting* to a bar *pull-out* as the sizes of voids increase. If imperfections cover half of the developed length of a bar, a larger *un-bonded* perimeter of up to 30% might be allowed.

The limits established here could become acceptable void sizes that could be considered during the design phase of structures for the use of corrective measures such as modification factors for the *development length* equation. During the inspection of pre-construction panels, the actions taken during the design phase could be validated. Although the development of the actual modification factors was not part of the scope of this study, an upcoming phase of this research will focus on their development keeping in mind the limits established herein.

Overall, the strategy adopted herein to model the bond mechanism provided a comprehensive understanding of the stress of reinforcing bars with different sizes of *un-bonded* perimeters. Moreover, it illustrated the interest in validated non-linear 3D FE models to generate extensive parametric studies to complement experimental results and provide a strong basis to establish

rational recommendations for the design and the inspection of reinforced concrete structures. Nevertheless, additional research is needed to validate these findings using full-scale specimens including different parameters and configuration (more than one test bar with, longer bonded lengths, stirrups, fibers, etc.).

5.10 Acknowledgements

The authors are grateful to the Concrete Infrastructure Research Center (CRIB) of Québec and the Natural Sciences and Engineering Research Council of Canada (NSERC), the Canadian Council of Independent Laboratories (CCIL), The American Shotcrete Association (ASA), the Québec and East Ontario Chapter of the American Concrete Institute (ACI) and the Tunnelling Association of Canada (TAC) for their financial support to this project.

5.11 References

[5] ACI Committee 318, "318-19 Building code requirements for structural concrete and commentary," American Concrete Institute, Michigan, 2019, 559 p.

[6] CSA, "A23.3-19 Design of concrete structures," Canadian Standards Association, Ontario, 2019, 297 p.

[9] Crom, T. R., "Dry mix shotcrete nozzling," Concrete International, Vol. 3, No. 1, 1981, pp. 80-93.

[10] Beaupré, D., Jolin, M., "Effect of shotcrete consistency and nozzleman experience on reinforcement encasement quality," Shotcrete Magazine, Vol. 3, No. 4, 2001, pp. 20-23.

[15] ACI Committee 506, "506.2-13 Specification for shotcrete," American Concrete Institute, Michigan, 2013, 12 p.

[16] ACI Committee 506, "Visual shotcrete core quality evaluation technote (ACI 506.6T-17)," American Concrete Institute, Michigan, 2017, 4 p.

[17] ASTM, "A944-10(2015) standard test method for comparing bond strength of steel reinforcing bars to concrete using beam-end specimens," American Society of Testing and Materials, 2015, 4 p. https://doi.org/10.1520/A0944-10R15

[28] ACI Committee 506, "506.2-95 Specification for shotcrete," American Concrete Institute, 1995, 8 p.

[36] Rabbat, B. G., Russell, H. G., "Friction coefficient of steel on concrete or grout," Journal of structural engineering, Vol. 111, No. 3, 1985, pp. 505-515.

[37] FIB, "Bond of reinforcement in concrete – Bulletin No. 10," The International Federation of Structural Concrete, 2000, 434 p.

[39] Choi, C. O., Darwin, D., McCabe, S. L., "Bond strength of epoxy-coated reinforcement to concrete", University of Kansas, 1990, 217 p.

[40] Treece, R. A., Jirsa, J. O., "Bond strength of epoxy-coated reinforcing bars," ACI Materials Journal, Vol. 86, No. 2, 1989, pp. 167-174.

[45] Fei, J., Darwin, D., "Fatigue of high relative rib area of reinforcing bars," University of Kansas Center for Research, Kansas, 1999, 76 p.

[64] Cox, J. V., Herrmann, L. R., "Development of a plasticity bond model for steel reinforcement," Mechanics of cohesive-frictional materials, Vol. 3, No. 2, 1998, pp. 155-180.

[66] Ftima, M. B., "Utilisation de la méthode des éléments finis non-linéaires pour la conception des structures en béton armé: application aux structures massives, " 2013, Université de Montréal, 189 p.

[71] Tholen, M. L., Darwin, D., "Effects of deformation properties on the bond of reinforcing bars," University of Kansas center for research, Kansas, 1996, 370 p.

[72] Brown, C. J., Darwin, D., McCabe S. L., "Finite element fracture analysis of steel-concrete bond," University of Kansas center for research, Kansas, 1993, 100 p.

[73] Salem, H. M., Maekawa, K., "Pre- and postyield finite element method simulation of bond of ribbed reinforcing bars," Journal of Structural Engineering, Vol. 130, No. 4, 2004, pp. 671-680, https://doi.org/10.1061/(ASCE)0733-9445(2004)130:4(671)

[74] Lagier, F., Massicotte, B., Charron, J-P., "3D Nonlinear finite element modeling of lap splices in UHPFRC," Journal of structural engineering, Vol. 1452, No. 11, 2016, 14 p.

[75] Bandelt, M. J., Frank, T. E., Lepech, M. D., Billington, S. L., "Bond behavior and interface modeling of reinforced high-performance fiber-reinforced cementitious composites," Cement and concrete composites, Vol. 83, 2017, pp. 188-201.

[77] Orangun, C. O., Jirsa, J. O., Breen, J. E., "Re-evaluation of test data on development length and splices," Journal of the American Concrete Institute, Vol. 74, No. 3, 1977, pp. 114-122.

[90] ASTM, "C234-91a Standard test method for comparing concretes on the basis of the bond developed with reinforcing steel," American Society of Testing and Materials, 1991, 5 p.

[101] ASTM, "C496-17 Standard test method for splitting tensile strength of cylindrical concrete specimens," American Society of Testing and Materials, 2017, 5 p. https://doi.org/10.1520/C0496_C0496M-17

[107] Dassault Systems, "ABAQUS Theory Manual V. 6.14," 2014, unpaged.

[108] Lubliner, J., Oliver, J., Oller, S., Onate, E., "A plastic-damage model for concrete," International Journal of Solids and Structures, Vol. 25, No. 3, 1989, pp. 299-326.

[109] Lee, J., Fenves, G. L., "Plastic-damage model for cyclic loading of concrete structures," Journal of engineering mechanics, Vol. 124, No. 8, 1998, pp. 892-900.

[121] Basso Trujillo, P., Jolin, M., Massicotte, B., Bissonnette, B., "Bond strength of reinforcing bars encased with shotcrete," Construction and Building Materials, Vol. 169, 2018, pp. 678-688. https://doi.org/10.1016/j.conbuildmat.2018.02.218

[124] Basso Trujillo, P., Malo, R., Jolin, M., "Alternative set-up apparatus to test ASTM A944-10 beam-end specimens," Journal of Testing and Evaluation, Vol. 46, No. 4, 2018, pp. 1741-1748. https://doi.org/10.1520/JTE20170645

[126] Jolin, M., Beaupré, D., Mindess, S., "Rheology of dry-mix shotcrete," Concrete Science and Engineering, Vol. 12, No. 3, 2001, pp. 195-201.

[127] Basso Trujillo, P., Jolin, M., Massicotte, B., Bissonnette, B., "Bond strength of reinforcing bars with varying encapsulation qualities," ACI Structural Journal, Vol. 115, No. 6, 2018, pp. 1707-1717.

[128] Unauthored, "Essais portant sur l'adhérence des armatures du béton - 2. Essai par traction," Materials and Structures, Vol. 3, 1970, pp. 175-178.

[129] Chen, W.-F., "Plasticity in reinforced concrete," McGraw Hill, 2007, 474 p.

[130] Popovics, S., "A numerical approach to the complete stress-strain curve of concrete," Cement and concrete research, Vol. 3, No. 5, 1973, pp. 583-599.

[131] Thorenfeldt, E., Tomaszewicz A., Jensen J. J., "Mechanical properties of high-strength concrete and application to design," Utilization of high-strength concrete, 1987, pp. 149-159.

[132] Wight, J. K., MacGregor J. G., "Reinforced concrete : Mechanics and design," 2009, 1157 p.

[133] De Nicolo, B., Pani, L., Pozzo, E., "Strain of concrete at peak compressive stress for a wide range of compressive strengths," Materials and Structures, Vol. 27, No. 4, 1994, pp. 206-210

[134] Collins, M. P., Mitchell, D., MacGregor, J. G., "Structural design considerations for high-strength concrete," Concrete international, Vol. 15, No. 5, 1993, pp. 27-34.

[135] Collins, P., Porasz, A., "Shear design for high-strength concrete," Bulletin d'information No. 193 - Comité Euro-International du béton, 1989, pp. 77-83.

[136] Cornelissen, H. A. W., Hordijk, D. A., Reinhardt, H. W., "Experimental determination of crack softening characteristics of normal weight and lightweight concrete," Heron, Vol. 31, No. 2, 1986, pp. 45-56.

[137] Rocco, C., Guinea, G. V., Planas, J., Elices, M., "Review of the splitting-test standards from a fracture mechanics point of view," Cement and concrete research, Vol. 31, No. 1, 2001, pp. 73-82.

[138] Vos, E., "Influence of loading rate and radial pressure on bond in reinforced concrete," Delft University, 1983, 235 p.

[139] Pavlović, M., Marković, Z., Veljković, M., Buđevac, D., "Bolted shear connectors vs. headed studs behavior in push-out tests," Journal of constructional steel research, Vol. 88, 2013, pp. 134-149.

[140] Derringer, G., Suich, R., "Simultaneous optimization of several response variables," Journal of quality technology, Vol. 12, 1980, pp. 214-219.

[141] Hussein, A., Marzouk, H., "Behaviour of high-strength concrete under biaxial stress," ACI Materials Journal, Vol. 97, No. 1, 2000, pp. 27-36.

[142] Vogel, T., Schenkel, M., "Bond behavior of reinforcement with inadequate concrete cover," 3rd international symposium of bond in concrete - from research to standards, 2002, pp. 359-366.

Chapter 6 Shotcrete modification factors for the *development length* equation

Pasquale Basso Trujillo[a], Marc Jolin[a], Bruno Massicotte[b], Benoît Bissonnette[a]
[a] *Dept. of Civil and Water Engineering, Université Laval*
[b] *Department of Civil, Geological and Mining Engineering, École Polytechnique de Montréal*

This paper is part of the ACI Structural Journal, ISSN 0889-3241, https://doi.org/10.14359/51730539. Paper submitted on July 13th, 2020; approved on October 22nd, 2020 and published on May 1st, 2021.

6.1 Résumé

Le développement des paramètres de conception pour les structures en béton projeté est devenu un aspect pressant pour l'industrie. Ceci est particulièrement vrai quand des imperfections peuvent être crées derrière les barres d'armature lors de la projection du béton. Les recommandations courantes catégorisent les imperfections de façon qualitative et font référence à l'inspection du béton projeté pour des raisons de contrôle de qualité seulement. De plus, elles ne considèrent pas la force d'adhérence entre les barres d'armature et le béton en lien avec la qualité de l'enrobage des barres limitant ainsi leur utilité pour les ingénieurs en structure qui veulent proprement inclure l'usage du béton projeté dans la conception des structures. Dans cette étude, les résultats obtenus avec des éprouvettes d'adhérence dont leur barre d'armature possédait différentes qualités d'enrobage ont été utilisés pour proposer des facteurs de correction pour l'équation de la *longueur de développement* des barres d'armature. Les facteurs de correction représentent le rapport entre la performance d'adhérence des barres d'armature parfaitement bien enrobées et celles ayant des imperfections en utilisant des principes de la *théorie de possibilité*. Ainsi, les facteurs de modification peuvent être sélectionnés en fonction de la taille des vides et de la probabilité d'adhérence égale à une barre parfaitement enrobée associée à différents niveaux de risque des bâtiments.

6.2 Abstract

The development of design criteria intended for reinforced shotcrete structures has become a pressing matter for the industry. This is particularly true when imperfections behind reinforcing bars might be created during spraying operations. Current guidelines categorize imperfections qualitatively and only address the inspection of shotcrete for quality control

purposes. Moreover, they disregard the bar-concrete bond strength as a function of the bars' encapsulation quality limiting their usefulness for structural engineers wanting to rightfully include shotcrete in the design. In this paper, data from bond specimens with varying reinforcing bar encapsulation qualities was used to derive modification factors for the *development length* equation of straight bars. The modification factors were computed as *bar stress ratios* between perfectly encapsulated bars and those having imperfections using notions of *possibility theory*. As such, modification factors can be selected based on the void size and an equal bar stress probability associated to a building's risk category.

keywords: Shotcrete; Sprayed concrete; Encapsulation; Voids; Bond strength; Development length; Possibility theory; Fuzzy number; Modification factor.

6.3 Introduction

The use of shotcrete to build complete reinforced concrete elements has become a practical alternative relative to cast in-place (CIP) concrete because, among others, little formwork (if any) is needed [13]. Its use is particularly appealing for irregular shaped thin structures such as tunnel linings, tanks and domes as well as more common elements such as walls, columns and beams. Nowadays, shotcrete mixtures are engineered to be extremely robust by including carefully selected mineral and chemical admixtures. The outcome has been a considerable reduction of rebound and dust and an improvement of the placement quality, which consequently improved the mechanical and durable properties of the in-place shotcrete [13, 21, 143, 144]. The equipment, although not at the same rate as the shotcrete mixtures, has also evolved over the years [145] and guidelines for the proper shotcrete placement have been enforced [121]. Still, issues related to the encapsulation quality of reinforcing bars can arise if, among others, the experience of nozzle operators is insufficient, the elements present heavily congested zones of reinforcement or the accessibility to the spraying area is difficult.

A particular concern that has not been properly addressed in guidelines nor in design codes involves the actions that need to be taken if imperfections (such as voids or poorly compacted aggregates) are created specifically behind reinforcing bars. An early attempt to deal with this issue came with the introduction of the core-grading system in the American Concrete Institute's (ACI) "506.2-95 Specification for shotcrete" [28] in which grades ranging from 1 (perfect encapsulation) to 5 (poorest encapsulation) were attributed to the encapsulation quality of the

reinforcing bars by visual inspection of the cores. Nonetheless, despite the effort put into its creation, the reliability of the system was widely questioned [31-33] and it has even lead some engineers to make unsupported design decisions [34]. Consequently, the core-grading system was removed in the 2013 version of the same document (ACI 506.2-13) [15] and was recently replaced by the ACI's technical note 506.6T-17, "Visual shotcrete core quality evaluation technote" [16]. In this document, imperfections are characterized based on the percentage of the bars' perimeter they cover (here called *un-bonded* perimeter or *u.p.*) and on their overall size to categorize the encapsulation quality from "very good" to "poor". While the past core-grading system remains active only the for the nozzlemen accreditation exam, the ACI's 506.6T-17 [16] technical note is intended to be a supporting document for structural engineers to determine the quality of the reinforcing bars' encapsulation by visually inspecting cores taken from sprayed pre-construction panels[15]. Unfortunately, the decision to accept or to refuse the inspected cores is still experienced based and often subjective because the limits established in ACI's 506.6T-17 do not account for the bond strength of the bars as a function of their quality of encapsulation.

It has now long been argued [121, 127, 146] that a viable alternative and perhaps a more advantageous way to deal with possible imperfections behind reinforcement could be to establish an *un-bonded* perimeter limit below which design criteria should be adopted and beyond which imperfections should be considered unacceptable. A suitable design parameter that could be used to compensate for the bond strength reduction in the presence of imperfections behind reinforcement (by means of *modification factors* for shotcrete) could be the *development length* (ℓ_d) for reinforcing bars in tension required by the ACI design code [5] and computed according to Equation 6.1a and 6.1b (or the equivalent Canadian Standards Association version [6]) where C_u = 1/1.1 or 3/40 depending if S.I. units or U.S. customary units are used respectively. This equation provides the anchorage length at the end of a reinforcing bar to guarantee attaining its yield stress and therefore comply with the assumptions made during the design of reinforced concrete elements with the ultimate limit states design criteria. Each of the variables presented in the following equations is described in the notation section of this article.

$$\ell_d = C_u \frac{f_y}{\lambda\sqrt{f'_c}} \frac{\Psi_t\Psi_e\Psi_s\Psi_g}{\left(\frac{C_b+K_{tr}}{d_b}\right)} d_b \qquad (6.1a)$$

[15] Panels often sprayed in complex shotcrete projects to recreate the challenging parts of actual structures.

$$K_{tr} = \frac{40A_{tr}}{sn} \quad (6.1b)$$

Moreover, the restrictions expressed in Equation 6.2a, 6.2b, 6.2c and 6.2d must be respected.

$$\ell_d \geq 300 \text{ mm (12 in.)} \quad (6.2a)$$

$$\Psi_t \Psi_e \leq 1.7 \quad (6.2b)$$

$$(c_b + K_{tr}) / d_b \leq 2.5 \quad (6.2c)$$

$$\sqrt{f'_c} \leq 8.3 \text{ MPa (100 psi)} \quad (6.2d)$$

The ACI 318 Committee proposed Equation 6.1a and 6.1b by adapting the one proposed by Orangun et al. [76] using *modification factors*. The "top-bar" factor (Ψ_t) [83-85] accounts for the adverse effect of bleeding water accumulating under reinforcing bars as the height of concrete below them increases. The "bar coating" factor (Ψ_e) [38, 40] accounts for the effect of epoxy or zinc coating over reinforcing bars. The "bar size" factor (Ψ_s) [5] acknowledges the more favorable bond performance of small size bars. The "reinforcement grade" factor (Ψ_g) [5] accounts for the effect of reinforcement yield on the required *development length*. Historically, *modification factors* have been developed by computing *bond performance ratios*. Depending on the investigation, they have been computed as ratios between the ultimate loads, the ultimate slip or the loads at a given slip between "reference" laboratory bond specimens and those accounting for the variable under study.

Since the bond performance reduction of inadequately encased reinforcing bars (as it may occur in shotcrete) is not accounted in Equation 6.1a and 6.1b, the aim of this investigation is to propose scientifically supported *bar performance ratios* (here using *bar stress ratios* or BSR's) as a function of a bar's *un-bonded* perimeter and the equal bar stress probability to a perfectly encased reinforcing bar that can be associated to a building's risk category. For this purpose, the results from a comprehensive investigation [121, 127, 146] which includes an experimental and a Finite Element (FE) campaign completed previously by the authors was used and is summarized in the following sections. The shotcrete and the cast in-place (CIP) "pull-out" specimens' results obtained from the laboratory [121] served to validate the analytical methodology used in this

research to propose the modification factors for shotcrete. However, only the results from the CIP "beam-end" specimens tested in the laboratory (as explained later in this paper) were used to create the actual modification factors that are proposed. Since the encasement quality of the reinforcing bars in the "beam-end" specimens was investigated using *artificial voids* made of silicone inserts to replicate the voids found in shotcrete, the results from the shotcrete "pull-out" specimens also served to include the variability of actual voids found in shotcrete using principles of *possibility theory*. The results from the FE campaign [146] served to establish the *un-bonded* perimeter limits within which the modification factors should or should not be used. A total of 60 specimens (45 from the experimental and 15 from the FE program) have been used to reach the conclusions of this study.

6.4 Research significance

The proposed *bar stress ratios* are intended to be employed as *modification factors* for the *development length* of straight bars' equation of North American design codes. This will help structural engineers to make supported design decisions in case imperfections are foreseen with the placement of shotcrete. In that regard, quality control decisions after pre-construction panels are sprayed, cored and inspected could be better supported and even relaxed knowing that measures were considered during the design phase of a given shotcrete structure. This will ultimately guarantee bar yielding at the ultimate limit state design criteria and thus, ensure the ductile behavior of reinforced shotcrete elements.

6.5 Summary of previous experimental and Finite Element results

6.5.1 "Pull-out" specimens

The impact of voids behind a single reinforcing bar was studied by Basso et al. [121] using "pull-out" specimens made with *dry-mix* process shotcrete. Various sizes of imperfections were created behind the reinforcing bars of the specimens as the nozzle operator deliberately changed the *consistency* of the mixture. The bond performance of the specimens was evaluated based on the strength and the slip of the reinforcing bar as well as on their mode of failure. To build the specimens, a pre-packaged concrete mixture was sprayed into wooden rectangular panels as the one shown in Figure 6.1 After curing, the blocks were cut following the dotted lines shown over the mold to obtain three "pull-out" specimens per panel. If voids were observed, their *un-bonded* perimeter (*u.p.*) was precisely measured on the bottom of each specimen

and at four additional locations taken from two 40 mm concrete plates cut below the specimens. The rest of the concrete in the mold was used to characterize the properties of the shotcrete using cores. All specimens possessed 16.0 mm (5/8 in.) nominal diameter (d_b) reinforcing bars and bonded lengths of $2.5d_b$ at their bottom which were controlled with a PVC sleeve on the top section of the reinforcing bar.

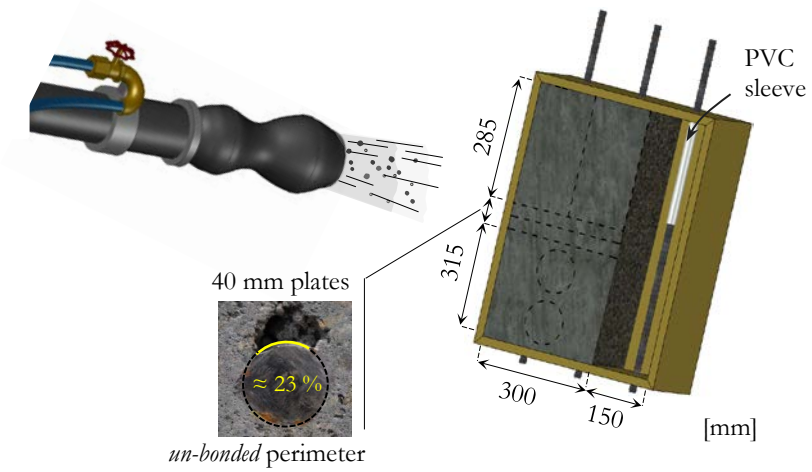

Figure 6.1: Spraying representation of "pull-out" specimens (Note: 25.4 mm = 1 in.)

The *u.p.* frequency distribution of 7 specimens (refer to Appendix H) in which voids were observed behind the reinforcing bar are presented in Figure 6.2. The results show how the scatter of the *u.p.* ranges from as much as 60% to as little as 10% from one location to another and a clear frequency distribution cannot be determined making the analysis of data considerably challenging.

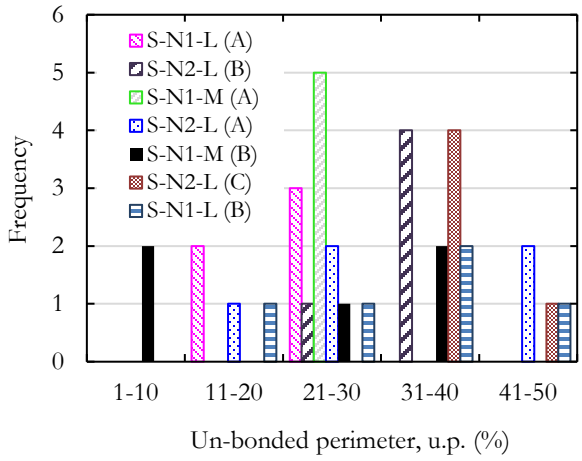

Figure 6.2: Frequency distribution of *un-bonded* perimeters

To facilitate the data analysis and to limit the size variability of the voids, cast in-place (CIP) specimens were built using the same mixture of *dry-mix* process shotcrete and the imperfections were recreated using silicone inserts placed over the entire bonded length of the specimens' test bar[16]. This strategy allowed to obtain well-defined tendencies of the bar strength reduction with known void sizes and consequently limited the number of specimens needed to be tested in the laboratory. The results showed that beyond *un-bonded* perimeters of 20%, the bar stress at failure is considerably reduced and that the failure mode of the specimens tends to change from concrete *splitting* to a bar *pull-out* failure setting therefore this *un-bonded* perimeter as a threshold beyond which the bond behavior of reinforcing bars considerably changes. Despite results from shotcrete and CIP specimens showing the same tendencies, only the bar stresses at failure were statistically equivalent between both methods of concrete placement. For this reason, the modification factors for shotcrete proposed herein were created considering only the bar stress at failure. It needs to be noted that the height of the voids was not found to have a significant impact on the bar stress reduction as the results of specimens with double the void height did not differ from those with a single void height [121].

6.5.2 "Beam-end" specimens

6.5.2.1 Experimental program

To further investigate the impact voids behind a reinforcing bar have on bond, ASTM A944-10 [17] "beam-end" specimens were tested by Basso et al. [124, 127]. Only cast in-place (CIP) specimens with silicone inserts placed over the entire bonded length of the test bar were built (refer to Figure 6.3a and 6.3b) because reliably spraying this type of specimens proved to be extremely challenging in the laboratory. Bonded lengths of $6.3d_b$ were tested for 15.9 and 19.0 mm nominal diameter reinforcing bars. In all cases, a concrete cover (c_b) of $2.5d_b$ was used. To avoid excessive bleed water accumulating under the test bars, a mixture with a *w/b* ratio of 0.45 and a polycarboxylate based water reducer was used; bleeding tests [103] were performed to confirm this expectation. The results showed that only after an *u.p.* of 20% is reached, the bar stress at failure starts to decrease considerably. For these type of bond specimens, the transition from a concrete *splitting* (refer to Figure 6.3c) to a bar *pull-out* failure occurred at *u.p.* values of around 30%. Therefore, it was suggested that bars having *u.p. of* 30% or more should be carefully

[16] The height of the bar, i.e., the cross-sectional length of the void from the top of the test bar towards the outer surface of the specimens, measured half the *un-bonded* perimeter length. For *un-bonded* perimeters of 10%, 20% and 30% and a 16 mm bar this represents height in between 2.5 and 7.5 mm.

treated as higher confinement provided by the concrete cover could cause a premature failure mode transition [127].

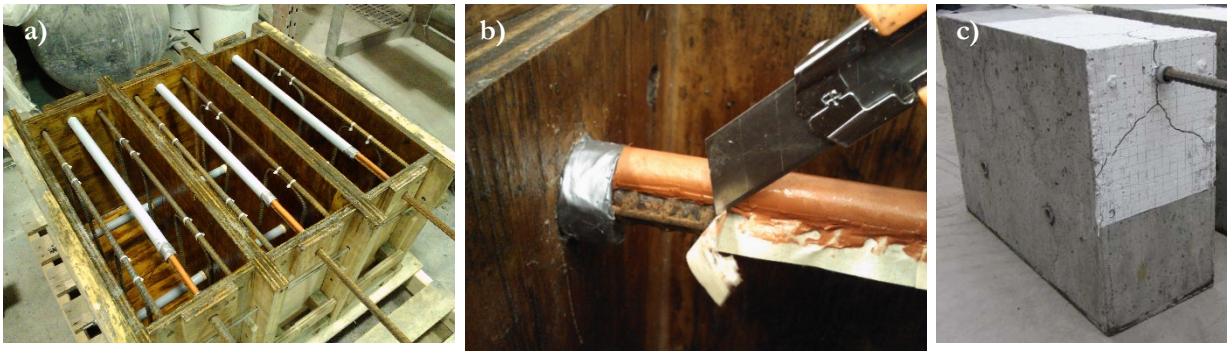

Figure 6.3: (a) Interior reinforcement of "beam-end" specimens (b) installation of the silicone insert and (c) concrete splitting failure

6.5.2.2 Finite element program

To broaden the knowledge obtained from the experimental program, Basso et al. [146] modeled the ASTM A944-10 "beam-end" specimens using the Finite Element (FE) package Abaqus 6.14 as shown in Figure 6.4. This specimen was favored over the "pull-out" because its geometry and stress distribution better represent the ones observed in most structures [42, 124]. The concrete was idealized as a homogeneous material and the test bar was modeled at *rib-scale*, i.e., the geometry of the ribs was explicitly discretized [64]. After the model was statistically calibrated, a parametric analysis was performed to study the effect of the concrete cover in conjunction with different sizes of voids behind the test bar. Based on the FE model's bar stress-slip relationship and the stresses around the reinforcing bars, a 20% *un-bonded* perimeter (*u.p.*) was found to be the threshold at which a considerable stress distribution change was observed. *Un-bonded* perimeters of 30% or more either considerably increased the bar slip for small concrete cover specimens ($2.5d_b$) or increased the chances of a premature failure mode change for larger concrete cover specimens ($5.0d_b$) when the voids covered the entire bonded length of the reinforcing bar. When voids covered half of the reinforcing bar's bonded length, it was observed that the *un-bonded* perimeter limit could increase from 10% to 20% or from 20% to 30% without impacting the bond performance of the specimens in comparison to voids covering the entire bonded length of the reinforcing bars. In other words, a specimen with a 30% *u.p.* covering half of the bonded length behaved in a similar way as one with a 20% *u.p.* covering the entire bonded length of the reinforcing bar for example.

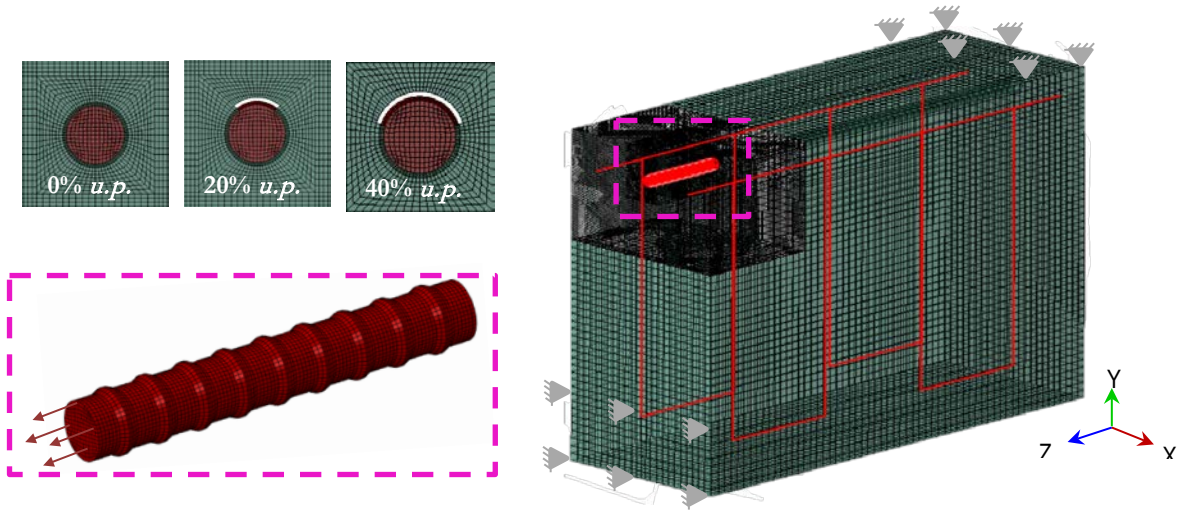

Figure 6.4: "Beam-end" FE model created with Abaqus 6.14

6.6 Analytical procedure to develop modification factors

6.6.1 *Possibility theory*

An important challenge resulting from ACI's 506.6T-17 technote [16] is the fact that the size of voids is regarded as precise values whereas in reality, their dimensions incorporate an intrinsic level of uncertainty because of their irregular shape. For that reason, it is believed that *un-bonded* perimeters should instead be treated as imprecise quantities characterized using *possibility theory* [147]. Representing this type of imprecision with classic probability theory would not be adequate since the *un-bonded* perimeters do not follow a clear probability distribution. This would probably still be true even if more data was available as the presence of a given *u.p.* value is not subject to random sampling.

With *possibility theory*, the uncertainty of a variable (x) is defined using a *possibility function* ($\pi(x)$) rather than using a probability function. Consider the triangular *possibility function* ($\pi(u.p.)$) on the [15%, 45%] *u.p.* interval and a *mode* of 30% as shown in Figure 6.5. The distribution represents, in a gradual manner, the range of *un-bonded* perimeters that are less plausible than others given a value of the $\pi(u.p.)$. When $\pi(u.p.) = 0$, it is considered that *un-bonded* perimeters smaller than 15% and greater than 45% are not a possible outcome at all. On the other hand, when $\pi(u.p.) = 1$, it is considered that a 30% *u.p.* is "completely possible", "unsurprising" or simply the "closest value to the reality". Quantities represented with *possibility functions* are usually called *fuzzy* numbers and are written with a tilde (~) over them [148, 149]. Thus, the quantity depicted in

Figure 6.5 can be denoted as $\widetilde{30}\%$ and should be interpreted as "an *un-bonded* perimeter close to 30%".

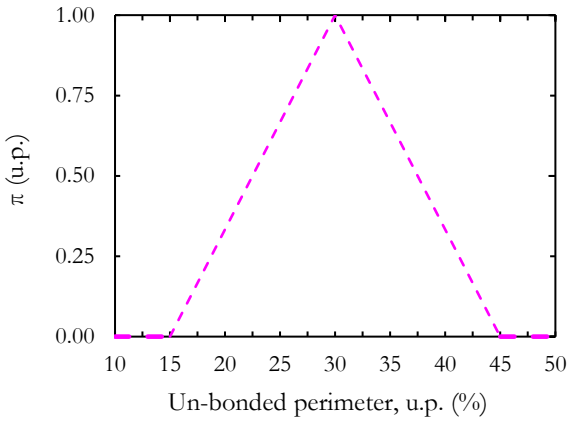

Figure 6.5: Triangular possibility function of a given *u.p.*

Although *possibility theory* and classic *probability theory* seem similar at a first glance, uncertainty in the former is treated with two types of measures (*possibility* (Π) and *necessity* (N) measures) instead of the single uniform probability distribution used in the latter [149-151]. Both Π and N are expressed in Equation 6.3 and 6.4 for a *fuzzy* number $\tilde{F}$ and its complement $\bar{F}$. While Π expresses the uncertainty of the variable x, N evaluates its degree of acceptance.

$$\Pi(\tilde{F}) = \sup_{x \in \tilde{F}} \pi(x) \tag{6.3}$$

$$N(\tilde{F}) = 1 - \Pi(\bar{F}) = \inf_{x \notin \tilde{F}} (1 - \pi(x)) \tag{6.4}$$

Based on *possibility theory*, the largest values of Π are required to be one and the smallest values of N are required to be zero as expressed in Equation 6.5 and 6.6. These requirements differ substantially from the one established in *probability theory* where the sum of the values under each probability distribution (Prob) are required to add precisely 1 as expressed by Equation 6.7 for a value A and its complement $\bar{A}$.

$$\Pi(\tilde{F}) + \Pi(\bar{F}) \geq 1 \tag{6.5}$$

$$N(\tilde{F}) + N(\bar{F}) \leq 1 \tag{6.6}$$

$$Prob(A) + Prob(\bar{A}) = 1 \tag{6.7}$$

Despite such differences, a link between both theories exists as a consequence of the *consistency principle* which states that the degree of possibility of a value is greater than, or equal, to its probability as expressed in Equation 6.8.

$$\Pi(\tilde{F}) \geq \text{Prob}(A) \geq N(\tilde{F}) \tag{6.8}$$

The simplest, yet most advantageous, shape of a *possibility function* is a triangular one since $\Pi(\tilde{F})$ and $N(\tilde{F})$ encompass any possible *probability* distribution that can be built using the same interval of values. This is shown in Figure 6.6 where the cumulative functions $\Pi(-\infty, u.p.)$ and $N(-\infty, u.p.)$, computed for the *fuzzy* number $\tilde{30}\%$ defined in Figure 6.5, encompass a normal cumulative probability distribution with the same interval. As mentioned above, any other cumulative probability distribution would have been encompassed by $\Pi(\tilde{F})$ and $N(\tilde{F})$ within the same *u.p.* interval. Therefore, $\Pi(\tilde{F})$ and $N(\tilde{F})$ can be interpreted as upper and lower probability limits that must be favored over probability theory whenever uncertain or incomplete information is studied as it is the case of *un-bonded* perimeters.

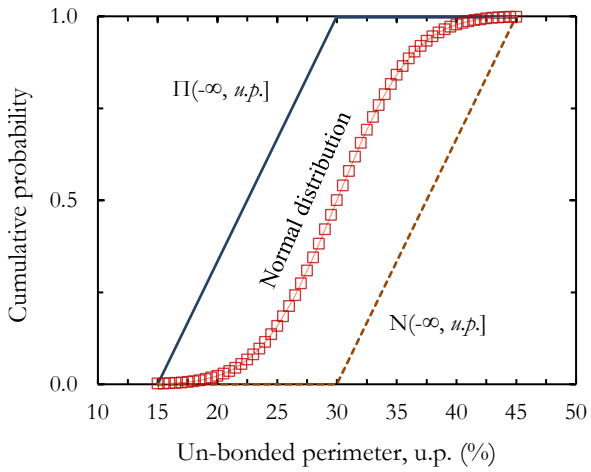

Figure 6.6: Bounds of cumulative measures based on a triangular possibility distribution

6.6.2 From precise to *fuzzy un-bonded* perimeters using CIP "pull-out" specimens

The uncertainty linked to *un-bonded* perimeters can be incorporated to the precise (or "crisp") ones measured from cast in-place (CIP) laboratory specimens with *artificial voids* to create *fuzzy* numbers. Here, the uncertainty was accounted by increasing each "crisp" *u.p.* with a randomly chosen symmetric bound in between $\gamma_{ij} = \pm 10$ and $\pm 60\%$ to represent the scatter

found in the laboratory with shotcrete "pull-out" specimens [121]. A fixed bound $e_i = \pm 2\%$ was added to the bar strength at bond failure (P_{max}) obtained from the experimental tests. A triangular *possibility function,* which turns out to be a pyramidal distribution for the two variables under consideration (P_{max} and *u.p.*), was used as shown in Figure 6.7. The space inside the pyramid represents all possible values that could have been obtained if shotcrete specimens were tested. However, as $\pi(P_{max}, u.p.)$ increases towards 1, the "closest value" of a P_{max} similar to the mean of a series of shotcrete specimens with a given *u.p.* would be obtained. This is true as the bar strengths at bond failure obtained from shotcrete specimens are equivalent to the ones obtained with CIP specimens for a given size of imperfection (real or artificial) [121]. With *fuzzy* numbers, it is now possible to plot both the P_{max} linked to an *u.p.* including their value of uncertainty to represent actual shotcrete results. *Fuzzy* regression models can thereafter be computed to establish relationships with the added uncertainty.

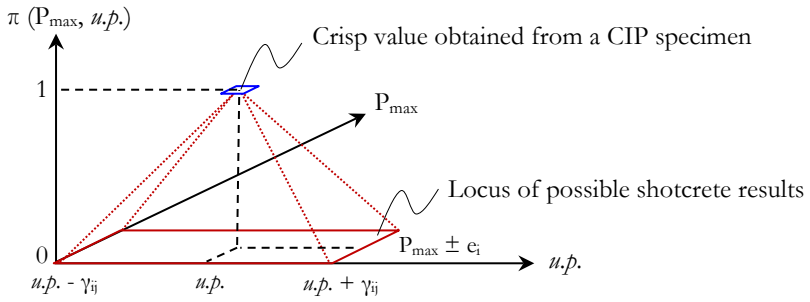

Figure 6.7: *Fuzzy* number representation of cast in-place results with *artificial voids*

6.6.3 Fuzzy linear regression using CIP "pull-out" specimens

The linear regression (adequate for the results obtained with "pull-out" specimens [121]) for *fuzzy* input and output values [152] as expressed by Equation 6.9a was used for the results obtained with CIP "pull-out" specimens. *Fuzzy* regressions, contrary to classic regressions based on the *least squares* method, require the resolution of a Linear Program (LP). Nonetheless, *fuzzy* regression models are also composed of an output ($\tilde{Y}$), regression coefficients ($\tilde{A}_j$) and input variables ($\tilde{X}_j$), all of which are *fuzzy* numbers with their own mode (y_i, A_j and x_{ij} respectively) and bounds (e_i, α_j and γ_{ij} respectively). To solve the *fuzzy* regression model, the objective is to minimize its "vagueness" ($J(A,\alpha)$) determined by its coefficients whilst maximizing its predictability as depicted by Equations 6.9b and 6.9c respectively.

$$\tilde{Y} = \sum_j^p \left(\tilde{A}_j \otimes \tilde{X}_j\right) = \sum_j^p \left((A_j, \alpha_j) \otimes (x_{ij}, \gamma_{ij})\right) \tag{6.9a}$$

$$\text{Min.} \quad J(A, \alpha) = \sum_{i=1}^{n} \max_{0 \le j \le p} \left(|A_j|\gamma_{ij}, |x_{ij}|\alpha_j\right) \tag{6.9b}$$

$$\text{S. t.} \quad \left|y_i - \sum_j^p A_j x_{ij}\right| \le \left|L^{-1}(h)\right| \max_{0 \le j \le p} \left(|A_j|\gamma_{ij}, |x_{ij}|\alpha_j\right) - \left|L^{-1}(h)\right| e_i \tag{6.9c}$$

Where $\alpha_j \geq 0$ for all i = 1,2, …, n, j = 0, …, p.

The degree of fitting *h* (refer to Equation 6.9c) is equivalent in some way to the Pearson coefficient (R^2) of classic regression theory and must satisfy the inequality $0 \leq h < 1$. In *possibility theory*, its value is not an outcome of the analysis but rather a value that needs to be specified; it is a way to *control* the vagueness (or the uncertainty) of the model since there is little information available. Higher values result in a better predictability of the *fuzzy* regression model but induce higher (undesirable) values of J(A,α). Therefore, the highest value of *h*, without considerably increasing the value of J(A, α) must be specified to increase the model predictability but to limit its "vagueness". Typical values of *h* range in between 0.5 and 0.7 [153, 154]. If *h* is set to 0.6 and the LP from Equations 6.9a, 6.9b and 6.9c is solved for the 14 *fuzzy* numbers derived from CIP "pull-out" specimens **(**refer to Table H.1 in Appendix H), the *fuzzy* linear model $\tilde{Y}$ = (51.0, 16.2) $\oplus$ (-1.11, 0.0) $\otimes \tilde{X}_1$ as shown in Figure 6.8 is obtained **(**refer to Table H.2 in Appendix H). Because many solutions exist for α_0 and α_1, the smallest number respecting all of the constrains was selected to minimize the spread of the *u.p.*

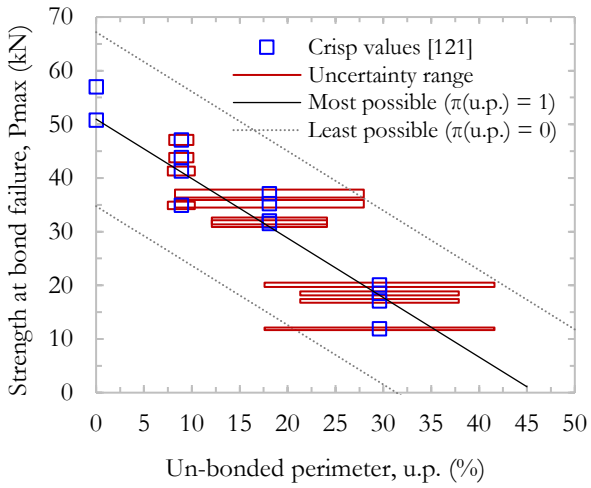

Figure 6.8: Linear *fuzzy* regression from "pull-out" specimens' results

The *fuzzy* regression model, in a similar way to *fuzzy* numbers, involves the creation of a "closest to the true path" ($\pi(u.p.) = 1$) and its upper and lower regression bounds beyond which values are not considered to be a possible outcome ($\pi(u.p.) = 0$). It needs to be noted that the LP was solved 10 times using randomly selected values of γ (from $\pm$ 10 to $\pm$ 60%) attributed to each precise *un-bonded* perimeter value and a significant influence on the *fuzzy* model shape was not observed. In fact, it was found that it is the degree of fitting h that has the greater impact on its upper and lower bounds and this is discussed in the following section.

6.6.4 Model adequacy using shotcrete "pull-out" specimens

To properly select the degree of fitting h, the LP was also solved for $h = 0.5$ and 0.7. The prediction capabilities of the *fuzzy* models were then compared to the bar strength at bond failure of the 10 shotcrete specimens (refer to Table H.1 in Appendix H) as shown in Figure 6.9a. The results of seven specimens correspond to those shown in Figure 6.2 whereas the other three correspond to shotcrete specimens in which the bar was perfectly encapsulated [121]. As can be seen, h only influences the "spread" of the *fuzzy* models as all of the 3 models share the same "closest to the true" regression line ($\pi(P_{max}, u.p.) = 1$). Choosing the best suited value of h is subjective and the influence on the "vagueness" J(A,α) of the model needs to be verified with each choice as shown in Figure 6.9b.

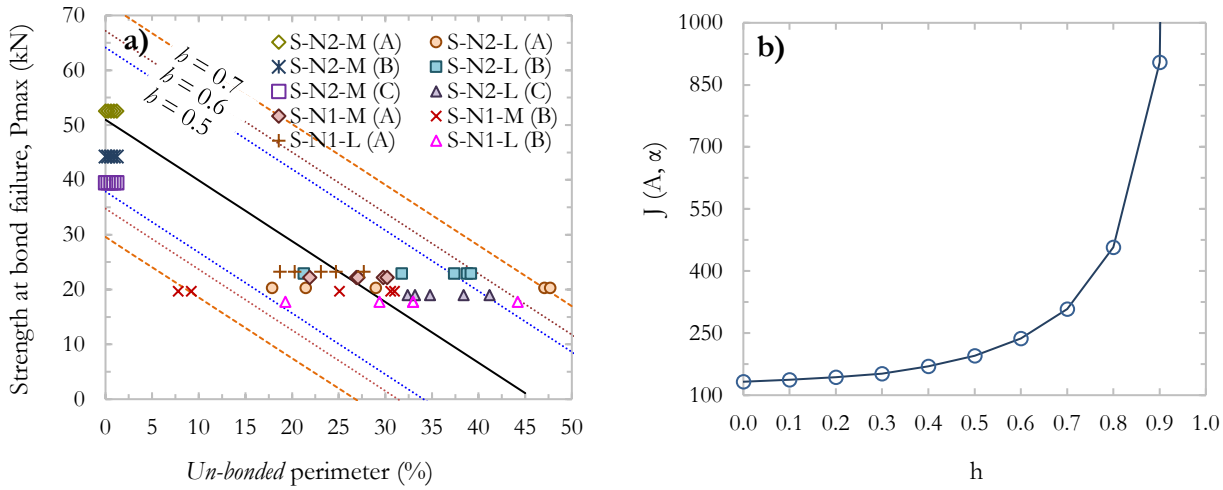

Figure 6.9: (a) Model level of predictability and (b) effect of h on the model's vagueness

In this particular case, a value of h = 0.6 seems to be the most appropriate since most of the experimental results lie within its bounds. Moreover, the onset of considerable "vagueness" seems to occur beyond h = 0.6 where J(A,α) passes from 237 to 308 at h = 0.7. This represents an increase of (308-237) / 237 = 30% over the previous value instead of (237-195) / 195 = 22% at h = 0.6. Thus, a value of h = 0.6 was selected for all subsequent analysis.

6.6.5 *Fuzzy* polynomial regression using CIP "beam-end" specimens

With regard of the "beam-end" specimens, the polynomial regression is the most adequate model for the data [127]. Therefore, the *fuzzy* input and output regression model [155] expressed by Equation 6.10a was used in this case. The objective function and the constraints of the *fuzzy* polynomial model are expressed in Equation 6.10b and 6.10c.

$$\widetilde{Y} = \sum_{j=1}^{p}\left(\widetilde{A}_j \otimes \widetilde{X}_j\right) \oplus \sum_{1 \le l \le k \le p}\left(\widetilde{A}_{l,k} \otimes \widetilde{X}_l \otimes \widetilde{X}_k\right) \quad (6.10a)$$

$$\text{Min.} \quad J(A, \alpha) = \sum_{i=1}^{n} \ldots$$

$$\ldots \max\left\{ \max_{1 \le j \le p}\left(|A_j|\gamma_{ij}, |x_{ij}|\alpha_j\right), \max_{1 \le l \le k \le p}\left(\alpha_{l,k}|x_{il}||x_{ik}|, |A_{l,k}|\gamma_{il}|x_{ik}|, |A_{l,k}||x_{il}|\gamma_{ik}\right)\right\} \quad (6.10b)$$

$$\text{S. t.} \quad \left|y_i - \left(\sum_{j=1}^{p} A_j x_{ij} + \sum_{1 \le l \le k \le p} A_{l,k} x_{ik} x_{il}\right)\right| \le \left|L^{-1}(h)\right| \max\left\{ \max_{1 \le j \le p}\left(|A_j|\gamma_{ij}, |x_{ij}|\alpha_j\right) \ldots \right.$$

$$\left. \ldots, \max_{1 \le l \le k \le p}\left(\alpha_{l,k}|x_{il}||x_{ik}|, |A_{l,k}|\gamma_{il}|x_{ik}|, |A_{l,k}||x_{il}|\gamma_{ik}\right)\right\} - \left|L^{-1}(h)\right| e_i \quad (6.10c)$$

Where α_j and $\alpha_{l,k} \ge 0$ for $i = 1, 2, \ldots, n$, $j = 0,1, \ldots, p$ and $1 \le l \le k \le p$.

Solving the LP with the 24 *fuzzy* numbers (transformed from the precise experimental results shown in Table H.1 in Appendix H) as shown in Figure 6.10 and using h = 0.6 results in the *fuzzy* polynomial model $\widetilde{Y}$ = (224.6, 46.9) ⊕ (1.3, 0.0) ⊗ $\widetilde{X}_1$ ⊕ (-0.1, 0.0) ⊗ $\widetilde{X}_1$ ⊗ $\widetilde{X}_1$ (refer to Table H.3 in Appendix H). In this case, the output is expressed as the bar stress at bond failure (f_{smax}) because No. 16 (#5) and No. 19 (#6) reinforcing bar sizes are included.

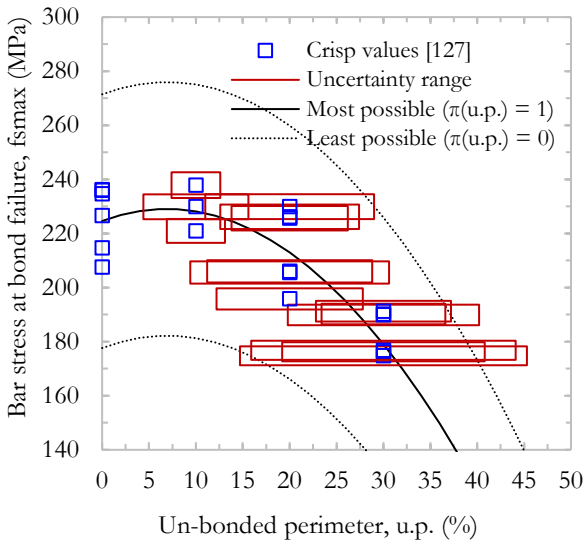

Figure 6.10: Polynomial *fuzzy* regression using "beam-end" specimens

Although shotcrete results are not available in this case to verify the adequacy of the model, the *linear fuzzy* model proved that the bar strength at bond failure of actual shotcrete specimens could be adequately predicted using this technique. Moreover, similar to the *fuzzy* linear model, varying the uncertainty range of the *u.p.* (γ) does not considerably change the shape of the *fuzzy* polynomial regression model.

6.6.6 Development of *bar stress ratios* and discussion

The *fuzzy* regression models previously developed can be used to create *bar stress ratios* (BSR's), i.e., ratios between the results obtained with perfectly encapsulated bars and those having imperfections. The polynomial *fuzzy* regression will be used for this purpose since "beam-end" specimens most accurately recreate the stress distribution of most reinforced concrete elements [42, 124]. Here, the BSR have been computed using Equation 6.11 for *un-bonded* perimeters equal to 10% and 20%. *Bar stress ratios* (BSR) for larger *u.p.* values are not proposed because either the bond failure of the element would likely change to a bar *pull-out* or an excessive slip bar would occur [127, 146]. Moreover, past experience with shotcrete has shown that other issues such as excessive rebound leading to inhomogeneities such as rock pockets would be present where *un-bonded* perimeters higher than 20% are produced resulting in an application that would be deemed inadequate.

$$Bar\ stress\ ratio = \frac{\widetilde{Y}_{u.p.\,=\,0\%}}{\widetilde{Y}_{u.p.\,>\,0\%}} \tag{6.11}$$

Since Equation 6.11 involves the division of two *fuzzy* numbers, arithmetic operations subject to interval analysis need to be used [148, 149]. In the case of a division, the operation is expressed by Equation 6.12 and therefore, the resulting *bar stress ratios* represent *fuzzy* numbers with a non-linear possibility function as those shown in Figure 6.11.

$$[a, b] / [d, e] = [\min(a/d, a/e, b/d, b/e), \max(a/d, a/e, b/d, b/e)] \tag{6.12}$$

The intervals [a, b] and [d, e] represent the bounds of each *fuzzy* number taken from the polynomial regression needed to compute a BSR at a given α-cut, i.e., the subset of bar stresses at bond failure (f_{smax}) having a greater *possibility* ($\pi(f_{smax})$) than the threshold defined by the α-cut. For instance, the α-cut at $\pi(f_{smax}) = 0.5$ of the *fuzzy* number $\widetilde{Y}_{u.p.\,=\,0\%}$ taken from the polynomial regression (refer to Figure 6.10) encompasses the interval [201.2, 248.1]. When that interval is divided by the interval $\widetilde{Y}_{u.p.\,=\,20\%}$ [189.6, 236.5], the result is the 20% *u.p.* BSR interval [0.85, 1.31] at π(BSR) = 0.5 as seen in Figure 6.11.

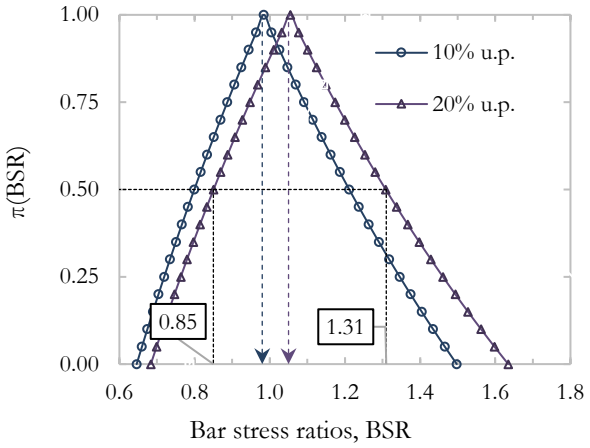

Figure 6.11: Possibility distributions of *bar stress ratios*

As can be observed, the "completely possible" BSR's for the 10 and 20% *un-bonded* perimeters are 0.98 and 1.05 respectively. As previously stated, such BSR's could be used as modification factors for the *development length* equation of reinforcing bars in tension of North American reinforced concrete design codes [5, 6] as it has been done for the "top-bar", "coating" and "bar size" effects. If judged necessary by structural engineers, larger BSR's could be selected

depending upon the type of structure to be built. However, doing so based on *possibility* distributions represents a big challenge because an entirely objective decision cannot be made. In that regard, a less subjective way to interpret the BSR's can be made if they are transformed into probability distributions. Such transformation is feasible given that the *possibility* (Π) and the *necessity* (N) measures of a *possibility* distribution are considered upper and lower probabilities respectively. Here, the *possibility/probability* transformation method proposed by Dubois et al. [156] (refer to Equation 6.13) was used to obtain the probability density function (Prob(BSR)) of the 10% and the 20% BSR's. The transformation method conservatively chooses a single probability distribution with the highest possible level of uncertainty.

$$\text{Prob(BSR)} = \int_0^{\pi(\text{BSR})=1} \frac{d\alpha}{|L_\alpha|} \tag{6.13}$$

Where $|L_\alpha|$ is the interval length of the α-cut.

In reality, the *possibility/probability* procedure enables us to determine the probability (somewhat subjective since it comes from a *possibility* distribution) that a reinforcing bar with a given *u.p.* over its entire bonded length will perform in the same manner as a reinforcing bar having a perfect encapsulation with the use of a given BSR.

The cumulative probabilities of equal bar stress performance resulting from Equation 6.13 for the *un-bonded* perimeters under consideration are shown in Figure 6.12; they were computed with each of the aforementioned 10 *fuzzy* regression models obtained by randomly changing the range of the *u.p.* uncertainty (γ_{ij}) in between ± 10 and ± 60%.

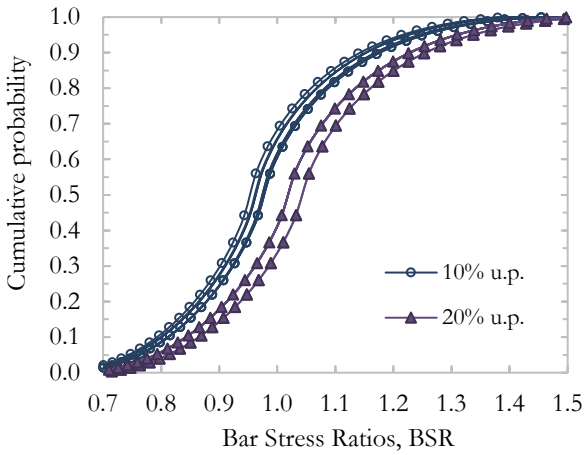

Figure 6.12: Cumulative probability linked to *bar stress ratios*

The mean BSR's above and equal to 1.0 are shown in Table 6.1. The coefficient of variance between all models' cumulative probability are shown in parenthesis in the same table. As can be observed, the largest value was found to be 7.0% which is deemed an adequate level of variance.

The minimum acceptable cumulative probability was set to 60% as it is the one that was achieved with a 10% *u.p.* for a 1.0 BSR. This is also because BSR's of less than 1.0 are not logical to be used with the appearance of voids. For this reason, a BSR of 1.0 is not suggested for a 20% *u.p.* as its mean cumulative probability of equal bar stress performance represents 35% (refer to Figure 6.12). Table 6.1 allows structural engineers to select a BSR and use them as modification factors for the *development length* equation (refer to Equation 6.1a and 6.1b) based on the size of voids or imperfections (if any) that are foreseen when shotcrete is used.

Table 6.1: Cumulative probability of equal bar stress performance

Un-bonded perimeter, *u.p.*	*Bar Stress Ratios,* BSR (C.O.V.)					
	1.0	**1.1**	**1.2**	**1.3**	**1.4**	**1.5**
0%	100% (-) I – IV	-	-	-	-	-
10%	60 % (7.0) I	82 % (1.2) I / II	92 % (0.7) II / III	97 % (0.8) III / IV	100 % (0.5) IV	-
20%	-	72 % (6.2) I	87 % (1.3) I / II	93 % (0.8) II / III	98 % (0.4) III / IV	100 % (0.2) IV

* Values in parenthesis represent the standard deviation of the cumulative probability obtained from 10 model iterations

The expected voids' size needs to be determined based on the structural engineer's expertise. For such purpose, it is expected that the experience of the spraying crew, the extent of the quality control campaign, the difficulty level of the spraying operations (congestion of reinforcing bars, number of reinforcing layers, etc.) and other parameters of the project are reviewed. The suggested approach to help structural engineers choose a BSR based on the probability of equal bar stress is to link such probabilities to the risk categories of buildings as adopted by the

"Minimum Design Loads for Buildings and Other Structures" Standard [157]. A summarized description of each risk category is provided in Table 6.2.

Table 6.2: Risk Category of buildings as established by the ASCE [157]

Use or occupancy of buildings and structures	Risk Category
Buildings and other structures that represent a low risk to human life in the event of failure	I
All buildings and other structures except those listed in Risk Categories I, III and IV	II
Buildings and other structures, the failure of which could pose a substantial risk to human life, cause a substantial economic impact and/or mass disruption of day-to-day civilian life in the event of failure	III
Buildings and other structures designated as essential facilities, the failure of which could pose a substantial hazard to the community and required to maintain the functionality of other Risk Category IV structures.	IV

As can be seen, the risk categories go from I to IV for low to high-level risk structures respectively. The levels suggested for each BSR have been integrated in Table 6.1 for the appropriate cumulative probability of equal bar stress performance. In that regard, greater values of modification factors could be selected based on the risk associated to the structure. In the case of essential structures such as a city shelter (category IV), an engineer might be prompt to use a 1.5 modification factor for shotcrete if 20% *u.p.* could be created during spraying operations. Based on the information presented in Table 6.1, in conjunction with the findings made by Basso et al. [146] using the FE method regarding the percentage of the reinforcing bar's bonded length covered by a void (refer to the Finite Element program presented in Chapter 5), guidelines have been proposed for the reinforcement detailing and the inspection of shotcrete structures if voids or imperfections are foreseen or are created behind a reinforcing bar. It has to be noted that despite the BSR's presented in Table 6.1 were developed using specimens with a $2.5d_b$ concrete cover, the result should be applicable to concrete covers up to $5.0d_b$ as the bar stress loss from 0 to 20% *u.p.* between specimens with concrete covers in between those values are not considerably different [146].

6.7 Guidelines for design and evaluation

Based on the analytical procedure presented in this research paper, the proposed *bar stress ratios* (BSR) to be used as modification factors for the *development length* equation to guarantee an adequate bond strength *could* go as follows:

A. In the case of voids appearing over the entire bonded length of a bar being developed

   a) Use a modification factor of at least 1.0 when *un-bonded* perimeters of around 10% or less might be created.

   b) Use a modification factor of at least 1.1 when *un-bonded* perimeters of around 20% might be created.

B. In the case of voids appearing sporadically[17] over the bonded length of a bar being developed

   a) Use a modification factor of at least 1.0 when *un-bonded* perimeters of around 20% or less might be created.

   b) Use a modification factor of at least 1.1 when *un-bonded* perimeters of around 30% might be created.

C. The acceptance or correction with modification factors of *un-bonded* perimeters larger than 20% if voids cover the entire bonded length of the bar or larger than 30% if voids appear sporadically over the bonded length of the bar is not recommended.

D. *Modification factors* greater than the minimal recommended might be prescribed by the structural engineer based on the risk category of the building for a given expected encapsulation quality of the reinforcing bars. Table 6.1 can be used for such purpose.

E. The *modification factors* proposed herein are not recommended to be used in conjunction with Ψ_t or Ψ_e as shotcrete presents little (if any) bleeding and because coated bars are not normally used with shotcrete.

[17] Sporadic voids could be regarded as those covering a total of 50% or less of the reinforcing bar's developed length. Such limit is based on the findings of the Finite Element parametric analysis described in the "Finite Element program" section.

6.8 Further research

The modification factors proposed in this research are the result of a long-term investigation in which different types of small-scale laboratory bond specimens with different qualities of reinforcement encapsulation were tested [121, 124, 127, 146]. Both shotcrete and cast in-place concrete were used for such purpose and even additional results were obtained using the Finite Element method. Additional research should address the use of large-scale bond specimens to confirm the accuracy of the *bar stress ratios*. Additional scenarios encountered in real life, such as the presence of stirrups over the bonded length of the bars and cyclic loading, should also need to be studied as well as the impact of voids on the durability of structures. More research is also needed in cases where shotcrete is properly applied and no voids are encountered since past research suggests that the performance of reinforcing bars encases with shotcrete is better than with cast in-place concrete and therefore modification factors could be less than 1.0 for shotcrete in this case.

6.9 Conclusion

In this research, the bar strength at bond failure obtained with cast in-place "beam-end" specimens having *artificial voids* were used to develop *bar stress ratios* (BSR) between perfectly encapsulated bars and those having different sizes of imperfections. Since it is believed that voids or imperfections behind reinforcing bars (if created during spraying operations) should be regarded as imprecise values, BSR were computed using notions of *possibility theory* as it does not require data to follow any specific probability function and allows to define the *un-bonded* perimeter as "close to" a certain size. Initially, each precise *un-bonded* perimeter measured from *artificial voids* was converted into an imprecise quantity (*fuzzy* numbers) to incorporate the bounds of actual voids created with shotcrete specimens. In a subsequent stage, a *fuzzy* regression model was created with the *pseudo-shotcrete* data to compute the BSR's for *un-bonded* perimeters of up to 20%. This is the threshold beyond which several studies have found that the bar stress at failure reduces significantly for large concrete covers or that the bar slip increases considerably for small covers. As a way to validate the procedure, a *fuzzy* linear model was built in a similar way and was validated using the bar strength at bond failure of actual shotcrete "pull-out" specimens.

The resulting BSR's are intended to be used as modification factors in conjunction with the *development length* equation for reinforcing bars in tension required by North American design

codes to compensate for the bar stress reduction caused by imperfections behind the bonded length of reinforcing bars. To ease their selection based on a given void size, the equal bar stress probability (in comparison to a perfectly encapsulated reinforcing bar) was computed and then associated to a building risk category. Guidelines were developed for their selection and accounted for various parameters such as void size, void location or the concrete cover which were obtained from the experimental and Finite Element programs, but they represent the first series of modification factors developed for shotcrete to the knowledge of the authors so more research is needed to validate them of enhance them.

Overall, the selected modification factor could be used to multiply the *development length* equation during the design phase of reinforced shotcrete structures to guarantee an equal bar stress as perfectly encapsulated bars in case imperfections behind reinforcing bars are foreseen during spraying operations. As a consequence, such measures could ease the severity of core acceptance during the inspection phase.

6.10 Acknowledgements

The authors are grateful to the Concrete Infrastructure Research Center (CRIB) of Québec, the Natural Sciences and Engineering Research Council of Canada (NSERC), King Packaged Materials and Co., the Canadian Council of Independent Laboratories (CCIL), the American Shotcrete Association (ASA) and the Québec and East Ontario Chapter of the American Concrete Institute (ACI) for their financial support. Furthermore, special thanks are extended to Jean-Daniel Lemay and Mathieu Thomassin-Mailhot (research engineers), to René Malo (expert laboratory technician) and to Pierre-André Tremblay and Alain Melançon (laboratory technicians) of the Department of Civil and Water Engineering at Université Laval for their outstanding work and support during the casting and the testing operations.

6.11 References

[5] ACI Committee 318, "318-19 Building code requirements for structural concrete and commentary," American Concrete Institute, Michigan, 2019, 559 p.

[6] CSA, "A23.3-19 Design of concrete structures," Canadian Standards Association, Ontario, 2019, 297 p.

[13] ACI Committee 506, "506R-16: Guide to shotcrete," American Concrete Institute, Michigan, 2016, 52 p.

[15] ACI Committee 506, "506.2-13 Specification for shotcrete," American Concrete Institute, Michigan, 2013, 12 p.

[16] ACI Committee 506, "Visual shotcrete core quality evaluation technote (ACI 506.6T-17)," American Concrete Institute, Michigan, 2017, 4 p.

[17] ASTM, "A944-10(2015) standard test method for comparing bond strength of steel reinforcing bars to concrete using beam-end specimens," American Society of Testing and Materials, 2015, 4 p. https://doi.org/10.1520/A0944-10R15

[21] Gagnon, A., Fily-Paré, I., Jolin, M., "Rethinking shotcrete mixture design through sustainable ingredients," Shotcrete Magazine, Vol. 18, No. 4, 2016, pp. 28-31.

[28] ACI Committee 506, "506.2-95 Specification for shotcrete," American Concrete Institute, 1995, 8 p.

[31] Warner, J., "Understanding shotcrete - Structural applications," Concrete International, Vol. 17, No. 10, 1995, pp. 55-61.

[32] Warner, J., "Bond strength of reinforcing bars in reinforced shotcrete - Discussion by James Warner," ACI Materials Journal, Vol. 95, No. 1, 1998, pp. 196-197.

[33] Concrete Construction Staff, "Shotcrete core grading: Is it working?," Concrete Construction, Vol. 45, No. 10, 2000.

[34] Fischer, M., Hofmann, M., "Reinforced shotcrete with bar diameters up to 32 mm," Crossrail learning legacy, 2015, 13 p.

[38] Johnston, D. W., Zia, P., "Bond characteristics of epoxy-coated reinforcing bars," North Carolina State University, 1982, 163 p.

[40] Treece, R. A., Jirsa, J. O., "Bond strength of epoxy-coated reinforcing bars," ACI Materials Journal, Vol. 86, No. 2, 1989, pp. 167-174.

[42] ACI Committee 408, "408R-03 Bond and development of straight reinforcing bars in tension," American Concrete Institute, Michigan, 2003, 49 p.

[64] Cox, J. V., Herrmann, L. R., "Development of a plasticity bond model for steel reinforcement," Mechanics of cohesive-frictional materials, Vol. 3, No. 2, 1998, pp. 155-180.

[76] Orangun, C. O., Jirsa J.O., Breen J.E., "The strength of anchor bars: A revaluation of the test data on development length and splices," The University of Texas, Texas, 1975, 78 p.

[83] Clark, A. P., "Comparative bond efficiency of deformed concrete reinforcing bars," Journal of Research, Vol. 37, December, 1946, pp. 399-407.

[84] Jirsa, J. O., Breen, J. E., "Influence of casting position and shear on development and splice length - Design recommendations," The University of Texas, Texas, 1981, 45 p.

[85] Jeanty, P. R., Mitchell, D., Mirza, M. S., "Investigation of 'top bar' effects in beams," ACI Structural Journal, Vol. 85, No. 3, 1988, pp. 251-257.

[103] Josserand, L., de Larrard F., "A method for concrete bleeding measurement," Materials and Structures, Vol. 37, 2004, pp. 666-670. https://doi.org/10.1007/BF02480511

[121] Basso Trujillo, P., Jolin, M., Massicotte, B., Bissonnette, B., "Bond strength of reinforcing bars encased with shotcrete," Construction and Building Materials, Vol. 169, 2018, pp. 678-688. https://doi.org/10.1016/j.conbuildmat.2018.02.218

[124] Basso Trujillo, P., Malo, R., Jolin, M., "Alternative set-up apparatus to test ASTM A944-10 beam-end specimens," Journal of Testing and Evaluation, Vol. 46, No. 4, 2018, pp. 1741-1748. https://doi.org/10.1520/JTE20170645

[127] Basso Trujillo, P., Jolin, M., Massicotte, B., Bissonnette, B., "Bond strength of reinforcing bars with varying encapsulation qualities," ACI Structural Journal, Vol. 115, No. 6, 2018, pp. 1707-1717.

[143] Fily-Paré, I., Jolin, M., "The use of recycled glass in shotcrete," Shotcrete Magazine, Vol. 15, No. 4, 2013, pp. 14-16.

[144] Lemay, J-D., Jolin, M., Gagné, R., "Ultra rapid strength development in dry-mix shotcrete for ultra-rapid support in challenging mining conditions," Shotcrete Magazine, Vol. 16, No. 4, 2014, pp. 14-19.

[145] Bridger, P., "The history of shotcrete equipment," Shotcrete Magazine, Vol. 19, No. 4, 2017, pp. 34-37.

[146] Basso Trujillo, P., Lagier, F., Jolin, M., Massicotte, B., Bissonnette, B., "Finite element model of beam-end specimen with different qualities of reinforcing bar encapsulation," Engineering Structures Journal (submitted).

[147] Zadeh, L. A., "Fuzzy sets as a basis for a theory of possibility," Fuzzy Sets and Systems, Vol. 1, No. 1, 1978, pp. 3-28.

[148] Pedrycz, W., Gomide, F., "An introduction to fuzzy sets: Analysis and design,", The MIT press, London, 1998, 490 p.

[149] Klir, G. J., Yuan, B., "Fuzzy Sets and Fuzzy Logic - Theory and Applications," Upper Saddle River: Prentice Hall PTR, 1995, 574 p.

[150] Dubois, D., Prade, H., "Fundamentals of fuzzy sets," Kluwer academic publishers, 2000, 647 p.

[151] Aven, T., Baraldi, P., Flage, R., Zio, E., "Uncertainty in risk assessment - The representation and treatment of uncertainties by probabilistic and non-probabilistic methods," West Sussex: Wiley, 2014, 200 p.

[152] Hong, D. H., Lee, S., Do, H. Y., "Fuzzy linear regression analysis for fuzzy input-output data using shape-preserving operations," Fuzzy Sets and Systems, Vol. 122, No. 3, 2001, pp. 513-526.

[153] Heshmaty, B., Kandel, A., "Fuzzy linear regression and its implications to forecasting in uncertainty environment," Fussy sets and systems, Vol. 15, No. 2, 1985, pp. 159-191.

[154] Bardossy, A., "Fuzzy regression in hydrology," Water resources research, Vol. 26, No. 7, 1990, pp. 1497-1508.

[155] Hong, D. H., Do, H. Y., "Fuzzy polynomial regression analysis using shape preserving operation," Journal of Computational & Applied Mathematics, Vol. 8, No. 3, 2001, pp. 645-656.

[156] Dubois, D., Prade, H., Sandri, S., "On possibility/probability transformations," Fuzzy Logic: State of the Art, 1993, pp. 103-112.

[157] ASCE, "Minimum design loads for buildings and other structures," American Society of Civil Engineers, 2010, 209 p.

Chapter 7 Discussion

7.1 Introduction

This chapter seeks to discuss the findings of each article presented in this document to broaden the insight around the impact of the encapsulation quality of reinforcing bars on the bar-concrete bond strength. This chapter will be divided in two main sections. The first one will concentrate on the findings from Chapters 3, 4 and 5 which presented the results from the experimental program and the Finite Element model. The discussion focuses on the performance of properly placed shotcrete versus cast in-place concrete and on the relationship between the concrete cover and the mode of failure of bond specimens in combination with different sizes of the voids in case they are created specifically behind the reinforcing bars during the spraying operations. The impact voids may have on additional reinforcing bar confinement (e.g., fibers and stirrups) is also discussed. The second section discusses the proposed approach for structural engineers to implement the modification factors for the *development length* equation of reinforcing bars in tension proposed in this study during the inspection and the design of new shotcrete structures.

7.2 Reinforcing bar encapsulation and bond strength

It has been stated, mainly in Chapter 1 and Chapter 3, that the *consistency* of shotcrete plays a significant role on the encapsulation quality of reinforcing bars. The *dry-mix* process is perhaps the most challenging shotcrete process in this regard as nozzlemen need to adjust the water content of the mixture without knowing, *a priori*, its actual *w/b* ratio. Nonetheless, voids can also be created behind reinforcing bars when using the *wet-mix* process if, among others, a mixture is sprayed "too wet" leading to concrete sagging or if an excessive use of set-accelerator prevents the proper flow of the mixture behind the reinforcing bars. As a consequence, the *wettest stable limit* of the mixtures is still nowadays sought in the industry. This is, not only to achieve a proper encapsulation, but also to avoid excessive rebound and to maximize the build-up thickness of the mixture. Moreover, past research suggests that the *wettest stable limit* needs to be considered as range of adequate *consistency* values within which a shotcrete mixture can be properly sprayed. The results from this research indicate that the driest limit within that range should be sought for a given shotcrete mixture in order to achieve the highest possible bond of reinforcing bars without creating voids. This is of paramount importance since the slip at bond

failure and the slip stiffness of reinforcing bars in shotcrete was significantly enhanced in comparison to cast in-place concrete when the reinforcing bars were properly encapsulated in this study (refer to Section 3.5.5). For this reason, it is conceivable that smaller *development length*s, i.e. modification factors smaller than one, could be used with good quality and properly sprayed shotcrete where a perfect reinforcing bar encapsulation is guaranteed. However, more data needs to be gathered before actual modification factors applicable to this particular situation can be rightfully determined and proposed for the building codes.

The better bar-concrete slip stiffness of shotcrete in comparison to cast in-place concrete when spraying operations are adequate could also open the debate about the Serviceability Limit States (SLS) currently used when shotcrete structures are designed. Indeed, under the same loads, shotcrete elements might tend to deflect less and therefore could be less prone to premature flexural cracking in comparison to regular cast in-place concrete. As a consequence, some serviceability limits might be worth studying in detail for shotcrete structures. As an example, the *crack control* parameter (or z factor) currently required for the design of flexural members in the CSA A23.3-19 code (changed to an actual reinforcing bar spacing verification in the 1999 version of the ACI-318 code) indirectly limits the widths of the cracks to 0.33 and 0.40 mm for exterior and interior exposures by controlling the spacing of reinforcing bars. If epoxy coated reinforcing bars are used, they are required to be closer together with the use of a modification factor of 1.2 as an increased number of cracks can occur with their use because of an increased slip. In the case of shotcrete, a modification factor might be considered to alleviate these spacing restrictions as less slip is expected if a proper mixture and placement techniques are used. Needless to say, more research is needed in this regard to determine the actual factors for shotcrete in this case.

If voids are indeed created behind reinforcing bars, the interaction between their size and the concrete cover resulted to have a critical impact on the specimens' mode of failure. Firstly, it was found that the void's *un-bonded* perimeter (or *u.p.*) was enough to characterize the bar stress reduction and that other parameters like the voids' height and their position over the reinforcing bar (refer to Section 4.5.3) represented secondary parameters. Care has to be exerted in this regard as concrete durability, which was not investigated herein, might be impacted with these parameters. Secondly, it was found that *un-bonded* perimeters beyond 20% could either considerably increase the bar-concrete slip or drastically decrease the stress at bond failure of a

single reinforcing bar depending on the amount of concrete cover. The Finite Element (FE) model presented in Chapter 5 suggested that the failure mode change from concrete *splitting* to a bar *pull-out* could occur more promptly with an increased amount of concrete cover as the *un-bonded* perimeter increases. These observations were extremely helpful to better understand the impact of a void on the bond performance of a reinforcing bar and establish a 20% *un-bonded* perimeter as the threshold beyond which the structural performance of elements could be put at risk if the voids cover all of the anchorage region of a reinforcing bar. One of the key aspects that helped determine this limit was the fact that experimental "beam-end" specimens with a 30% *un-bonded* perimeter and a $2.5d_b$ concrete cover showed signs of a *pull-out* failure and therefore, increasing the concrete cover to $5.0d_b$ would truly cause a *pull-out* failure. Another important aspect that helped determine this limit was the fact that FE specimens with 30% or more *un-bonded* perimeters and $5.0d_b$ concrete cover developed a smaller bar stress at failure than specimens with a $2.5d_b$ concrete cover (refer to Section 5.7). This is extremely interesting as this phenomenon goes against the well-known bond behavior of perfectly encapsulated bars where increasing the concrete cover, after the specimen's mode of failure changes from *splitting* to *pull-out*, does not cause the bar stress at failure to decrease; yet it was observed in the presence of voids. This shows that a high confinement could dangerously decrease the sought ductile behavior of structural elements when *un-bonded* perimeters larger than 20% are present behind reinforcing bars all along their anchorage length. It needs to be noted that the 20% *un-bonded* perimeter threshold was established by analyzing the results of bond specimens whose reinforcing bar confinement was only provided by the concrete cover. Albeit it was not studied herein, it is believed that additional reinforcing bar confinement provided with stirrups or fibers in the concrete matrix could amplify this effect for *un-bonded* perimeters larger than 20%. Despite this, larger *un-bonded* perimeters were still deemed acceptable in case they do not cover the entire developed length of a reinforcing bar. In such cases, *un-bonded* perimeters of up to 30% were considered to provide an acceptable bond behavior if longer *development lengths* with the use of modification factors, are used.

Perhaps one of the most difficult aspects regarding the findings of this research is to determine the level of precision of the aforementioned *un-bonded* perimeter limits. It is well known that the type, geometry and other parameters of the chosen specimens can influence the results obtained from the tests. Of course the results of the "pull-out" and the "beam-end" specimens are

different because the stress distribution is also different between them. However, even for the same type of bond specimen, comparing the results of specimens with and without voids could provide slightly different tendencies if one chooses longer or smaller bonded lengths for instance. Indeed, if one compares the performance of the "beam-end" specimens presented in Chapter 4 and 5, it can be observed that the bonded length of the reinforcing bar plays an important role in the bar stress at failure reduction with increasing *un-bonded* perimeters. The reduction of the bar stress at failure of "beam-end" specimens presented in Chapter 4, which possessed a $6.3d_b$ bonded length, was more pronounced than the one of specimens presented in Chapter 5 whose bonded length was $12.5d_b$. Certainly, stress redistribution plays an important role that cannot be omitted so longer bonded lengths should be tested to verify the limits of the *un-bonded* perimeter established here. This would, of course, require to use bigger "beam-end" specimens or even another type such as "beam-splice" specimens. Regardless, it is believed that the limits suggested here are conservative and represent the starting point for the development of scientific-based guidelines for the inspection and design of shotcrete structures (or even other types such as 3D printed structures) in which the encapsulation quality of reinforcing bars is considered. There is still a great amount or research that needs to be done in this regard and the impact of voids on other parameters such as the configurations of reinforcing bars (e.g., size, bundles, *development length*, etc.) and types of anchorage systems (e.g., hooked or headed reinforcing bars) needs to be done to enhance design codes of concrete constructions and the safety of its users.

7.3 Development of inspection and design guidelines for shotcrete

Regardless of the *un-bonded* perimeter limit that will be adopted by a structural engineer in case voids (if any) are present along the bonded length of a reinforcing bar, a correction to the *development length* equation needs to be considered to compensate for the bar stress at failure loss caused by voids. In the current version of the North American design codes, correction factors are already used to account for the detrimental effect of a reinforcing bar coating (epoxy or zinc), the "top-bar" effect or the more beneficial bond strength achieved with small size reinforcing bars. In Chapter 4, the "top-bar" effect of a reinforcing bar was found to be comparable to the effect of *un-bonded* perimeters in between 20% and 30%. As such, it was deemed necessary to use modification factors for the *development length* equation of reinforcing bars in tension if voids are created behind reinforcing bars with shotcrete.

The modification factors proposed in this research were created in a similar way as the other ones already included in the *development length* equation for other situations. However, because voids in actual shotcrete specimens are highly irregular, the voids were reproduced in cast in-place "beam-end" specimens using artificial silicone inserts. This was without a doubt the best way to recreate them if their precise size was to be measured. In reality, structural engineers will be faced with difficult decisions regarding the actual *un-bonded* perimeter size and how much the developed length of a reinforcing bar is actually affected. The selection of such size is critical and requires a great deal of judgment as the selected size would be linked to a given modification factor. Whether this choice is conservative or not depends greatly on the judgment of the structural engineer who will have to take into account many parameters like the location of the void (over the developed portion of the reinforcing bar, over a splice, near the maximum moment, etc.), the level of reinforcing bar congestion, difficult job site conditions, the experience of the shotcrete crew, etc. Because modification factors were created using principles of *possibility theory*, any chosen *un-bonded* perimeter will actually represent an approximate or "close" value as the one selected; this approach greatly facilitates the selection process of the *un-bonded* perimeter by the structural engineer. Thus, even if a "crisp" value is chosen, a range in the vicinity of the chosen value will be taken into account. The proposed procedure is intended to be iterative. If it is known that shotcrete will be used for a project, a given *un-bonded* perimeter can be estimated by the structural engineer if there is concern about the encapsulation quality of reinforcing bars. A modification factor can thereafter be chosen based on the probability of equal bond performance in comparison to a perfectly encapsulated reinforcing bar (refer to Table 6.1 in Section 6.6.6). Such probability of equal bond performance was linked to the American Society of Civil Engineering's risk category of buildings so structural engineers could more easily make a selection. During the pre-construction phase of the project, where panels or mock-ups are sprayed, the choice of the modification factor can be validated. Proper corrections to the *development length* of the reinforcing bars (by either decreasing or increasing their length) can be made thereafter if deemed necessary based on the encapsulation quality of the reinforcement.

Perhaps the most difficult aspect of the process would be to determine the portion of the reinforcing bar's developed length that is in contact with the void (if any). For an inspection, the process could rely on the number of cores presenting defects in a given area of interest within the pre-construction panel. Then, based on the number of cores with imperfections around the

reinforcing bar, the presence of voids could be determined to be on less or more than 50% of the developed length of the reinforcing bar. During the design, where the inspection results are not available, a conservative approach could be to expect the presence of voids all along the bonded length of the bars if they are truly expected for any reason. Then, a proper modification factor could be chosen depending on the size of the void. During the inspection of cores taken from the pre-construction panels or mock-ups, the appropriate corrections can be made to the *development lengths* or even accept slightly larger *un-bonded* perimeters in case they are not present over the entire bonded length of the reinforcing bar.

As stated before, the experience and judgment of the structural engineers are essential in this process and the same modification factor might not be necessarily the same if two different engineers are faced with the same challenge. However, the procedure to increase the confidence level by which structural engineers specify *development length*s for shotcrete structures has believed to be greatly improved with these guidelines in which a scientific approach linking the bond strength of reinforcing bars with the size and location of voids has been used.

Conclusion and recommendations

General conclusions

The objective of this research was to increase the current knowledge regarding the impact of the encapsulation quality of reinforcing bars on their bond performance with concrete. On one hand, it was observed that a better bond performance can be obtained with shotcrete than with regular cast in-place concrete if a reinforcing bar is perfectly encapsulated due to the high impact velocity with which shotcrete is placed. On the other hand, in case imperfections are created behind reinforcing bars, a limit on the size of imperfection needed to be established to avoid an excessive bar stress at failure loss and bar slip and therefore, an undesirable failure mode such as the bar *pullout*. This limit was determined to be a 20% or a 30% *un-bonded* perimeter if the voids covered the entire or half of the bonded length of the reinforcing bar of the specimens respectively. However, even before these limits are attained, some bar stress at failure reduction is still observed. As a consequence, modification factors for the *development length* equation of reinforcing bars in tension were created. The modification factors were developed to provide inspectors and structural engineers with rational criteria for the evaluation of pre-construction panels and during the design of new shotcrete structures if imperfections below the established limits are foreseen.

Reinforcing bar encapsulation and bond strength

In the first part of this research, the influence of the mixture *consistency* on the bond performance of a reinforcing bar was investigated. Since the *wettest stable limit* of a shotcrete mixture is in fact a range, the "driest" *consistency* within this acceptable range should be sought to maximize the bond between the concrete and the reinforcing bars. Seeking this value should not have a negative impact on other shotcrete properties such as rebound, build-up thickness, mechanical and durability properties but more research should be conducted in this area. Regarding bond strength, using *consistencies* below the optimal range ("too wet") will cause reinforcing bars to slip further even though a perfect reinforcing bar encasement with an optimal bar stress at failure could be obtained. Using *consistencies* above the optimal range ("too dry") will increase the chances of creating imperfections behind reinforcing bars; the *consistency* of the shotcrete mixture can be measured using a pocket penetrometer on the job site. Comparatively with regular cast in-place concrete, shotcrete can provide a better or equal bond performance

(mainly in terms of the bar slip stiffness) if a perfect encapsulation quality is obtained due to the high velocity at which the concrete is placed.

If voids are created behind the reinforcing bars during the spraying operations, a 20% *un-bonded* perimeter limit is suggested if the voids cover the entire developed length of the reinforcing bar. A 30% *un-bonded* perimeter can be considered if voids cover only half of the developed length of the reinforcing bar. These limits were established based on the combined results of the "pull-out" and the "beam-end" specimens presented in Chapters 3, 4 and 5 with both the experimental and the Finite Element programs. The limits also took into account the failure mode change from *splitting* to *pullout* as the void size and the concrete cover increased in order to avoid an undesirable brittle behavior of an element. It has to be noted that even within the suggested limits, a bar stresses at bond failure reduction was still observed and thus, modification factors for the *development length* equation of reinforcing bars in tension were created to compensate for such bond strength loss.

Inspection and design of shotcrete structures

In the second part of this research, modification factors for the *development length* of reinforcing bars in tension equation were proposed using notions of *possibility theory* along with the results of cast in-place "beam-end" specimens with silicone inserts. Modification factors can be applied to the *development length* of reinforcing bars calculation during the design of shotcrete structures if voids are expected or their use can be verified based on the inspected encapsulation quality of a reinforcing bar observed from cores taken from pre-construction panels. For design purposes, the modification factors could be chosen based on the expected *un-bonded* perimeter of voids and on the allowed risk of a structural engineer based on the risk category to which the structure belongs. The modification factors associated to the *un-bonded* perimeter of reinforcing bars and their equal bond performance confidence level relative to a perfectly encapsulated reinforcing bar that has been linked to the risk category of buildings established by the ASCI (from I to IV or the less to the most critical respectively) to help structural engineers better select the appropriate modification factor if needed are shown in Table C.1.

Table C.1: Selection table for the shotcrete modification factors

Un-bonded perimeter, *u.p.*		Modification factor					
On 100% ℓ_d	On ≤ 50% ℓ_d	**1.0**	**1.1**	**1.2**	**1.3**	**1.4**	**1.5**
0%	0%	100% (I – IV)	-	-	-	-	-
10%	20%	60% (I)	82% (I / II)	92% (II / III)	97% (III / IV)	100% (IV)	-
20%	30%	-	72% (I)	87% (I / II)	93% (II / III)	98% (III / IV)	100% (IV)

The proposed selection procedure of the modification factors for shotcrete *could* go as follows:

A. In the case of voids appearing over the entire bonded length (100% of ℓ_d) of the reinforcing bar being developed

   a) Use a modification factor of at least 1.0 when *un-bonded* perimeters of around 10% or less might be created.

   b) Use a modification factor of at least 1.1 when *un-bonded* perimeters of around 20% might be created.

B. In the case of voids not covering the entire bonded length (50% or less of ℓ_d) of the reinforcing bar being developed[18]

   a) Use a modification factor of at least 1.0 when *un-bonded* perimeters of around 20% or less might be created.

   b) Use a modification factor of at least 1.1 when *un-bonded* perimeters of around 30% might be created.

C. The acceptance or correction made with modification factors for *un-bonded* perimeters larger than 20% if voids cover the entire bonded length of the bar or larger than 30% if voids appear sporadically (50% or less of ℓ_d) over the bonded length of the bar is not recommended.

[18] A value of 50% is determined based on the results of "beam-end" specimens testes using the Finite Element method where voids were only placed over half of the bonded length of the test bar.

D. *Modification factors* greater than the minimal recommended above might be prescribed by the structural engineer based on the risk category of the building given an expected encapsulation quality of the reinforcing bars. Table C.1 can be used for such purpose.

E. The *modification factors* proposed herein are not recommended to be used in conjunction with Ψ_t or Ψ_e as shotcrete presents little (if any) bleeding and because coated bars are not normally used with shotcrete.

Future research recommendations

Based on the research performed, the chosen methodology and the conclusions that resulted from it, some recommendations for future research regarding the encasement quality of reinforcing bars with shotcrete are enumerated below:

1) Experimental tests using cast in-place "beam-end" specimens should further explore parameters like the concrete cover and the *developed length* in combination with different *un-bonded* perimeters using silicone inserts. In this regard, it would be extremely interesting and beneficial for the proposed guidelines of this research to study the influence of concrete covers smaller than $2.5d_b$, bonded lengths of a minimum of 300 mm and 25M (No. 25) reinforcing bars on the failure mode of the specimens and the bar stress at failure reduction with an increasing *un-bonded* perimeter. "Beam-end" specimens with such parameters could also be tested using shotcrete. One of the main difficulties encountered in this research when trying to spray bond specimens was to provide a proper bracing of the reinforcing bars and the PVC sleeves. In the case of the "beam-end" specimen, the displacement of all of these components occurred during the spraying operations when it was placed shot perpendicular to its longitudinal plane (parallel to the longitudinal axis of the reinforcing bar) due to the high velocity at which shotcrete was sprayed. A possible solution which was not attempted is to cast half of the "beam-end" specimen using regular cast in-place concrete so that a portion of the stirrups can be embedded in the concrete. The mold could be tilted before pouring the concrete so that the

hardened concrete stays at an angle providing an escape for rebound. The rest of the specimen can be then sprayed providing the proper formwork around it. A standardized procedure can be developed to test "beam-end" specimens using shotcrete. An alternative to provide even more realistic data, albeit more time consuming and expensive, would be to test "beam-splice" specimens.

2) As the proposed modification factors were developed based on cast in-place concrete "beam-end" specimens, the minimal modification factor recommended was established as 1.0 for perfectly reinforcing bars. However, it was demonstrated that properly placed shotcrete could reduce the bond slip of reinforcing bars in comparison with cast in-place concrete. As such, it is possible that smaller modification factors could be used for shotcrete. However, there is still scarce information in this regard so an experimental program designed to investigate this phenomenon should be undertaken before smaller modification factors for shotcrete can be established.

3) During the Finite Element (FE) program, the concrete elements around the reinforcing bar were given the same material properties as the bulk concrete. This approach was selected as the literature review revealed that the interfacial transition zone around reinforcing bars for highly stable concrete mixes was considerably small. However, due to the high impact with which concrete is sprayed, the concrete around reinforcing bars could be modeled with even higher mechanical properties than the bulk. This might cause the FE model to better predict the slip stiffness measured experimentally.

4) The Finite Element model proved to be a powerful tool to study the impact of parameters that could not be investigated during the experimental program. It also served to screen parameters which would have caused a significant amount of effort if they were tested experimentally. As such, it would be extremely beneficial to study the impact of voids using specimens with stirrups over the bonded length of the specimens' bonded length and study different types of reinforcing bar anchorages such as hooked or headed bars to determine the effect of voids on bond in these

cases. Experimental validation can be thereafter undertaken for the cases in which valuable and interesting data is obtained.

5) The *un-bonded* perimeter limits that were developed were completely based on the bond strength results provided by different interface qualities between a reinforcing bar and the concrete surrounding it affected by voids. Albeit some investigations have studied the effect of voids on the durability properties of reinforced concrete members, a thorough research program should be done to determine if the *un-bonded* perimeter limits proposed here do not jeopardize the service life of structures.

The continuous research in this domain will help to confirm or enhance the modification factors for the *development length* equation of reinforcing bars in tension proposed herein with the ultimate goal to increase the safety of the shotcrete structures being built in the years to come.

Bibliography

[1] Davis, B., "Holcim New Zealand cement terminal," Shotcrete Magazine, Vol. 19, No. 1, 2017 pp. 26-30.

[2] Townsend III, F. E., "Northern boulevard crossing tunnel CQ039," Shotcrete Magazine, Vol. 18, No. 1, 2016, pp. 34-36.

[3] Townsend III, F. E., "The plaza substation and queen structures," Shotcrete Magazine, Vol. 18, No. 1, 2016, pp. 22-23.

[4] Panian, L., Steyer, M., Tipping, S., "Post-tensioned shotcrete shearwalls," Concrete International, Vol. 29, No. 10, 2007, pp. 39-45.

[5] ACI Committee 318, "318-19 Building code requirements for structural concrete and commentary," American Concrete Institute, Michigan, 2019, 559 p.

[6] CSA, "A23.3-19 Design of concrete structures," Canadian Standards Association, Ontario, 2019, 297 p.

[7] Ghio, V.A., The rheology of fresh concrete and its effects on the shotcrete process," The University of California, California, 1993, 193 p.

[8] Ghio, V. A., Monteiro, P. J. M., "Bond strength of reinforcing bars in reinforced shotcrete," ACI Materials Journal, Vol. 94, No. 2, 1997, pp. 111-118.

[9] Crom, T. R., "Dry mix shotcrete nozzling," Concrete International, Vol. 3, No. 1, 1981, pp. 80-93.

[10] Beaupré, D., Jolin, M., "Effect of shotcrete consistency and nozzleman experience on reinforcement encasement quality," Shotcrete Magazine, Vol. 3, No. 4, 2001, pp. 20-23.

[11] Jolin, M., Beaupré, D., Mindess, S., "Quality control of dry-mix shotcrete during construction," Concrete International, Vol. 24, No. 10, 2002, pp. 69-74.

[12] Jolin, M., Gagnon, F., Beaupré, D., "Determination of criteria for the acceptance of shotcrete for certification," Shotcrete: More engineering developments, 2004, pp. 175-181.

[13] ACI Committee 506, "506R-16: Guide to shotcrete," American Concrete Institute, Michigan, 2016, 52 p.

[14] Zynda, C., "Shotcrete panels for evaluation and testing," Shotcrete magazine, Vol. 18, No. 3, 2016, pp. 10-14.

[15] ACI Committee 506, "506.2-13 Specification for shotcrete," American Concrete Institute, Michigan, 2013, 12 p.

[16] ACI Committee 506, "Visual shotcrete core quality evaluation technote (ACI 506.6T-17)," American Concrete Institute, Michigan, 2017, 4 p.

[17] ASTM, "A944-10(2015) standard test method for comparing bond strength of steel reinforcing bars to concrete using beam-end specimens," American Society of Testing and Materials, 2015, 4 p. https://doi.org/10.1520/A0944-10R15

[18] Jolin, M., "Mechanisms of placement and stability of dry-process shotcrete," University of British Columbia, British Columbia, 1999, 152 p.

[19] Millette, D., Jolin, M., "Shotcrete accelerators for wet-mix," Shotcrete Magazine, Vol. 16, No. 4, 2014, pp. 44-46.

[20] Gagnon, A., "Développement de mélanges de béton projeté à valeurs environnementales ajoutées, " Université Laval, Québec, 2017, 116 P.

[21] Gagnon, A., Fily-Paré, I., Jolin, M., "Rethinking shotcrete mixture design through sustainable ingredients," Shotcrete Magazine, Vol. 18, No. 4, 2016, pp. 28-31.

[22] ASTM, "C143/C143M-20 standard test method for slump of hydraulic-cement concrete," American Society of Testing and Materials, 2020, 4 p. https://doi.org/10.1520/C0143_C0143M-20

[23] Bell, J., "Reinforcing bar shadowing and what you can do," Shotcrete Magazine, Vol. 18, No. 2, 2016, pp. 40-41.

[24] Norton, M., "Wet-process shotcrete placement formula for nozzlemen: M+A+R+V+S=PHD," Shotcrete Magazine, Vol. 12, No. 3, 2010, pp. 34-35.

[25] Armelin, H. S., "Rebound and toughening mechanisms in steel fiber reinforced dry-mix shotcrete," The University of British Columbia, British Columbia, 1997, 262 p.

[26] Armelin, H. S., Banthia, N., Morgan, D. R., Steeves, C., "Rebound in dry-mix shotcrete," Concrete international, Vol. 19, No. 9, 1997, pp 54-60.

[27] Von der Hofen, M. H., "Structural shotcrete reinforcing," Shotcrete Magazine, Vol. 11, No. 4, 2009, pp. 22.

[28] ACI Committee 506, "506.2-95 Specification for shotcrete," American Concrete Institute, 1995, 8 p.

[29] ACI, "CP-60(15) Craftsman workbook for ACI certification of shotcrete nozzleman," American Concrete Institute, Michigan, 2015, 120 p.

[30] ACI Committee C660, "ACI CPP 660.1-20 Certification policies for shotcrete nozzleman and shotcrete nozzleman in training," American Concrete Institute, Michigan, 2017, 12 p.

[31] Warner, J., "Understanding shotcrete - Structural applications," Concrete International, Vol. 17, No. 10, 1995, pp. 55-61.

[32] Warner, J., "Bond strength of reinforcing bars in reinforced shotcrete - Discussion by James Warner," ACI Materials Journal, Vol. 95, No. 1, 1998, pp. 196-197.

[33] Concrete Construction Staff, "Shotcrete core grading: Is it working?," Concrete Construction, Vol. 45, No. 10, 2000.

[34] Fischer, M., Hofmann, M., "Reinforced shotcrete with bar diameters up to 32 mm," Crossrail learning legacy, 2015, 13 p.

[35] Lutz, L. A., Gergely, P., "Mechanics of bond and slip of deformed bars in concrete," American Concrete Institute Journal, Vol. 64, No. 11, 1967, pp. 711-721.

[36] Rabbat, B. G., Russell, H. G., "Friction coefficient of steel on concrete or grout," Journal of structural engineering, Vol. 111, No. 3, 1985, pp. 505-515.

[37] FIB, "Bond of reinforcement in concrete – Bulletin No. 10," The International Federation of Structural Concrete, 2000, 434 p.

[38] Johnston, D. W., Zia, P., "Bond characteristics of epoxy-coated reinforcing bars," North Carolina State University, 1982, 163 p.

[39] Choi, C. O., Darwin, D., McCabe, S. L., "Bond strength of epoxy-coated reinforcement to concrete", University of Kansas, 1990, 217 p.

[40] Treece, R. A., Jirsa, J. O., "Bond strength of epoxy-coated reinforcing bars," ACI Materials Journal, Vol. 86, No. 2, 1989, pp. 167-174.

[41] Brown, C. J., Darwin, D., McCabe S. L., "Finite Element Fracture Analysis of Steel-Concrete Bond," University of Kansas Center for research, Kansas, 1993, 100 p.

[42] ACI Committee 408, "408R-03 Bond and development of straight reinforcing bars in tension," American Concrete Institute, Michigan, 2003, 49 p.

[43] Darwin, D., Graham, E. K., "Effect of deformation height and spacing on bond strength of reinforcing bars," ACI Structural Journal, Vol. 90, No. 6, 1993, pp. 646-657, http://dx.doi.org/10.14359/4459

[44] Cairns, J., Jones, K., "Influence of rib geometry on strength of lapped joints: An experimental and analytical study," Magazine of concrete research, Vol. 47, No. 172, 1995, pp. 253-262.

[45] Fei, J., Darwin, D., "Fatigue of high relative rib area of reinforcing bars," University of Kansas Center for Research, Kansas, 1999, 76 p.

[46] Rehm, G., "The fundamental law of bond," Symposium on bond and crack formation, RILEM, Stockholm, 1957, pp. 491-498.

[47] Ghods, P., Isgor, O. B., McRae, G. A., Li, J., Gu, G. P., "Microscopic investigation of mill scale and its proposed effect on the variability of chloride-induced depassivation of carbon steel rebar," Corrosion science, Vol. 53, No. 3, 2011, pp. 946-954.

[48] Alexander, M. G., Arliguie, G., Ballivy, G., Bentur, A., Marchand, J., "Engineering and transport properties of the Interfacial Transition Zone in cementitious composites," RILEM, 1999, 404 p.

[49] Kenny, A., Katz, A., "Statistical relationship between mix properties and the interfacial transition zone around embedded rebar," Cement and concrete composites, Vol. 60, 2015, pp. 82-91.

[50] Horne, A. T., Richardson, I. G., Brydson, R. M. D., "Quantitative analysis of the microstructure of interfaces in steel reinforced concrete," Cement and concrete research, Vol. 37, No. 12, 2007, pp. 1613-1623.

[51] Zhang, R., Castel, A., François R., "Influence of steel-concrete interface defects owing to the top-bar effect on the chloride-induced corrosion of reinforcement," Magazine of concrete research, Vol. 63, No. 10, 2011, pp. 773-781.

[52] Soylev, T. A., François, R., "Quality of steel-concrete interface and corrosion of reinforcing steel," Cement and Concrete Research, Vol. 33, No. 9, 2003, pp. 1407-1415. https://doi.org/10.1016/S0008-8846(03)00087-5

[53] Soylev, T. A., François, R., "Défauts d'adhérence acier-béton dus au ressuage et au tassement du béton frais," Annales du bâtiment et des travaux publics, 2001.

[54] Soylev, T. A., "Rôle de la qualité de l'interface acier-béton sur la corrosion de l'armature du béton armé," INSA, Toulouse, 2002, 225 p.

[55] Spiratos, N., Pagé, M., Mailvaganam, N. P., Malhotra, V. M., Jolicoeur, C, "Superplasticizers for concrete: fundamentals, technology and practice," Supplementary cementing materials for sustainable development Inc, Ontario, 2003, 322 p.

[56] Darwin, D., Zuo J., Tholen M. L., Idun, E. K., "Development length criteria for conventional and high relative rib area reinforcing bars," ACI Structural Journal, V. 93, No. 3, 1996, pp. 347-359, https://doi.org/10.14359/9694

[57] Zuo, J., Darwin, D., "Splice strength of conventional and high relative rib area bars in normal and high-strength concrete," ACI Structural Journal, Vol. 97, No. 4, 2000, pp. 630-641, https://doi.org/10.14359/7428

[58] Miller, G. G., Kepler J. L., Darwin, D., "Effect of epoxy coating thickness on bond strength of reinforcing bars," ACI Structural Journal, Vol. 100, No. 3, 2003, pp. 314-320, https://doi.org/10.14359/12606

[59] Whiting, D., Seegebrecht, G. W., Tayabji, S., "Effect of degree of consolidation on some important properties of concrete," Special Publication 96, 1987, pp. 125-160.

[60] Brettmann, B. B., Darwin, D., Donahey, R. C., "Bond of reinforcement to superplasticized concrete," Journal of The American Concrete Institute, Vol. 83, No. 1, 1986, pp. 98-107. https://doi.org/10.14359/1743

[61] Brettmann, B. B., Darwin, D., Donahey, R. C., "Effects of superplasticizers on concrete-steel bond strength," University of Kansas Center for Research, Kansas, 1984, 32 p.

[62] Gagnon, F., "Enrobage de l'armature dans le béton projeté: Évaluation et effets," Université Laval, Québec, 2004, 166 p.

[63] Garcia T., Cavalero, S. H. P., Perez, J., Rueda, A., Figueiredo, A. "Evaluation of concrete-steel bond strength in wet mix sprayed concrete," The 7th international symposium on sprayed concrete, Sandefjiord, 2014, pp. 161-172.

[64] Cox, J. V., Herrmann, L. R., "Development of a plasticity bond model for steel reinforcement," Mechanics of cohesive-frictional materials, Vol. 3, No. 2, 1998, pp. 155-180.

[65] Panedpojaman, P., Pothisiri, T., "Bond characteristics of reinforced normal-strength concrete beams at elevated temperatures," ACI Structural Journal, Vol. 111, No. 6, 2014, pp. 1351-1362.

[66] Ftima, M. B., "Utilisation de la méthode des éléments finis non-linéaires pour la conception des structures en béton armé: application aux structures massives, " 2013, Université de Montréal, 189 p.

[67] Tastani, S., "Analytical investigation of bond between ECC matrix and steel reinforcement," 6th International conference on concrete repair, Thessaloniki, 2016, 6 p.

[68] Lura, P., Plizzari, G. A., Riva, P., "3D finite-element modeling of splitting crack propagation," Magazine of concrete research, Vol. 54, No. 6, 2002, pp. 481-493.

[69] Reinhardt, H. W., J. Blaauwendraad, E. Vos, "Prediction of bond between steel and concrete by numerical analysis" Materials and structures, Vol. 17, No. 4, 1984, pp. 311-320.

[70] Ozbolt, J., Eligehausen, R., "Numerical simulation of cyclic bond-slip behavior," Proceedings of bond in concrete: From research to practice, 1992, pp. 12(27)-12(33).

[71] Tholen, M. L., Darwin, D., "Effects of deformation properties on the bond of reinforcing bars," University of Kansas center for research, Kansas, 1996, 370 p.

[72] Brown, C. J., Darwin, D., McCabe S. L., "Finite element fracture analysis of steel-concrete bond," University of Kansas center for research, Kansas, 1993, 100 p.

[73] Salem, H. M., Maekawa, K., "Pre- and postyield finite element method simulation of bond of ribbed reinforcing bars," Journal of Structural Engineering, Vol. 130, No. 4, 2004, pp. 671-680, https://doi.org/10.1061/(ASCE)0733-9445(2004)130:4(671)

[74] Lagier, F., Massicotte, B., Charron, J-P., "3D Nonlinear finite element modeling of lap splices in UHPFRC," Journal of structural engineering, Vol. 1452, No. 11, 2016, 14 p.

[75] Bandelt, M. J., Frank, T. E., Lepech, M. D., Billington, S. L., "Bond behavior and interface modeling of reinforced high-performance fiber-reinforced cementitious composites," Cement and concrete composites, Vol. 83, 2017, pp. 188-201.

[76] Orangun, C. O., Jirsa J.O., Breen J.E., "The strength of anchor bars: A revaluation of the test data on development length and splices," The University of Texas, Texas, 1975, 78 p.

[77] Orangun, C. O., Jirsa, J. O., Breen, J. E., "Re-evaluation of test data on development length and splices," Journal of the American Concrete Institute, Vol. 74, No. 3, 1977, pp. 114-122.

[78] Ferguson, P. M., Thompson, J. N., "Development length for large high strength reinforcing bars," Journal of the American Concrete Institute, Vol. 62, No. 1, 1965, pp. 71-94.

[79] Ferguson, P. M., Thompson, J. N., "Development length for large high strength reinforcing bars in Bond," Journal of the American Concrete Institute, Vol. 59, No. 7, 1962, pp. 887-922

[80] Chamberlin, S. J., "Spacing of reinforcement in beams," Journal of the American Concrete Institute, Vol. 53, No. 1, 1956, pp. 113-134.

[81] ACI Committee 318, "318-95 Building code requirements for structural concrete and commentary," American Concrete Institute, Michigan, 1995, 369 p.

[82] ACI Committee 318, "318-14 Building code requirements for structural concrete and commentary," American Concrete Institute, Michigan, 2014, 520 p.

[83] Clark, A. P., "Comparative bond efficiency of deformed concrete reinforcing bars," Journal of Research, Vol. 37, December, 1946, pp. 399-407.

[84] Jirsa, J. O., Breen, J. E., "Influence of casting position and shear on development and splice length - Design recommendations," The University of Texas, Texas, 1981, 45 p.

[85] Jeanty, P. R., Mitchell, D., Mirza, M. S., "Investigation of 'top bar' effects in beams," ACI Structural Journal, Vol. 85, No. 3, 1988, pp. 251-257.

[86] Hadje-Ghaffari, H., Choi, O. C., Darwin, D., McCabe, S. L., "Bond of epoxy-coated reinforcement: Cover, casting position, slump, and consolidation," ACI Structural Journal, Vol. 91, No. 1, 1994, pp. 59-68.

[87] ACI Committee 408, "Database 10-2001 (635 development and splice tests of uncoated bars)," American Concrete Institute, 2001.

[88] Canbay, E., Frosch, R. J., "Bond Strength of Lap-Spliced Bars," ACI Structural Journal, Vol. 102, No. 4, 2005, pp. 605-614.

[89] Paultre, P., "Structures en béton armé: Analyse et dimensionnement," Presses internationales Polytechnique, Québec, 2011, 928 p.

[90] ASTM, "C234-91a Standard test method for comparing concretes on the basis of the bond developed with reinforcing steel," American Society of Testing and Materials, 1991, 5 p.

[91] ACI Committee E703, "CCS-4(08) Shotcrete for the craftsman," American Concrete Institute, Michigan, 2008, 85 p.

[92] ASTM, "C192/C192M-16a standard practice for making and curing concrete test specimens in the laboratory," American Society of Testing and Materials, 2016, 8 p. https://doi.org/10.1520/C0192_C0192M-16A

[93] Nagi, M., Whiting, D., "Determination of water content of fresh concrete using a microwave oven," Cement, Concrete and Aggregates, Vol. 16, No. 2, 1994, pp. 125-131. https://doi.org/10.1520/CCA10290J

[94] AASHTO, "T 318-15 Standard method of test for water content of freshly mixed concrete using microwave oven drying," American Association of State and Highway Transportation Officials, Washington, 2015, 6 p.

[95] ASTM, "C117-13 standard test method for materials finer than 75-μm (No. 200) sieve in mineral aggregates by washing," American Society of Testing and Materials, 2013, 3 p. https://doi.org/10.1520/C0117-17

[96] ASTM, "C231/C231M-17 standard test method for air content of freshly mixed concrete by the pressure method," American Society of Testing and Materials, 2017, 9 p. https://doi.org/10.1520/C0231_C0231M-17A

[97] ASTM, "C1604/C1604M-05(2019) standard test method for obtaining and testing drilled cores of shotcrete," American Society of Testing and Materials, 2012, 5 p. https://doi.org/10.1520/C1604_C1604M-05R19

[98] ASTM, "C642-13 standard test method for density, absorption, and voids in hardened concrete," American Society of Testing and Materials, 2013, 3 p. https://doi.org/10.1520/C0642-13

[99] ASTM, "C39/C39M-17a standard test method for compressive strength of cylindrical concrete specimens," American Society of Testing and Materials, 2017, 8 p. https://doi.org/10.1520/C0039_C0039M-17B

[100] ASTM, "C1611-14 Standard test method for slump flow of self-consolidating concrete," American Society of Testing and Materials, 2014, 6 p. https://doi.org/10.1520/C1611_C1611M-14

[101] ASTM, "C496-17 Standard test method for splitting tensile strength of cylindrical concrete specimens," American Society of Testing and Materials, 2017, 5 p. https://doi.org/10.1520/C0496_C0496M-17

[102] ASTM, "C469-14 Standard test method for static modulus of elasticity and poisson's ratio of concrete in compression," American Society of Testing and Materials, 2014, 5 p. https://doi.org/10.1520/C0469_C0469M

[103] Josserand, L., de Larrard F., "A method for concrete bleeding measurement," Materials and Structures, Vol. 37, 2004, pp. 666-670. https://doi.org/10.1007/BF02480511

[104] ASTM, "C232-20 Standard test method for bleeding of concrete," American Society of Testing and Materials, 2020, 3 p. https://doi.org/10.1520/C0232_C0232M-20

[105] ASTM, "A370-20 Standard test methods and definitions for mechanical testing of steel products," American Society of Testing and Materials, 2020, 50 p. https://doi.org/10.1520/A0370-20

[106] ASTM, "C494/C494M-19 Standard specification for chemical admixtures for concrete," American Society of Testing and Materials, 2019, 15 p. https://doi.org/10.1520/C0494_C0494M-19

[107] Dassault Systems, "ABAQUS Theory Manual V. 6.14," 2014, unpaged.

[108] Lubliner, J., Oliver, J., Oller, S., Onate, E., "A plastic-damage model for concrete," International Journal of Solids and Structures, Vol. 25, No. 3, 1989, pp. 299-326.

[109] Lee, J., Fenves, G. L., "Plastic-damage model for cyclic loading of concrete structures," Journal of engineering mechanics, Vol. 124, No. 8, 1998, pp. 892-900.

[110] Jankowiak, T, Lodygowski, T., "Identification of parameters of concrete damage plasticity constituitive model," Foundations of civil and environmental engineering, No. 6, 2005, pp. 53-69.

[111] Ftima, M., B., "Utilisation de la méthode des éléments finis non-linéaires pour la conception des structures en béton armé: application aux structures massives," Université de Montréal, Québec, 2013, 189 p.

[112] Studebaker, C. H., "Report on gunite at Arrow dam," U.S. Bureau of Reclamation Memorandum, 1939, 66 p.

[113] ASTM, "C42/C42M-20 standard test method for obtaining and testing drilled cores and sawed beams of concrete," American Society of Testing and Materials, 2020, 7 p. https://doi.org/10.1520/C0042_C0042M-20

[114] Austin, S. A., Robins, P. J., "Sprayed concrete: properties, design and application," McGraw-Hill, New York, 1995, 382 p.

[115] Mor, A., "Steel-concrete bond in high-strength lightweight concrete," ACI Materials Journal, Vol. 89, No. 1, 1992, pp. 76-82.

[116] Carmer, S. G., Swanson, M. R., "An evaluation of ten pairwise multiple comparison procedures by Monte Carlo methods," Journal of the American Statistical Association, Vol. 68, No. 341, 1973, pp. 66-74. https://doi.org/10.2307/2284140

[117] Montgomery, D. C., "Design and analysis of experiments," 7th ed, 2009, 725 p.

[118] Quinn, G. P., Keough, M. J., "Experimental design and data analysis for biologists," Cambridge University Press, New York, 2002, 537 p.

[119] Morgan, D. R., McAskill, N., Neill, J., Duke, N. F., "Evaluation of silica fume shotcrete," International workshop on condensed silica fume in concrete, Montréal, 1987, 34 p.

[120] Milliken, G. A., Johnson, D. E., "Analysis of messy data - Volume III: Analysis of covariance," Champman & Hall / CRC, New York, 2002, 605 p.

[121] Basso Trujillo, P., Jolin, M., Massicotte, B., Bissonnette, B., "Bond strength of reinforcing bars encased with shotcrete," Construction and Building Materials, Vol. 169, 2018, pp. 678-688. https://doi.org/10.1016/j.conbuildmat.2018.02.218

[122] Jirsa, J.O., Lutz L.A., Gergely P., "Rationale for suggested development, splice, and standard hook provisions for deformed bars in tension," Concrete International, Vol. 1, No. 7, 1979, pp. 47-61.

[123] ASTM, "A615-20 Standard specification for deformed ad plain carbon-steel bars for concrete reinforcement," American Society of Testing and Materials, 2020, 8 p. https://doi.org/10.1520/A0615_A0615M-20

[124] Basso Trujillo, P., Malo, R., Jolin, M., "Alternative set-up apparatus to test ASTM A944-10 beam-end specimens," Journal of Testing and Evaluation, Vol. 46, No. 4, 2018, pp. 1741-1748. https://doi.org/10.1520/JTE20170645

[125] ASTM, "Significance of tests and properties of concrete and concrete-making materials," American Society of Testing and Materials, 2006, 664 p., https://doi.org/10.1520/STP169D-EB

[126] Jolin, M., Beaupré, D., Mindess, S., "Rheology of dry-mix shotcrete," Concrete Science and Engineering, Vol. 12, No. 3, 2001, pp. 195-201.

[127] Basso Trujillo, P., Jolin, M., Massicotte, B., Bissonnette, B., "Bond strength of reinforcing bars with varying encapsulation qualities," ACI Structural Journal, Vol. 115, No. 6, 2018, pp. 1707-1717.

[128] Unauthored, "Essais portant sur l'adhérence des armatures du béton - 2. Essai par traction," Materials and Structures, Vol. 3, 1970, pp. 175-178.

[129] Chen, W.-F., "Plasticity in reinforced concrete," McGraw Hill, 2007, 474 p.

[130] Popovics, S., "A numerical approach to the complete stress-strain curve of concrete," Cement and concrete research, Vol. 3, No. 5, 1973, pp. 583-599.

[131] Thorenfeldt, E., Tomaszewicz A., Jensen J. J., "Mechanical properties of high-strength concrete and application to design," Utilization of high-strength concrete, 1987, pp. 149-159.

[132] Wight, J. K., MacGregor J. G., "Reinforced concrete : Mechanics and design," 2009, 1157 p.

[133] De Nicolo, B., Pani, L., Pozzo, E., "Strain of concrete at peak compressive stress for a wide range of compressive strengths," Materials and Structures, Vol. 27, No. 4, 1994, pp. 206-210

[134] Collins, M. P., Mitchell, D., MacGregor, J. G., "Structural design considerations for high-strength concrete," Concrete international, Vol. 15, No. 5, 1993, pp. 27-34.

[135] Collins, P., Porasz, A., "Shear design for high-strength concrete," Bulletin d'information No. 193 - Comité Euro-International du béton, 1989, pp. 77-83.

[136] Cornelissen, H. A. W., Hordijk, D. A., Reinhardt, H. W., "Experimental determination of crack softening characteristics of normalweight and lightweight concrete," Heron, Vol. 31, No. 2, 1986, pp. 45-56.

[137] Rocco, C., Guinea, G. V., Planas, J., Elices, M., "Review of the splitting-test standards from a fracture mechanics point of view," Cement and concrete research, Vol. 31, No. 1, 2001, pp. 73-82.

[138] Vos, E., "Influence of loading rate and radial pressure on bond in reinforced concrete," Delft University, 1983, 235 p.

[139] Pavlović, M., Marković, Z., Veljković, M., Buđevac, D., "Bolted shear connectors vs. headed studs behavior in push-out tests," Journal of constructional steel research, Vol. 88, 2013, pp. 134-149.

[140] Derringer, G., Suich, R., "Simultaneous optimization of several response variables," Journal of quality technology, Vol. 12, 1980, pp. 214-219.

[141] Hussein, A., Marzouk, H., "Behaviour of high-strength concrete under biaxial stress," ACI Materials Journal, Vol. 97, No. 1, 2000, pp. 27-36.

[142] Vogel, T., Schenkel, M., "Bond behavior of reinforcement with inadequate concrete cover," 3rd international symposium of bond in concrete - from research to standards, 2002, pp. 359-366.

[143] Fily-Paré, I., Jolin, M., "The use of recycled glass in shotcrete," Shotcrete Magazine, Vol. 15, No. 4, 2013, pp. 14-16.

[144] Lemay, J-D., Jolin, M., Gagné, R., "Ultra rapid strength development in dry-mix shotcrete for ultra-rapid support in challenging mining conditions," Shotcrete Magazine, Vol. 16, No. 4, 2014, pp. 14-19.

[145] Bridger, P., "The history of shotcrete equipment," Shotcrete Magazine, Vol. 19, No. 4, 2017, pp. 34-37.

[146] Basso Trujillo, P., Lagier, F., Jolin, M., Massicotte, B., Bissonnette, B., "Finite element model of beam-end specimen with different qualities of reinforcing bar encapsulation," Engineering Structures Journal (submitted).

[147] Zadeh, L. A., "Fuzzy sets as a basis for a theory of possibility," Fuzzy Sets and Systems, Vol. 1, No. 1, 1978, pp. 3-28.

[148] Pedrycz, W., Gomide, F., "An introduction to fuzzy sets: Analysis and design,", The MIT press, London, 1998, 490 p.

[149] Klir, G. J., Yuan, B., "Fuzzy Sets and Fuzzy Logic - Theory and Applications," Upper Saddle River: Prentice Hall PTR, 1995, 574 p.

[150] Dubois, D., Prade, H., "Fundamentals of fuzzy sets," Kluwer academic publishers, 2000, 647 p.

[151] Aven, T., Baraldi, P., Flage, R., Zio, E., "Uncertainty in risk assessment - The representation and treatment of uncertainties by probabilistic and non-probabilistic methods," West Sussex: Wiley, 2014, 200 p.

[152] Hong, D. H., Lee, S., Do, H. Y., "Fuzzy linear regression analysis for fuzzy input-output data using shape-preserving operations," Fuzzy Sets and Systems, Vol. 122, No. 3, 2001, pp. 513-526.

[153] Heshmaty, B., Kandel, A., "Fuzzy linear regression and its implications to forecasting in uncertainty environment," Fussy sets and systems, Vol. 15, No. 2, 1985, pp. 159-191.

[154] Bardossy, A., "Fuzzy regression in hydrology," Water resources research, Vol. 26, No. 7, 1990, pp. 1497-1508.

[155] Hong, D. H., Do, H. Y., "Fuzzy polynomial regression analysis using shape preserving operation," Journal of Computational & Applied Mathematics, Vol. 8, No. 3, 2001, pp. 645-656.

[156] Dubois, D., Prade, H., Sandri, S., "On possibility/probability transformations," Fuzzy Logic: State of the Art, 1993, pp. 103-112.

[157] ASCE, "Minimum design loads for buildings and other structures," American Society of Civil Engineers, 2010, 209 p.

[158] FIB, "fib Model code for concrete structures," The International Federation of Structural Concrete, 2010, 402 p.

[159] Angst, U., M., et al., "The steel-concrete interface," Materials and Structures, Vol. 50, No. 2, 2017, 143 p.

Appendix A Alternative set-up apparatus to test ASTM A944-10 "beam-end" specimens

Pasquale Basso Trujillo[a], René Malo[a], Marc Jolin[a]
[a] *Dept. of Civil and Water Engineering, Université Laval*

This paper is part of the Journal of Testing and Evaluation, ISSN 0090-3973, doi.org/10.1520/JTE20170645. Paper submitted on November 9th, 2017; approved on March 15th, 2018 and published on July 1st, 2018.

A.1 Résumé

L'appareil d'essai décrit dans la norme ASTM A944-10, *Standard test method for comparing bond strength of steel reinforcing bars to concrete using beam-end specimens* a été conçu pour appliquer la charge de façon horizontale respectivement au plancher du laboratoire. Cependant, la plupart des laboratoires en génie civil utilisent (ou ont accès à) des cadres rigides d'essai conçus pour appliquer la charge de façon verticale. Ainsi, un appareil d'essai adapté aux dits cadres rigides, donnant une alternative à celui décrit dans la norme ASTM A944-10, a été conçu et est présenté ici. Après une brève description des caractéristiques les plus importantes de l'éprouvette d'essai décrite par la norme ASTM A944-10, l'appareil d'essai proposé ainsi que la procédure pour installer l'éprouvette sont décrits. Par la suite, les résultats de trois groupes d'éprouvettes ayant trois répliques sont présentés et sont suivis par une discussion portant sur l'analyse de l'information obtenue par l'essai.

A.2 Abstract

The set-up apparatus described in the ASTM A944-10, *Standard test method for comparing bond strength of steel reinforcing bars to concrete using beam-end specimens* is designed to apply the load horizontally with respect to the laboratory floor. However, many civil engineering laboratories currently use (or have access to) rigid testing frames designed to apply the load vertically. Thus, a set-up apparatus adapted to the current frames in use and alternate to the one described in the ASTM A944-10 standard was developed and is presented. Following a brief review of the major characteristics of a typical ASTM A944-10 "beam-end" specimen, the proposed set-up apparatus and the procedure to mount and test the specimen are described. Thereafter, the results of three groups of specimens having three replicas each are presented and are followed by a discussion on how to interpret and analyze the information obtained from the test.

Keywords : Beam-end, ASTM A944-10, Bond, Concrete reinforcement, Reinforced concrete, Reinforcement, Steel reinforced concrete

A.3 Introduction

The ASTM A944-10, *Standard test method for comparing bond strength of steel reinforcing bars to concrete using beam-end specimens* [17] is based on original research done at the University of Kansas [61] in the mid 80s and has since become an important reference for researchers studying the mechanical properties of the interface between reinforcing bars and concrete. The specimen was designed to reproduce accurately the stress state of most real-life reinforced concrete elements in flexure (both the reinforcing bar and the concrete surrounding it are placed in tension) and the bond strengths obtained closely match (although they are in general slightly higher [17]) those of full-scale specimens with similar embedment lengths [42]. Because of the representative stress state and because it usually requires less effort and cost to test than full-scale specimens, its use has gained an enormous amount of popularity in the past few decades. In fact, its use has been the basis for the proposal of *modification factors* [38, 39] for the *development length* equation for bars in tension specified in North American reinforced concrete design codes [5, 6].

In the ASTM A944-10 [17] standard, the described procedure suggests to place the "beam-end" specimens over a pedestal with their test bar in a horizontal position with respect to the laboratory floor. However, many civil engineering laboratories nowadays possess (or have access to) rigid testing frames configured to apply the load vertically. In order to avoid taking additional space in the laboratory and to minimize costs, one of the existing test frames in the civil engineering laboratory at the Université Laval in Québec City, Canada, has been adapted to test ASTM A944 "beam-end" specimens with the test bar in a vertical position and is presented subsequently.

A.4 Review of a typical "beam-end" specimen

The typical configuration of a specimen with all its parts is shown in Figure A.1. As can be seen, the *bonded length* of the test bar and its location are controlled by front and back PVC sleeves. The length of the front sleeve is referred to as the *lead length* in the ASTM A944-10 standard [17] and is required to prevent a cone-type failure of the concrete on the front surface of the specimen. Moreover, the interior end of the bond breaking sleeves must be sealed in some way to prevent mortar seepage and the same orientation of the test bar's ribs needs to be

respected for all the specimens. Additional bars and stirrups guarantee that the specimen will not fail in flexure or in shear. The stirrups are placed parallel to the test bar so they don't cross the failure plane of the concrete but they can be placed transversally over the *bonded length* if their contribution to the bond strength is to be studied [43]. Moreover, transversal PVC sleeves can be placed between the stirrups so that the specimen can be transported easily when inserting reinforcing bars inside them. This is convenient as these reinforcing bars can be removed once the specimen has been moved. The dimensions of the specimen and the procedure to place and cure the concrete are detailed in the ASTM A944-10 standard [17].

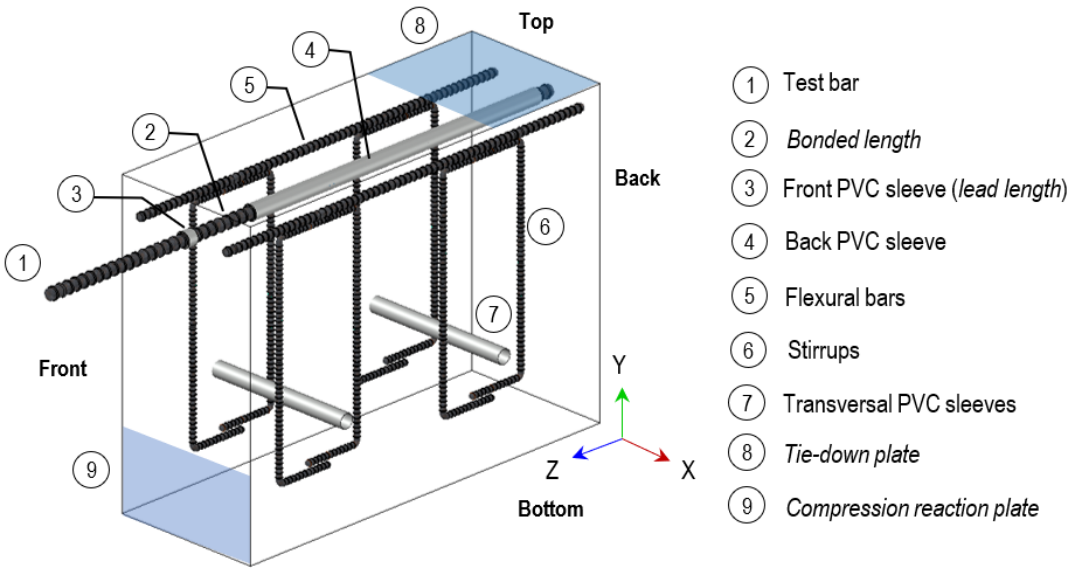

Figure A.1: Geometry of a typical ASTM A944-10 "beam-end" specimen

An important limit regarding the distance between the upper part of the *compression reaction plate* and the center of the test bar is specified in the ASTM A944-10 standard [17]. This distance must be greater than 0.9 times the embedment length (l_e) of the bar, i.e., the sum of the *bonded* and the *lead length*. This limit is needed to guarantee the stress distribution shown in Figure A.2 in which radial tensile stresses cause the concrete to split as the test bar is loaded [42].

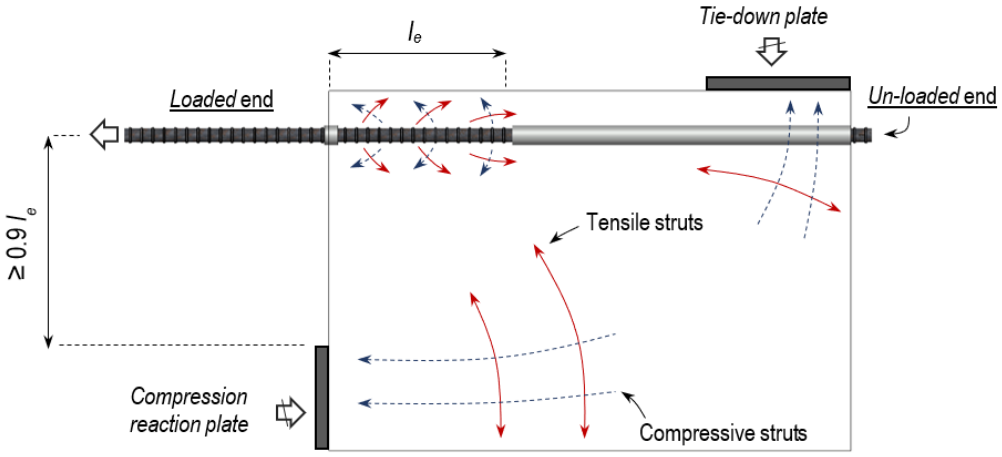

Figure A.2: Stress distribution in an ASTM A944 "beam-end" specimen

A.5 Alternative testing apparatus

In order to use a 311 MTS high force servo hydraulic rigid frame to test a specimen such as the one shown in Figure A.1, the assembly shown in Figure A.3 was built within the limits of the frame. For clarity, a detailed representation of the assembly with all of its components is shown in Figure A.4 and the size of the major components is provided in Table A.1 of the Appendix.

Figure A.3: Assembly of the alternative testing apparatus

Firstly, a steel box was anchored to the base of the frame and then a steel plate with four alignment bolts (one at each corner) was placed over it. Using an overhead crane and the lifting device shown in Figure A.5a, the "beam-end" specimen was carefully lifted (to avoid damaging the test bar) and was placed over the steel plate with the four alignment bolts. The bolts of the steel plate served to tilt the specimen on its Y-Z and its X-Z planes (refer to Figure A.1 and Figure A.4) so that the test bar's longitudinal axis was precisely vertical.

A steel piece soldered to the back of the steel plate, provided support for the back alignment plate and held the *tie-down plate* in place with two horizontal threaded rods on each side. As the top-back border of the "beam-end" specimen (refer to Figure A.1) rested over the *tie-down plate*'s support (previously leveled with respect to the plate with four alignment bolts using the *tie-down plate*'s structure), the back alignment plate was used to push the specimen along the Y axis to align the test bar with the testing actuator. Leveling lasers (as shown in Figure A.5b) were used throughout the alignment process and once the specimen was correctly positioned, the bolts holding all the pieces together were tightened.

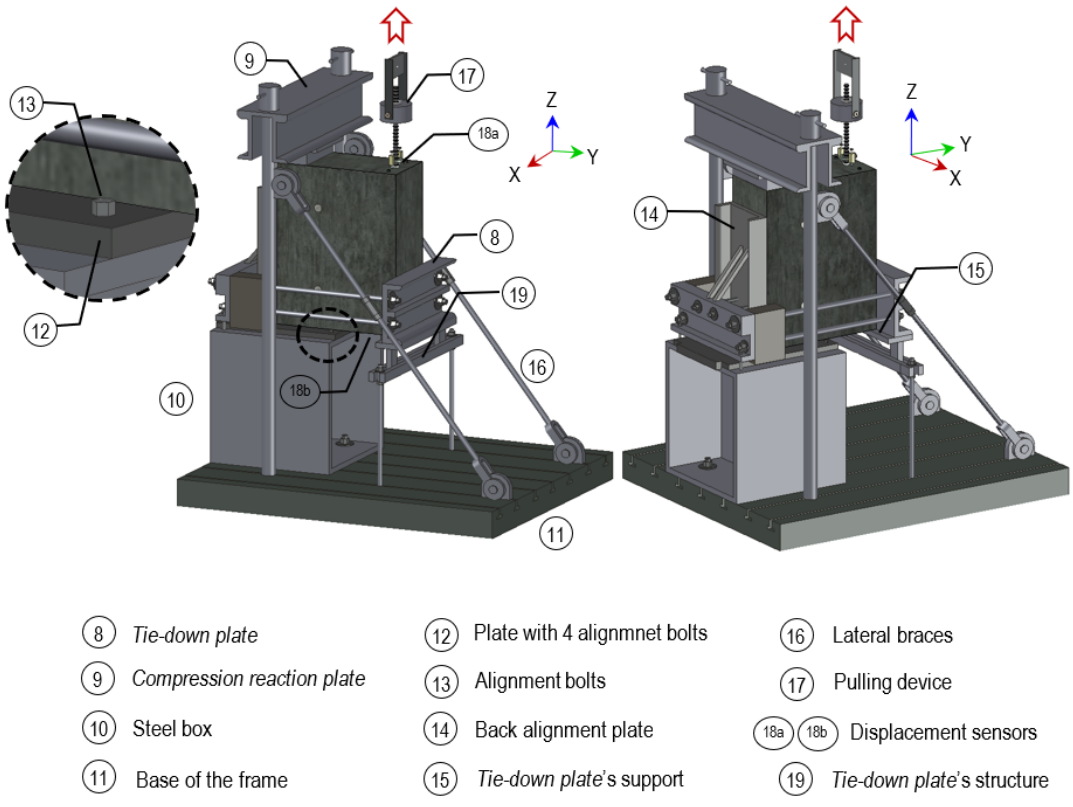

Figure A.4: Detailed representation of the assembly

Once the specimen was properly aligned and secured in place, the *compression reaction plate* was lowered and tightened. It consisted of two C sections welded together by means of two parallel steel plates (one on top and one at the bottom) which in turn, was held in place by two steel columns on each side. The columns passed in between the C sections and were anchored to the base of the frame. Moreover, they were restrained by lateral braces so that the columns would maintain their verticality throughout the entire duration of the test. A rubber sheet and a thick steel block were placed over the specimen at that location to transfer the compression reaction force to the assembly uniformly.

Finally, the pulling device (see Figure A.5c) was installed around the test bar; it consisted of two square shafts (linked together at the top by a plate) pin-holding a thick cylinder with a concentric opening throughout its entire thickness. A wedge grip was placed around the test bar and above the thick cylinder so that it would bear against the wedge while the pulling device was being displaced. According to the ASTM A944-10 standard [17], the loading rate is required to be between 10 and 30% of the bond strength per minute so that the test lasts no less than approximately 3 minutes.

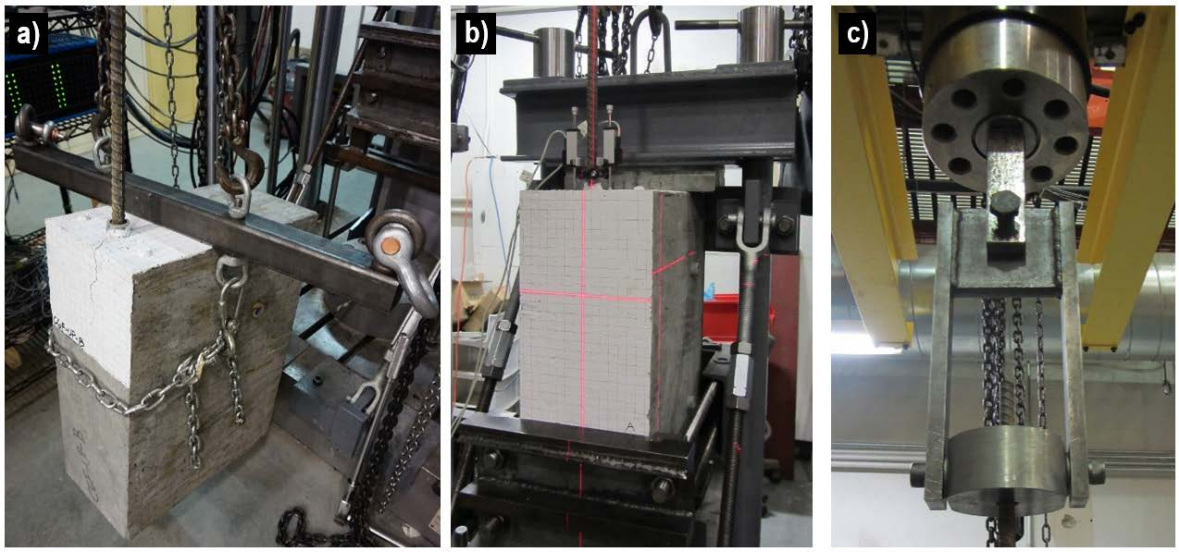

Figure A.5: a) Lifting device, b) leveling lasers, and c) pulling device

Special devices (refer to Figure A.6a) were built to hold two *TR series novotechnik* linear position sensors with return spring (refer to Figure A.6b) and were placed around the test bar at its loaded and un-loaded ends (refer to Figure A.2). Each position sensor was mounted on a c-shaped

aluminum piece which in turn was mounted on a hinged steel shaft collar. Threaded holes for two additional thumb screws (in addition to the existing one on the side used to close the collar) were made on opposite sides of the collar with respect to the plane of the hinge. Once the collar was closed around the test bar, the additional screws were tightened to hold the adapted collar securely in place during the entire test; one of the screw tips bore against the barrel of the bar and the other one wedged the test bar from the side. The used position sensors had linearity up to ±0.075 % and repeatability to ±0.002 mm (±7x10^{-5} in.) in accordance with the precision requirements of the ASTM A944-10 standard [17]. All sensors, and the 1500 kN load cell that was used, were connected to a 7000-128-SM Micro-Measurements data acquisition system.

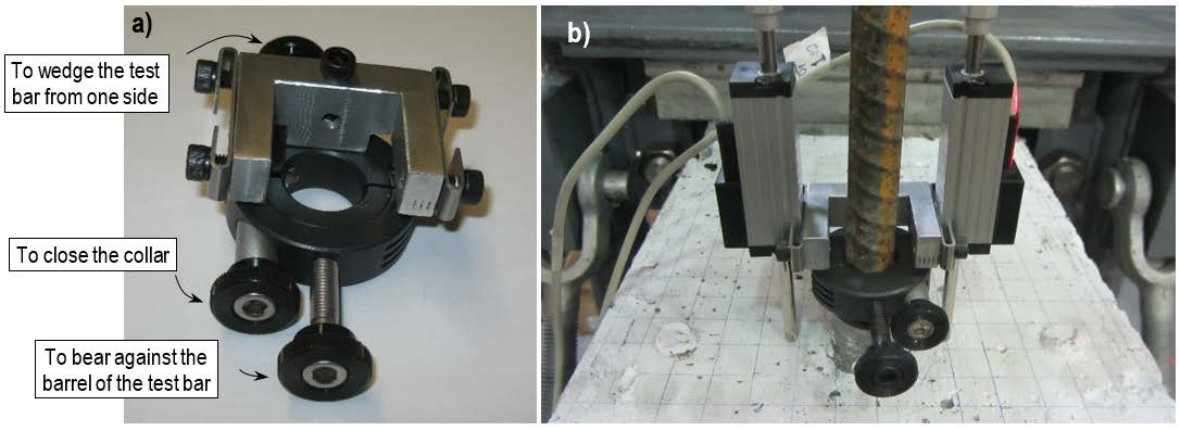

Figure A.6: a) Adapted collar, and b) the device placed around the test bar at the loaded end

A.6 Typical results and discussion

The results of three groups of specimens tested using the previously described set-up are presented in this section. Each group consisted of three identical specimens which have been identified by the size of the test bar (#16) and the *w/b* ratio of the concrete used (0.45, 0.48, and 0.55). All specimens had *lead lengths* of 12.5 mm (0.5 in.), *bonded lengths* of 100 mm (3.9 in.), concrete covers of 40 mm (1.6 in.) and test bars of 16 mm (0.6 in.) nominal diameter with a *relative rib* area of 0.080 (calculated in accordance with [45]). Additional information regarding the configuration of the specimens and the properties of the steel and the concrete can be found in Ref. [127]. The load-slip curves of group #16-0.45 are shown in Figure A.7 for the measurements taken at the loaded and at the un-loaded ends of the test bar (refer to Figure A.2).

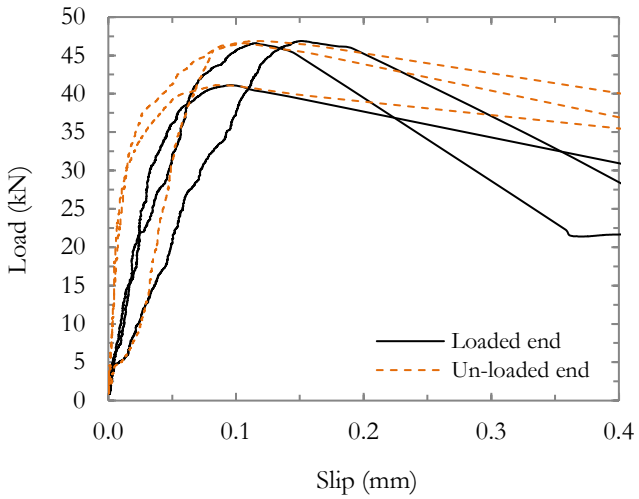

Figure A.7: *Load–slip* curves of group #16-0.45 of "beam-end" specimens

At the loaded end, the elastic deformations of the reinforcing bars have been subtracted from the slip measurements. Load-slip curves provide extremely valuable information as they express the bond behavior of the entire system, i.e., the concrete and the bar under study as well as their interface. The difference between the loaded and the un-loaded end curves represents the lengthening of the reinforcing bar for a given load [42]. Moreover, the un-loaded end curve provides a measure unit of the "stiffness" of the entire bonded region [39]. However, contrary to full-scale specimens, the curves are representative of the *local* bond behavior of the system and therefore they are not directly applicable to the design of reinforced concrete structures [17]; for such reasons the results are mostly used for comparison purposes. The most widely used parameter for comparison is the ultimate load. The ultimate load of the specimens of each group (labeled alphabetically) as well as their average (Avg.) and coefficient of variation (C.O.V.) are presented in Table A.1. The compressive strength (f_c), the splitting tensile strength (f_s) and the elastic modulus (E_c) of the concrete at the time of testing are also provided for each group of ASTM A944-10 "beam-end" specimens. As it can be seen, the C.O.V. within each group is lower than the usual value of 10 % that has been reported in the literature for this type of test [38, 39]. Thus, despite the fact that specimens tested using the traditional set-up configuration are not available, the results can be regarded as being adequate. Indeed, the results are not affected by testing the specimen vertically as their self-weight does not induce additional stresses on the test bar.

Table A.1: Ultimate load and concrete properties of the "beam-end" specimens

Group	Specimen	Ultimate load, kN	Avg., kN	C.O.V., %	f'_c, MPa	f_s, MPa	E_c, GPa
	A	41.2					
#16-0.45	B	46.9	44.9	7.1	57.7	3.9	33.3
	C	46.6					
	A	42.1					
#16-0.48	B	42.5	42.3	0.5	48.3	3.7	29.4
	C	42.3					
	A	34.1					
#16-0.55	B	33.9	33.8	0.9	34.7	2.5	25.4
	C	33.5					

Note: 1 kN = 225 lbf and 0.001 GPa = 1 MPa = 0.145 ksi

Another parameter that may be used for comparison is the load at a given value of slip. Many researchers have used a *critical slip* value of 0.05 mm (0.002 in.) when using "beam-end" specimens or other bond specimens of similar nature [38-40]. Load-slip curves have also served to develop *bond slip laws* and used as inputs in Finite Element models [37, 64] to predict the response of reinforced concrete members without the need to explicitly model the geometry of the reinforcing bars and account for the interface properties between steel and concrete. Such *bond slip laws* are inevitably linked to the bond specimen used for their development and therefore, special care is needed when choosing one. For example, *bond slip laws* developed using data gathered from "beam-end" tests would only be useful in situations where a relatively low confinement is provided by the concrete cover and *splitting* of the concrete governs the bond failure (e.g., the clear span of a flexural member).

In ASTM A944-10 "beam-end" specimens, two types of concrete *splitting* patterns may be encountered. At the front surface of the specimen (refer to Figure A.1) the crack may run down from the test bar and fan out to the sides of the specimen once it reaches the *compression reaction plate* or it may develop as two cracks running from the test bar to the sides of the specimen at approximately 120° between one another. These two different cracking patterns on the front surface may occur in specimens of the same group due to slightly different concrete's compressive strengths [60, 61, 127]. On the top surface, a common pattern usually involves a crack running parallel to the *bonded length* and then fanning out towards the sides of the specimen.

A proper characterization of the failure mode is of vital importance as it provides information about the reliability and validity of the tests. The *splitting* patterns of the ASTM A944 "beam-end" specimens belonging to group #16-0.48, and in accordance with the patterns described above, are presented in Figure A.8.

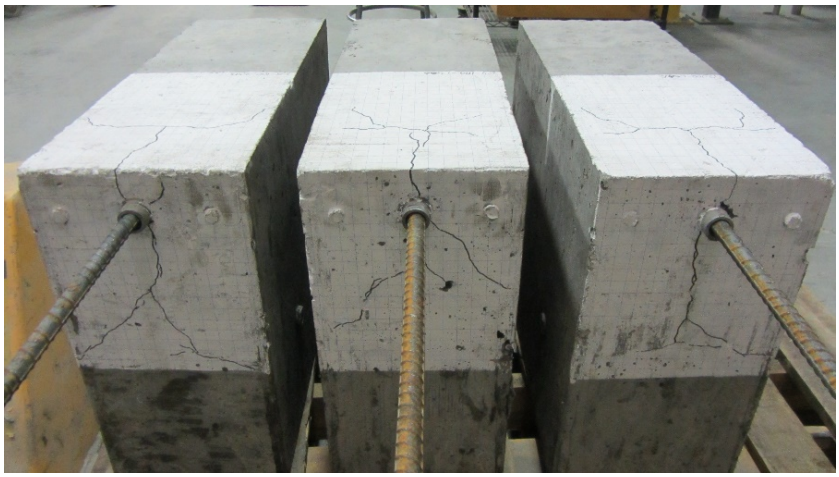

Figure A.8: Cracking patterns of group #16-0.48 of "beam-end" specimens

A.7 Conclusions

The configuration of a typical ASTM A944 "beam-end" specimen, its stress distribution and the way to interpret and possibly use the results of the test have been briefly explained in this technical note. It has been pointed out how many civil engineering laboratories currently possess (or have access to) rigid testing frames designed to apply the load vertically. For this reason, an alternate set-up apparatus to the one described in the ASTM A944-10 standard (in which the load is applied horizontally) was built over a 311 MTS high-force servo hydraulic rigid frame to avoid taking additional space in the laboratory and to minimize costs. Moreover, a special device was designed to attach the position sensors easily to the loaded and the un-loaded ends of the test bar. The results of three groups of ASTM A944-10 "beam-end" specimens having three replicas each resulted in coefficients of variation lower than 10% and similar cracking patterns to the ones reported in the literature demonstrating the adequacy of the alternative set-up apparatus presented.

A.8 Acknowledgments

The authors are grateful to the Concrete Infrastructure Research Center (CRIB) of Québec, the Natural Sciences and Engineering Research Council of Canada (NSERC), King Packaged Materials and Co., the Canadian Council of Independent Laboratories (CCIL), The American Shotcrete Association (ASA), and the Québec and East Ontario Chapter of the American Concrete Institute (ACI) for their financial support. Furthermore, special thanks are extended to Jean-Daniel Lemay and Mathieu Thomassin-Mailhot (research engineers) and to Pierre-André Tremblay and Alain Melançon (laboratory technicians) of the Department of Civil and Water Engineering at Université Laval for their outstanding work and support during casting and testing operations.

A.9 References

[5] ACI Committee 318, "318-19 Building code requirements for structural concrete and commentary," American Concrete Institute, Michigan, 2019, 559 p.

[6] CSA, "A23.3-19 Design of concrete structures," Canadian Standards Association, Ontario, 2019, 297 p.

[17] ASTM, "A944-10(2015) standard test method for comparing bond strength of steel reinforcing bars to concrete using beam-end specimens," American Society of Testing and Materials, 2015, 4 p. https://doi.org/10.1520/A0944-10R15

[37] FIB, "Bond of reinforcement in concrete – Bulletin No. 10," The International Federation of Structural Concrete, 2000, 434 p.

[38] Johnston, D. W., Zia, P., "Bond characteristics of epoxy-coated reinforcing bars," North Carolina State University, 1982, 163 p.

[39] Choi, C. O., Darwin, D., McCabe, S. L., "Bond strength of epoxy-coated reinforcement to concrete", University of Kansas, 1990, 217 p.

[40] Treece, R. A., Jirsa, J. O., "Bond strength of epoxy-coated reinforcing bars," ACI Materials Journal, Vol. 86, No. 2, 1989, pp. 167-174.

[42] ACI Committee 408, "408R-03 Bond and development of straight reinforcing bars in tension," American Concrete Institute, Michigan, 2003, 49 p.

[43] Darwin, D., Graham, E. K., "Effect of deformation height and spacing on bond strength of reinforcing bars," ACI Structural Journal, Vol. 90, No. 6, 1993, pp. 646-657, http://dx.doi.org/10.14359/4459

[45] Fei, J., Darwin, D., "Fatigue of high relative rib area of reinforcing bars," University of Kansas Center for Research, Kansas, 1999, 76 p.

[60] Brettmann, B. B., Darwin, D., Donahey, R. C., "Bond of reinforcement to superplasticized concrete," Journal of the American Concrete Institute, Vol. 83, No. 1, 1986, pp. 98-107. https://doi.org/10.14359/1743

[61] Brettmann, B. B., Darwin, D., Donahey, R. C., "Effects of superplasticizers on concrete-steel bond strength," University of Kansas Center for Research, Kansas, 1984, 32 p.

[64] Cox, J. V., Herrmann, L. R., "Development of a plasticity bond model for steel reinforcement," Mechanics of cohesive-frictional materials, Vol. 3, No. 2, 1998, pp. 155-180.

[127] Basso Trujillo, P., Jolin, M., Massicotte, B., Bissonnette, B., "Bond strength of reinforcing bars with varying encapsulation qualities," ACI Structural Journal, Vol. 115, No. 6, 2018, pp. 1707-1717.

A.10 Appendix

Table A.2: Dimensions of the major components of the alternative set-up apparatus

Component	Subcomponent	Property or designation	Value, mm
Steel box (welded plates)	N/A	Height	600
		Depth	400
		Width	380
		Thickness	25
Steel plate (with 4 alignment bolts)	N/A	Depth	400
		Width	310
		Thickness	25
Back support for the back alignment plate	C section[a] (along the X axis)	MC150 x 22.5[c]	-
	C section (along the Y axis)	C200 x 17.0	-
Alignment plate	C section	C200 x 21.0	-
Tie-down plate	C section[b]	C200 x 21.0	-
Horizontal threaded rods (4)	N/A	Diameter	25
Compression reaction plate	C sections (2)	MC150 x 22.5	-
	Steel plates (2)	Depth	200
		Width	600
		Thickness	25
Columns	N/A	Diameter	65
Lateral braces	N/A	Diameter	25
Rubber sheet	N/A	Thickness	2
Thick Steel block	N/A	Depth	150
		Width	250
		Thickness	100

Table A.2 (continued): Dimensions of the major components of the alternative set-up apparatus

Pulling device	Vertical shafts	Depth	50
		Width	20
	Linking plate	Thickness	25
	Thick cylinder	Diameter	150
		Thickness	65

Note: 1 mm = 0.039 in.
a Reinforcing shaft of 75 by 50 mm cross section on top of the C section
b One reinforcing shaft of 80 by 30 mm cross section on bottom and two of 50 by 30 mm on the middle and top of the C section; the extra 30 mm on the bottom served as the support for the "beam-end" specimen.
c Units are expressed in kg/m; 1 kg/m = 0.672 lb./ft

Appendix B Comparison between the ACI 318-19 and CSA A23.3-19 equations for ℓ_d

The CSA A23.3-19 *development length* equation (Equation 12.1 in [6]) is:

$$\ell_d = 1.15 \frac{k_1 k_2 k_3 k_4}{(d_{cs}+K_{tr})} \frac{f_y}{\sqrt{f'_c}} A_b \tag{B.1}$$

Where:

$K_{tr} = A_{tr} f_{yt} / 10.5sn$

$(d_{cs} + K_{tr}) \leq 2.5d_b$

By substituting the transverse section of the reinforcing bar (A_b) with $\pi d_b^2/4$, Equation B.1 becomes Equation B.2.

$$\ell_d = \frac{1.15\pi}{4} \frac{k_1 k_2 k_3 k_4}{(d_{cs}+K_{tr})} \frac{f_y}{\sqrt{f'_c}} d_b^2 \approx 0.9 \frac{k_1 k_2 k_3 k_4}{(d_{cs}+K_{tr})} \frac{f_y}{\sqrt{f'_c}} d_b^2 \tag{B.2}$$

If the term 0.9 in Equation B.2 is put as a denominator, it would take the form of 1/1.1 as shown in Equation B.3.

$$\ell_d = \frac{1}{1.1} \frac{k_1 k_2 k_3 k_4}{(d_{cs}+K_{tr})} \frac{f_y}{\sqrt{f'_c}} d_b^2 \tag{B.3}$$

The same can be done for the lightweight concrete factor k_3 if its value is computed inversely; the 1.3 value for low-density concrete in the CSA A23.3-19 code would be approximately equal to the recommended 1 / 1.3 ≈ 0.75 value in the ACI 318-19 code. Thus, the equation can be rewritten as expressed in Equation B.4.

$$\ell_d = \frac{1}{1.1k_3} \frac{k_1 k_2 k_4}{(d_{cs}+K_{tr})} \frac{f_y}{\sqrt{f'_c}} d_b^2 \tag{B.4}$$

Then, rearranging the values expressed in Equation B.4, Equation B.5 is obtained.

$$\ell_d = \frac{f_y}{1.1k_3\sqrt{f'_c}} \frac{k_1 k_2 k_4}{(d_{cs}+K_{tr})} d_b^{\,2} \tag{B.5}$$

Moreover, the square of the reinforcing bar diameter can be rearranged as expressed in Equation B.6 which is essentially the same one appearing in the ACI 318-19 code (Equation 24.4.2.3 in [5]), differing only due to nomenclature.

$$\ell_d = \frac{f_y}{1.1k_3\sqrt{f'_c}} \frac{k_1 k_2 k_4}{\left(\frac{d_{cs}+K_{tr}}{d_b}\right)} d_b \tag{B.6}$$

As for the confining factor K_{tr}, if the yielding stress of the transverse reinforcement in the CSA A23.3-19 equation is replaced by 420 MPa (Grade 60 bars), the term becomes $K_{tr} = 40A_{tr}/sn$ as the one appearing in the ACI 318-19 design code.

The only difference resides now on the fact that the modification factor Ψ_g, which accounts for the grade of the reinforcing bar, has been added to the ACI 318-19 version of the code. This modification factor did not appear in the ACI 318-14 version and is not accounted for in the Canadian A23.3-19 version of the code.

Appendix C Creation of *artificial voids*

Artificial voids consisted of hardened silicone tubes cut in halves and glued over the bonded region of the test bars with the same materials. A silicone gasket maker was used for this purpose. Firstly, the silicone was inserted into hollow plastic tubes as those shown in Figure C.1 and was let to cure for approximately 2 to 3 weeks. The plastic tubes had 4.8, 9.5 and 15.9 mm of nominal inner diameter for the 15M (No. 16) bars and 6.4, 12.7 and 19.1 mm of nominal inner diameter for the 20m (No. 19) test bars. Once the silicone had completely hardened, the tubes were cut longitudinally with a cutter knife to extract the silicone tubes.

Figure C.1: Material needed to create *artificial voids*

The extracted silicone tubes were also cut longitudinally to obtain two halves of equal size to be used as *artificial voids*. Each half was then glued over the entire bonded length of the bond specimens' test bar using the same silicone as seen in Figure C.2a. Before this was done, the exact size of the insert was outlined over the bonded length using masking tape to ensure no silicone was deposited elsewhere over the surface of the reinforcing bar. The masking tape was removed using the cutter knife once the *artificial* voids were securely glued in place as seen in Figure C.2b.

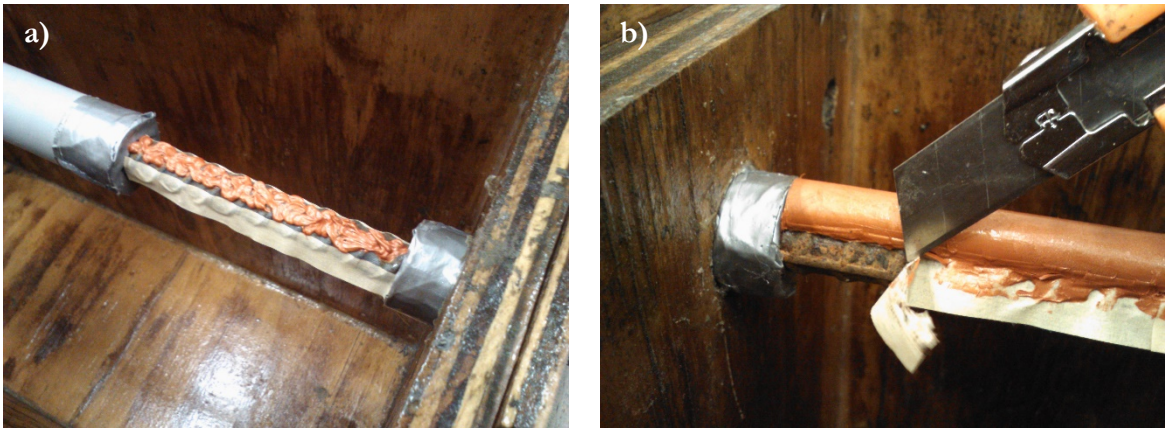

Figure C.2: *Artificial voids* being secured over the bonded length of a test bar

The manufacturer's technical sheet specifies that the hardened silicone has a tensile strength of about 1.5 MPa with an elongation of 350% of its initial length after 7 days at 25°C and 50% humidity. Based on this information, the modulus of elasticity of the material can be approximated as $E_{a.v.} = \sigma_t / (\Delta L/L) = 1.5$ MPa $/ 2.5 = 0.6$ MPa and thus, its resistance can be completely neglected.

Appendix D Water to binder ratio of in-place shotcrete

The water content (w) of a sample of shotcrete was computed as shown in Figure D.1 where the main components of the equation are described. Because the mixing time is considerably short in the *dry-mix* process (0.05 to 0.5 seconds of actual mixing [18]) and the aggregates do not absorb all of the mixing water, a (subjective) coefficient (C_{ag}) equal to 0.5 was applied to the absorption coefficient of the total weight of fine and coarse aggregates (a_{ag}) whose value was weighted based on their proportion in the mixture; 0.6 and 0.4 for the coefficient of the fine and the coarse aggregates respectively. Moreover, a sieve analysis showed that the particles passing the No. 200 sieve (PS_{200}) represented 0.87% of the pre-bagged mixture.

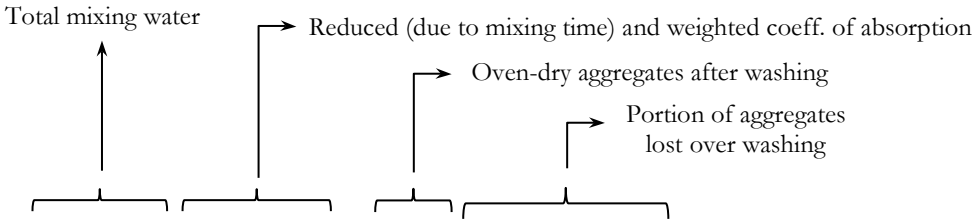

$$w = \frac{w_{c1} - w_{dry\ c1}}{w_{c1}} - C_{ag} \cdot {}^{a_{ag}}/_{100} \cdot \left[\left(w_{dry\ ag} - \frac{{}^{PS_{200}}/_{100} \cdot w_{dry\ ag}}{{}^{PS_{200}}/_{100} - 1} \right) / w_{c1} \right]$$

Figure D.1: Expression to calculate the water content of in-place shotcrete

For the binder, as shown in Figure D.2, the calculation assumes it is composed of particles finer than 75 μm and determines its weight when the sample is washed over a No. 200 sieve [95].

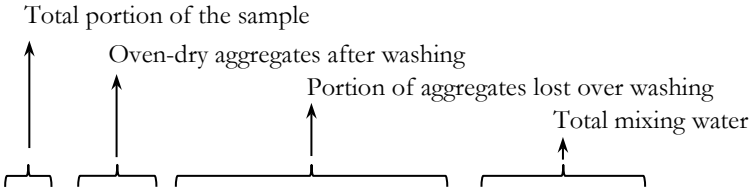

$$b = 1 - \left[w_{dry\ ag} - \frac{{}^{PS_{200}}/_{100} \cdot w_{dry\ ag}}{{}^{PS_{200}}/_{100} - 1} / w_{c2} \right] - \frac{w_{c1} - w_{dry\ c1}}{w_{c1}}$$

Figure D.2: Expression to calculate the binder content of in-place shotcrete

The remaining notation used in Figures D.1 and D.2 is detailed as follows:

$w_{c1,c2}$ = Weight of the fresh concrete sample 1 or 2

$w_{dry\ c1}$ = Weight of the sample after several cycles of drying in the microwave

$w_{dry\ ag}$ = Weight of the sample after 48 hours of drying in the oven

Appendix E Linear position sensors

The TR-0025 Novotechnik position transducer with return spring that was used in this experimental phase of this research is shown in Figure E.1

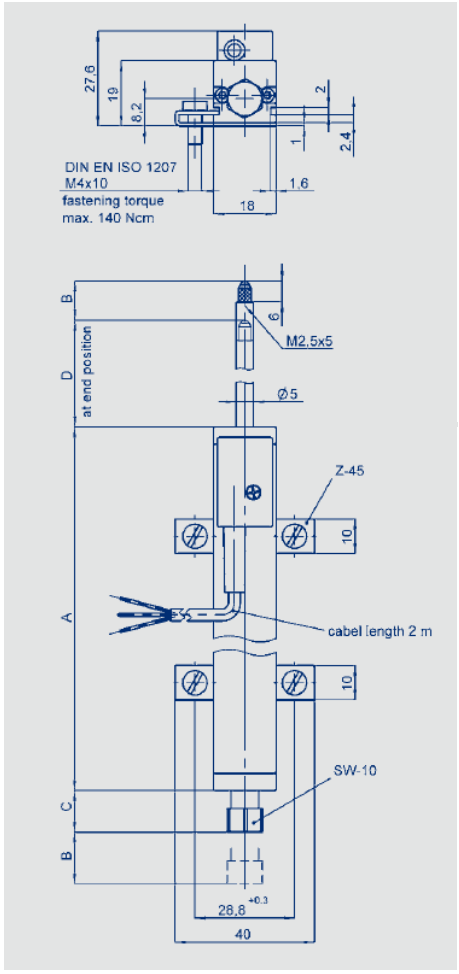

Type designations	TR-0025 TRS-0025
Electrical Data	
Defined eletrical range	25
Electrical stroke	27
Nominal resistance	
Resistance tolerance	
Independent linearity	0.2
Repeatability	
Recommended operating wiper current	
Maximum wiper current in case of malfunction	
Maximum permissible applied voltage	42
Effective temperature coefficient of the output-to-applied voltage ratio	
Insulation resistance (500 VDC)	
Dielectric strength (500 VAC, 50 Hz)	
Mechanical Data	
Body length (dimension A)	63
Mechanical stroke(dimension B)	55
Dimension C (TR series)	12
Dimension D (TR series)	32
Weight with cable with plug	 120 74
Weight of shaft with coupling	25
Operating force extended (horizontal) Operating force retracted (horizontal)	≤ 2.5 ≤ 5.0
Operating force to end stop	
Operating frequency (maximum) (in critical applications, mount probe tip upwards)	18
Maximum permitted torque for mounting screws (with washer)	

Figure E.1: Position transducer used in the experimental phase

Appendix F Additional data of Chapter 3

F.1 Section 3.4.7 of Chapter 3

The concrete properties of each group of "pull-out" specimens in which concrete was poured is shown in Table F.1.

Table F.1: Properties of cast in-place groups

Family	***u.p.***	**Air (%)**	**Slump (mm)**	***w/b***	**$f_{c\,21d}$ (MPa)**	**B.W.A. (%)**	**P. V. (%)**
CIP	0						
CIP-h	9	5.0	157	0.45	48.9	6.3	14.0
CIP-h	18						
CIP-h	30	4.5	190	0.45	49.1	6.9	15.4
CIP-2xh	9						
CIP-2xh	18	4.5	195	0.45	49.8	7.1	15.8
CIP-2xh	30						
Mean		4.7	180	0.45	49.3	6.8	15.1
S. D.		0.3	20.6	0.0	0.5	0.4	0.9
C.O.V.		6.2	11.4	0.0	1.0	6.2	6.3

F.2 Section 3.5.1 of Chapter 3

The precise measurements of the *un-bonded* perimeter taken at the bottom of the "pull-out" specimens is shown in Table F.2.

Table F.2: Measurements of the *u.p.* in "pull-out" specimens

Specimen I.D.	Comments*	*Un-bonded* perimeter (*u.p.*)					
		Cut A	Cut B	Cut C	Cut D	Cut E	Average
S-N1-L (A)	V.	28	25	23	20	19	23
S-N2-L (B)	V.	39	39	37	32	21	34
S-N1-M (A)	V.	30	30	27	27	22	27
S-N2-L (A)	V.	48	47	29	22	18	33
S-N1-M (B)	V.	31	31	25	9	8	21
S-N2-L (C)	V.	41	38	35	33	32	36
S-N1-L (B)	V.	44	33	33	29	19	32
CIP-h (A)	10 % *u.p.*	9	-	-	-	-	9
CIP-h (B)		8	-	-	-	-	
CIP-2xh (A)		9	-	-	-	-	
CIP-2xh (B)		10	-	-	-	-	
CIP-h (A)	20 % *u.p.*	15	-	-	-	-	18
CIP-h (B)		19	-	-	-	-	
CIP-2xh (A)		18	-	-	-	-	
CIP-2xh (B)		21	-	-	-	-	
CIP-h (A)	30 % *u.p.*	31	-	-	-	-	30
CIP-h (B)		33	-	-	-	-	
CIP-2xh (A)		27	-	-	-	-	
CIP-2xh (B)		28	-	-	-	-	

*V.: Voids

F.3 Section 3.5.2 of Chapter 3

The results observed in section 3.5.2 have been obtained from the ANOVA shown in Table F.3.

Table F.3: Analysis of variance for the *consistency* families

Parameter	S. of variation	Sum of squares	df	MSE	F_0	*p-value*	$F_{0.05}$
$P_{0.25}$	Between treatments	501.0	5	100.2	5.90	0.011	3.48
	Error	152.8	9	17.0			
	Total	653.8	14	46.7			
P_{max}	Between treatments	1,647.1	5	329.4	25.28	0.000	3.48
	Error	117.3	9	13.0			
	Total	1,764.3	14	126.0			
K_{su}	Between treatments	11,570.0	5	2,315.4	4.34	0.027	3.48
	Error	4,796.4	9	532.9			
	Total	16,373.5	14	1,169.5			

Verifications need nevertheless to be computed to guarantee the following assumptions while using such statistical test:

1. The variances between the populations under comparison are equal and;
2. That the errors and observations are normally and independently distributed.

The equality of the population variances assumption was verified using the Modified Levene Test in which the hypothesis expressed in Equation F.1 are tested:

$$H_0: \sigma_1^2 = \sigma_2^2 = \ldots = \sigma_n^2 \text{ for n families}$$

$$\text{vs.} \qquad \text{(F.1)}$$

$$H_a: \sigma_i^2 \neq \sigma_j^2 \text{ for at least one pair (i, j)}$$

The absolute deviations of each treatment's observations (y_{ij}) from their median ($\overline{y}_i$), as expressed in Equation F.2, are presented in Table F.4 and the ANOVA testing the equality of these deviations is presented in Table F.5.

$$d_{ij} = \left| y_{ij} - \overline{y}_i \right| \quad \begin{cases} i = 1, 2, \ldots, n \\ j = 1, 2, \ldots, a_i \end{cases} \tag{F.2}$$

Table F.4: Deviations for the Modified Levene Test

Parameter	S-N2-H	S-N2-M	S-N1-H	S-N1-M	S-N1-L	S-N2-L
	6.0	10.3	0.7	2.1	3.5	1.0
$P_{0.25}$	0.3	2.7	0.7	2.1	3.5	0.3
	0.0	0.0	-	-	-	0.0
	0.4	8.3	0.4	1.3	2.8	0.0
P_{max}	2.0	4.8	0.4	1.3	2.8	2.6
	0.0	0.0	-	-	-	1.3
	0.0	22.9	8.9	4.4	3.9	0.0
K_{su}	24.2	63.0	8.9	4.4	3.9	8.9
	6.9	0.0	-	-	-	3.7

The results indicate that the variances of the treatments within each parameter are equal for any important level of significance considered herein (*p-value* ≤ 0.05).

Table F.5: Modified Levene test for the *consistency* families

Parameter	S. of variation	Sum of squares	df	MSE	F_0	*p-value*	$F_{0.05}$
$P_{0.25}$	Between treatments	30.7	5	6.1	0.69	0.643	3.48
	Error	80.0	9	8.9			
	Total	110.6	14	7.9			
P_{max}	Between treatments	29.7	5	5.9	1.33	0.332	3.48
	Error	40.0	9	4.4			
	Total	69.7	14	5.0			
K_{su}	Between treatments	1,267.5	5	253.5	0.96	0.491	3.48
	Error	2,383.3	9	264.8			
	Total	3,650.8	14	260.8			

The population's normality assumption was verified by visually inspecting the normal probability plot of the residuals as shown in Figure F.1a), b) and c) for each parameter under study; it can be observed that this assumption is not seriously violated. Moreover, the independence assumption is not violated since the results do not depend on time or on the sequence of concrete projection (each specimen was sprayed and tested in a controlled environment).

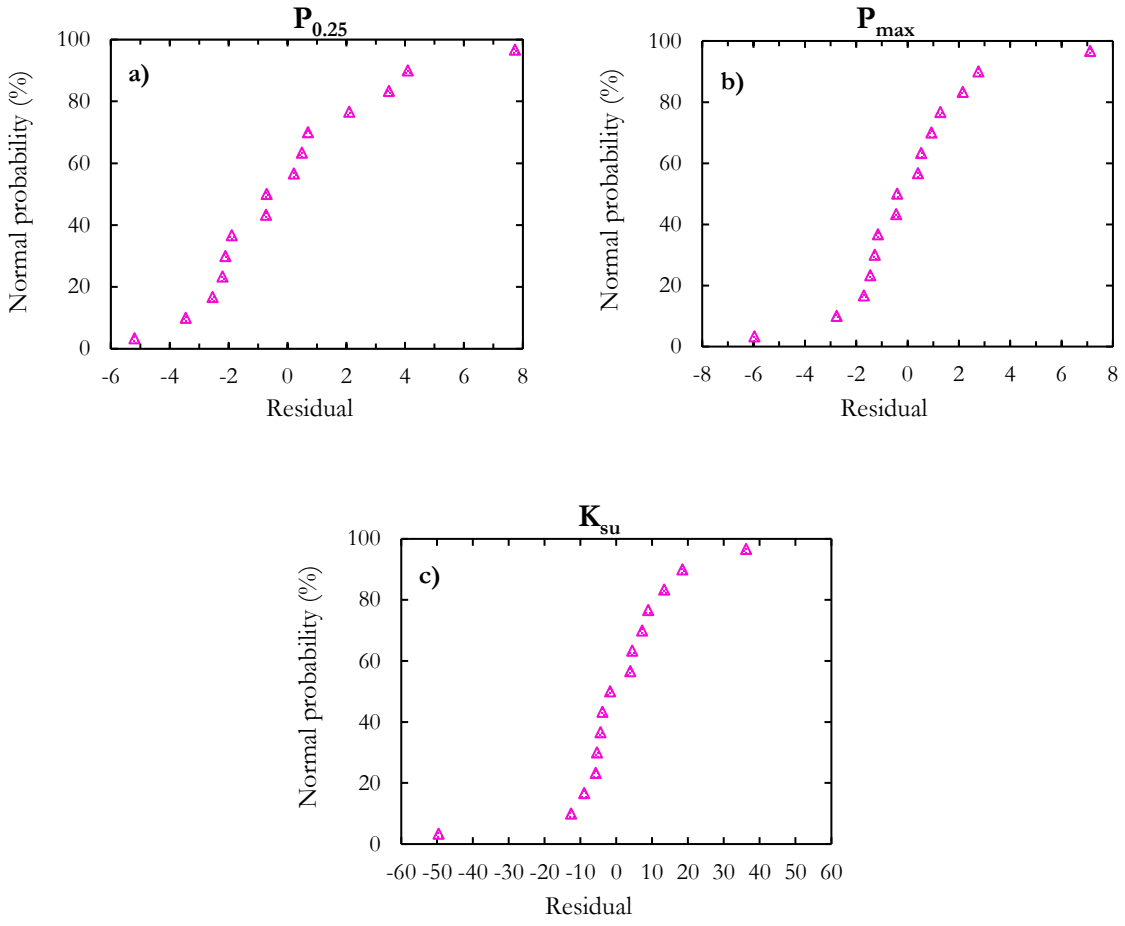

Figure F.1: Normal probability plot for the residuals

Lastly, no outliers were detected since the largest standardized residual ($d_{ij} = \frac{e_{ij}}{\sqrt{MSE}}$) for the $P_{0.25}$, P_{max} and K_{su} were 1.9, 1.7 and 2.1 respectively and therefore did not surpass the 3.0 limit normally defined in the literature as the threshold for this purpose.

F.4 Section 3.5.4 of Chapter 3

The model comparison test is a special type of hypothesis testing procedure designed to test the equality between the intercept (β_{0i}) and the slope (β_i) of linear regression models. In this case, the F-statistic is calculated as the ratio between the *residual* sum of squares of a "combined" model (which uses the overall data) and the *pooled* sum of squares of each individual model with their respective degrees of freedom. When applying the test, it is assumed that: 1) a linear regression model is adequate and 2) that the intercept and the slope are significant. Thus, once the test is performed, these assumptions need to be verified. For the models compared, the F-statistic is computed as expressed in Equation F.3 where the values were obtained from ANOVA tests performed on the "combined" and the individual models as shown in Table F.6.

$$F_{0(2,12)} = \frac{SSH_0 \ / \ df(SSH_0)}{SSRES(Pooled) \ / \ df(SSRES(Pooled))} = \frac{(205.3 - 101.1 - 74.4) \ / \ (14 - 6 - 6)}{(101.1 + 74.4) \ / \ (6 + 6)} = 1.02 \qquad (F.3)$$

Table F.6: Analysis of variance for the linear regression models

Model	S. of variation	Sum of squares	df	MSE	F_0	*p-value*	R^2_{adj}
CIP & CIP-h	Between treatments	1550.3	1	1550.3	91.98	< 0.000	0.929
	Error	101.1	6	16.9			
	Lack of fit	41.0	2	20.5	1.37	0.353	
	Pure error	60.1	4	15.0			
	Total	1651.4	7	235.9			
CIP & CIP-h	Between treatments	1311.7	1	1311.7	105.78	< 0.000	0.937
	Error	74.4	6	12.4			
	Lack of fit	33.6	2	16.8	1.65	0.301	
	Pure error	40.8	4	10.2			
	Total	1386.1	7	198.0			
Combined	Between treatments	2857.0	1	2857.0	194.86	< 0.000	0.928
	Error	205.3	14	14.7			
	Lack of fit	27.8	2	13.9	0.94	0.418	
	Pure error	177.5	12	14.8			
	Total	3062.2	15	204.2			

Based on these results, it can be observed that each individual model is adequate and their coefficients are significant.

Appendix G Additional data of Chapter 4

G.1 Section 4.6.1 of Chapter 4

The results observed in section 4.6.1 have been obtained from the ANOVA shown in Table G.1.

Table G.1: Analysis of Variance of the polynomial regression model

Model	S. of variation	Sum of squares	df	MSE	F_0	*p-value*	R^2_{adj}
#16-0.45 T + #19-0.45 T	Between treatments	7097.5	2	3548.8	28.89	< 0.000	0.736
	Error	2211.0	18	122.8			
	Lack of fit	0.4	1	0.4	0.00	1.000	
	Pure error	2210.6	17	130.0			
	Total	9308.6	20	465.4			

As explained in Appendix F, the assumptions of equal variance between populations and the normality and independence of errors and observations have not been seriously violated in this section or any other section of the chapter.

G.2 Section 4.6.4 of Chapter 4

The bleeding capacity of the two *w/b* ratio mixtures studied in Chapter 4 has been presented for the tallest container only (h=43 cm) because that was the approximate amount of concrete beneath the reinforcing bars in the ASTM A944-10 "beam-end" specimens. The bleeding capacity of all containers used to measure the average bleeding rate is shown in Figure G.1.

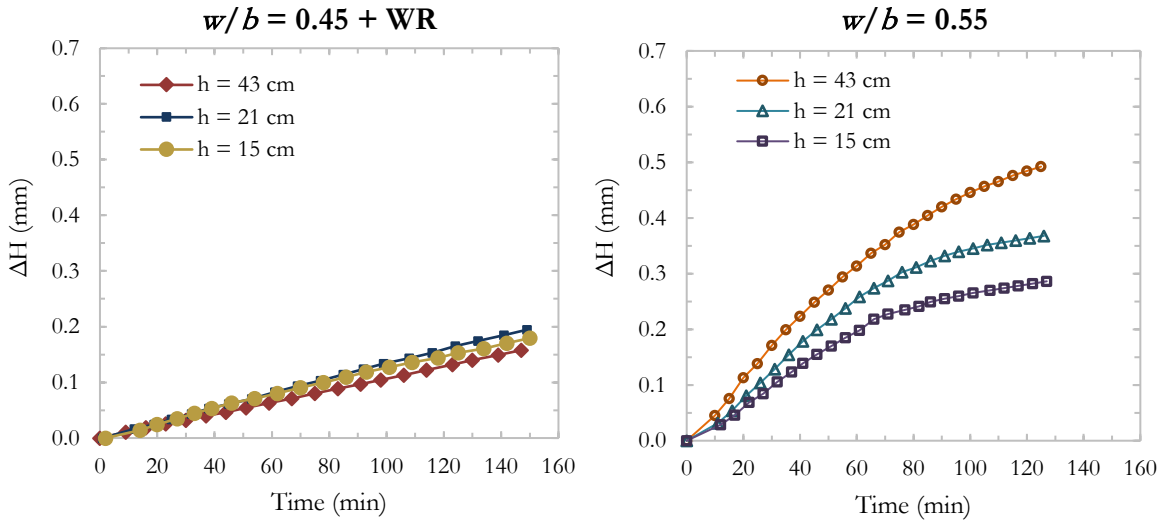

Figure G.1: Individual bleeding capacity of concrete mixtures

G.3 Section 4.6.5 of Chapter 4

The individual failure mode of each specimen presented in Chapter 4 is presented in Table G.2.

Table G.2: Individual failure mode of specimens

Family	*Nominal u.p.* (%)	Failure[§]		
		A	B	C
#16-0.45	0	S-Y	S-T	S-T
#16-0.45 T	10	S-Y	S-Y	S-Y
	20	S-T	S-Y	S-Y
	30	S-Y	S→P	S-Y
#16-0.45 B	20	S-Y	S-T	S-Y
	30	S-T	S-Y	S-Y
#19-0.45	0	S-T	S-T	S-Y
#19-0.45 T	20	S-T	S-T	S-Y
	30	S-Y	S-T	S-Y
#19-0.45 B	20	S-T	S-Y	S-T
	30	S-T	S-Y	S-Y
#16-0.55	0	S-T	S-Y	S-T

[§] S: Early *splitting failure*; S-Y: Y-shape *splitting* failure; S-T: T-shape *splitting* failure; P: *Pull-out* failure

Appendix H Additional data of Chapter 6

H.1 Section 6.6.3 of Chapter 6

The experimental and Finite Element results used for the development of the *bar stress ratios* are presented in Table H.1.

Table H.1: Bar strength/stress at bond failure of each bond specimen

Research article	Type of specimen	Specimen I.D.	Bonded length	*Un-bonded* perimeter (*u.p.*)	Comments on the *u.p.*	P_{max}, kN	f_{smax}, MPa
Ref. 121	Laboratory "pull-out" (24 specimens)	S-N2-M (A)	$2.5d_b$	0 % *u.p.*	0	52.6	-
		S-N2-M (B)			0	44.3	-
		S-N2-M (C)			0	39.5	-
		S-N1-L (A)		Voids	23*	23.3	-
		S-N2-L (B)			34*	22.9	-
		S-N1-M (A)			27*	22.2	-
		S-N2-L (A)			33*	20.3	-
		S-N1-M (B)			21*	19.7	-
		S-N2-L (C)			36*	19.0	-
		S-N1-L (B)			32*	17.8	-
		CIP (A)		No voids	0	50.8	-
		CIP (B)			0	57.0	-
		CIP-h (A)		10 % *u.p.*	9	47.1	-
		CIP-h (B)			8	43.8	-
		CIP-2xh (A)			9	34.9	-
		CIP-2xh (B)			10	41.3	-
		CIP-h (A)		20 % *u.p.*	15	35.2	-
		CIP-h (B)			19	37.1	-
		CIP-2xh (A)			18	31.5	-
		CIP-2xh (B)			21	32.0	-
		CIP-h (A)		30 % *u.p.*	31	11.9	-
		CIP-h (B)			33	20.1	-
		CIP-2xh (A)			27	18.5	-
		CIP-2xh (B)			28	17.1	-

Table H.1 (continued): Bar strength/stress at bond failure of each bond specimen

Ref. 127	Laboratory "Beam-end"† (21 specimens)	No. 16-0.45 (A)	6.3d_b	0 % *u.p.*	-	-	207.5
		No. 16-0.45 (B)			-	-	236.2
		No. 16-0.45 (C)			-	-	234.7
		No. 19-0.45 (A)			-	-	214.6
		No. 19-0.45 (B)			-	-	235.9
		No. 19-0.45 (C)			-	-	226.6
		No. 16-0.45 T (A)		10 % *u.p.*	-	-	220.9
		No. 16-0.45 T (B)			-	-	237.9
		No. 16-0.45 T (C)			-	-	229.9
		No. 16-0.45 T (A)		20 % *u.p.*	-	-	229.9
		No. 16-0.45 T (B)			-	-	225.6
		No. 16-0.45 T (C)			-	-	206.0
		No. 19-0.45 T (A)			-	-	226.2
		No. 19-0.45 T (B)			-	-	205.6
		No. 19-0.45 T (C)			-	-	195.8
		No. 16-0.45 T (A)		30 % *u.p.*	-	-	189.9
		No. 16-0.45 T (B)			-	-	174.8
		No. 16-0.45 T (C)			-	-	190.2
		No. 19-0.45 T (A)			-	-	176.3
		No. 19-0.45 T (B)			-	-	191.3
		No. 19-0.45 T (C)			-	-	176.8
Ref. 146	F. E. "Beam-end"§ (15 specimens)	2.5cb-0up-1.0VL	6.3d_b	0 % *u.p.*	-	-	201.4
		2.5cb-20up-1.0VL		20 % *u.p.*	-	-	219.0
		2.5cb-30up-1.0VL		30 % *u.p.*	-	-	192.6
		2.5cb-0up-1.0VL	12.5d_b	0 % *u.p.*	-	-	297.1
		2.5cb-20up-1.0VL		20 % *u.p.*	-	-	289.4
		2.5cb-30up-1.0VL		30 % *u.p.*	-	-	292.9
		2.5cb-40up-1.0VL		40 % *u.p.*	-	-	213.8
		5.0cb-0up-1.0VL		0 % *u.p.*	-	-	335.3
		5.0cb-20up-1.0VL		20 % *u.p.*	-	-	322.7
		5.0cb-30up-1.0VL		30 % *u.p.*	-	-	231.4
		5.0cb-40up-1.0VL		40 % *u.p.*	-	-	102.7
		2.5cb-30up-0.5VL		30 % *u.p.*	-	-	303.1
		2.5cb-40up-0.5VL		40 % *u.p.*	-	-	299.6
		5.0cb-30up-0.5VL		30 % *u.p.*	-	-	327.8
		5.0cb-40up-0.5VL		40 % *u.p.*	-	-	286.1

*Average of 5 locations

†The actual size of *un-bonded* perimeters could not be verified and the value represents a nominal one

§The *un-bonded* perimeter represents the exact value as modeled

The data of the linear *fuzzy* model, $\tilde{Y} = (A_0, \alpha_0) \oplus (A_1, \alpha_1) \otimes \tilde{X}_1$, presented in Section 6.6.3 is shown in Table H.2.

Table H.2: *Fuzzy* linear regression by Hong et al., 1999

Sample i	$\widetilde{u.p}_{.i1} = (x_i, \gamma_i)$	$\tilde{P}_i = (y_i, e_i)$
1	(0.0, 0.0)	(50.8, 1.0)
2	(0.0, 0.0)	(57.0, 1.1)
3	(8.9, 1.3)	(43.8, 0.9)
4	(8.9, 2.7)	(47.1, 0.9)
5	(18.1, 9.9)	(35.2, 0.7)
6	(18.1, 9.0)	(37.1, 0.7)
7	(29.6, 12.0)	(11.9, 0.2)
8	(29.6, 17.1)	(20.1, 0.4)
9	(8.9, 1.4)	(34.9, 0.7)
10	(8.9, 1.6)	(41.3, 0.8)
11	(18.1, 6.0)	(31.5, 0.6)
12	(18.1, 9.7)	(32.0, 0.6)
13	(29.6, 8.3)	(17.1, 0.3)
14	(29.6, 7.2)	(18.5, 0.4)

The solution of the linear problem using the data presented in Table H.2 is as follows:

Minimize $J(A,\alpha) = \max(\alpha_0,|A_1|*0.0, 0.0*\alpha_1) + \ldots + \max(\alpha_0,|A_1|*7.2, 29.6*\alpha_1)$

Subject to:

$|50.8 - (A_0 + A_1*0.0)| \leq |1 - 0.6|\max(\alpha_0,|A_1|*0.0, 0.0*\alpha_1) - |1 - 0.6|*1.0$

$\vdots$

$|18.5 - (A_0 + A_1*27.6)| \leq |1 - 0.6|\max(\alpha_0, |A_1|*8.3, 27.6*\alpha_1) - |1 - 0.6|*0.4$

Where :

α_0 and $\alpha_2 \geq 0$ for i = 1, 2, …, 14 and j = 0, 1

Resulting in:

$\tilde{Y} = (51.0, 16.2) \oplus (-1.11, 0.0) \otimes \tilde{X}_1$

H.2 Section 6.6.5 of Chapter 6

The data of the polynomial *fuzzy* model, $\widetilde{Y} = (A_0, \alpha_0) \oplus (A_1, \alpha_1) \otimes \widetilde{X}_1 \oplus (A_2, \alpha_2) \otimes \widetilde{X}_1 \otimes \widetilde{X}_1$, presented in Section 6.6.5 is shown in Table H.3.

Table H.3: *Fuzzy* polynomial regression by Hong et al., 2001

Sample i	$\widetilde{u.p}_{.i1} = (u.p_i, \gamma_i)$	$\widetilde{P}_i = (P_i, e_i)$
1	(0.0, 0.0)	(207.5, 4.1)
2	(0.0, 0.0)	(236.2, 4.7)
3	(0.0, 0.0)	(234.7, 4.7)
4	(0.0, 0.0)	(214.6, 4.3)
5	(0.0, 0.0)	(235.9, 4.7)
6	(0.0, 0.0)	(226.6, 4.5)
7	(10.0, 3.1)	(220.9, 4.4)
8	(10.0, 2.6)	(237.9, 4.8)
9	(10.0, 5.6)	(229.9, 4.6)
10	(20.0, 9.0)	(229.9, 4.6)
11	(20.0, 6.2)	(225.6, 4.5)
12	(20.0, 8.8)	(206.0, 4.1)
13	(20.0, 7.4)	(226.2, 4.5)
14	(20.0, 10.6)	(205.6, 4.1)
15	(20.0, 7.8)	(195.8, 3.9)
16	(30.0, 10.2)	(189.9, 3.8)
17	(30.0, 15.3)	(174.8, 3.5)
18	(30.0, 6.6)	(190.2, 3.8)
19	(30.0, 10.8)	(176.3, 3.5)
20	(30.0, 7.2)	(191.3, 3.8)
21	(30.0, 14.1)	(176.8, 3.5)

The solution of the linear problem using the data presented in Table H.3 is as follows:

Minimize $J(A, \alpha) = \max(\alpha_0, |A_1|*0.0, 0.0*\alpha_1, \alpha_2*0.0*0.0, |A_2|*0.0*0.0) + \ldots$

$\ldots + \max(\alpha_0, |A_1|*0.0, 0.0*\alpha_1, \alpha_2*0.0*0.0, |A_2|*0.0*0.0),$

Subject to:

$|207.5 - (A_0 + A_1*0.0 + A_2*0.0*0.0)| \leq |1 - 0.6|\max(\alpha_0, |A_1|*0.0, 0.0*\alpha_1, \alpha_2*0.0*0.0, \ldots$

$$\ldots |A_2|*0.0*0.0) - |1 - 0.6|*4.1$$

$$\vdots$$

$$|176.8 - (A_0 + A_1*30.0 + A_2*30.0*30.0)| \leq |1 - 0.6|\max(\alpha_0, |A_1|*14.1, 30.0*\alpha_1, \alpha_2*30.0*30.0, \ldots$$

$$|A_2|*14.1*30.0) - |1 - 0.6|*3.5$$

Where:

α_0, α_1 and $\alpha_2 \geq 0$ for i = 1, 2, …, 21 and j = 0, …, 2

Resulting in:

$$\tilde{Y} = (224.6, 46.9) \oplus (1.3, 0.0) \otimes \tilde{X}_1 \oplus (-0.1, 0.0) \otimes \tilde{X}_1 \otimes \tilde{X}_1$$